Schweizerischer Erdbebendienst
Service Sismologique Suisse
Servizio Sismico Svizzero
Swiss Seismological Service

ETH
Eidgenössische Technische Hochschule Zürich
Swiss Federal Institute of Technology Zurich

Seismic Hazard Model 2015 for Switzerland (SUIhaz2015)

Report

19.07.2016

Imprint

Publisher
Swiss Seismological Service (SED) at ETH Zurich

Authors
Stefan Wiemer, Laurentiu Danciu, Ben Edwards, Michèle Marti, Donat Fäh, Stefan Hiemer, Jochen Wössner, Carlo Cauzzi, Philipp Kästli, Katrina Kremer

Compilation and Layout
Michèle Marti

Cover picture
Swiss Seismological Service

Publication date
19.07.2016

DOI
10.12686/a2

Seismic hazard online

Maps
Discover and compare additional maps of effects, hazard, and magnitudes with different parameters and periods by using our web tool:

www.seismo.ethz.ch/en/knowledge/seismic-hazard/maps/

Background information
You can find further information and an extensive scientific report about the seismic hazard model on this site:

www.seismo.ethz.ch/en/knowledge/seismic-hazard/background-information/

For professionals
Professionals can find additional information, specific data, and parameters on this site:

www.seismo.ethz.ch/en/knowledge/seismic-hazard/for-professionals/

Contents

Imprint **3**

Contents **5**

1. Introduction and context **7**
1.1 Why we need a Swiss national seismic hazard assessment 7
1.2 Mandate and role of the SED 9
1.3 History of seismic hazard assessment in Switzerland 9
1.4 Elements and data requirements for probabilistic seismic hazard assessment 12

2. General seismotectonic context **15**
2.1 Where earthquakes occur in Switzerland 15
2.2 Relationship between mountain building processes and earthquakes 16
2.3 The largest historical earthquakes in the Alps 18
2.4 The role of strain in creating earthquakes 19

3. Earthquake activity in Switzerland **23**
3.1 The challenge of understanding past earthquakes 23
3.2 Information on paleo-earthquakes in Switzerland 25
3.3 Information on historical and instrumental earthquake 27
3.4 ECOS09: a new earthquake catalogue for Switzerland 28
3.5 References 31
3.6 References ECOS-09 32

4. Seismic source model for the 2015 Swiss seismic hazard **35**
4.1 Motivation and overview 35
4.2 Seismotectonic context 36
4.3 Datasets of relevance for deriving the seismogenic zonation 38
4.4 Style of faulting and preferred rupture orientations 41
4.5 Estimating activity rates 46
4.6 Estimating the maximum magnitude 47
4.7 Defining a seismogenic zoning approach 50
4.8 SEIS-15 model 52
4.9 SEIS-04 model 53
4.10 CH-15 smoothed seismicity model 53
4.11 SHARE combined earthquake rate model 56
4.12 Rate forecast comparison and model weights 57
4.13 Consistency checks and adjustment for Basle 59
4.14 References 63

5. Assessment, adjustment and weighting of ground motion prediction models **67**
5.1 Introduction 67
5.2 GMPE selection 69
5.3 Empirical GMPEs: calibration and adjustment 71
5.4 Prediction uncertainties 78
5.5 Adopted logic tree 79
5.6 Conclusions 87
5.7 Data and resources 88
5.8 Acknowledgements 88
5.9 References 88

6. Hazard integration and computational aspects 93
6.1 Computational Aspects of PSHA 93
6.2 Software framework used for the hazard integration 93
6.3 Validation against FRISK88 94
6.4 Single source parameterization 96
6.5 Master logic tree 97
6.6 Computational settings 98

7. Swiss hazard 2015: main results 101
7.1 Seismic hazard curves 101
7.2 Seismic hazard maps 102
7.3 Intensity probability maps for Switzerland, including indicative local site amplification 105
7.4 Uniform Hazard Spectra (UHS) 107
7.5 Disaggregation results 109
7.6 Comparison with the 2004 national hazard model 111
7.7 References 117

8. Sensitivity analysis and comparison with other models 119
8.1 Seismogenic depth 119
8.2 Stochastic versus empirical GMPEs 120
8.3 Individual GMPE contribution 121
8.4 Mapping the uncertainty ratio 123
8.5 Comparison with SIA 124
8.6 Comparison with ESHM13 126
8.7 Comparison with PRP 127
8.8 References 130

9. Communicating seismic hazard 133
9.1 Introduction and context 133
9.2 Best practices in communicating seismic hazard 133
9.3 Improvements in the 2015 hazard model communication 135
9.4 Products 138
9.5 Literature 143

10. Summary and outlook 145

11. Acknowledgements 149

Appendix A 150

Appendix B 151

Appendix C 155

1. Introduction and context

1.1 Why we need a Swiss national seismic hazard assessment

Switzerland is an earthquake country! In 2014 alone, more than 900 earthquakes were recorded within or near Switzerland by the seismic network operated by the Swiss Seismological Service (SED, www.seismo.ethz.ch) at ETH Zurich. Although only 21 of them attained a magnitude of 2.5, large enough to be potentially felt. They are part of a rich earthquake history of Switzerland including numerous damaging earthquakes, which are recorded in the historical reports of the past 800 years, including the strongest earthquake ever documented north of the Alps in Basle in 1356.

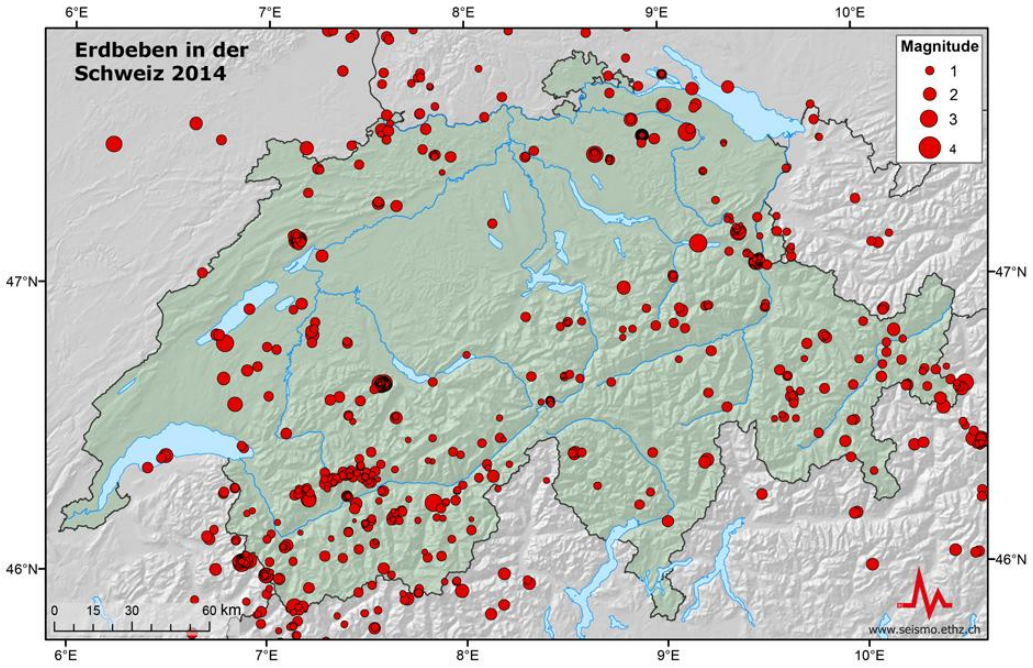

Figure 1: Map of Switzerland, red dots show the locations ('epicentres') of earthquakes recorded in 2014.

Unknown to most citizens, of all natural hazards in Switzerland earthquakes pose the greatest damage potential. Large-scale earthquakes are fortunately quite rare, but if they strike, they can cause far-reaching and very costly damage and lead, potentially, to hundreds or even thousands of fatalities. Recent estimates by the federal office of civil protection and SwissRe indicate that a repeat of the 1356 Basle earthquake with a magnitude of 6.7 would result in staggering casualties: direct damage costs of 70 to 140 billion Swiss Francs, 600 to 1,000 fatalities, and 45,000 to 1,600,000 people rendered homeless. How large the damage footprint of such an event would be is shown in a Scenario ShakeMap in Figure 2; the earthquake would be very strongly felt across Switzerland and light damages could occur as far as Zurich and Berne.

While such a devastating event might only occur every 1,000 or 2,000 years (that is, with an annual probability of 0.05 to 0.1 percent), slightly smaller events of approximate magnitude 6 could also be catastrophic were they to occur beneath urbanized zones. From historical records we know that since the 13th century, 12 earthquakes have occurred which caused substantial damages, meaning that every 50 to 150 years (statistically seen, with a 1% chance every year) such a disaster might strike Switzerland. A repeat of the 1855 Visp (VS) earthquake, magnitude 6.2, would for example cost 2 to 5 billion Swiss Francs in direct damages alone.

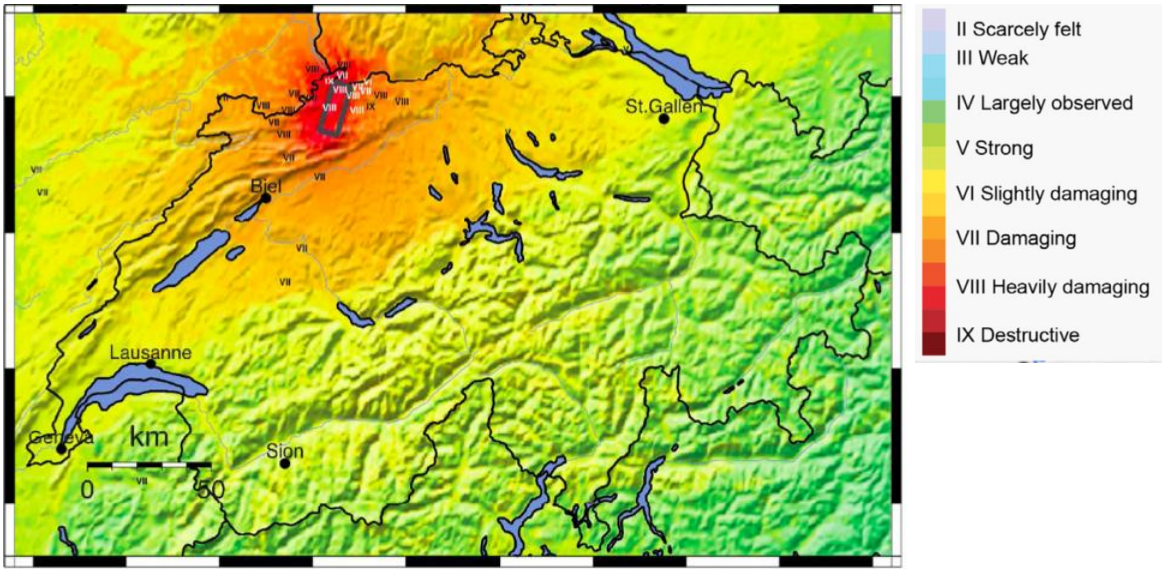

Figure 2: Scenario ShakeMap for an assumed repeat of a 1356-type earthquake near Basle, (magnitude 6.7). Colour-coded is the expected level of shaking and damaging, expressed on the macro-seismic intensity scale (EMS-98).

At present, earthquakes cannot be prevented or even reliably predicted. But thanks to extensive research, much is now known about how often and how intensely the earth could shake at a given location in future. Switzerland's seismic hazard model 2015 (SUIhaz2015) presented in this report is a comprehensive elucidation of this knowledge. It forecasts potential earthquakes and the resulting ground motions over the next fifty years. The model is based on integrating knowledge of tectonics and geology, information about the history of earthquakes, damage reports and wave propagation models.

Probabilistic seismic hazard assessment (PSHA) at a national level enables societies to make well-informed decisions on earthquake safety. It is a fact of life that zero risks of natural hazard is impossible to achieve, even through near-infinite investments. Therefore, authorities, experts and society need to balance those risks, costs and benefits. The SUIhaz2015 is in this endeavour a starting point for making decisions regarding earthquake mitigation and risk management at local, regional and national levels. A hazard, and to an even greater degree a risk model, allows us to prioritize actions in a rational way by identifying the most cost-effective and most needed actions, thereby ensuring that every citizen is protected against earthquakes to a minimum standard, as defined by society.

On a technical level, a PSHA defines for building engineers the kind of ground motions which can be expected in an earthquake and to couple them to the response of local soil and the building characteristics. This is essential to know for residential buildings, and even more so for infrastructures such as hospitals, bridges, waterlines, power lines, trains, chemical facilities, etc. The national Swiss seismic building codes defined in the SIA norms 261ff are, for that reason, partially based on the seismic hazard model.

For scientists and engineers, a PSHA is especially important because it captures as much as reasonably possible the variability of the relevant processes coupled to the uncertainty in our understanding these processes. By systematically analyzing where the largest uncertainties lie, using a so-called sensitivity analysis, scientists and engineers can identify the most-relevant gaps in our understanding and thereby help to guide and prioritize future research. A PSHA is also a quantitative and replicable forecast of the future seismicity and can be tested against observations. The performance of the various model components, as well as the model overall, can be evaluated, giving model developers important feedback on potential problems and misconceptions, but also (to a certain degree) independently validating the model.

Last but not least, seismic hazard models serve as a reminder that Switzerland is an earthquake country. Despite its moderate seismic activity, Switzerland manifests a high seismic risk due to the high population and infrastructure density. For the release of SUIhaz2015 we thus aspired to facilitate public access to results and implications especially for non-experts who would like to learn more about the threat of earthquakes.

1.2 Mandate and role of the SED

The Swiss Seismological Service (SED) at ETH Zurich is the federal agency responsible for monitoring earthquakes and assessing the seismic hazards of Switzerland. Its origins date back to the Swiss Earthquake Commission founded in 1878, which made Switzerland the first country to establish a permanent organization for the evaluation of earthquakes, even before countries such as Italy or Japan. In 1914, the earthquake monitoring mandate was defined in a federal law. Thus, what had previously been a voluntary activity was transformed into an institution which since 1957 has been located at ETH Zurich. Today, the SED has a staff of about 60 people, 2/3 of them are scientists and engineers, including about ten PhD students.

The SED's main tasks are:

- earthquake surveillance
- providing information to the authorities and the public, including alerting
- earthquake hazard assessment
- research and development on earthquakes and their effects
- education and outreach-related activities
- contributions to the international program monitoring the nuclear-test-ban treaty

The SED has had a federal mandate for many decades to produce and regularly update the national hazard model. The hazard model presented here is specifically in fulfilment of the Federal Council resolution of January 30, 2013 addressing earthquake precautionary measures to be taken by the federal government for the period 2013 – 2016.[1]

1.3 History of seismic hazard assessment in Switzerland

Probabilistic seismic hazard assessment is by its very nature an attempt to capture state-of-the-art of the knowledge and understanding of seismic hazard at a certain point in time. It is important and customary around the world to regularly update a PSHA in order to integrate new data and new scientific findings. The 2015 assessment is the latest stage in the evolution of such snapshots in time. It builds on a number of studies related to hazard assessment in Switzerland which have been performed during the past three decades:

- In **1978**, Sägesser and Mayer-Rosa (1978) published the first PSHA for Switzerland. The hazard was based on the historical catalogue available at the time which contained epicentral Intensities, I_o, as a quantification of size. To compute hazard, an intensity-based attenuation function was used. Hazard was computed, based on the Cornell-McGuire approach (Cornell 1968), with a zoning model including about 20 zones, which to a large degree mirrored the spatial distribution of seismicity. This study produced the input for the Swiss building code (SIA code 160) as well as for critical facilities, such as nuclear power plants and large dams.

[1] Resolution of Federal Council of 30 January 2013 on "Precautionary measures for earthquakes. National programs 2013 – 2016,

- In **1995,** a comprehensive study by Rüttener (1995), based on a historical parametric method, estimated the hazard and associated uncertainties at twelve sites in Switzerland. The computed parameter was once again macroseismic intensity.
- **In 1998,** Grünthal et al. (1998) significantly updated the hazard map, and provided a harmonized assessment including Germany, Austria and Switzerland (D-A-CH). The D-A-CH map was used as test region for Global Seismic Hazard Assessment Program (GSHAP) region 3 (Grünthal 1999), which depicted the first unified seismic hazard model for Northern Europe (north of 46° latitude), including the majority of Switzerland. To express epistemic uncertainty in ground motions modelling, Grünthal (1999) used three attenuation relationships of equal weight: Ambraseys et al. (1996), Boore et al. (1997) and Sabetta and Pugliese (1996).
- **In 2002**, the SESAME project (Seismotectonics and Seismic Hazard Assessment in the Mediterranean Region; IGCP Project 382) published a first unified seismic hazard model for the entire European-Mediterranean region (Jiménez et. al 2003). For the SESAME computations, Ambraseys et al. (1996) attenuation relationships in terms of peak ground acceleration (PGA) and spectral acceleration (SA) were applied. For Switzerland, the zonation of the GSHP test region 3 (Grünthal 1999) was adopted with minor modifications to the southernmost source zones.
- **In 2004**, the SED published the first fully probabilistic national seismic hazard assessment for Switzerland in spectral ordinates rather than intensities (Giardini et al., 2004; Wiemer et al., 2009). The study was based on a revised moment-magnitude earthquake catalogue for Switzerland and the surrounding regions, covering the period 1300 to 2003 (ECOS02). Information on active faulting in Switzerland was judged as too sparse to be used as source model; instead, the SED developed two models of areal sources. The first aimed at capturing historical and instrumental seismicity (SEIS), the second was guided largely by tectonic principles and expressed the alterative view that seismicity is less stationary, and thus, future activity may occur in previously quiet regions (TECT). Using a specific predictive spectral ground-motion model for Switzerland (Bay et al., 2005), the SED estimated the expected ground-motions in units of the 5% damped acceleration response spectrum at frequencies of 0.5 to 10 Hz for all of Switzerland, and referenced to rock sites with an estimated shear wave velocity of approximately 1500 m/s^2 in the upper 30 m. The resulting map is shown in Figure 3.

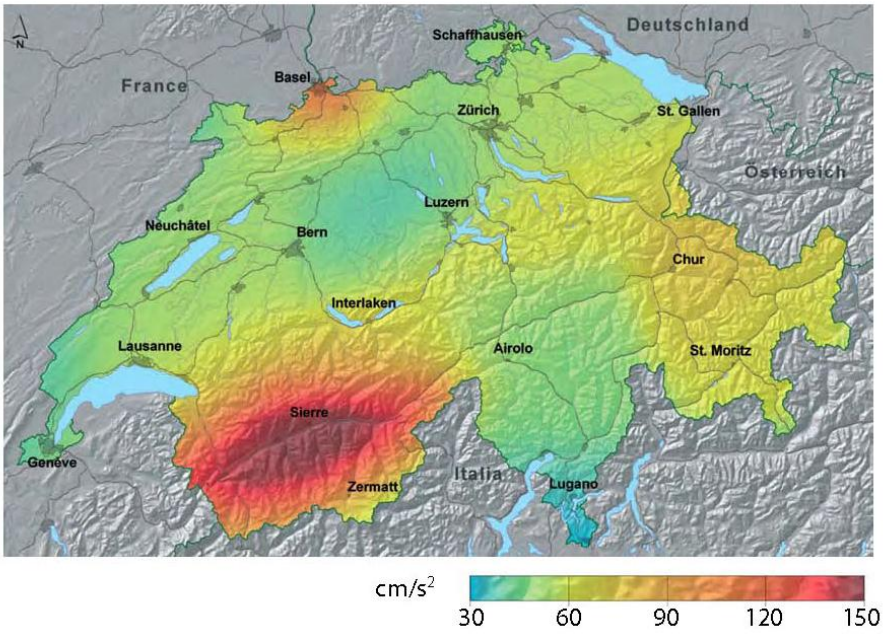

Figure 3: 2004 Version of the Seismic hazard map of Switzerland, depicting the level of horizontal ground-motion in cm/s^2 (in units of 5% damped acceleration response spectrum at 5 Hz frequency) expected to be reached or exceeded in a period of 475 years (10% exceedance chance in 50 years). The map is assumed to be valid for a rock ground condition (V_s approximately 1500 m/s). Overall, the hazard level of Switzerland ranges between 5 and 15% of the acceleration of gravity (50-150 cm/s^2).

- In **2013**, the collaborative EU-FP7 project Seismic Hazard Harmonization in Europe (SHARE, www.share-eu.org) coordinated by ETH Zurich brought together scientists and engineers from around Europe to update general understanding of earthquake activity and the related ground motions. SHARE produced more than sixty time-independent European Seismic Hazard Maps (ESHMs, see Figure 4 for an example) spanning spectral ordinates from PGA (Peak Ground Acceleration) to 10 seconds and exceedance probabilities ranging from 10^{-1} to 10^{-4} annual probability. The hazard values are referenced to a rock velocity of vs_{30}=800m/s. SHARE models earthquakes as finite ruptures and includes all events with magnitudes MW≥4.5 in the computation of hazard values. The so called ESHM13 (European Seismic Hazard Model) will be updated around 2018, still in time for the next release of the EuroCode 8 in 2020. The update will specifically focus on integrating recent progress made in modeling the ground motions of earthquakes.
- **Between 1999 and 2004** The PEGASOS study[2] (Probabilistic Seismic Hazard Analysis for Swiss Nuclear Power Plant Sites) was initiated in 1999 by the Swiss Federal Nuclear Safety Inspectorate (HSK, now ENSI) in order to incorporate scientific advances into engineering practice. The PEGASOS Refinement Project was initiated in 2008 and concluded in 2016. These site-specific hazard assessments followed the American SSHAC Level 4 procedure (NUREG-CR 6372). SUIhaz2015 was able to benefit indirectly in a number of ways from the ongoing PEGASOS and PRP studies. Most notably, the revision of the ECOS09 catalogue as well as the geophysical measurements of the local amplification at SDSNet sites and the development of a stochastic ground motion prediction model was in part financed by funding from ENSI/swissnuclear.

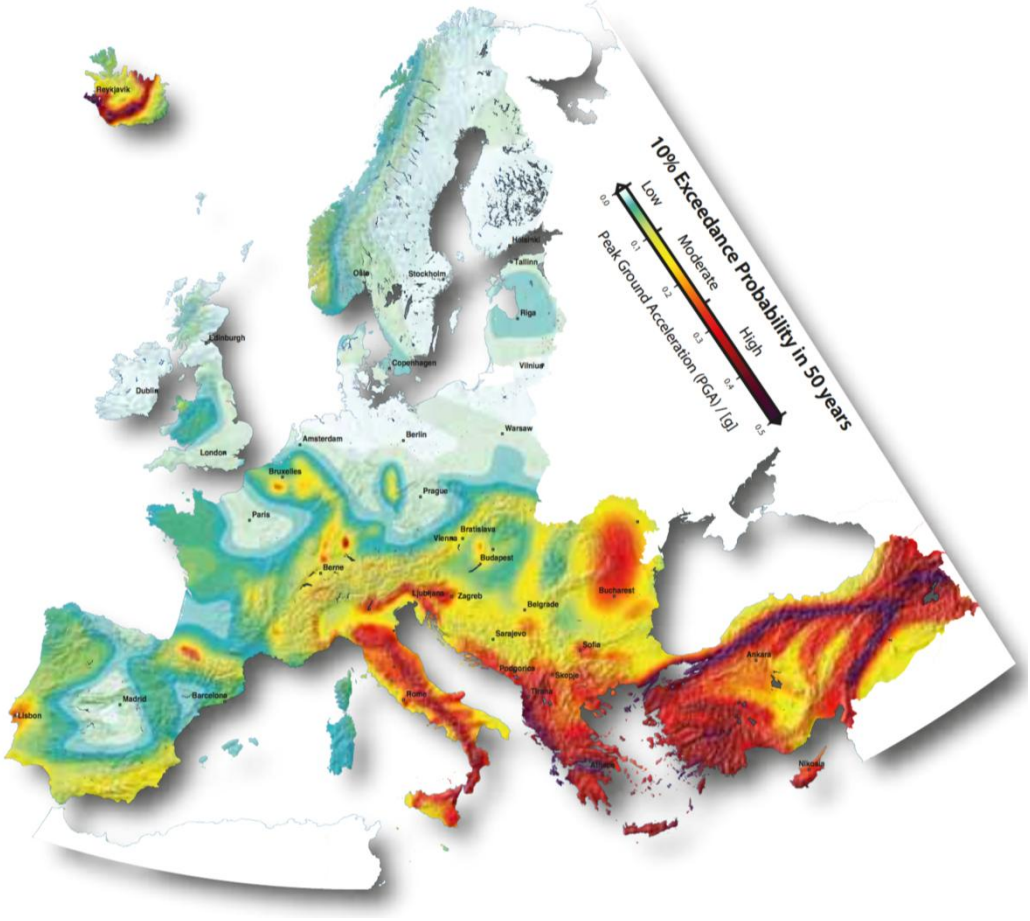

Figure 4: The SHARE European Seismic Hazard Map displays the ground motion (i.e. the Peak Ground Acceleration PGA) expected to be reached or exceeded with a 10% probability in 50 years, i.e. these values repeat themselves on average every 475 years. Cold colours indicate comparatively low hazard areas (PGA≤0.1g), yellow to orange colours indicate moderate hazard areas (0.1<PGA≤0.25g) and red colours indicate high hazard areas (PGA>0.25g**).**

[2]http://www.swissnuclear.ch/en/earthquake-safety-_content---1--1027.html

1.4 Elements and data requirements for probabilistic seismic hazard assessment

Overall objectives of a PSHA

The goal of probabilistic seismic hazard analysis (PSHA) is to quantify the rate (or probability) of exceeding various ground-motion levels at a site (or a map of sites) given all possible earthquakes (Reiter, 1990). A PSHA is a forecast of the possible ground motions to be expected at every location in Switzerland within 50 years, and for all relevant frequencies of ground motions. The forecast references to an idealized rock site with well-specified conditions, not the actual local site conditions because these are generally not known on a national scale; and are then applied locally in a second step.

Significantly, this forecast must cover all possible scenarios and specifically include also unlikely or extreme earthquake shaking caused by larger events very near a site and possibly with unusually high ground motions at the source. Such a shaking may not be very likely in a 50 year time frame since such an event may occur only every 500, or even 5,000 years. However, by capturing all possible scenarios, a PSHA permits us to make decisions for different kinds of uses and the levels of safety required. While a residential building may be designed to withstand a shaking that will only occur with less than a 10% likelihood within 50 years, a critical facility may be designed to a higher safety standard, for example withstanding shaking that will occur only with a 2% or 0.5% in 50 years.

The concept of a low probability event, such as a shaking that will only occur with a 2% change within 50 years, is in principle interchangeable with the idea of earthquake recurrence: a low probability event of 2% within 50 years is one that will re-occur only rarely, roughly every 2,500 years (to be precise: 2475.9 years, see appendix A for a conversion between recurrence rates and return periods). Likewise, the hazard can be shown annualized.

Note, however, that the concept of 'return period' sometimes inspires a misunderstanding in the sense that the underlying earthquakes recur at regular intervals (e.g., every 500 years) and that consequently earthquakes can be 'overdue' - or the reverse, safe periods because such events have recently occurred. Earthquakes, however, as in hazard models as explained in Chapter 4 in more detail, are assumed to be random in time and independent of each other. While a certain shaking or event will be forecast to occur on average every 500 years, this is only a statistical average that will prove correct over the long term. The likelihood that such an event will occur is assumed to be constant in the models, the same tomorrow, next year and in 500 years. This concept is easily understood when using dice as an example: while we know well how often a '6' will be rolled on average (1 in 6, with a 16.66 percent chance), the fact that one did just roll a six, or did not roll one for 10 times in sequence has no implication for the next roll of the dice. Each roll of the dice is independent. The same is assumed for earthquakes and the analogue can be stretched a bit further: the reason why there are more often earthquakes in the Valais or Basle than in other areas of Switzerland can be seen as more dice being rolled there, on average.

It is worth noticing that the confidence levels (50^{th}, 84^{th} and 95^{th}) and probability level (10% in 50 years, 2% in 50 years and 1% in 50 years) of ground motions are interrelated. Generally, the 84th percentile of the 10% in 50 years is coincidentally very similar to the median (50^{th} percentile) of the 2% in 50 years results. These measures of uncertainties are interchangeable when used for engineering design. One might base the seismic loading on a median value of a lower probability level (2% in 50 years) or the upper confidence level (84^{th}) of the median value of 10% in 50 years. Both options will provide satisfactory ground motion for engineering design. Conservatism can thus be built in by choosing a lower probability level or by choosing a higher fractile.

A PSHA is also a formalized and systematic way to capture the various types of uncertainties that are inherent to making forecasts in natural systems. In doing so, the final PSHA model will satisfy the SSHAC requirement of representing the centre, body and range of the informed technical community; it will characterize not only the mean (or median) expected ground motion but also a full uncertainty distribution around it (expressed as standard deviation or fractiles). Knowing just how certain an assessment is can be important, and if established correctly, the uncertainty of a forecast is an important way to judge its quality and usefulness, as well as to track progress. One of the major advances of the new model, compared to previous one, is that the uncertainty in the forecast has been substantially reduced.

A key statement that describes well the objected of a PSHA is: "*Regardless of the scale of the PSHA study the goal remains the same: to represent the centre, the body, and the range that the larger informed technical community would have if they were to conduct the study*" (NUREG/CR-6372). This principle was also adopted for our PSHA. The hazard model we have compiled is not intended to be the personal opinion of the experts involved, or the official position of the SED, it must be a weighted assessment of the wider technical community. The SED was in a unique position to take advantage of the parallel PEGASOS and PEGASOS Refinement project ongoing at the same time. Thanks to these projects, primary data sources (such as ECOS09) and models (such as GMPE's) were developed which otherwise may have been out of scope. More importantly, however, SED scientists were exposed over the past ten years to numerous expert opinions of many of the world leading experts in their respective domains. This exposure and the countless in-depth discussions and exchanges are in our opinion a highly important contribution to ensuring the breath and quality of the Swiss national model.

Elements of a PSHA

To meet the objectives outlined above, it is necessary to perform a number of analytical steps, which define the input parameters needed for performing a PSHA following the Cornell-McGuire approach (Cornell 1968; McGuire 1976; Figure 5):

1. **Seismogenic source model** (sometimes termed as earthquake rupture forecast): This model describes what kind of earthquakes are possible in the future. It can be based on area sources, on fault sources, or on a mixture; it must also specify the size distribution of the future earthquakes, their depth distribution and faulting styles. The historical and instrumental **catalogue** is the primary information source for defining a source model.

2. **A set of Ground Motion Predictions** (GMPE), which describes the attenuation of amplitudes (PGA, response spectral values at a number of frequencies) as a function of frequency, distance and magnitude.

3. **A computational framework** is also needed to do the hazard integration and keep track of all uncertainties etc.

Uncertainties in all steps need to be systematically evaluated and characterized. The distinction between aleatory variability and epistemic uncertainty is now widely viewed as a useful paradigm for seismic hazard analysis (e.g., Toro et al. 1997). In PSHA, aleatory variability determines the shape of the hazard curve, whereas epistemic uncertainties, captured by the branches of the logic tree, lead to families of hazard curves (e.g., Bommer and Scherbaum 2005). Note, however, that while the distinction between aleatory and epistemic uncertainties is conceptually useful, in practice the separation of the two is sometimes far from clear-cut (Anderson and Brune, 1999; Wiemer et al., 2009).

Output products of the hazard model are primarily:

1. A set of **hazard curves**, which define the annual probability of exceedance as a function of ground motion (e.g. spectral acceleration) for all relevant frequencies of ground motion and for a specific assumed reference rock site. Our model spans the range down to return periods of 10,000 years (annual probability 10^{-4}).

2. A set of **hazard maps**, showing the ground motion for a given return period and frequency.

3. A set of **uniform hazard curves**, depicting the ground motion as a function of spectral period for a given return period.

4. **Disaggregation** at each site, identifying for a given return period and spectral period the dominating contribution to the hazard as a function of distance, magnitude and ground motion variance.

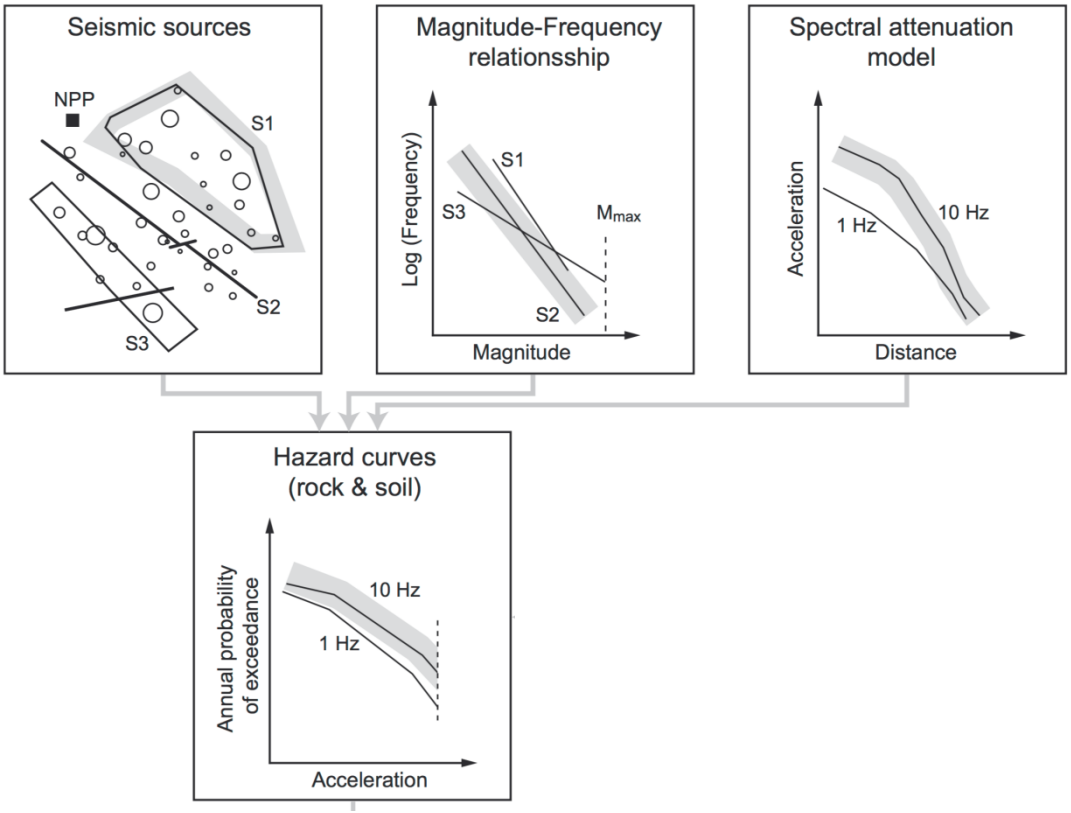

Figure 5: Elements of a PSHA (adopted from Reiter (1990) and swissnuclear).

In the subsequent chapters, we describe the data and processing steps relevant for the computation of the hazard model: the general seismo-tectonic context (Chapter 2); the catalogue (Chapter 3), and the 2015 seismogenic source model (Chapter 4) and the Ground Motion Prediction Equations (Chapter 5). We will then present and discuss the computational aspects and hazard results (Chapters 6, 7 and 8) and close with some word on the goals of our communication strategy (Chapter 8).

2. General seismotectonic context[3]

2.1 Where earthquakes occur in Switzerland

The SED has been operating a digital network of seismic stations since 1975. This network monitors the seismic activity in Switzerland and in neighbouring countries. On average, the SED records 500 to 800 earthquakes per year. Of those, however, the public notices only a few. The majority of the recorded earthquakes take place in the Swiss Alps, especially in Valais and Grisons (Figure 6). Seismic activity is also particularly high in the northern foothills of the Alps, in Central Switzerland, and in the Jura and Basle regions.

Earthquakes occur at markedly different depths (Figure 7) within the Alps and in the region north of it. Earthquakes in the northern foothills and the Jura occur throughout the entire crust of the Earth down to the Moho, the boundary between the crust and the mantle, outside the Alps at a depth of about 30 km. On the other hand, seismic activity underneath the Alps is limited to the upper part of the crust; here, quakes occur to depths of 20 km only while the Moho reaches a depth of more than 50 kilometres.

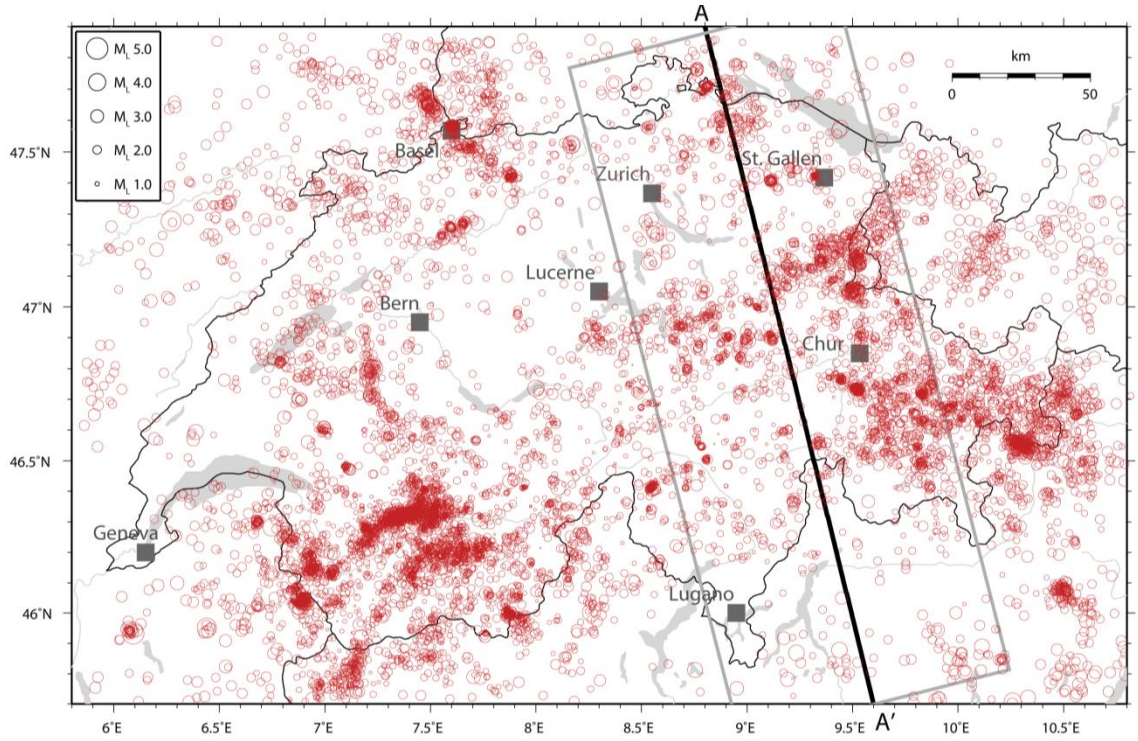

Figure 6: Map of all earthquakes (red circles) with a magnitude of 1 or more in Switzerland between January 1975 and January 2014. Valais and Grisons are regions in the Swiss Alps that have increased seismicity. The size of the circles indicates the local magnitude (ML) of the earthquakes. The thick black line shows the location of the deep cross section through Eastern Switzerland (see Figure 7). Only quakes within the gray rectangle were used for the profile in Figure 7.

[3] This section has been adopted from snapshot no. 5 of the SED 100-years celebration.

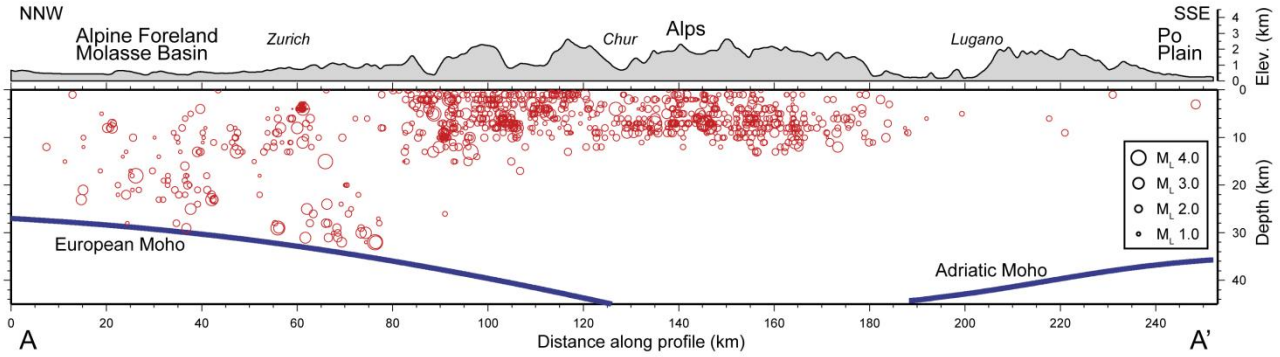

Figure 7: Vertical cross section through Switzerland documenting the depth distributions of earthquakes: in the Alps, the occurrence of earthquakes is restricted to the upper crust; below the northern foothills and the Swiss plateau, earthquakes take place throughout the entire crust. The crust/mantle boundary is marked by Moho (see text). The size of the circles indicates the local magnitude (ML) of the earthquakes. The location of the profile is shown in Figure 6 (modified and updated from Deichmann et al. 1999, Eclogae).

2.2 Relationship between mountain building processes and earthquakes

The Alps are the result of a complex geological history involving two large lithospheric plates (Figure 8): Europe and Africa. The lithosphere is the outermost solid shell of the Earth. It is about 100 km thick and consists of two layers, the crust on top and the mantle lithosphere below. The global lithosphere is fractured into numerous large and small plates that move in different directions on the viscous mantle, rubbing against or colliding with one another. The entity of all of these processes is called plate tectonics.

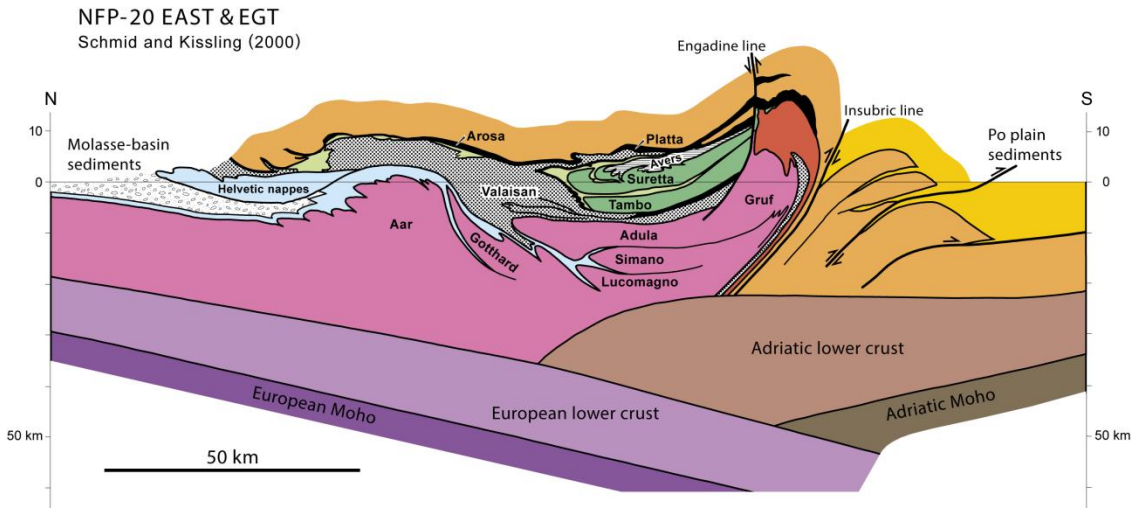

Figure 8: Geological depth profile through Eastern Switzerland. The European (from the left) and the Adriatic plates (from the right) collided, forming the Alps as we know them today (modified and updated from Schmid and Kissling 2000, Tectonics).

Due to their composition, we differentiate between two types of lithosphere: continental and oceanic. The oceanic lithosphere is denser than the viscous mantle below it and can therefore sink. The continental lithosphere is less dense than the mantle and therefore remains floating on top of it. When oceanic lithosphere meets continental lithosphere during the collision of two plates, the oceanic lithosphere dives into the viscous mantle below it – a process that is called subduction and that is usually associated with large earthquakes and volcanic activity. If two continental lithosphere plates collide, a mountain range develops along the plate boundary.

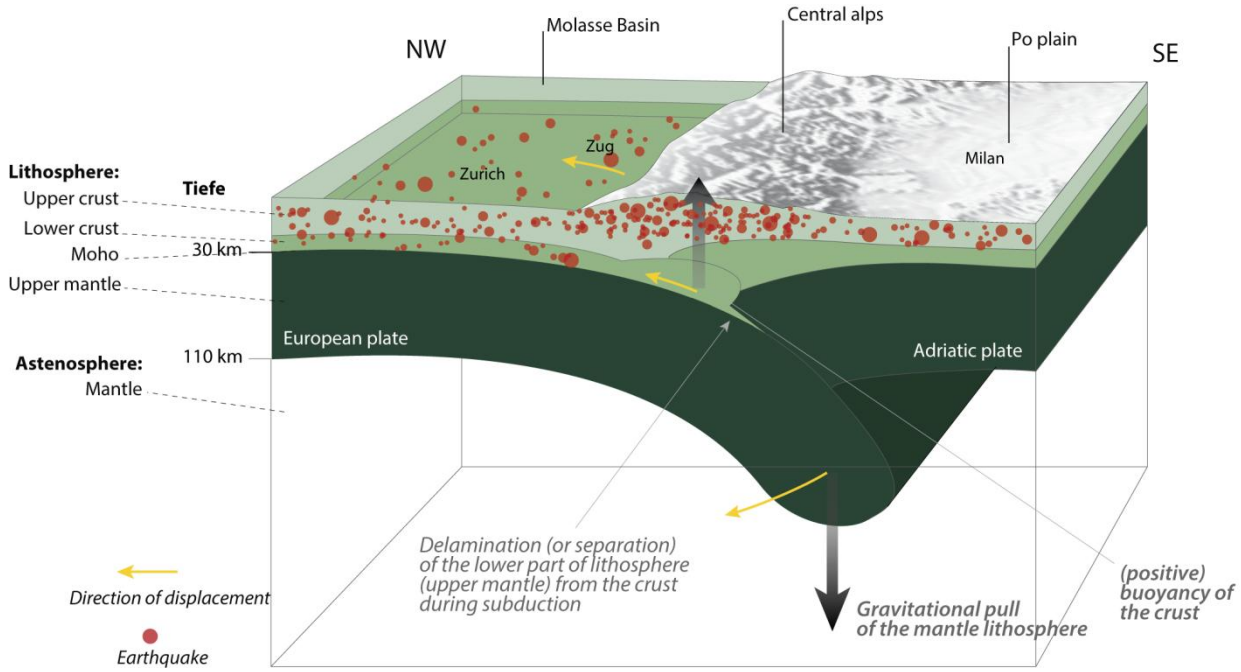

Figure 9: Cross section through the lithosphere schematically showing the various forces acting at depth on the Alps. The hanging European slab (mantle lithosphere) causes a downward force, while the lower crust detaches from the slab and the large crustal root generates buoyancy to compensate for loads by topography (mountains) and by the slab (Singer et al. 2014, EPSL).

Not only the European and African plates participated in the formation of the Alps, but also several smaller lithospheric plates, which are known as micro plates. Particularly important is the Adriatic micro plate. Following the complete subduction of the oceanic lithosphere, and thus the closing of the original ocean (called Alpine Tethys by scientists) between Europe and Africa about 35 million years ago, the continental parts of the European and the Adriatic/African plates collided, initiating the formation of the Alps. Similar to a floating iceberg, the weight of the mountains is supported by the buoyancy of a large crustal root. With increasing height of the mountains, erosion of rocks at the Earth's surface plays an ever more important role. With the removal of rock material at the surface the weight of the mountains decreases and the crust beneath the Alps rises again to retain the isostatic equilibrium. The massive erosional debris of the mountains has accumulated on both sides of the Alps over the last 30 million years, as the Molasse sediments in the north and as sediments filling the basin beneath the Po plain in the south. The Alps as we know them today have thus been shaped by forces from the earth's interior and by erosion. Today, the Alps are rising by approximately 1 millimetre per year and are simultaneously eroding. Post-glacial rebound remains also an important contribution to the current vertical motions.

Generally speaking, the earthquakes that we observe in Switzerland (see Figure 6, Figure 7) are the results of the collision between the European and the African lithospheric plates as they reflect the underlying mechanics of these processes. Seismic waves penetrate the subsurfaces, thus illuminating the deep parts of the lithosphere beneath the Alps. One important detail has been discovered in the last few years: after the complete subduction of the oceanic lithosphere and the subsequent collision of the two continents, a piece of the original mantle lithosphere is still attached to the European plate (known as the mantle slab). This slab is bending the lithosphere in the northern foothills of the Alps downward (see Figure 9 and Figure 10), thus indirectly causing the widely distributed seismicity on the Swiss plateau. Since plate tectonic processes take place over geological time scales, it can be assumed that the current seismicity in the region of the Alps will remain the same for millions of years to come.

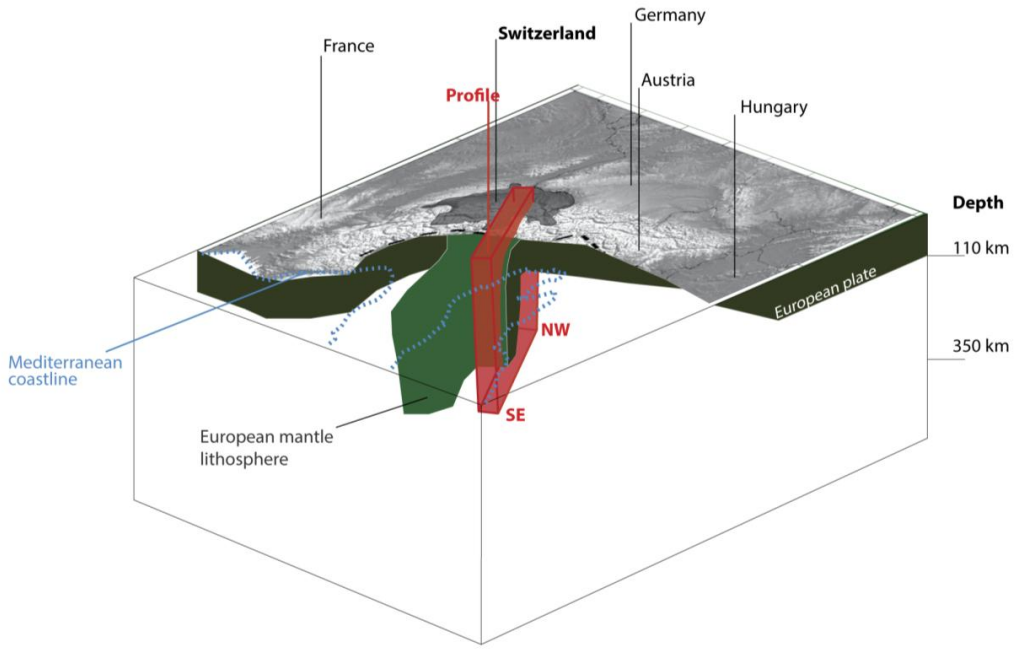

Figure 10: Three-dimensional depiction of the hanging European mantle lithosphere slab, which is one of the main driving forces for earthquake activity in the Alps. The NW-SE profile that is marked in red is shown in Figure 7 (Singer et al. 2014).

2.3 The largest historical earthquakes in the Alps

As a result of plate collision, severe earthquakes have occurred in the Alps and their surroundings time and time again in the past (Figure 11). Information from historical sources and modern earthquake catalogues show that there were at least 12 earthquakes with a magnitude of 6 or more in the past thousand years (see Table 1 and the orange circles in Figure 11). The last major earthquake took place in 1976 in northern Italy (M 6.5) followed by two aftershocks with magnitudes greater than 6 within a few months. This Friuli quake claimed 989 lives and injured 2,400 people; about 45,000 were left homeless as a result. Although the extent of damage for historical events can sometimes be difficult to estimate, it is likely that at least three of the quakes listed in the table caused more than 10,000 deaths.

	Date	Latitude (°)	Longitude (°)	Magnitude [source]	Location
1	1117.01.03.	45.309	11.023	6.7 [a]	Verona (IT)
2	1222.12.25.	45.313	10.697	6.0 [a], 6.1 [b]	Basso Bresciano (IT)
3	1295.09.03.	46.78	9.54	6.2 [a, b]	Churwalden (CH)
4	1348.01.25	46.579	13.540	7.0 [a]	Villach (AT)
5	1356.10.18.	47.47	7.6	6.5 [a], 6.6 [b]	Basle (CH)
6	1511.03.26.	46.198	13.431	6.9 [a]	Idrija (SI)
7	1590.09.15.	48.275	16.014	6.1 [a]	Neulengbach (AT)
8	1690.12.04.	46.633	13.880	6.6 [a]	Carinthia (AT)
9	1695.02.25.	45.801	11.949	6.5 [a]	Asolano (IT)
10	1855.07.25.	46.23	7.85	6.1 [a], 6.2 [b]	Visp (CH)
11	1873.06.29.	46.16	12.383	6.3 [a]	Belluno (IT)
12	1976.05.06.	46.262	13.300	6.5 [c, d]	Friuli (IT)

Table 1: List of the strongest mainshocks in the Alps (including the Swiss plateau). The magnitudes are taken from the following sources: a = SHEEC, b = ECOS-09, c = NEIC, d = ISC. The uncertainties in the magnitudes (if listed) are less than 0.5.

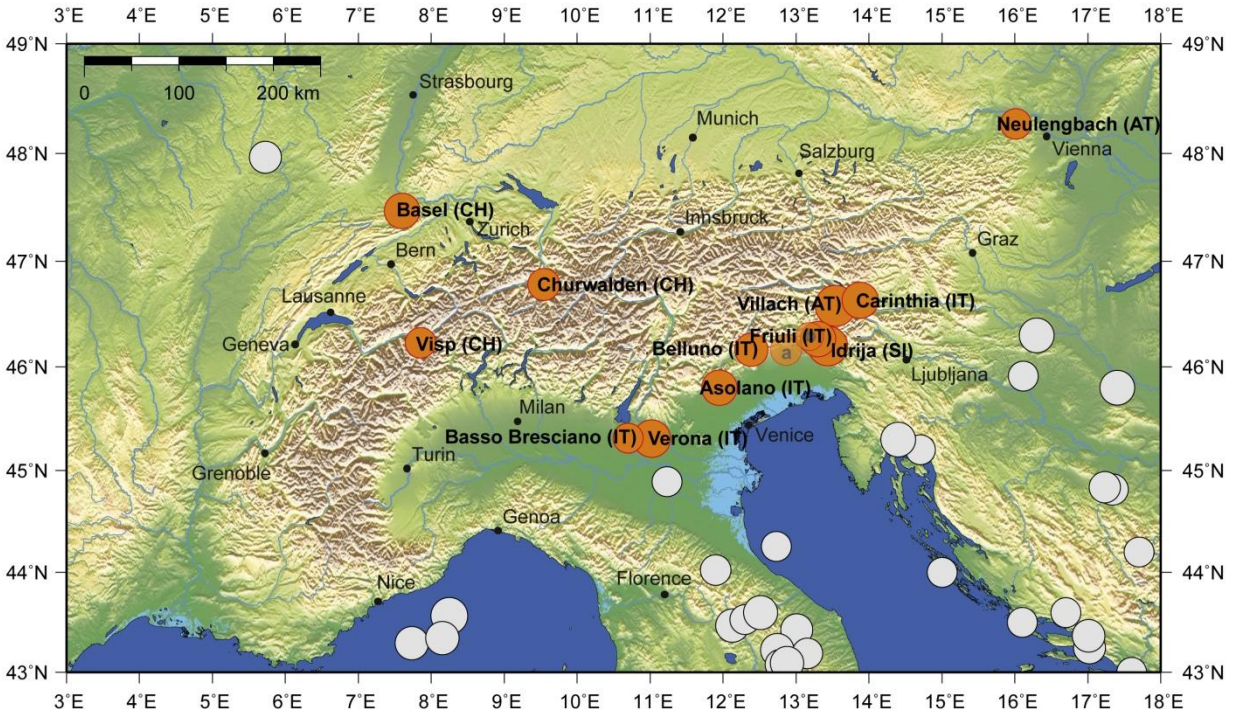

Figure 11: Map with the largest earthquakes (magnitude ≥ 6) in and around the Alps in the last millennium. The orange circles indicate the quakes in the Alps and on the Swiss plateau listed in the table. The size of the circles is proportional to the magnitude. The gray circles mark quakes outside the region of the Alps. The aftershocks of the Friuli quake of 1976 are labeled 'a' and 'b'.

Earthquakes cannot be predicted. As the time series in Figure 12 shows, they also occur at irregular intervals. Therefore, we do not know where and when the next major quake will occur. A quake with a magnitude around 6 or more usually occurs every 50 to 150 years in Switzerland; quakes with a magnitude of 7 are expected to occur about 10 times less often (not observed in historical times).

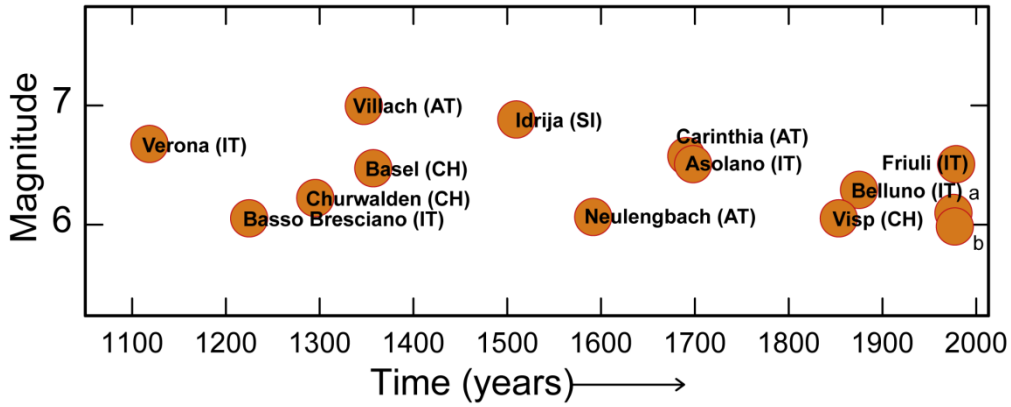

Figure 12: Time series of the largest earthquakes in the last millennium in the Alpine region. The aftershocks of the Friuli quake of 1976 are labeled 'a' and 'b'.

2.4 The role of strain in creating earthquakes

Earthquakes are to a first order principle a response of the earth to deformation caused by strain. The Earth crust and lithosphere is moving and in many places deforming because of a number of forces acting upon the plates. Deformation can be a-seismic, continuous and creep-like, but a good fraction of the deformation takes place episodically in large earthquakes. Strain, therefore, is a first order predictor of seismicity rate on a global scale, reflecting the basic physical principle of energy conversation. While short- and medium-term fluctuations in seismicity rate are common, the long-term rate much respect the plate-tectonic input.

An illustrative example of this general relation is shown in Figure 13, which compares the annualized rate of earthquakes in California, Japan and Switzerland from instrumental data between 1980 and 2013. Many more earthquakes occur overall in Japan and California than in Switzerland, but the difference decreases somewhat when normalizing to the respective areas. If we then normalize also by the average deformation (or straining) rate, as determined from geodetic data, the output of earthquakes per area and per strain is starting to be quite comparable between the different regions. This pertains to the rate of events but also, to a first order, to their average frequency-size distribution (the slope of the lines). So the difference in seismic activity rates is to a first order a result of the different deformation rates, which in California or Japan are 30 - 100 time higher than in Switzerland. A consequence, earthquakes occur at a rate 30-100 time higher.

Using the previously mentioned dice analogue again, one can argue that in California and Japan the dice is rolled on average much more often - but the dice is the same. This also applies to large events: A magnitude 7 is expected in Japan of onshore Californian maybe every 10 years or so, while in Switzerland we expect such an event with a rate 100 times lower, every 1000 years or so. One of the challenges in seismic hazard assessment is, however, to decide where the curves start to role of: The maximum possible magnitude and its dependence on the tectonic environment and the local strain rate remains poorly understood.

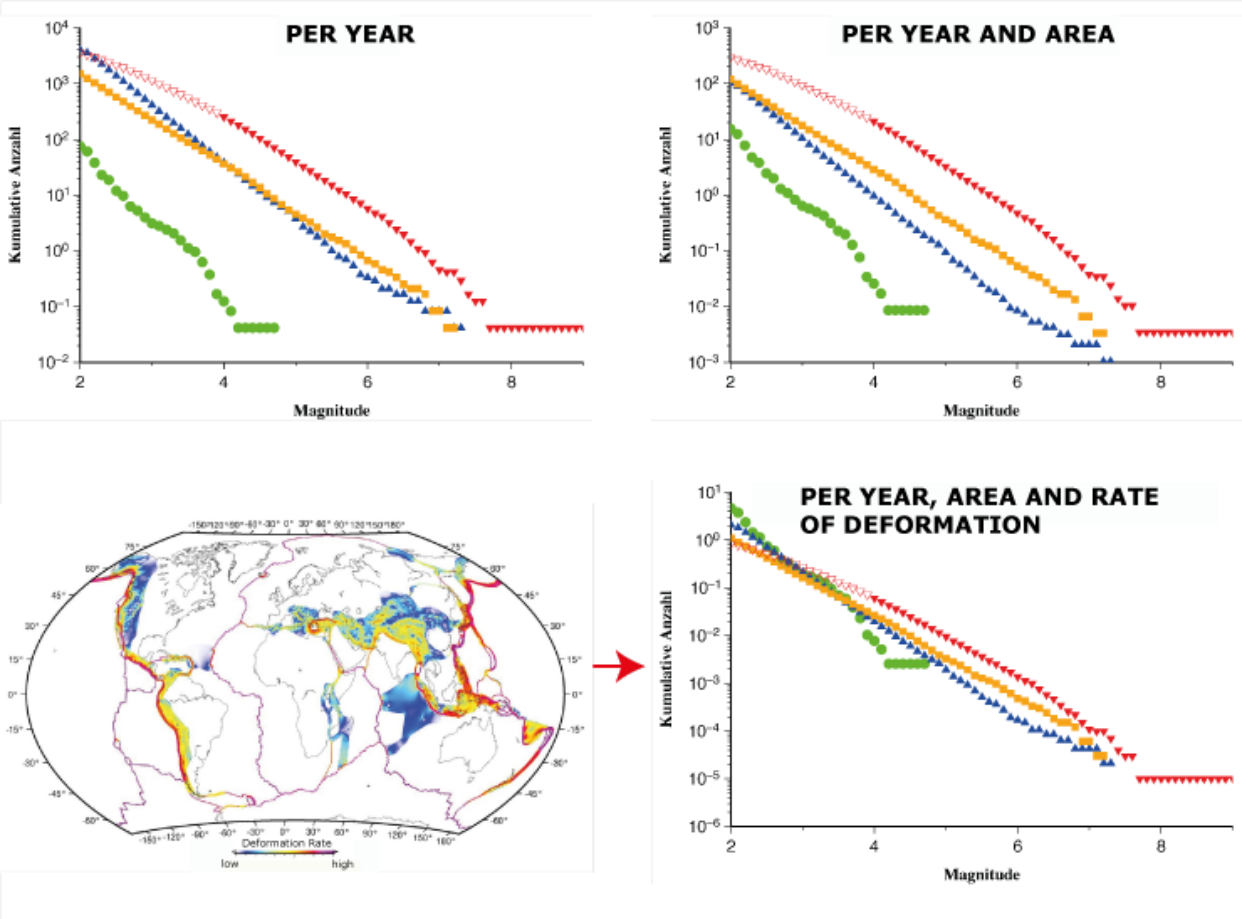

Figure 13: Top Left: Annualized rate of earthquakes as a function of magnitude for Switzerland (green), California (blue), onshore Japan (yellow) and offshore Japan (red). Top right: The same, but normalized to a unit areas; Bottom right: The same, but normalized also by unit deformation, as taken from the global earthquake rate model (Bottom left; From GEM: https://www.globalquakemodel.org/what/seismic-hazard/strain-rate-model/)

Strain as a proxy for earthquake rate and hazard can also be applied as a first order principle at the European scale and to a lesser extend also to Switzerland. Areas of high strain rate in Europe are also the areas of higher hazard; however, when going beyond first order the simple correlation partially breaks down. First of all, strain can be release not only seismically in earthquakes but also a-seismically through steady creep. The portioning between seismic and a-seismic is in many

areas poorly known and can change with space and time. In addition, how strain is distributed throughout a region and on which faults it is concentrated on is also often poorly known. In addition, we do not know well in what size earthquakes the strain may be released, in very rare larger ones or more frequent moderate ones? Finally, in places of low strain rate, such as Switzerland, the measured deformation using GNSS (Global Navigate Satellite System) day is just at the resolution limit.

3. Earthquake activity in Switzerland

3.1 The challenge of understanding past earthquakes

Seismic hazard assessment uses primarily the past seismicity and past earthquake recordings as the key to understand and forecast future seismicity and ground motions. Larger earthquakes are fortunately rare, even in tectonically active regions. Therefore, the further we can reach back into the past, and the more complete our record is, the better. However, seismic monitoring together with the resulting earthquake catalogue and ground motion records are constantly evolving, forming complex and heterogeneous space-time patterns, ultimately making the understanding of the past seismicity and seismic records of past events a formidable challenge and a science on its own. A good fraction of any PSHA is invested in compiling earthquake information from paleoseismology, historical seismology and instrumental recordings into a consistent data set.

The first seismometer in Switzerland was installed in 1907 in Davos (GR). Today, almost 150 instruments record earthquakes in near real-time, forming one of the densest and most modern seismic networks on earth (Figure 14). The number of stations, the quality of the sensors but also the processing approaches and the available algorithm and computers have evolved enormously in the past decades, a steady evolution with several jumps when a new generation of networks or technology was installed. To make this already complex story even more challenging, the information available in Switzerland needs to be combined with the information from neighbouring countries in a consistent way, for example ensuring that the magnitudes of earthquakes are computed with consistency through time and across borders.

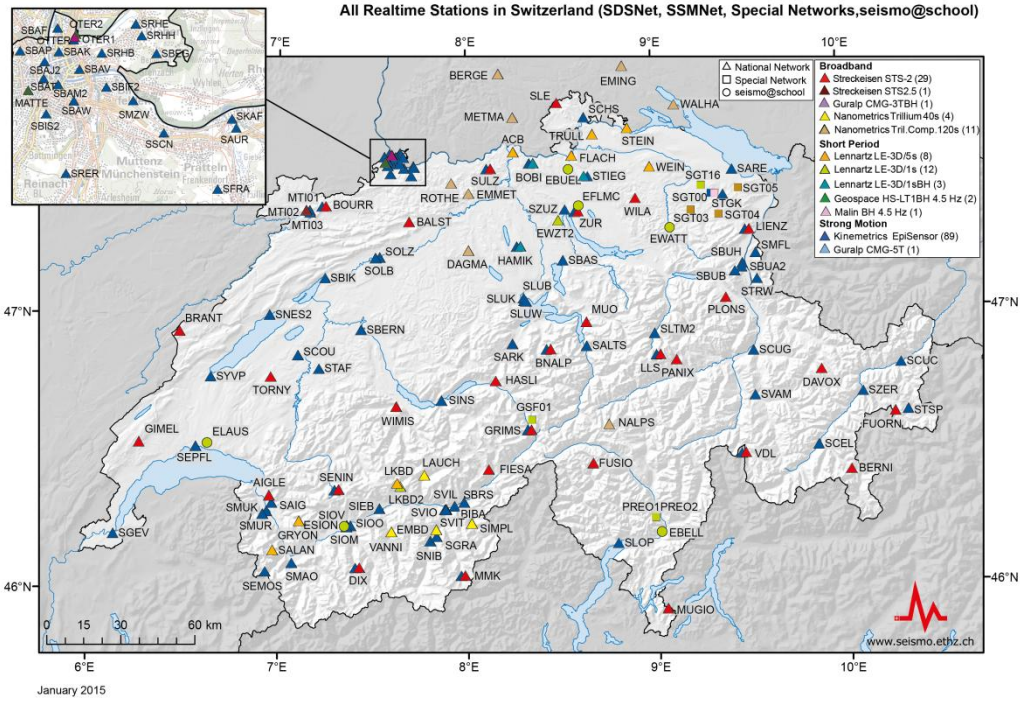

Figure 14: Map of Switzerland, showing the location of seismometers if different kind operated by the Swiss Seismological Service (Status January, 2015).

To illustrate the heterogeneity of the space time evolution of seismic recording, but also highlight the current ability to detect earthquakes in Switzerland, we show in Figure 15 an estimate of the magnitude of completeness with time (Diehl, personal communication, 2015). The assessment is based on the pick statistics of past earthquakes at each station, combined with a probabilistic model (PMC: Probabilistic Magnitude of Completeness; Schorlemmer and Wössner, 2008). Note

how in some areas of Switzerland, where the station density and station quality is the highest, magnitude 1,0 events can always be detected, while in other places, such as the Ticino, or Geneva, a magnitude 2.0 might be missed.

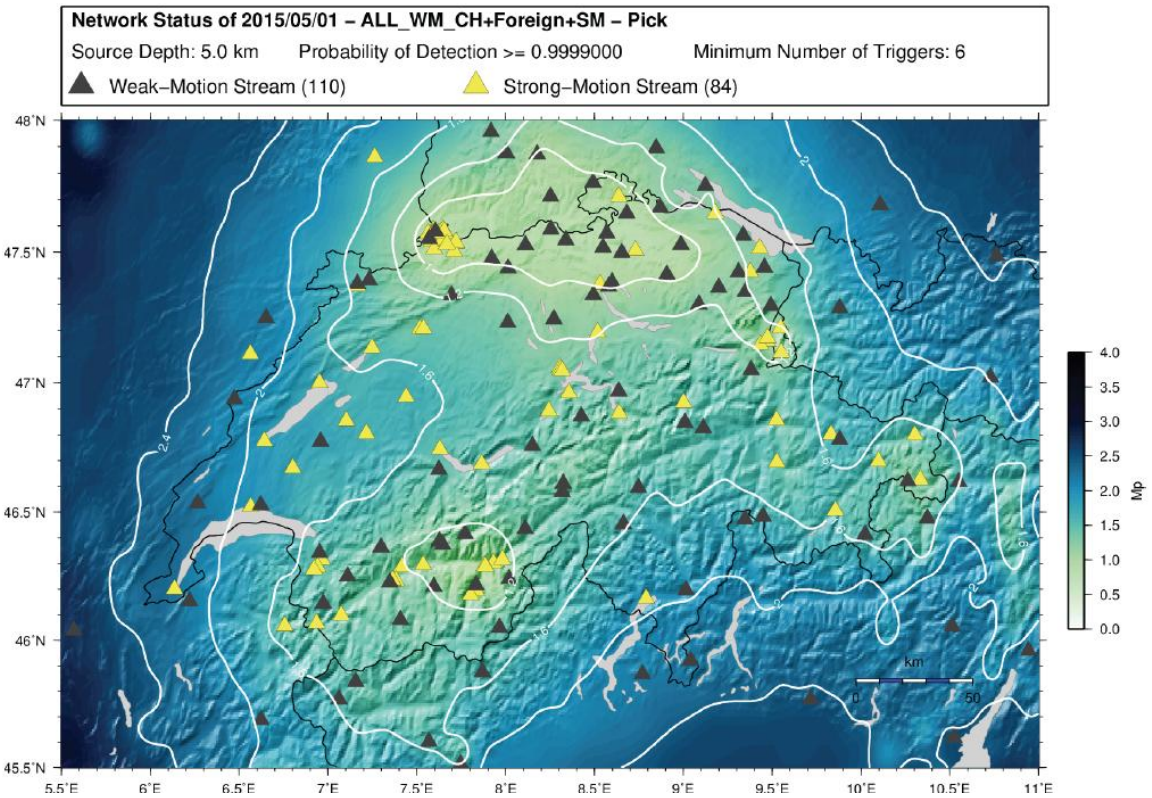

Figure 15: Map of Switzerland, colour-coded is the magnitude of complete recording. Above this magnitude, no earthquake should be missed by the network.

In addition to instrumental seismicity, historical records of felt events as well as damaging earthquakes are highly relevant, because they allow us to extend the seismic record back several hundred years. A systematic recording of felt reports on earthquakes started in Switzerland already in 1887, with the founding of the Earthquake Commission ("Erdbebenkommission") by ETH Geology Professor Albert Heim[4] (* 12. April 1849 in Zurich; † 31. August 1937). It was triggered by a magnitude 4.4 earthquake on May 2nd 1877 near Hinwil (ZH) that was strongly felt all the way to Olten and Lucerne, causing small cracks in buildings in the vicinity of the epicentre. A modern re-interpretation of this earthquake is shown in Figure 16, where the historically reported intensities are shown as well as a scenario ShakeMap that illustrates the level of shaking.

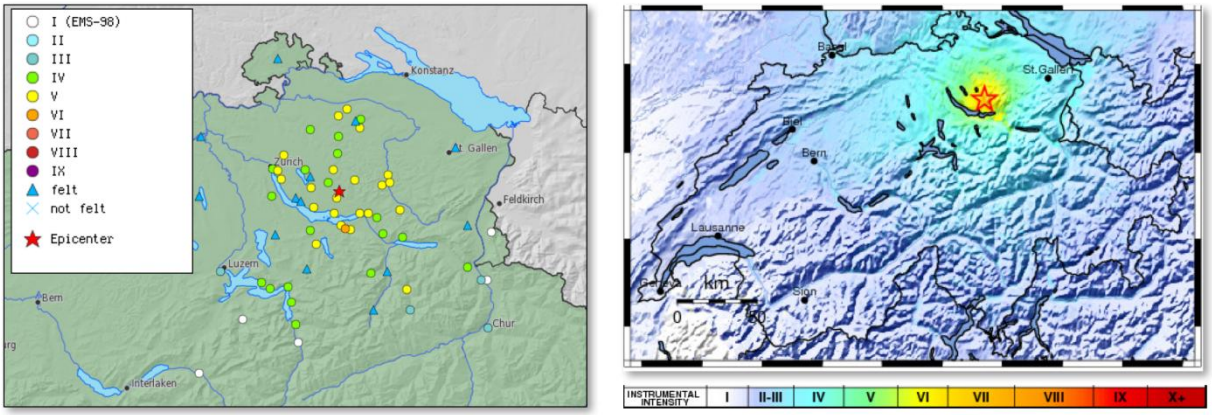

Figure 16: Intensity map (left) and ShakeMap (right) of the magnitude 4.4 earthquake near Hinwil (ZH) in 1877.

[4] https://de.wikipedia.org/wiki/Albert_Heim

Learning about earthquakes before 1878 is also possible, because earthquakes, particularly the stronger ones, are events which are noted by people, and historical reports on such events in newspaper, city records, monasteries, or even in family diaries exist through the centuries. The detective work of finding and deciphering these records, combining them with modern knowledge on earthquake effects, and eventually interpreting them so that the location and magnitude can be derived is the domain of macroseismic analysis, also called historical seismology.

The fact that collecting felt information from earthquakes pays off can be seen from one of the very first compilations of historical earthquakes, shown in Figure 17. After the earthquake commission had collected felt reports from earthquakes for 35 years, Prof. Früh[5] compiled in 1911 a map of these events, which is reproduced in Figure 17. The map is based on about 7,000 felt reports from 230 earthquakes. It is quite remarkable in the sense that many of the patterns that are seen in the current hazard map – the activity centres Valais and Grisons, can be clearly seen already. Prof. Früh detected also that earthquakes are more often felt at night, and speculated correctly that this is likely due to the fact that people perceive them better when it is quieter and people are lying down.

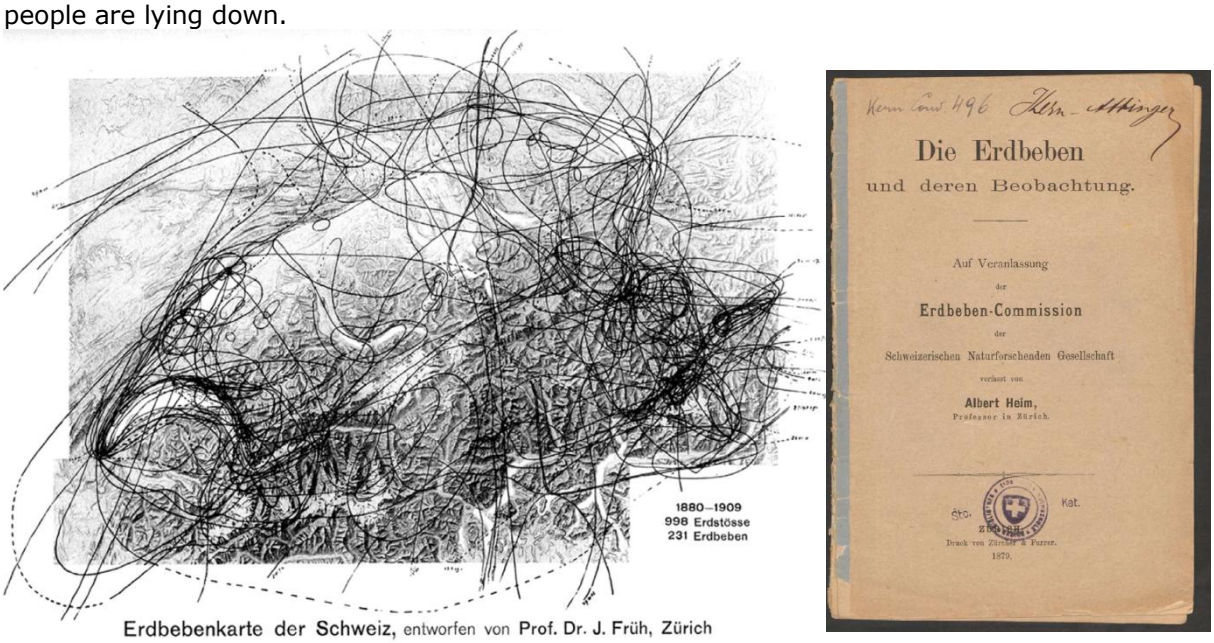

Figure 17: Left: Map of Switzerland, indicated are the felt areas based on 7000 felt areas from 230 earthquakes between 1878 and 1911. Right: Cover page of the first report by the Earthquake commission by Albert Heim, 1878.

3.2 Information on paleo-earthquakes in Switzerland

In regions with moderate seismicity and large intervals between strong earthquakes, paleoseismological archives that exceed the historical and instrumental timescale are needed to establish reliable estimates of earthquake recurrence for long return periods. Prehistoric earthquake investigations rely on paleoseismic archives registering the on-fault and the off-fault earthquake-induced effects. To extend the seismological catalogue for prehistoric timescales several geological archives that are susceptible to record seismic shaking-induced evidences have been studied. For this purpose, the following geological archives have been used: (1) lakes sediments, (2) active faults (3) rockfalls and (4) caves. All these methods have been used to show evidences for paleoearthquakes in Northern and Central Switzerland and are published in several peer-reviewed articles: Lemeille et al., 1999; Rodŕiguez-Pascua et al., 2000; Meghraoui, 2001; Becker et al., 2002; Monecke et al., 2004; Becker et al., 2005; Ferry et al., 2005; Monecke et al., 2006; Strasser et al., 2006; Strasser et al., 2013; Kremer et al., 2015; Reusch et al., 2016.

[5] http://www.library.ethz.ch/Ressourcen/Digitale-Bibliothek/Kurzportraets/Johann-Jakob-Frueh-1852-bis-1938

The major limitation of all these methods remains the dating of these evidences. In most cases, dating intervals are large (several hundreds of years), thus, interpreting events in different settings as simultaneous remains tentative. If within a dating interval, several possible earthquake-induced evidences are recorded, these events can either considered as simultaneous and thus, lead to define single and large events or as not simultaneous and thus, lead to define periods of intensified local and smaller events close to the studied sites.

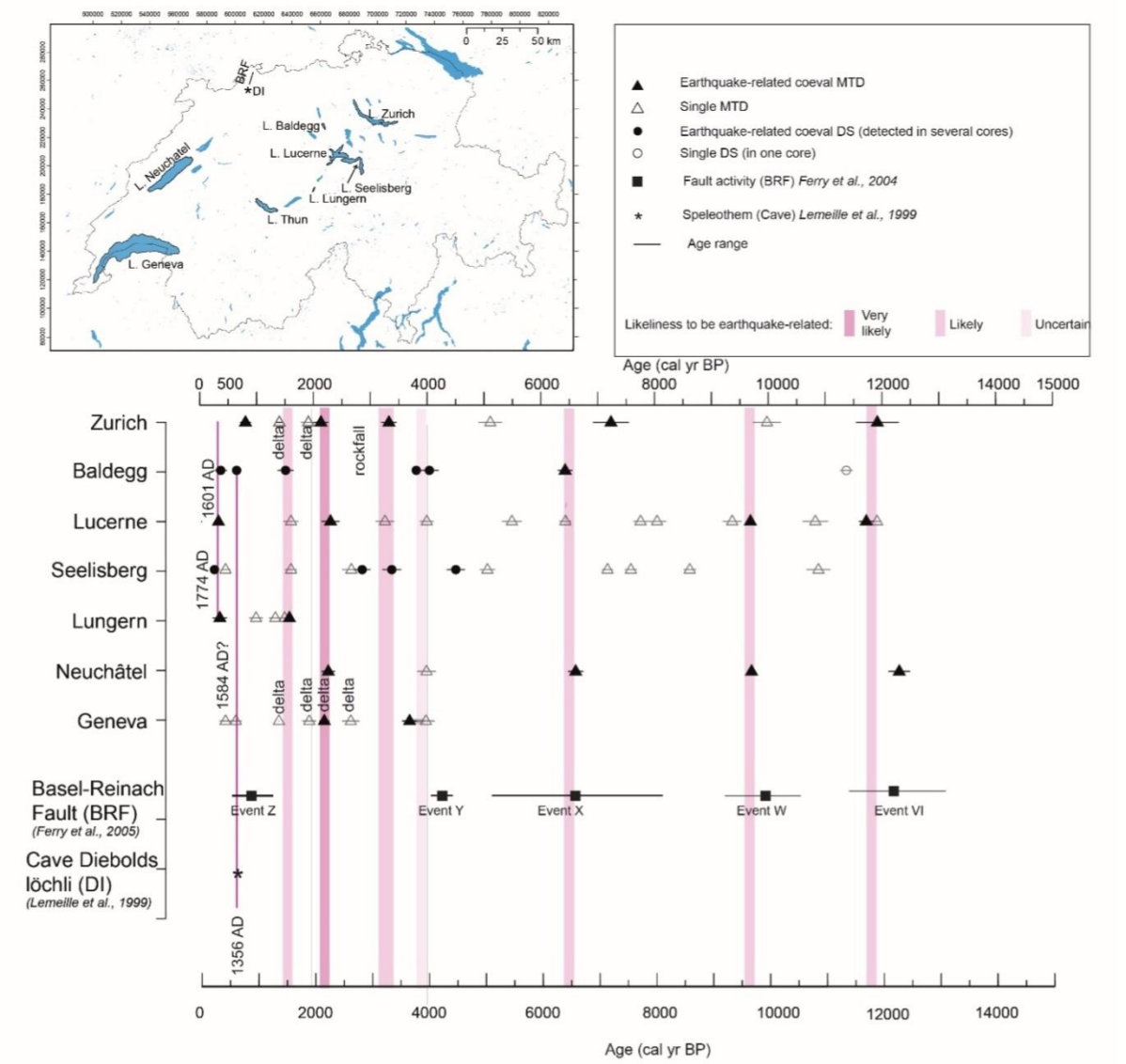

Figure 18: Map of Switzerland showing the different studied lakes, the location of the Basle Reinach Fault (BRF) and the Cave (Diebolds Löchli, DI). The most probable earthquake-induced effects are marked in black filled symbols, and time intervals characterized by either single large events or periods of intensified smaller and more local events are marked by pink vertical bars. "L.": Lake (Kremer et al., submitted to Quaternary Science Reviews)

In Switzerland most evidences are provided by lake records. In lakes, the occurrence of several coeval deposits imaged by seismic reflection data and ground-truthed by retrieving sediment cores are interpreted as caused by simultaneous slope failures within the lake basin(s) that are most probably triggered by earthquakes, when other mechanisms, such as storms, tsunamis, rockfalls, etc. can be excluded. Same interpretation is valuable for coeval sediment deformation observed in several sediment cores of different lake basin(s). This has been done by holistic understanding of environmental and sedimentary regime of the lakes. A new compilation based on re-dated event deposits and sediment deformation structures of previously published data has been submitted as Invited Research Article (Kremer et al., submitted) to Quaternary Science Reviews. This new compilation shows that during the past 14000 years, phases of "enhanced" seismicity and/or single large events are inferred at ~ 11900 cal yr BP (calibrated years before 1950), ~ 9700 cal yr BP

and at ~6500 cal yr BP. An increase in evidences is also noticed during the past 4000 years (~ 3900, ~3300, ~2200 and ~450 cal yr BP) (this is also true when the data when correcting the dataset for the length of the individual record). The last period at ~450 cal yr BP corresponds to the 1356 Basle, 1584 Aigle and 1601 Unterwalden earthquake-induced sublacustrine slope failures and sediment deformation. Comparing the dataset with the fault activity of the Basle-Reinach Fault from Ferry et al. (2004), that has been active during the 1356 Basle earthquake, at least 3 older periods (~ 11900, 9700 and 6500 cal yr BP) of similar geographical distribution of earthquake-induced evidences are observed. Thus, 1356 Basle-type earthquake might have been at the cause for this. However as dating intervals are large we are not able to be conclusive on that, but we get an idea on possibilities and maximum scenarios.

3.3 Information on historical and instrumental earthquake

Past earthquake activity in and around Switzerland has been documented interruptedly in a series of annual reports from 1879 until 1963 (*Jahresberichte des Schweizerischen Erdbebendienstes*). Three additional annual reports have been published for the years 1972-1974. These reports, together with historical records of earthquakes dating back to the 13th century, have been summarized by Pavoni (1977) and provide the basis for the first seismic hazard map of Switzerland (Sägesser and Mayer-Rosa 1978). With the advent of routine data processing by computer, the wealth of data acquired by the nationwide seismograph network has been regularly documented in bulletins with detailed lists of all recorded events (*Monthly Bulletin of the Swiss Seismological Service*). Since 1996, annual reports summarizing the seismic activity in Switzerland and surrounding regions have been published in the present form (Baer et al. 1997, 1999, 2001, 2003, 2005, 2007; Deichmann et al. 1998, 2000a, 2002, 2004, 2006, 2008, 2009, 2010, 2011, 2012; Diehl et al. 2013, 2014, 2015). A map of earthquake epicentres before 1974 is shown in Figure 19, a map all known events since 1975 with a magnitude Mw equal or greater than 2.0 is shown in Figure 20.

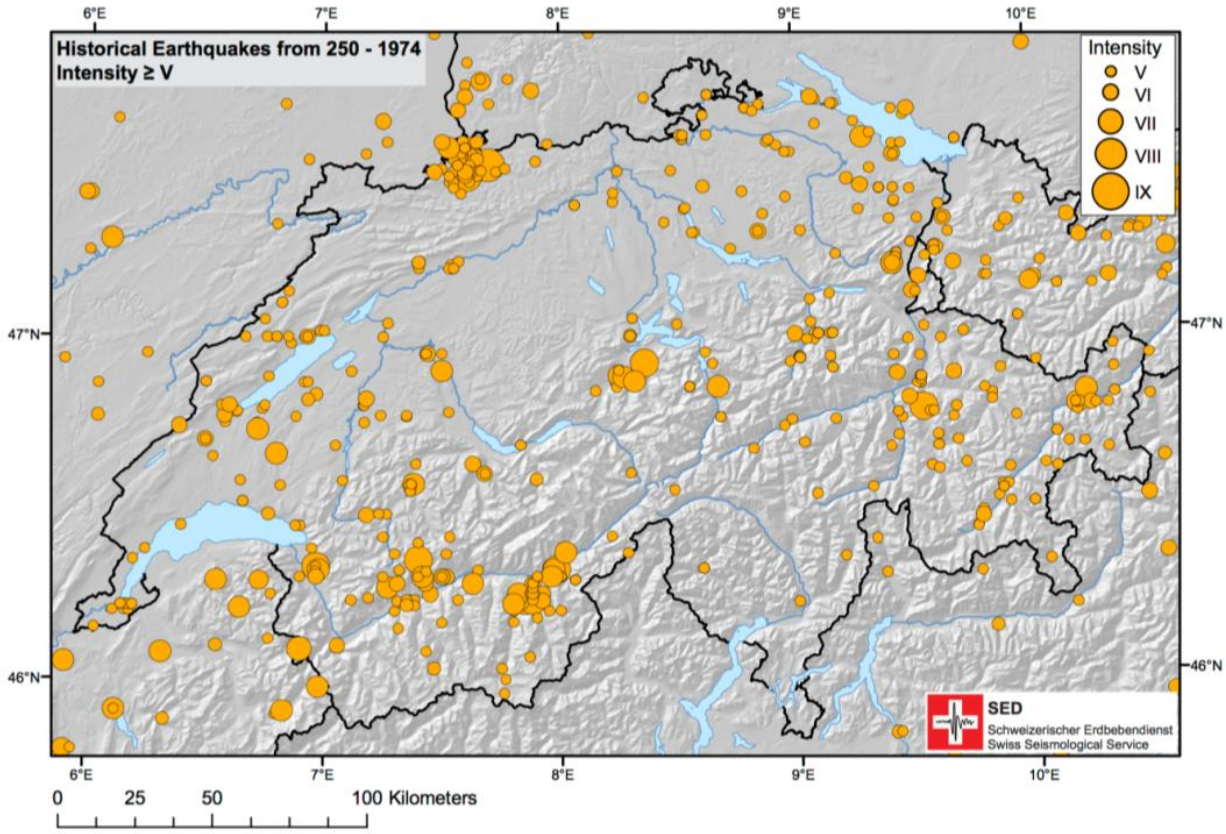

Figure 19: Map of Switzerland, shown are the epicentres of all known earthquakes from the ECOS09 database with macroseismic intensity >= V in the period 250 - 1974.

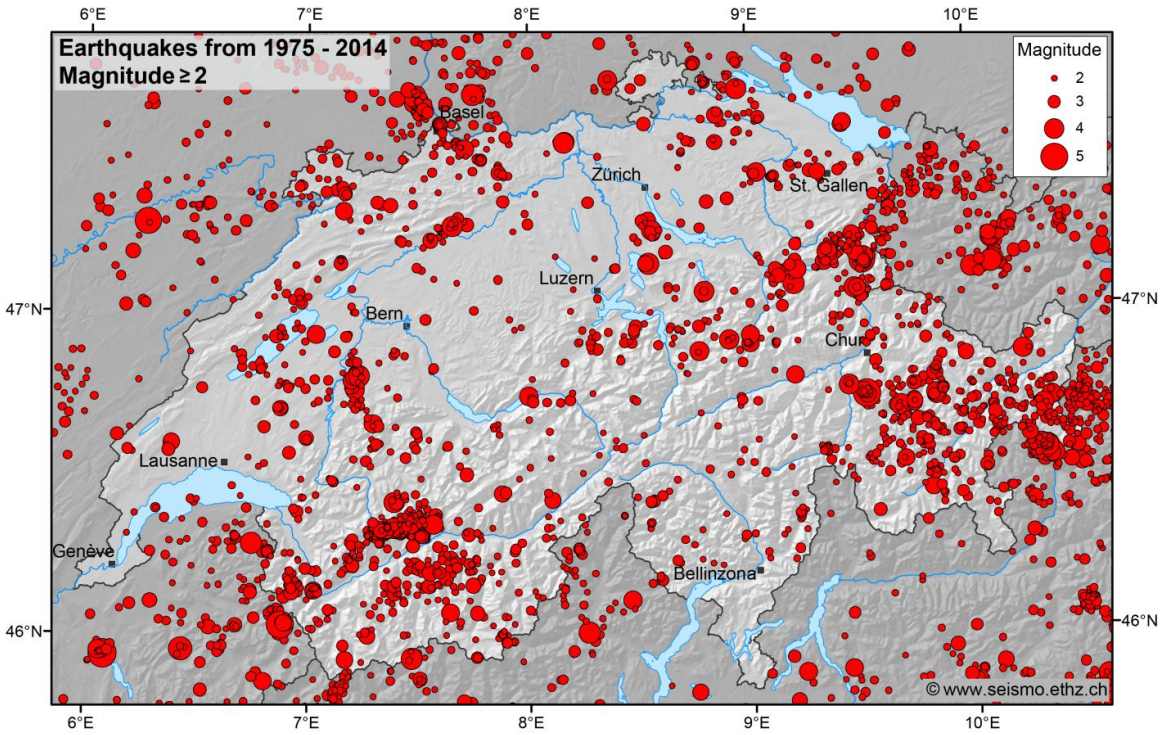

Figure 20: Map of Switzerland, shown are the epicentres of all known magnitude in the ECOS09 database with Mw >= 2.0 in the period 1974 - 2014.

In the course of reassessing the seismic hazards in Switzerland, a uniform earthquake catalogue was compiled in 2002 based on revised events of historical and instrumental periods (Fäh et al. 2003). The official seismic hazard map of Switzerland based on this catalogue was published in 2004 (Giardini et al. 2004; Wiemer et al. 2009). In 2009, the Earthquake Catalogue of Switzerland was revised (ECOS-09), as described in the next section.

Earthquakes recorded in the past decades are not only needed as an input for defining the rate of past earthquakes, together with calibrating the ground motion prediction models; they also serve as input for dozens of scientific studies. Many of these studies have relevance for PSHA. These studies cover a wide range of aspects of the recent seismicity of Switzerland and have been published in the scientific literature (for overviews and additional references see, e.g. Deichmann 1990; Pavoni and Roth 1990; Rüttener 1995; Rüttener at al. 1996; Pavoni et al. 1997; Deichmann et al. 2000b; Kastrup et al. 2004; Kastrup et al. 2007; Husen et al. 2007; Marschall et al. 2013, Singer et al. 2014).

3.4 ECOS09: a new earthquake catalogue for Switzerland

ECOS-09, the Earthquake Catalogue of Switzerland forming the basis of the seismogenic source model of SUIhaz2015. It is based on a multi-year project at the SED starting with the ECOS-02. It is a key step in the upgrade of the databases for earthquake hazard assessment for Switzerland and its neighbouring regions, and is documented fully in a number of publications and reports, listed below. In this section, we only provide a summary of the main elements.

ECOS-09 integrates in a consisted way the following basic information:

- the Macroseismic Earthquake Catalogue of Switzerland, with events from AD 250, revised and supplemented to 2008;
- yearly reports of the Swiss earthquake commission since 1879;
- earthquake locations of the instrumental networks of the SED since 1975;
- earthquake catalogue from neighbouring and international agencies.

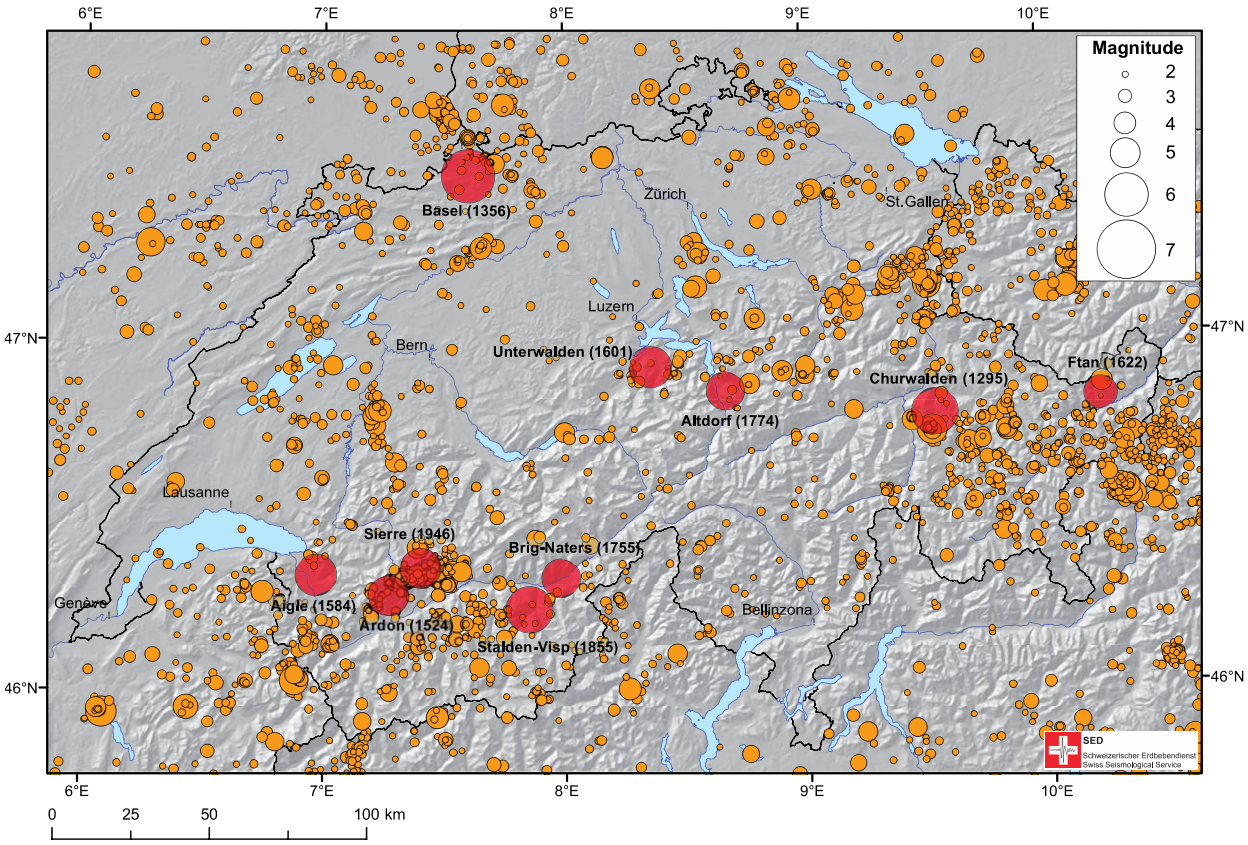

Figure 21: Epicentre map of Switzerland, shown are all earthquakes in the ECOS09 catalogue from magnitude Mw >= 2.0 since 1300. The 10 largest events are marked by red circles and listed in Table 2.

Depending on size and location of the events, the study of earthquakes before 1975 was undertaken in three steps: historical, macro-seismic and seismological.

Firstly, historical records were used to analyze known earthquakes. All available studies, catalogues of earthquakes and macroseismic databases from Switzerland and neighbouring countries were evaluated, matched, and stored in a database. Secondly, all earthquakes where significant effects were observed in Switzerland and its surroundings were re-evaluated and the associated intensity fields were determined. Intensity points for foreign locations were imported from available compilations. Earthquakes without significant damage (if known) were systematically reviewed for the years following 1878, while those from the period preceding 1878 were processed according to the availability of historical documents. At the same time Swiss earthquake seismograms from the main European earthquake observatories since the beginning of the 20th Century were analyzed to derive a relationship between magnitude and macroseismic fields. Thirdly, all earthquakes with sufficient seismologically determined intensity observations were evaluated: their strength was determined using a regression procedure to derive source parameters (epicentre, depth, epicentral intensity, maximum intensity and magnitude).

Location	Magnitude	Intensity	Date	Lat	Long
Basle (BS)	6.6	IX	18.10.1356	47.47	7.6
Churwalden (GR)	6.2	VIII	03.09.1295	46.78	9.54
Stalden-Visp (VS)	6.2	VIII	25.07.1855	46.23	7.85
Aigle (VD)	5.9	VIII	11.03.1584	46.33	6.97
Unterwalden (NW)	5.9	VIII	18.09.1601	46.92	8.36
Ardon (VS)	5.8	VII	04.1524	46.27	7.27
Sierre (VS)	5.8	VIII	25.01.1946	46.35	7.4
Brig-Naters (VS)	5.7	VIII	09.12.1755	46.32	7.98
Altdorf (UR)	5.7	VII	10.09.1774	46.85	8.67
Ftan (GR)	5.4	VII	03.08.1622	46.82	10.23

Table 2: The ten largest main shocks known to have occurred in Switzerland. Some were followed by strong aftershocks.

For the earthquakes after 1975, earthquake locations from the instrumental network of SED were reviewed. Due to the continual upgrade of the instrumental network over the years, the accuracy of locations has also become more reliable. In order to complete the catalogue, particularly in the border regions of Switzerland, it was supplemented with the available earthquake catalogues from neighbouring countries and international agencies. Existing since the mid-1980s, digital waveforms were used to calibrate different magnitude scales of other seismological observatories with the Richter magnitude (M_L scale) of the SED. In addition, for all earthquakes a homogeneous magnitude estimate, based on the moment magnitude (Mw), was derived.

The earthquake catalogue ECOS-09 and the associated macroseismic database is available online via the website of the Swiss Seismological Service. The data covers a region that includes the area of the Swiss national map at a scale of 1:500 000 plus a buffer zone of 30 kilometres (Swiss coordinates (km): 460-882 / 20-350; Geographical coordinates approx.: 5.6-11.1E / 45.4 - 48.3N). The expected completeness of ECOS is regional and temporal and varies for different earthquake intensities.

The ECOS09 catalogue creation is documented in a major report (Fäh et al., 2011) along with 12 appendices, as listed below and available from the SED web; they are not repeated as part of this report. ECOS-09 is also part of the European earthquake catalogues SHEEC 1000-1899 [6] (Stucchi et al., 2012) and SHEEC 1900-2006[7] (Grünthal & Wahlström, 2012). The work on ECOS-09 is based on a large number of studies which are given in the reference list in Chapter 3.6. ECOS-09 and its documentation is available on the SED website, the key references are given at the end of this chapter.

Main ECOS-09 reports:

– Fäh, D., Giardini, D., Kästli, P., Deichmann, N., Gisler, M., Schwarz-Zanetti, G., Alvarez-Rubio, S., Sellami, S., Edwards, B., Allmann, B., Bethmann, F., Wössner, J., Gassner-Stamm, G., Fritsche, S., Eberhard, D., 2011. ECOS-09 Earthquake Catalogue of Switzerland Release 2011 Report and Database. Public catalogue, 17. 4. 2011. Swiss Seismological Service ETH Zurich, Report SED/RISK/R/001/20110417. PDF

[6] http://www.emidius.eu/SHEEC/sheec_1000_1899.html

[7] http://www.gfz-potsdam.de/sektion/erdbebengeFährdung-und-spannungsfeld/daten-produkte-dienste/sheec/sheec-1900-2006/

The appendices to the main report are:

- **Appendix A:** ECOS – Earthquake Catalogue of Switzerland ECOS. Report to PEGASOS, Version 31.03.2002; ECOS Catalogue Version 31.03.2002. Swiss Seismological Service, ETH Zürich, 2002, 95.p. PDF
- **Appendix B:** Grundlagen des Makroseismischen Erdbebenkatalogs der Schweiz, Band 1, 1000–1680. Gabriela Schwarz-Zanetti and Donat Fäh. Herausgegeben vom Schweizerischen Erdbebendienst, Zürich. VDF, 2011.
- **Appendix C:** Grundlagen des Makroseismischen Erdbebenkatalogs der Schweiz, Band 2, 1681–1878. Monika Gisler and Donat Fäh. Herausgegeben vom Schweizerischen Erdbebendienst, Zürich. VDF, 2011.
- **Appendix D:** Calibration of historical earthquakes for the earthquake catalogue of Switzerland ECOS-09. Sonia Álvarez-Rubio, Philipp Kästli, Donat Fäh, Souad Sellami. Internal report of the Swiss Seismological Service, March 2010. PDF
- **Appendix E:** The BOXER method applied to the determination of earthquake parameters from macroseismic data – Verification of the calibration of historical earthquakes in the Earthquake Catalogue of Switzerland (ECOS2009). Sonia Álvarez-Rubio and Donat Fäh. Internal report of the Swiss Seismological Service, December 2009. PDF
- **Appendix F:** Catalogue for the period 1964 to 1974. Souad Sellami. Internal report of the Swiss Seismological Service, March 2010. PDF
- **Appendix G:** Documentation of the Swiss instrumental earthquake catalog, 1975-2008. Nicholas Deichmann and Souad Sellami. Internal report of the Swiss Seismological Service, December 2009. PDF
- **Appendix H:** Swiss instrumental local magnitudes. Nicholas Deichmann. Internal report of the Swiss Seismological Service, December 2009.PDF
- **Appendix I:** Determination of MW and calibration of ML (SED) – MW regression. Bettina Allmann, Benjamin Edwards, Falko Bethmann, and Nicholas Deichmann. Internal report of the Swiss Seismological Service, March 2010. PDF
- **Appendix J:** Merging catalogues with focus on the period 1975-2008. Jochen Wössner, David Eberhard, Philipp Kästli. Internal report of the Swiss Seismological Service, March, 2010. PDF
- **Appendix K:** Conversion of local magnitude from foreign catalogs to SED local magnitude Nicholas Deichmann. Internal report of the Swiss Seismological Service, December 2009. PDF
- **Appendix L:** ECOS-09 Catalogue Format. Philipp Kästli. Internal report of the Swiss Seismological Service, March 2010. PDF

3.5 References

Becker, A., et al., 2002. Palaeoseismicity studies on end-Pleistocene and Holocene lake deposits around Basle, Switzerland. Geophysical Journal International 149, 659-678.

Becker, A., Ferry, M., Monecke, K., Schnellmann, M., Giardini, D., 2005. Multiarchive paleoseismic record of late Pleistocene and Holocene strong earthquakes in Switzerland. Tectonophysics 400, 153-177.

Ferry, M., Meghraoui, M., Delouis, B., Giardini, D., 2005. Evidence for Holocene palaeoseismicity along the Basel—Reinach active normal fault (Switzerland): a seismic source for the 1356 earthquake in the Upper Rhine graben. Geophysical Journal International 160, 554-572.

Kremer et al., Lake sediment records as earthquake catlogue : limitations and perscpectives, submitted to Quaternary Science Reviews

Kremer, K., Hilbe, M., Simpson, G., Decrouy, L., Wildi, W., Girardclos, S., 2015. Reconstructing 4000 years of mass movement and tsunami history in a deep peri-Alpine lake (Lake Geneva, France-Switzerland). Sedimentology 62, 1305-1327.

Lemeille, F., Cushing, M., Carbon, D., Grellet, B., Bitterli, T., Flehoc, C., Innocent, C., 1999. Co-seismic ruptures and deformations recorded by speleothems in the epicentral zone of the Basel earthquake. Geodinamica Acta 12, 179-191.

Meghraoui, M., 2001. Active normal faulting in the Upper Rhine Graben and paleoseismic identification of the 1356 Basel earthquake (vol 293, pg 2070, 2001). Science 294, 57-57.

Monecke, K., Anselmetti, F.S., Becker, A., Sturm, M., Giardini, D., 2004. The record of historic earthquakes in lake sediments of Central Switzerland. Tectonophysics 394, 21-40.

Monecke, K., Anselmetti, F.S., Becker, A., Schnellmann, M., Sturm, M., Giardini, D., 2006. Earthquake-induced deformation structures in lake deposits: A late Pleistocene to holocene paleoseismic record for central Switzerland. Eclogae Geologicae Helvetiae 99, 343-362.

Reusch, A., Moernaut, J., Anselmetti, F.S., Strasser, M., 2016. Sediment mobilization deposits from episodic subsurface fluid flow—A new tool to reveal long-term earthquake records? Geology 44, 243-246.

Rodŕiguez-Pascua, M.A., Calvo, J.P., De Vicente, G., Gómez-Gras, D., 2000. Soft-sediment deformation structures interpreted as seismites in lacustrine sediments of the Prebetic Zone, SE Spain, and their potential use as indicators of earthquake magnitudes during the Late Miocene. Sedimentary Geology 135, 117-135.

Strasser, M., Anselmetti, F.S., Fäh, D., Giardini, D., Schnellmann, M., 2006. Magnitudes and source areas of large prehistoric northern Alpine earthquakes revealed by slope failures in lakes. Geology 34, 1005-1008.

Strasser, M., Monecke, K., Schnellmann, M., Anselmetti, F.S., 2013. Lake sediments as natural seismographs: A compiled record of Late Quaternary earthquakes in Central Switzerland and its implication for Alpine deformation. Sedimentology 60, 319-341.

3.6 References ECOS-09

Álvarez-Rubio, S., P. Kästli, D. Fäh, S. Sellami and D. Giardini, 2011. Parameterization of historical earthquakes in Switzerland. Journal of Seismology, 16, 1–24, DOI 10.1007/s10950-011-9245-8.

Bernardi, F., Braunmiller J. and D. Giardini (2005). Seismic Moment from Regional Surface-Wave Amplitudes: Applications to Digital and Analog Seismograms, Bull. Seism. Soc. Am., 95, pp. 408–418.

Braunmiller, J., Deichmann, N., Giardini, D., Wiemer, S. and the SED Magnitude Working Group (2005). Homogeneous Moment-Magnitude Calibration in Switzerland, Bull. Seism. Soc. Am., 95, pp. 58–74.

Breu, M. (2004). Ein Erdbeben verschwindet aus der Statistik. ethlife, 21.9.2004.

Cara, M., W. Brüstle, M. Gisler, P. Kästli, C. Sira, C. Weihermüller, J. Lambert (2005). Transfrontier macroseismic observations of the Ml=5.4 earthquake of February 22, 2003 at Rambervillers, France. Journal of Seismology 9/3, 317–328.

Edwards, B., B. Allmann, D. Fäh and J. Clinton, 2010. Automatic computation of moment magnitudes for small earthquakes and the scaling of local to moment magnitude, Geophysical Journal International 183, 407-420.

Fäh, D., D. Giardini, F. Bay, F. Bernardi, J. Braunmiller, N. Deichmann, M. Furrer, L. Gantner, M. Gisler, D. Isenegger, M.-J. Jimenez, P. Kästli, R. Koglin, V. Masciadri, M. Rutz, C. Scheidegger, R. Schibler, D. Schorlemmer, G. Schwarz-Zanetti, S. Steimen, S. Sellami, S. Wiemer, J. Wössner (2003). Earthquake Catalogue of Switzerland (ECOS) and the related macroseismic database. Eclogae geol. Helv. – Swiss J. Geosciences 96, 219–236.

Fäh, D., M. Gisler, B. Jaggi, P. Kästli, T. Lutz, V. Masciadri, C. Matt, D. Mayer-Rosa, D. Rippmann, G. Schwarz-Zanetti, J. Tauber, T. Wenk (2009). The 1356 Basel earthquake: an interdisciplinary revision. Geophys. J. Int. 178, 351–374.

Fäh, D., M. Gisler, D. Giardini (2004). Historische Erdbeben in der Schweiz. Bundesamt für Bevölkerungsschutz (ed.). KGS/PBC/PCP Forum, Bern, 18–28.

Fäh, D., S. Steimen, I. Oprsal, J. Ripperger, J. Wössner, R. Schatzmann, P. Kästli, I. Spottke, P. Huggenberger (2006). The earthquake of 250 A.D. in Augusta Raurica, a real event with a 3D site-effect? Journal of Seismology 10/4, 459–477; DOI: 10.1007/s10950-006-9031-1.

Fritsche, S. (2008). Large Historical Earthquakes in Switzerland. Multidisciplinary Studies on Damage Fields and Site Effects, Diss. ETH Zürich, No. 17710, Zürich.

Fritsche, S., D. Fäh, D. Giardini (2005). Damage Fields and Site-Effects. Investigations on the 1855 Earthquake in Switzerland. Proceedings of the international conference of the 250th Anniversary of the 1755 Lisbon Earthquake, Lisbon, 340–346.

Fritsche, S., D. Fäh, M. Gisler, D. Giardini (2006). Reconstructing the damage field of the 1855 earthquake in Switzerland: historical investigations on a well-documented event. Geophys. J. Int. 166, 719–731.

Fritsche, S., D. Fäh (2009). The 1946 Magnitude 6.1 Earthquake in the Valais: Site-Effects as Contributor to the Damage. Eclogae geol. Helv. – Swiss J. Geosciences 102, 423-439; DOI 10.1007/s00015-009-1340-2.

Fritsche, S., D. Fäh, B. Steiner, D. Giardini (2009). Damage Field and Site Effect: Multidisciplinary Studies of the 1964 Earthquake Series in Central Switzerland. Nat. Hazards 48, 203–227.

Fritsche, S., Fäh, D., Schwarz-Zanetti, G. (2012). Historical intensity VIII earthquakes along the Rhone valley (Valais, Switzerland): primary and secondary effects. Swiss J Geosci, 105(1), 1–18, DOI 10.1007/s00015-012-0095-3.

Gisler, M. (2003). Historical Seismology in Switzerland: Reflections on Issues and Insights. Environment and History 9/2, 215–237.

Gisler, M. (2005). Optimism and Theodicy. Perception of the Lisbon Earthquake in Protestant Switzerland. Studies on Voltaire and the Eighteenth Century (SVEC), 247–264.

Gisler, M. (2006). Die Anfänge der systematischen Erdbebenforschung in der Schweiz und der Beitrag der Innerschweiz. Der Geschichtsfreund 159, Altdorf, 29–38.

Gisler, M. (2007). Erdbeben in der Schweiz im ersten Jahrtausend – Evidenzen und Grenzen. In: G.H. Waldherr, A. Smolka (ed.). Antike Erdbeben im alpinen und zirkumalpinen Raum. Befunde und Probleme in archäologischer, historischer und seismologischer Sicht/Earthquakes in Antiquity in the Alpine and Circum-alpine Region. Findings and Problems from an Archaeological, Historical and Seismological Viewpoint, Stuttgart: Franz Steiner, 133–153 (= Geographica Historica 24).

Gisler, M. (2007). Göttliche Natur? Formationen im Erdbebendiskurs der Schweiz des 18. Jahrhunderts, Zürich: Chronos.

Gisler, M., D. Fäh (2011). Grundlagen des Makroseismischen Erdbebenkatalogs der Schweiz. Bd. 2: 1681–1878, Zürich: vdf.

Gisler, M., D. Fäh, D. Giardini (ed.) (2008). Nachbeben. Eine Geschichte der Erdbeben in der Schweiz. Bern: Haupt.

Gisler, M., D. Fäh, N. Deichmann (2004). The Valais Earthquake of December 9, 1755. Eclogae geol. Helv. – Swiss J. Geosciences 97, 411–422.

Gisler, M., D. Fäh, P. Kästli (2004). Historical Seismicity in Central Switzerland. Eclogae geol. Helv. – Swiss J. Geosciences 97, 221–236.

Gisler, M., D. Fäh, R. Schibler (2003). Two significant earthquakes in the Rhine Valley at the end of the 18th century: The events of December 6, 1795 and April 20, 1796. Eclogae geol. Helv. – Swiss J. Geosciences 96, 357–366.

Gisler, M., D. Fäh, R. Schibler (2004). Revising macroseismic data in Switzerland: The December 20, 1720 earthquake in the region of Lake Constance. Journal of Seismology 8/2, 179–192.

Gisler, M., D. Fäh, V. Masciadri (2007). "Terrae motus factus est": Earthquakes in Switzerland before A.D. 1000. A Critical Approach. Natural Hazards 43, 63–79.

Gisler, M., D. Giardini (2007). Erdbeben in Europa – eine kleine Kulturgeschichte. Vierteljahresschrift der Naturforschenden Gesellschaft in Zürich 152/4, 101–110.

Gisler, M., G. Schwarz-Zanetti, D. Fäh, V. Masciadri, D. Rippmann (2006). The 1356 Basel Earthquake from a Historical Standpoint: Old Wine in New Wineskins? Proceedings of the First European Conference on Earthquake Engineering and Seismology (ECEES), Genève, 1–5 (CD ROM).

Gisler, M., J. Kozák, J. Vanek (2008). The 1855 Visp (Switzerland) Earthquake: A Milestone in Macroseismic Methodology? In: J. Fréchet, M. Meghraoui, M. Stucchi (ed.). Historical Seismology: Interdisciplinary Studies of Past and Recent Earthquakes, Heidelberg (= Modern Approaches in Solid Earth Sciences 2), 225–241.

Gisler, M., M. Weidmann, D. Fäh (2005). Erdbeben in Graubünden. Vergangenheit, Gegenwart, Zukunft, Chur: Desertina, 135 p.

Gisler; M. (2006). Die Anfänge der systematischen Erdbebenforschung in der Schweiz und der Beitrag der Innerschweiz. Der Geschichtsfreund 159, 29–38.

Goertz-Allmann, B.P., B. Edwards, F. Bethmann, N. Deichmann, J. Clinton, D. Fäh, and D. Giardini, 2011. A new empirical magnitude scaling relation for Switzerland. Bull. Seism. Soc. Am., 101:3088-3095; doi:10.1785/0120100291.

Grolimund, R., S. Sellami, N. Deichmann, D. Fäh, und Swiss Seismological Service (2014), Earthquakes in Switzerland and Surroundings 1964–1974. An Interdisciplinary Approach to a 'Dark Age' of Earthquake Documentation. ETH-Zurich, doi:10.3929/ethz-a-010222529. [online] Available from: http://dx.doi.org/10.3929/ethz-a-010222529

Mayer-Rosa, D., G. Schwarz-Zanetti (2004). On historical earthquakes in Switzerland: summary of compilations and investigations. Annals of Geophysics 47/2–3.

Schwarz-Zanetti G., D. Fäh, R. Schibler, V. Masciadri, P. Kästli, D. Giardini (2003). The earthquake in Unterwalden and the rockslide from the Bürgenstock into Lake Lucerne on September 18, 1601. Eclogae geol. Helv. – Swiss J. Geosciences 96, 441–450.

Schwarz-Zanetti G., N. Deichmann, D. Fäh, V. Masciadri, J. Goll (2004). The Earthquake in Churwalden (CH) of September 3, 1295. Eclogae Geol. Helv. – Swiss J. Geosciences 97, 255–264.

Schwarz-Zanetti, G., D. Fäh (2011). Grundlagen des Makroseismischen Erdbebenkatalogs der Schweiz. Bd. 1: 1000–1680, Zürich: vdf.

Schwarz-Zanetti, G., D. Fäh, V. Masciadri, P. Kästli (2007). The Churwalden (CH) Earthquake of September 1295. Fauna and Flora in the Middle Ages. Investigations into the Medieval Environment and its Impact on Human Mind, Beihefte zur Mediävistik, Bd. 8, 249–266.

Schwarz-Zanetti, G., M. Gisler, D. Fäh, P. Kästli (2006). Interdisziplinäre Rekonstruktion des Basler Erdbebens von 1356 an der ETHZ. Ein Werkstattbericht. In: Moyen Age – Medioevo – Temp medieval, Zeitschrift des Schweizerischen Burgenvereins 11/3, 140–144.

Schwarz-Zanetti, G., N. Deichmann, D. Fäh, V. Masciadri, J. Goll (2004). The earthquake in Churwalden (CH) of September 3, 1295. Eclogae geol. Helv. – Swiss J. Geosciences 97, 255–264.

Schwarz-Zanetti, G., N. Deichmann, D. Fäh, V. Masciadri, P. Kästli, M. Schnellmann, M.-J. Jimenez (2006). Das Unterwaldner Erdbeben vom 18. September 1601. Der Geschichtsfreund 159, 11–28.

Schwarz-Zanetti, G., V. Masciadri, D. Fäh, P. Kästli (2007). The false Basel earthquake of May 12, 1021. Journal of Seismology 12/1, 125–129.

Swiss Seismological Service (2002). ECOS – Earthquake Catalog of Switzerland. ECOS Report to PEGASOS, Version 31. 3. 2002, SED: Zürich.

Würsten, F. (2003). Der neue Erdbebenkatalog der Schweiz: Ein kritischer Blick in vergangene Zeiten. ethlife, 9.4.2003.

4. Seismic source model for the 2015 Swiss seismic hazard

4.1 Motivation and overview

A seismogenic source model - also referred to as an earthquake rupture forecast - integrates all potential sources of information about location, size and faulting style of potential future earthquake into a probabilistic model. The national PSHA model of 2004 (Wiemer et al., 2009a) is the natural starting point of the analysis for the 2015 update. No major problems or inconsistencies of the 2004 model are known to us. When building the 2015 model, we started nevertheless with round of discussions inside a dedicated working group of experts within the SED, but also with many external stakeholders, on the deficits and limitations of the 2004 model. We were also able to benefit from the experience of the PEGASOS and PRP projects, and the SHARE-model building experience. These discussions and reflections helped us to define a list of priorities for the update of the 2004 model: Integrate new data collected in the past years into the model, for example 10 years of seismicity data. Integrate especially the new and newly harmonized ECOS09 (Chapter 3).

- Review the tectonic zonation approaches, especially considering alternative approaches for zone-less or smooth seismicity models.
- Consider if additional information of Earth's crust deformation, on faults, paleo-earthquake or the seismotectonic context has emerged that warrants changes to the zonation.
- Improve the representation of uncertainties in all parts of the seismogenic source model; while still maintaining, however, a reasonable model size and model complexity.
- Review the assessment of the maximum possible earthquakes, using also more data driven approaches.
- Support GMPE's that differentiate by faulting styles, as well as by extended ruptures (rather than point sources).

These priorities lead to a number of actions which are described in detail in this chapter. The work on seismotectonic zonation, and the ultimate decisions on model setup and model weights was performed by a working group of ETH scientist: Prof. Stefan Wiemer (Lead); Dr. Stefan Hiemer (main analyst); Dr. Jochen Wössner (now RMS); Dr. Laurentiu Danciu; Prof. E. Kissling; Prof. D. Giardini and Prof. Donat Fäh.

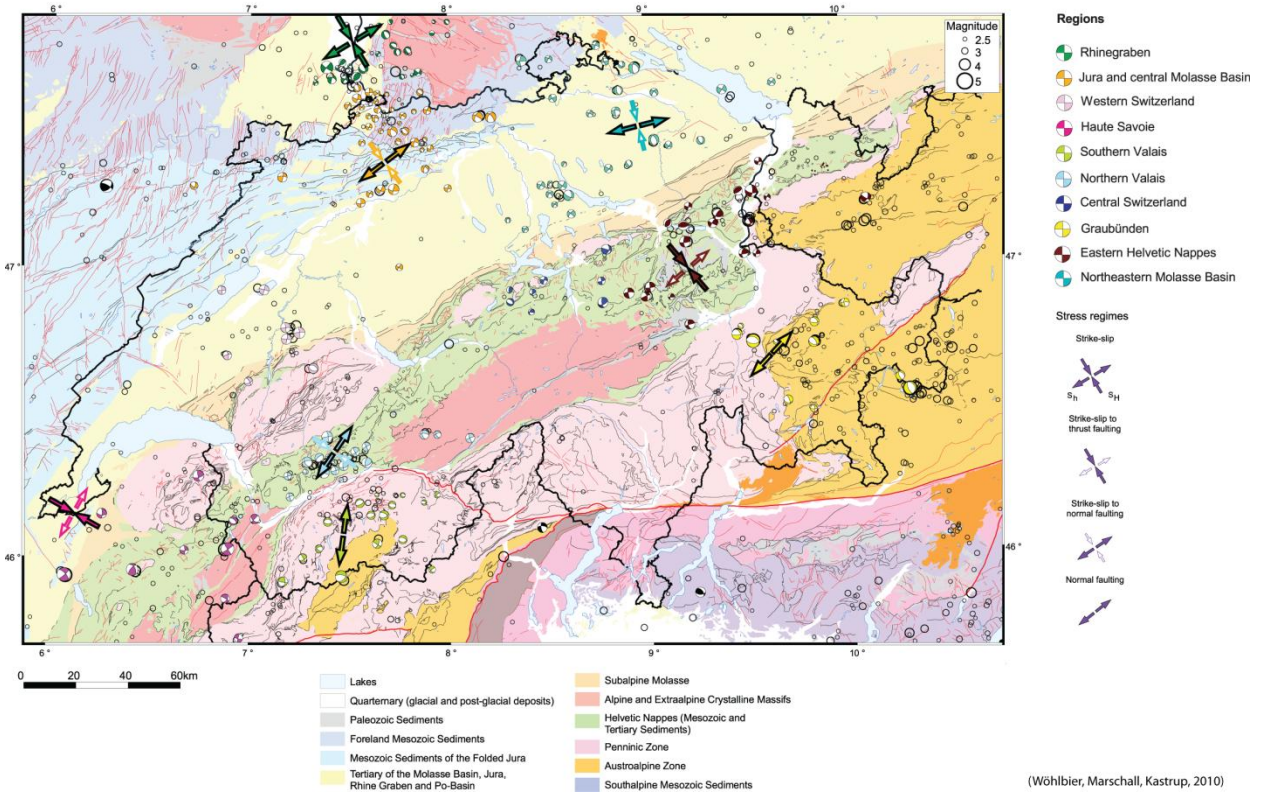

Figure 22: Seismotectonic map of Switzerland and surrounding region. Shown are the major tectonic/geological units differentiated by colour. Shown are also the focal mechanism based on stress tensor inversion, and epicentres of all earthquakes >= 2.5 from 1975 – 2009 (from Woehlbier et al., 2010)

4.2 Seismotectonic context

The tectonics of Switzerland are strongly affected by the Alpine orogeny, as already discussed in generic terms in Chapter 2. Switzerland is located inside the Tertiary collision zone between the African and the Eurasian plates. In terms of overall crustal strain rate and seismicity rate, Switzerland is located in the transition zones between areas of high seismic activity (Greece, Italy) and areas of low seismic activity (Northern Europe). The country can be subdivided into three main tectonic units (Figure 22): (1) The Alpine belt in the south, (2) the Jura in the north, and (3) the Molasse basin in between (e.g., Truempy 1985; Hsu¨ 1995; Pavoni et al. 1997; Kastrup et al., 2004). Moderate seismic activity occurs continuously beneath the Alpine belt and north of the Alps (particularly in the Molasse basin, Rhine Graben and Jura, e.g. Deichmann et al., 2000; Baer et al., 2005; Diehl et al., 2013, Marshall et al., 2013).

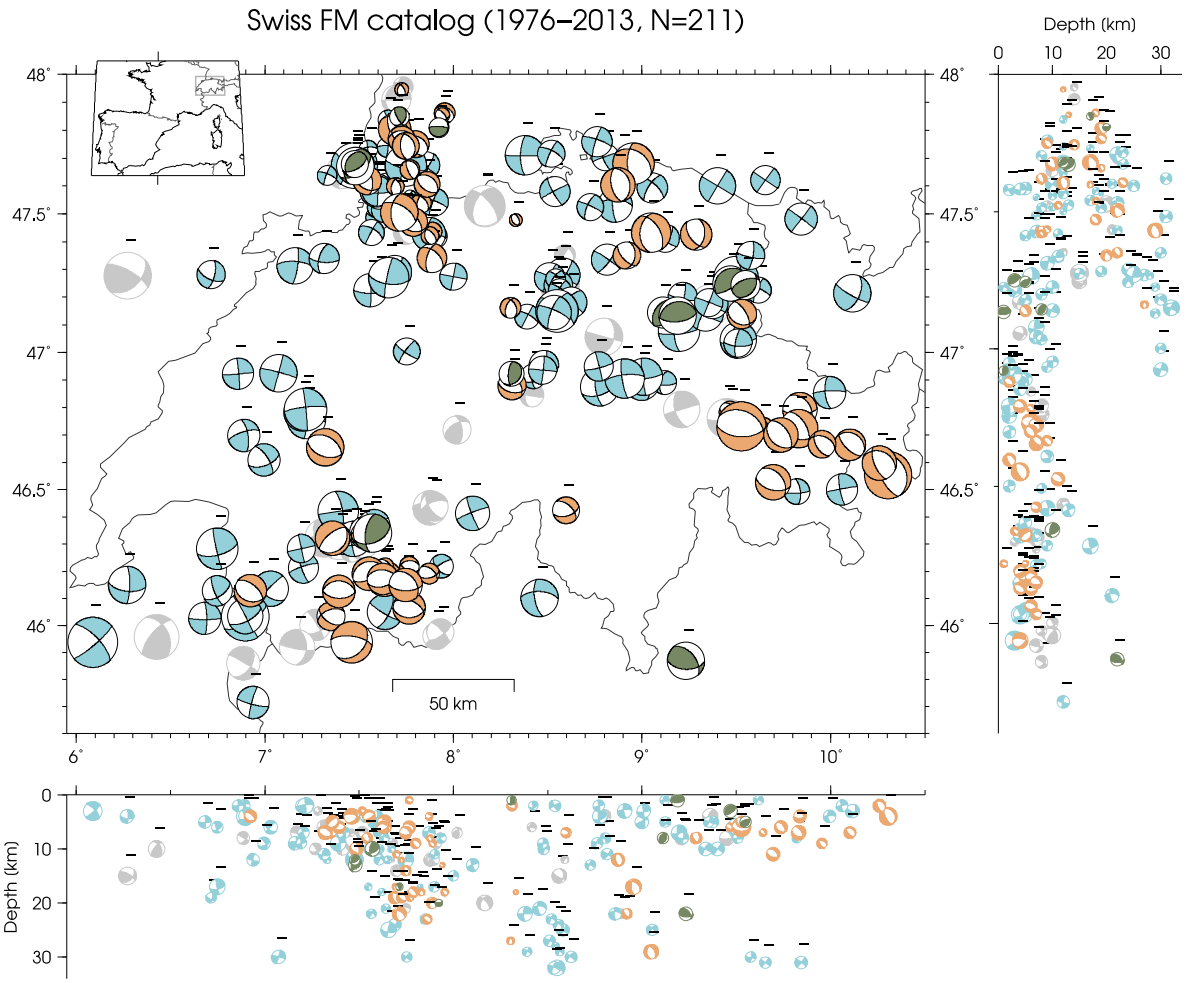

Figure 23: Focal mechanisms in Switzerland and surroundings for 211 events in the period 1976 - 2013. The colour coding indicates preferred faulting style (red: normal faulting; blue: strike-slip; green: thrust faulting).

A systematic analysis of to date 211 focal mechanisms in Switzerland and its surroundings shows (Figure 23) that the style of faulting and the orientation of the stress field vary significantly, both along strike and across the Alps (e.g. Kastrup et al., 2004; Reinecker et al., 2010; Marschall et al., 2013). Strike-slip mechanisms with a normal faulting component dominate in the Northern Alpine Foreland. The Upper Rhine Graben shows a complex mixture of very few thrust faulting events, a larger component of normal faulting mechanism along the borders of and to the south of the graben structure, and a majority of strike-slip faulting. Along the Northern Alpine Front, some shallow thrust mechanisms are observed. In contrast, the Penninic domains of the Valais and Grisons are characterized by normal faulting with extensional axes at a high angle to the strike of the Alps. In the Northern Foreland, the stress tensor reflects the large-scale convergence of Africa and continental Europe, with a maximum horizontal stress axis that rotates from east to west so as to remain roughly perpendicular to the Alpine arc. Thus, the least compressive stress in the Northern Foreland is roughly parallel to the Alpine front. Across the Alps, the variation in azimuth of the least compressive stress is defined by a progressive counterclockwise rotation of about 45° from the Foreland in the north across the Helvetic domain to the Penninic domains in the southern Valais. This apparent rotation of the stress field can be explained by the superposition of a local uniaxial deviatoric tension on the large-scale regional stress. The tensile nature and orientation of this local stress component is consistent with the spreading stress expected from lateral density changes due to the crustal root beneath the Alps (Kastrup et al., 2004).

Slab rollback orogeny in the Alps and its influence on the Molasse basing has recently been highlighted as an important mechanism that controls the evolution of the Alps, the seismotectonic en-

vironment as well as the much of the contemporary seismicity (Schlunegger and Kissling, 2015). Singer et al. (2014) illustrate how Alpine lithosphere slab rollback causes lower crustal seismicity in northern foreland. In addition, post-glacial rebound may add additional strain. However, there are to date no calibrated numerical models of alpine orogeny which link seismicity and orogeny with the resolution required for seismogenic zonation.

4.3 Datasets of relevance for deriving the seismogenic zonation

Seismogenic zonation needs to consider all potential sources of information which may be able to constrain the location, the rate and the maximum size of future earthquakes. For every kind of information, an important question is always how much the information about the past can be extrapolated into the future, an assessment of the stationarity of the underlying processes. For SUIhaz2015, we considered specifically the following data sets:

Paleoseismic, historical and instrumental earthquake catalogues. Past earthquakes remain, in our assessment, the primary informational source on future earthquakes. Our study is primarily based on the Earthquake Catalogue of Switzerland (ECOS-09), Fäh et al., 2011). For all details on the catalogue, please refer to Chapter 3.

Active fault information, including reliable slip rate estimates, persists in being, in our evaluation, too sparse in Switzerland to be used as part of a nation-wide seismogenic fault model. The situation in that respect is largely unchanged from the one in the 2004 model (Wiemer et al., 2009). The SHARE model and The European Database of Seismogenic Faults (EDSF8) positions a single fault in Switzerland, in the western Valais, with an estimated slip range of 0.1 – 1 mm, but states that these values are "unknown values assumed from geodynamic constraints". The geometrical constraints and maximum possible earthquake on this fault is also poor and largely constrained from seismological data. Because of these uncertainties and because adding a single fault is in our assessment potentially more biasing than beneficial, we did not explicitly consider active fault zones as seismogenic sources. However, paleoseismic information on recurrence of Basle does add an important constraint to the model, although it is used in our model more in a regional sense instead of being attributed to a single fault (i.e., the Reinach fault).

Geodetic data: Houilie et al. (2015) and Villiger et al., (2014) use geodetic and seismic datasets to check whether the surface deformation and the seismic activity are in agreement in terms of moment release and stress/strain orientations within the territory of Switzerland. They report that for most of the country, the stress released through earthquakes is consistent in amount and orientation with the lithosphere deformation measured by the Global Navigation Satellite System (GNSS). The surface strain rate ($<5.0\ 10^{-8}$ /yr) fits well with an average stress rate release of ~2.0 1011 Nm/yr, however, displays limited agreement with long-term (and deep) deformation. For three regions, Houlie et al., (2015) find seismic activity and surface deformation to be not in agreement. In the Basle area, deep seismicity exists while surface deformation is absent. This situation contrasts with what they found in the Ticino and the Swiss Jura, where the seismic activity is absent but surface deformation is detected ($\sim 2\ 10^{-8}$ /yr). This geodetic evidence will be used qualitatively as input to the seismogenic zonation as well as to the assessment of M_{max}. However, given the limited spatial resolution, the unknown role of a-seismic information and the general uncertainty of converting geodetic information into a seismicity forecast, especially in areas of moderate and distributed seismicity, geodetic data currently offers in our assessment only a limited constraint on seismogenic zonation in Switzerland.

Earthquake focal mechanisms are important to derive information about the style of deformation in the brittle layers of the Earth's crust. The spatial distribution of style of faulting is an important input parameter for many ground motion prediction equations. The focal mechanism earth-

[8] diss.rm.ingv.it/share-edsf/SHARE_WP3.2_Database.html

quake catalogue considered in this study contains 211 events in Switzerland and surrounding regions in the time period of 1976 -2013 (Fig. 3, update of the study by Kastrup et al., 2004; Marschall et al., 2013, N. Deichmann, pers. comm.). This database contains only focal mechanisms with focal depth information and published first-motions or waveform fits.

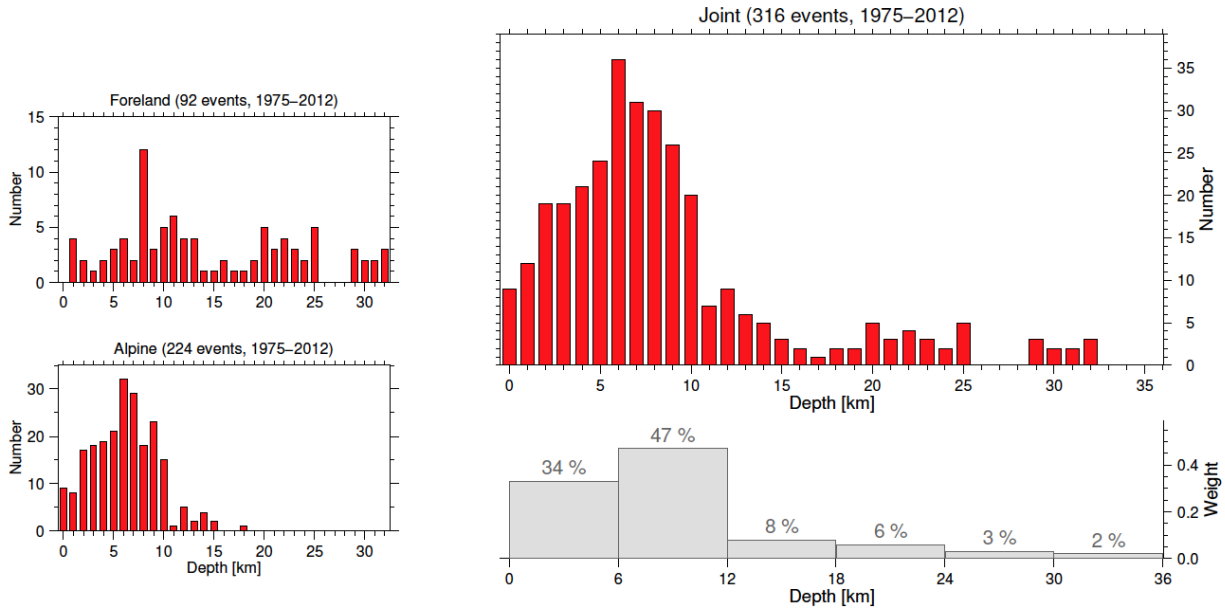

Figure 24: Left: depth distribution for Foreland and Alpine region, respectively. (b) and (c) are geographical subsets of the entire dataset (a) based on a straight WSW-ENE trending line (coordinates: from 46.35N/6.0E to 47.85N/11.0E). Percentages in top panels indicate relative weight between shallow (< 6 km) and deep part of the distribution. Percentages in bottom panels correspond to values used for the construction of the earthquake source model.

Hypocentral depth distributions of seismicity are an important input factor for PSHA, especially in Switzerland where seismicity is much deeper below the Foreland than in the Alps (Figure 24). We used and extended results from more specific studies (Deichmann et al., 2000; Husen et al., 2003), because the depth of many events in the ECOS-09 catalogue is poorly constrained (Fäh et al., 2011). In general, reliable hypocenter information can only be derived from earthquakes recorded with modern instrumental data, although depth does also play a role in estimating the macroseismic parameters of historical events. We considered the earthquakes recorded by the SED in Switzerland and surrounding regions over the time period 1975 -2012. The earthquakes induced by the geothermal project in Basle (e.g. Haring et al., 2008; Deichmann and Giardini, 2009) have been removed, but the data set was not declustered (N. Deichmann, pers. comm.).

The difficulty with focal depth statistics is to find selection criteria that minimize the poorly quantified uncertainty without introducing a systematic depth dependent bias. For this purpose, we followed the discussion in Deichmann et al. (2000) on selection criteria and applied the following values: minimum magnitude = 2.5, maximum gap = 180◦, minimum epicentral distance = 25 km, minimum number of P-or S-wave arrivals used for location = 9, and maximum root mean square of travel-time residuals = 0.4 seconds. These criteria result into a total number of 316 events to be used for estimating depth distributions, and shown in Figure 24. This dataset is subsequently used as the input for deriving a depth distribution for hazard calculations in the following way:

– for alpine and foreland shallow seismicity, we sum up all seismicity between 0 to 9km and place it on every point source at 4.5km.

– for deep sources we sum up all seismicity within 9 to the Moho depth Figure 25; the depth value of alpine sources is set to 13.50km, whereas for foreland deep sources two values are set to 13.5 and 22.5Km.

Note that extended rupture sourced from magnitude 5.5 are treated differently, as explained in Chapter 6.

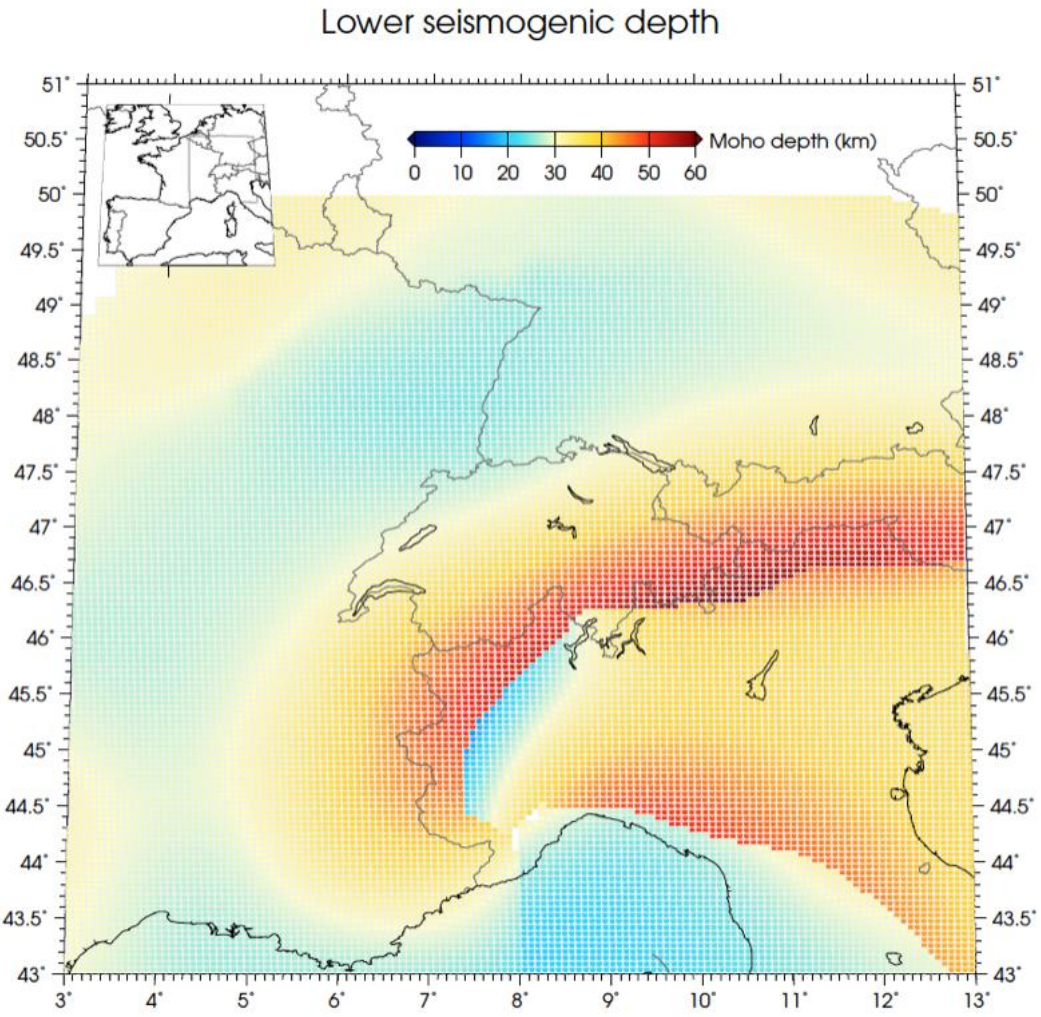

Figure 25: Map of the western Alpine region, Colour-coded is the depth of the Moho discontinuity. The crustal model is based combining controlled source seismology and local earthquake tomography (Wagner et al., 2012, c.f. their Figure 8a)

To constrain the lower end of the seismogenic zone, we use as an additional constraint the improved knowledge on the depth the Mohohorvic discontinuity that separates the brittle Earth crust from the more ductile upper Mantle. Using information from combining controlled source seismology and local earthquake tomography, Wagner et al. (2012) were able to constrain the depth of this layer with improved precious and spatial coverage (Figure 25). We use this information in our hazard assessment to limit both the earthquake hypocenters but also the maximum depth extents of extended ruptures.

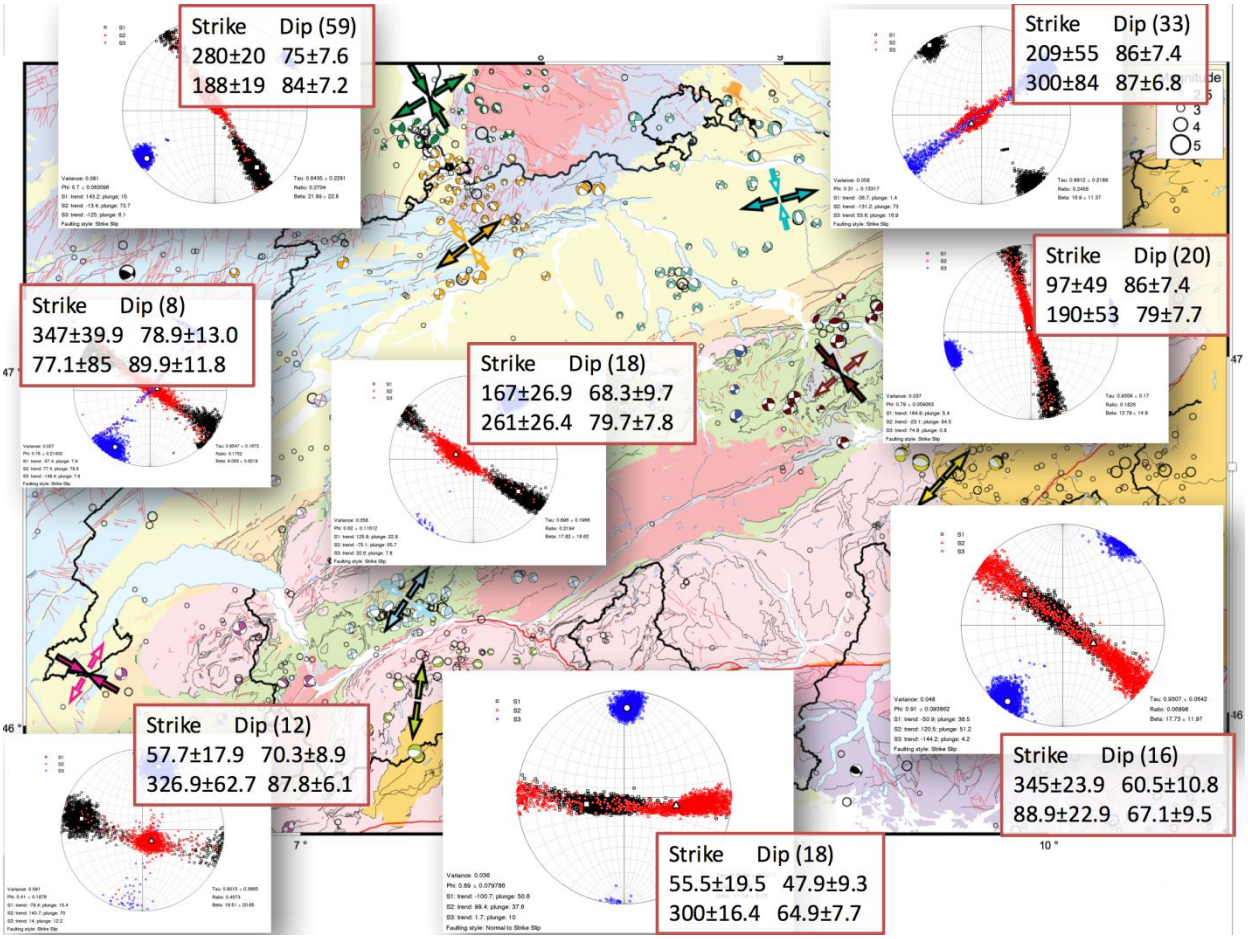

Figure 26: Results of the stress tensor inversions in eight sub-regions, using Michael's (1984) approach. The inversion is based on the reported focal mechanism shown in Figure 23. Blue dots represent the likely orientation of the first principle stress axis (S1), red the intermediate one (S2) and black minimal one (S3).

4.4 Style of faulting and preferred rupture orientations

Defining the faulting styles and preferred rupture orientations is a requirement for hazard computations for two reasons: 1) Some depend on faulting style if the GMPE is used (Chapter 5); 2) extended ruptures should be oriented preferentially in agreement with the existing stress regime and past rupture orientations.

The analysis of earthquake focal mechanisms in order to derive information about the style of deformation and the state of stress in the brittle layers of the Earth's crust is a well-established procedure. Kastrup et al. (2004) and Marschall et al. (2013) indicated the footprint of the large-scale stress field across Switzerland, and we are additionally interested in the local features of the style of faulting. Therefore, we used the spatial clustering and faulting style characteristics to further separate regions and infer the local stress tensor in these areas. Based on the defined spatial separation, we (1) estimate the orientation of the stress tensor axes and define the uncertainties with a bootstrap approach; then (2) calculate the optimally oriented style of faulting for these stress tensors resulting in two possible orientations for each region due to the focal mechanism ambiguity. We use the assessment of Deichmann (1992) to define preferred orientation for strike and dip. We defined the probability of the style of faulting based on the relative amount of focal mechanisms.

The principal components of the stress tensor and their uncertainties are calculated with the approach of Michael (1984, 1987). The inversion assumes that the stress field inverted from the set of focal mechanisms is constant, i.e. can be homogeneously describe with one tensor. The slip

events are assumed to be independent and the magnitude of the tangential traction on the fault plane is normalized, thus the traction is similar on all fault planes. The inversion minimizes the misfit angle between the observed slip direction of each fault plane solution and the assumed tangential traction, i.e. shear stress, on each fault pane, and results in the principal stress axis and their relative amplitude. Uncertainties in these results are calculated using a bootstrap approach.

Stress tensors were calculated for 12 areas (Figure 26), the Swabian Alb (Germany) and the Po Plain (Italy) were not included in the inversion. Between 8 and 59 focal mechanisms are available for the stress tensor inversion and thus the sampling in some regions is at the lower limit for determining the stress tensor from the focal mechanisms alone, in particular for the six regions with less than 20 available events. In addition, the stress field needs to be sampled from a variety of focal mechanisms in order to obtain reliable results (Hardebeck and Hauksson 2001). We used the original set of focal mechanisms to estimate the stress tensor and then a set of 1000 bootstrap samples, drawn from the focal mechanisms in each region, to estimate the uncertainty of the inversion, resulting in the principle stress axes. For each of the inverted sets of principal stress axis, we then calculated again the optimally oriented fault planes (strike, dip, rake) that is the stress tenor. The resulting optimal orientation of fault planes (Table 1) are in agreement with inferences of previous analyses (Kastrup et al., 2004, Marschall et al., 2013) and the seismotectonic map of Switzerland (Figure 22).

ID	N	FP 1			FP 2			Style			%	
		strike 1	dip 1	rake 1	strike 2	dip 2	rake 2	SS	TF	NF	FP 1	FP 2
2	59	280±23	75±8	-174±96	188±20	84±7	-15±35	50	10	40	70	30
6	11	203±36	85±10	-2±73	294±119	88±8	-175±80	80	10	10	50	50
7	8	347±39	79±13	0±87	77±81	90±12	-169±79	60	20	20	50	50
8	12	58±18	70±8	-178±170	327±65	88±6	-20±50	40	30	30	50	50
9	18	56±19	48±9	-145±46	301±16	65±8	-48±23	30	10	60	50	50
10	21	167±25	68±10	-11±52	261±25	80±8	-158±42	70	10	20	70	30
11	9	94±30	65±14	-178±160	3±146	88±6	-25±96	40	30	30	50	50
12	16	345±23	61±10	-27±40	89±21	67±9	-148±33	20	10	70	50	50
13	20	97±50	77±8	169±113	190±54	79±8	13±93	40	40	20	50	50
14	33	210±59	86±8	-3±97	300±94	87±8	-176±99	60	10	30	50	50

Table 1: Fault plane (FP) orientations optimally oriented to the obtained stress tensor of the set of focal mechanisms in each region. Listed are the identifier of the region (ID), number of events (N), strike, dip and rake of the two planes, and the assumed average percentage of faulting styles (SS = strike-slip, NF = normal faulting, TF = thrust faulting). Rake is not further considered. The percentage of earthquakes occurring on the two fault planes is defined in the last two columns.

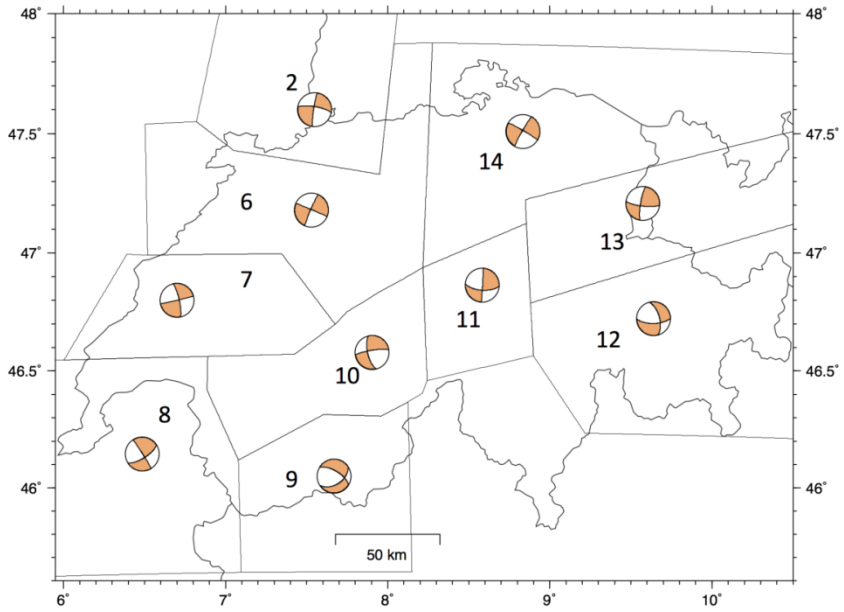

Figure 27: Regionalization of the preferred faulting style. See Table 2 for actual orientations.

Data preparation: declustering the ECOS catalogue

As a first step in most seismic hazard studies, the potentially biasing effect of temporal and spatial clustering of earthquakes is reduced through a process called 'declustering'. Declustering is the process of separating an earthquake catalogue into two parts: earthquakes that are independent of each other, and earthquakes that depend on each other, such as aftershocks, foreshocks, or multiplets (e.g., van Stiphout et al., 2011). The subset of independent events is expected to be time-independent, that is to follow a stationary Poisson process, which is a requirement for most hazard-related studies (Reiter, 1990; Frankel, 1995; Giardini et al., 1999). To understand the potential bias of clustering, consider that a recent large earthquake may have hundreds of large aftershocks in the weeks, month and years which follow. If we use this very rich aftershock sequence to estimate the long-term, average seismic activity, we would severely overestimate this rate, because our measurement is taken in an anomalously active period. Reducing this potential bias is the purpose of 'declustering'.

There is no unique way to decluster a seismicity, but fortunately the impact of declustering on the hazard is minor in the absence of major earthquake sequences (Wiemer at al., 2009b). In SUI-Haz15 we applied, as was done in the 2004 hazard, the space-time window approach by Gardner and Knopoff (1974) using window parameters optimized for Central Europe by Gruenthal (pers. comm., see also Wiemer et al., 2009b). In its original form, the ECOS-09 catalogue has a total of 52'399 entries (Fäh et al., 2011, Chapter 3). We separated the 21654 classified mainshocks from the time-dependent part of the catalogue. We also removed all entries that are known quarry blasts, indeed, earthquakes have no location or magnitude specified whose occurrences have not been classified as certain. Accordingly, our declustered ECOS-09 catalogue lists 20'998 events. Note that the envelope of all area source zones of model SEIS contains 12'513 events and the smoothed seismicity bounding box of SUIhaz15 features 7'954 events.

Data preparation: estimating the completeness

The magnitude of completeness, Mc, is the magnitude threshold below which only a fraction (i.e. less than 100%) of earthquakes in this magnitude bin are detected by the network (e.g. Wiemer and Wyss, 2000; Wössner and Wiemer, 2005). Completeness estimates as a function of time and sometimes space are a critical input for the correct estimation of earthquake activity rates. Completeness estimates for historical datasets was estimated as part of the historical reconstruction (Fäh et al., 2011; see also Chapter 3) and not repeated here in detail. These estimates are in general subjected to larger uncertainties and to some extend a matter of expert judgment based on an evaluation of various seismicity plots (Wiemer et al., 2009b; Musson et al., 2009).

Seismic network performance generally (but not always!) improves as more and higher quality sensors are installed in a region. Switzerland in particular underwent great changes in seismic monitoring around 2001, because a new network of broadband sensors replaced the old analogue sensors (Deichmann et al., 2012). This modification is known to have improved the completeness threshold (e.g., Nanjo et al., 2010).

Estimating Mc(x,y,t) for instrumental data is easier, relatively speaking, than for historical parts of the catalogue because in general estimates are based on numerous events with moderate uncertainty. The 'classical' approach to estimate Mc is based on the assumption of the power law behavior of seismicity ('Gutenberg-Richter law') which also underlies the recurrence model computations. Mc is defined as the point at which the rate of micro-earthquakes drops significantly below the forecasted one. In Figure 28 we show how Mc(t) can be derived for ECOS09 since 1975 using this approach. In addition, we show in Figure 28 for three periods the respective frequency-magnitude distribution. From these two graphs we can state that

- as expected from the M_L-to-M_w conversion (Fäh et al., 2011), the new ECOS09 Mc is "apparently" higher than the one of Mc(ECOS02);
- as expected, the Mc for the period 2002 onwards is about 0.3 Magnitude units lower than before due to the improved seismic monitoring capability.

The default completeness timetable for Switzerland used in our study is largely unchanged from previous findings (Wiemer et al., 2009b, Table 1). We interactively reviewed the cumulative frequency–magnitude distribution for each areal source zone and used adjusted completeness levels in some cases (see Table 1 and Appendix C). Thus, we defined the instrumental part of the catalogues all M ≥ 3.0 events following 1977.

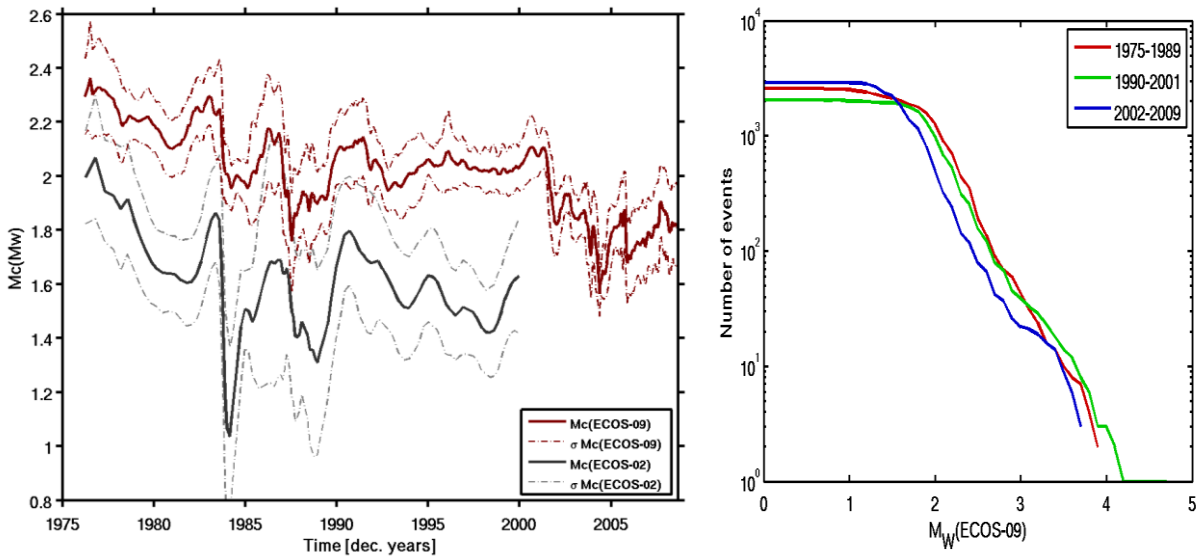

Figure 28: Left: Mc(t) for Switzerland, based on the Mw magnitudes of ECOS2009 (red) and ECOS-02 (black) together with 1-standard deviation uncertainty following the approach by Wössner and Wiemer (2005) with n=100 bootstraps sample. Right: Cumulative number of events as function of moment magnitude M_W(ECOS-09) for periods 01.01.1975-31.12.1989, 01.01.1990-31.12.2001, and 01.01.2002-31.12.2008.

The probability-based Magnitude of Completeness (PMC) method is a new approach to estimate completeness of earthquake catalogues and to improve the assessment a network's capabilities in recording earthquakes. It is based on empirical data, thus avoiding many of the assumptions traditional methods are based upon; specifically, it does not assume a power-law distribution of event sizes. It is a network-centric method in contrast to the catalogue-centric traditional method applied. For a detailed description of this method, please refer to Schorlemmer and Wössner (2008). Kazu et al (2010) have applied the PMC approach to Switzerland, providing an additional, independent estimation of Mc, based on the Ml scale. See also www.completenessweb.org, where for example the Swiss data and various documents can be downloaded.

Summary results of PMC from the Swiss work are shown in Figure 29; they in agreement with the estimated time-series based on the maximum curvature method shown in Figure 28. The maps for different time period emphasize that Mc varies starkly as a function of space and time, they also confirm the improvement in monitoring capability around 2001.

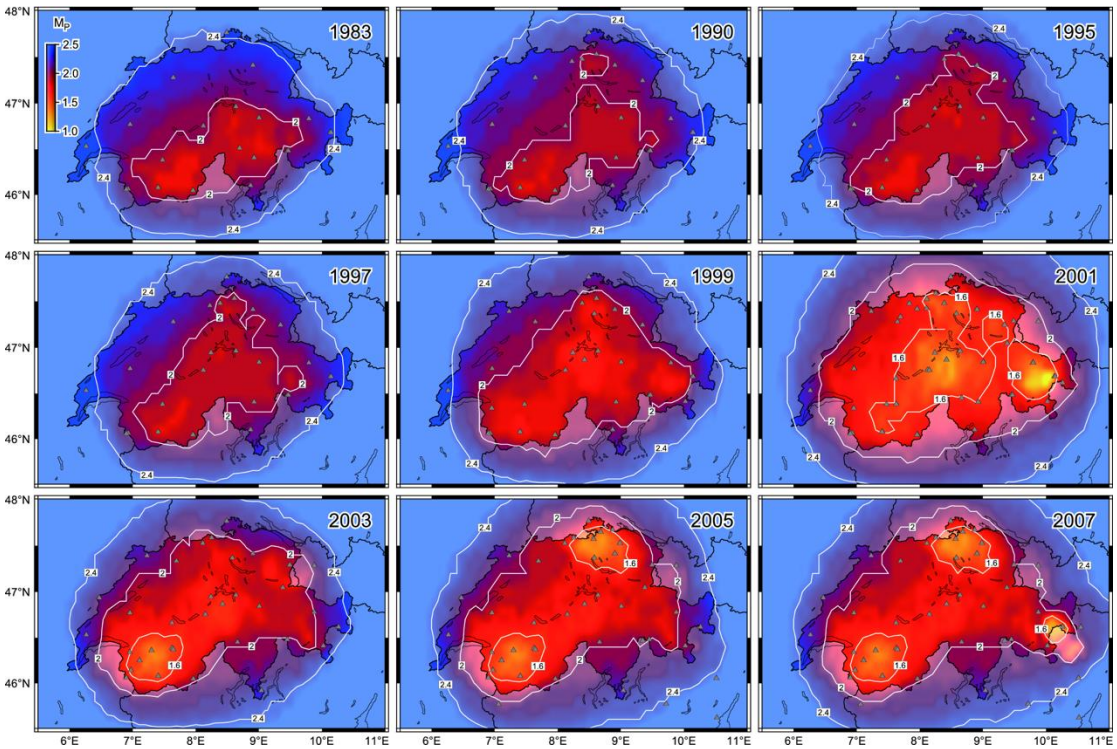

Figure 29: Maps of probability-based magnitude of completeness, MP, for different points in times. All maps show MP at 1 January of the respective year as indicated in the frames. White lines show contours for MP = 1.6, MP = 2.0, and MP = 2.4. Estimates are based on ML(SED) scale (From Nanjo et al., 2010).

The overall table of completeness used as a starting point for rate estimation is shown in Table 2. In each seismotectonic zone, completeness is then also checked manually and adjusted in selected cases. Before 1880, the default completeness values are largely different from the estimates for the 2004 model, albeit adjusted by 0.1 for the change in the Mw conversion. After 1880, the default completeness is substantially higher than in the 2004 model (Table 1), as explained in subsequent sections.

Completeness time	≥1200	≥1600	≥1680	≥1750	≥1880	≥1977
Default[1]	6.1	5.6	5.1	4.6	4.1	3.0
Italy[2]	6.1	5.6	5.1		4.6	3.0
Southern Switzerland[3]	6.1	5.6	5.1		4.1	3.0

Table 2: Completeness history of ECOS09 as a function of time for three sub-areas.

Catalogue preparation: removing quarry blast

The ECOS09 catalogue was checked to identify unidentified explosion events. Despite valiant efforts of network operators to identify these events, it is common in all regional earthquake catalogues to have such unidentified events because the separation of explosion events from tectonic ones is difficult (Fäh and Koch 2002; Koch and Fäh 2002; Wiemer and Baer 2000; Wuester 1993). These events are mainly limited to the most recent 30-year period of data. Their magnitudes are believed to be mostly smaller than M_W = 2.5; however, these small events have the potential to significantly bias the *a*- and *b*-value computation in some regions, especially because the size distribution of explosions is generally much steeper (higher *b* values) than of tectonic earthquakes (Wiemer and Baer 2000).

We re-applied to ECOS09 the methodology of creating the day-to-night time maps of event rates that can be used to identify areas of unusual daytime events rates (Wiemer and Baer, 2000; Wiemer et al., 2009). Only one remaining quarry region was identified, suggesting an improved ability

of the network to identify these events; events in this cluster are subsequently re-classified as explosions.

4.5 Estimating activity rates

For each seismogenic source zone defined later, we need to define the activity for all magnitudes, ranging from the minimum considered for hazard integration (M=4.0) all the way to the Mmax assumed for this source. This activity rate is based on interpolating and extrapolating the information of past earthquakes, since slip rates on fault do not exist. The SUIhaz2015 models uses the same assumptions as were applied in the 2004 Swiss hazard model, but a more refined rate estimate.

All seismic sources are assumed to follow a truncated exponential earthquake recurrence model. The completeness time history of each zone was assessed individually in order to estimate the corresponding recurrence parameters, staring from the default, overall assessment given in Table 1. For the description of the recurrence of seismic sources given the truncated exponential model, three parameters are required: the rate of earthquake activity N(m_0), the b-value and M_{max}.

We estimated activity rate parameters using a Bayesian penalized maximum likelihood (PML) approach (Johnston et al. 1994; Coppersmith et al. 2012) that updates the prior b-value only if it is supported by local data. The approach is described in more detail in Wössner et al. (2015) and was used in the SHARE project. We also adopted the weight of 0.25 – this means in the framework of PML that the believe in data is higher weighted (0.75). The prior b-value is estimated for the overall catalogue using Weichert (1980). The use of a prior was already included in the 2004 model (Wiemer et al., 2009); a prior estimate acts as a penalty function in order to stabilize the assessment in seismic sources with limited seismicity. The PML-estimates for the a– and b-value pairs and their associated uncertainty recover well the distribution of seismicity, also for sources with little data. The estimates are, however, guided by the more abundant small magnitude data, which is a desirable feature.

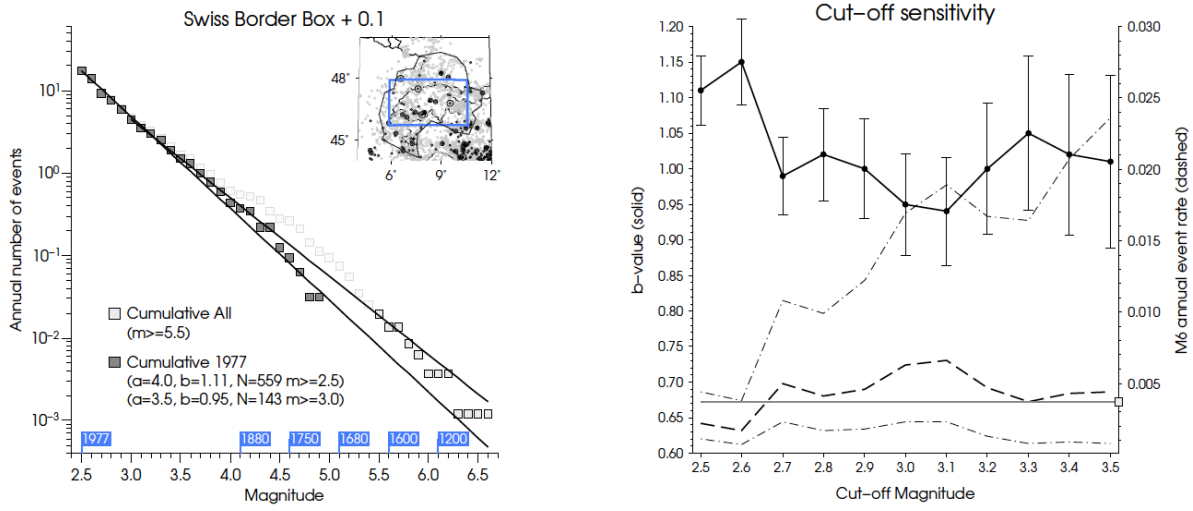

Figure 30: Magnitude-frequency distribution for Switzerland plus surrounding regions: (1) using all events and completeness time history as indicated at the bottom and given in Table 1, and (2) isolating the instrumental part of the catalogue (1977 - 2009). Right: Sensitivity of GR parameter estimation with respect to cut-off magnitude.

Figure 30 shows the overall magnitude frequency distribution of events in the ECOS 09 catalogue, limited to events near the Swiss border, and cut at the overall completeness indicated in Table 2. The historical and instrumental part of the catalogue are separated. From this figure, we can observe that the historical observation and instrumental data are consistent overall. However, the estimate of the b-value using only instrumental data (b=0.95) is somewhat higher than the one including the historical part of the catalogue (b=0.90). This degree of mismatch is typical for con-

temporary PSHA studies and was also observed in the 2004 study. As explained also in Wiemer et al. (2009), there can be at least two reasons for this observation: Differences in magnitudes scales between instrumental and historical periods, or natural fluctuations in rate, meaning that the period since 1977 by chance had a somewhat below average activity rate not respecting the long-term historical average. Because this ambiguity in interpretation cannot be resolved, we treat it as an additional source of epistemic uncertainty. The subsequently defined source models will represent the different views and consequently also use different b-values as priors. Note that while the difference in b-value of 0.05 is quite small, it does imply differences in overall rate of magnitude 6.5 earthquakes of a factor 2-3.

Figure 30 (right) also shows the sensitivity to the choice of the cut-off magnitude for estimating the overall b-value. For magnitudes 2.5 <Mw < 2.8, the b-values are significantly higher; this is a result of the conversion of Ml to Mw, as explained in the ECOS09 report (Fäh et al., 2011) as well as in Bethmann et al. (2011) and Goertz-Allmann et al., (2011). Above Mw 2.8, the b-value estimate is stable within the uncertainty range. This sensitivity to Mcut for values below 2.8 is a primary motivation to select a cut-off magnitude of 3.0 for the subsequent analysis.

For each area source region defined later, we then use the PML method and the prior value of 0.90 to estimate the b-value and its uncertainty. An example of such a fit for a zone in Grisons is shown in Figure 31. Using a prior of 0.90, we find a PML b-value of 0.91. We also show the 2004 model estimates for this zone for comparison, which in this case have barely changed.

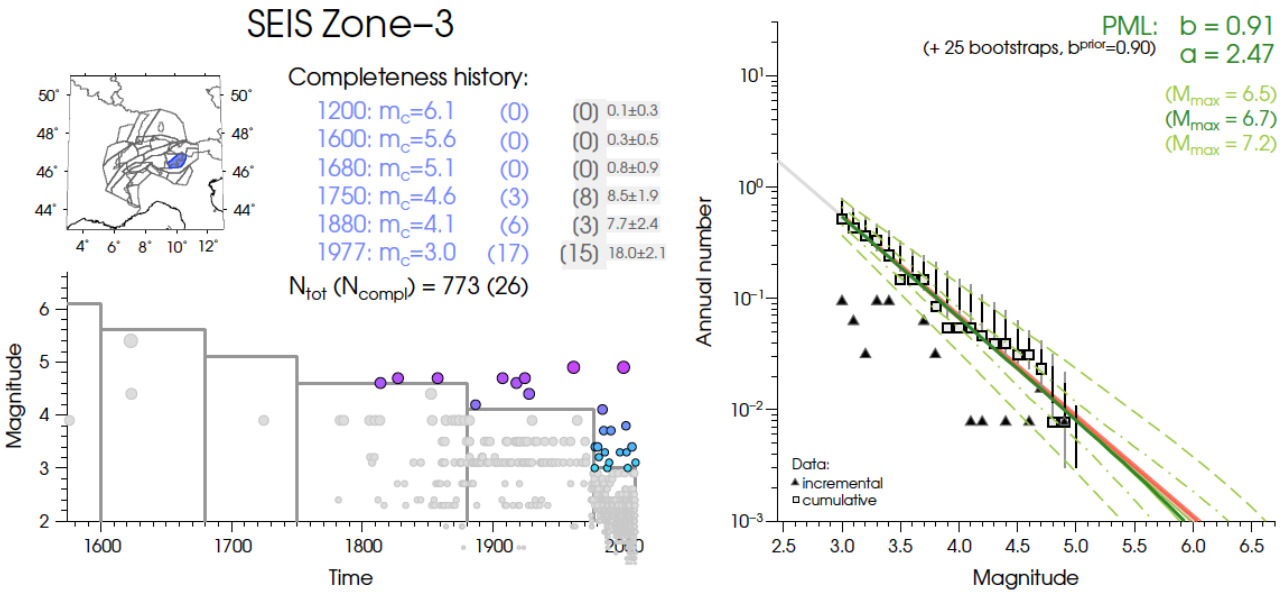

Figure 31: Left: map view of area sources (top) and the completeness-time history (bottom); events that are below the assume completeness are shown in grey. Right: Frequency-magnitude distribution of events above completeness. Green lines correspond to SEIS-15 estimates for different assume Mmax shown are the median estimates as well as plus/minus 1 and 2 sigma fractiles; the red line indicates the SEIS-04 values. Black vertical lines indicate the uncertainty in the rates of earthquakes for each magnitude bin, based on a bootstrap approach.

4.6 Estimating the maximum magnitude

The choice of the maximum possible earthquake, M_{max}, is typically quite critical for the hazard level in Switzerland at short return periods (< 500 – 1000 years;), but may have a considerable influence on the hazard at longer return period (Wiemer et al., 2009). It is possibly the most difficult recurrence parameter to assess in Switzerland, because the physical understanding of M_{max} is poor and the database of the rarest events is by definition statistically very limited, particularly in

areas of moderate seismicity, where the largest events may have recurrence rates of many thousands of years.

The very largest earthquakes of magnitude 8.0 – 9.5 on Earth are believed to be limited to selected special zones around the globe, typically subduction zones where both sufficiently long faults and homogeneous stress conditions exist to host a rupture of several hundreds of kilometers length. All experts in our team, and also the ones elicited in the PEGOSOS project, agree that ruptures of magnitudes larger than 8.0 can be excluded in Switzerland. However, most experts also agree that that in essentially in a critically stressed crust, earthquakes of magnitude of around 6.0 – 6.5 can happen more or less everywhere; albeit very seldom in areas of low strain. This statement is based on empirical evidence from around the globe; it is also consistent with the contemporary understating of earthquake ruptures processes and numerical modelling thereof. Finally, it is consistent with the historical and paleo-seismic record of earthquakes in Switzerland (see also Chapter 3). It is known that also areas where historically no magnitudes >5.5 events are known have experience such events in the past, but they may return only every 5,000 – 50,000 years. Faults of magnitudes up to 6.0 - 6.5 will typically not break the surface during rupture. It is also impossible to image such faults using geophysical techniques, especially blind faults or deep seated strike slip faults in the crystalline basement.

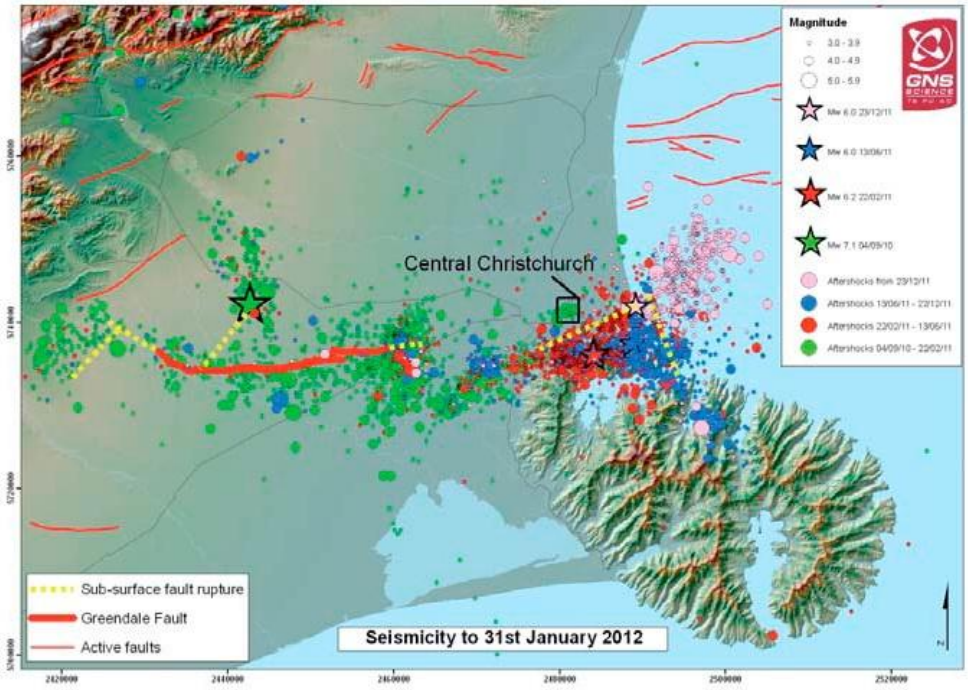

Figure 32: Earthquakes of the Canterbury sequence through to 31 January 2012. Major earthquakes are shown as stars, including the September 2010 Darfield main shock (green), the February (red), June (blue) and December (pink) 2011 Christchurch earthquakes. Yellow dashed lines represent subsurface rupture of subsidiary faults that ruptured in the Darfield earthquake (Holden, 2011), and the Christchurch earthquake of Feb 2011 (from Beryyman et al., 2012[2]).

A good example of large faults that rarely rupture in an area of straining rate comparable to Switzerland's (1-2 mm/year) are the Darfield and Christchurch earthquakes in 2010/2011, with magnitudes of 7.1 and 6.1[9]. While various faults and fault segments were known in the Canterbury region, it is unknown if they were active and in any case, the 2010 and 2011 quake ruptured on a previously unknown fault and actually involved slip on up to seven individual faults (Eliott et al., 2012). The return period of such events was estimated in the national hazard model to be more than several thousand years (Stirling et al, 2002). Likewise, about half of the earthquakes of magnitude 6 and above in California occurred on previously unmapped faults. These events serve

[9] http://www.mapfre.com/mapfrere/docs/html/revistas/trebol/n62/en/articulo2.html

as reminders that large earthquakes are possible in places that have historically not seen them, such as the Alpine Foreland in Switzerland.

The challenge for defining M_{max} in Switzerland is therefore to define a distribution that 1) reflects the view of the technical informed community that earthquake up to a magnitude 5.5 - 6 can happen everywhere; 2) magnitudes M>7.9 are excluded everywhere in Switzerland; 3) respect the fact that the available data that constrain M_{max} are very limited within Switzerland, even more so when looking into sub-areas; therefore, using global priors is sensible.

The SED seismogenic source experts evaluated various approaches taken in other PSHA studies and documented in the literature (e.g., Coppersmith et al., 2009, Wheeler 2009). It also evaluated the approaches taken by the PEGOSOS source experts as well as the regional SHARE zonation (Wössner et al., 2015). We decided to adopt the EPRI approach based on a global database (Johnston et al. 1994), which was also a prominent choice of PEGOSOS source experts. Although as stated below, none of the available methods provides a satisfying answer to the M_{max} problem, and for that reason we favour the EPRI approach for the estimation of M_{max} as the most satisfying compromise option. Specifically, we appreciate the broad uncertainty distribution of M_{max} and the fact that it combines global prior information with local data, depending on its availability. We consider the prior distribution for extended continental crust, with a mean magnitude of 6.4 and a standard deviation of 0.84, appropriate for Switzerland, because extension dominated the European crust in Permo-Carboniferous times (e.g., Burg et al. 1994), during the Mesozoic development of the Tethys passive margin (e.g., Ricou 1994) and during Tertiary extension (e.g., Ziegler 1992), and because the broader uncertainty distribution of extended crust expresses more accurately the notion that Mmax is uncertain.

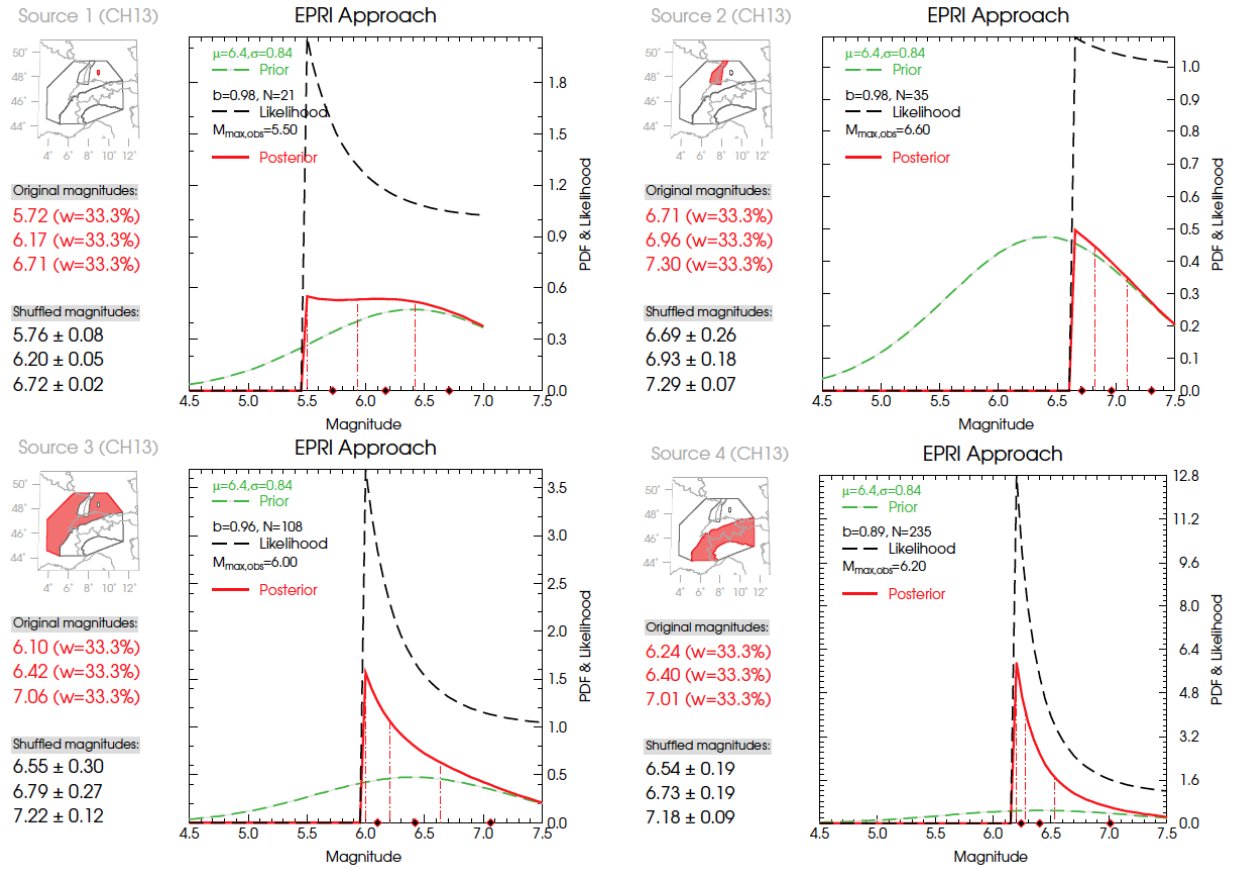

Figure 33: Large-scale zones used for estimating Mmax according to the EPRI approach and results of the assessment of Mmax for each of the four tectonic regions, . Note that respective likelihood functions depend on maximum observed magnitude, sample sizes and b-values. We discretized the resulting posterior distributions using 3 values for Mmax of equal probability. The Mmax distribution of the final source model is based on Monte Carlo perturbed catalogues (values in lower left corners).

In our assessment, M_{max} is a feature that is tied to the regional seismo-tectonic environment rather than the local seismicity. We therefore uncouple the assessment of rates and of M_{max} by using tree large-scale regions (see Figure 33 for regions). This is the approach similar to the one used in SHARE and by several of the PEGSOS source experts; this is reasonable, based also on the fact that large ruptures will extend for 50-100 km and more, and a M_{max} zone smaller than the actual rupture size makes little sense. In addition, the data in small zones is statistically too insignificant to allow for a robust estimation of M_{max} using EPRI. The one exception in our model, where we adopt the German and SHARE seismogenic area source models (Gruenthal et al., 2009; Wössner et al., 2014) in the sense that we treat this zone as a very special small-scale feature deserving its own tectonic region qualifier.

The prior distribution for extended continental crust ($\mu = 6.4$, $\sigma = 0.84$) is then combined with a likelihood function that is based on the zone-specific observed seismicity, assuming an exponential frequency-magnitude distribution. The likelihood function's decay starts at the largest observed magnitude in the area and depends on the b-value and the available number of data (see Figure 33 for values).

The posterior probability distribution for M_{max} is then derived by multiplying the generic prior distribution with the source-specific likelihood function. To derive a discrete distribution for M_{max} suitable as input into PSHA, we discretized the posterior distribution so that we obtained three values of equal weight of 33% (Figure 33). Note that we truncated the posterior distribution at an upper magnitude bound (7.0 in the Swabian Alp, 7.5 in all other zones) in order to exclude unrealistically high M_{max} values from the earthquake rate estimation. To also account for the uncertainty in location of events as well as for the uncertainty in magnitude, we apply a Monte Carlo resampling by repeating the same procedure 100 times but randomly varying the locations and their magnitudes within their uncertainty ranges. The reshuffled M_{max} values are sometimes larger, sometimes smaller than the original ones, see Figure 33 for values. The M_{max} ranges from 5.76 - 6.72 (Swabian Alp) to 6.69 - 7.29 (Rhinegraben). The M_{max} values thereby determined are then used on each zone as input for the rate computation for the double truncated frequency-magnitude distribution.

4.7 Defining a seismogenic zoning approach[10]

The key requirement for building a seismogenic source model is to capture the center, body and range of the knowledge of the informed technical community (Budnitz, 1997; Coppersmith et al., 2009). Capturing uncertainty in knowledge and diverging interpretation is as crucial as capturing the variability of the data, and is something that we like to further broaden, compared with the 2004 source model. We continue to use the commonly in PSHA applied weighted logic tree approach to capture the epistemic uncertainty in the understanding and modelling approaches. The different logic tree branches ideally represent the model space in a mutually exclusive but cumulatively exhaustive sense, although in practice this cannot be applied in a strict sense, since models as well as data overlap. We also capture the aleatory variability in parameters by estimating in formal ways the uncertainty ranges of relevant parameters. Weights in our model between branches were assigned based on discussions within the group of SED experts, reaching a consensus value.

Our modelling philosophy is based on a hierarchical approach featuring multiple layers (similar to Wössner et al., 2015). At its base lies a set of large-scale zones that provides an initial assessment essential for a homogeneous definition of model properties (such as maximum magnitude, tectonic regionalization and hypocentral depth distributions). This large scale tectonic regionalization is also important for the suitable selection of Ground Motion Prediction Equations (GMPEs,

[10] Note that we will refer to the SUIhaz2015 seismogenic source models as SEIS15 and CH15. In some figure the labeling will be SEIS14 and CH14, these model annotation are equivalent and identical to the CH15 and SEIS15 one.

Chapter 5). These properties are then mapped to the individual, smaller scale earthquake source models.

Note that all source models are time-independent seismicity forecasts, which are built under the assumption that earthquakes occur independently of each other at a constant average frequency (e.g. Cornell, 1968; Reiter, 1990).

Branching levels

Our final earthquake rate forecast is based on three different branching levels to represent uncertainties regarding (a) the seismic source modelling approach, (b) the recurrence rate parameter estimates, and (c) the maximum magnitude (Figure 34). The first branching level consists in itself of four branches, representing different earthquake source models that we will describe in more detail below:

(1) The area source model SEIS-15
(2) The smoothed seismicity model CH14
(3) The area source model SEIS04, based on ECOS02(Fäh et al, 2003; Wiemer et al., 2009b)
(4) The area source model SHARE, based on SHEEC (Stucchi et al., 2012; Wössner et al., 2014)

Models (3) and (4) were considered in order to capture epistemic uncertainties in the earthquake rate estimation process, since they represent viable alternatives that capture specific elements of uncertainty. Models (1) and (2) were constructed based on the ECOS-09 catalogue and feature two more branching levels dealing with aleatoric uncertainties regarding the earthquake rate parameter estimates: we used, as a explained below, a penalized maximum likelihood method for estimating recurrence rate and the aforementioned EPRI approach for estimating maximum magnitudes.

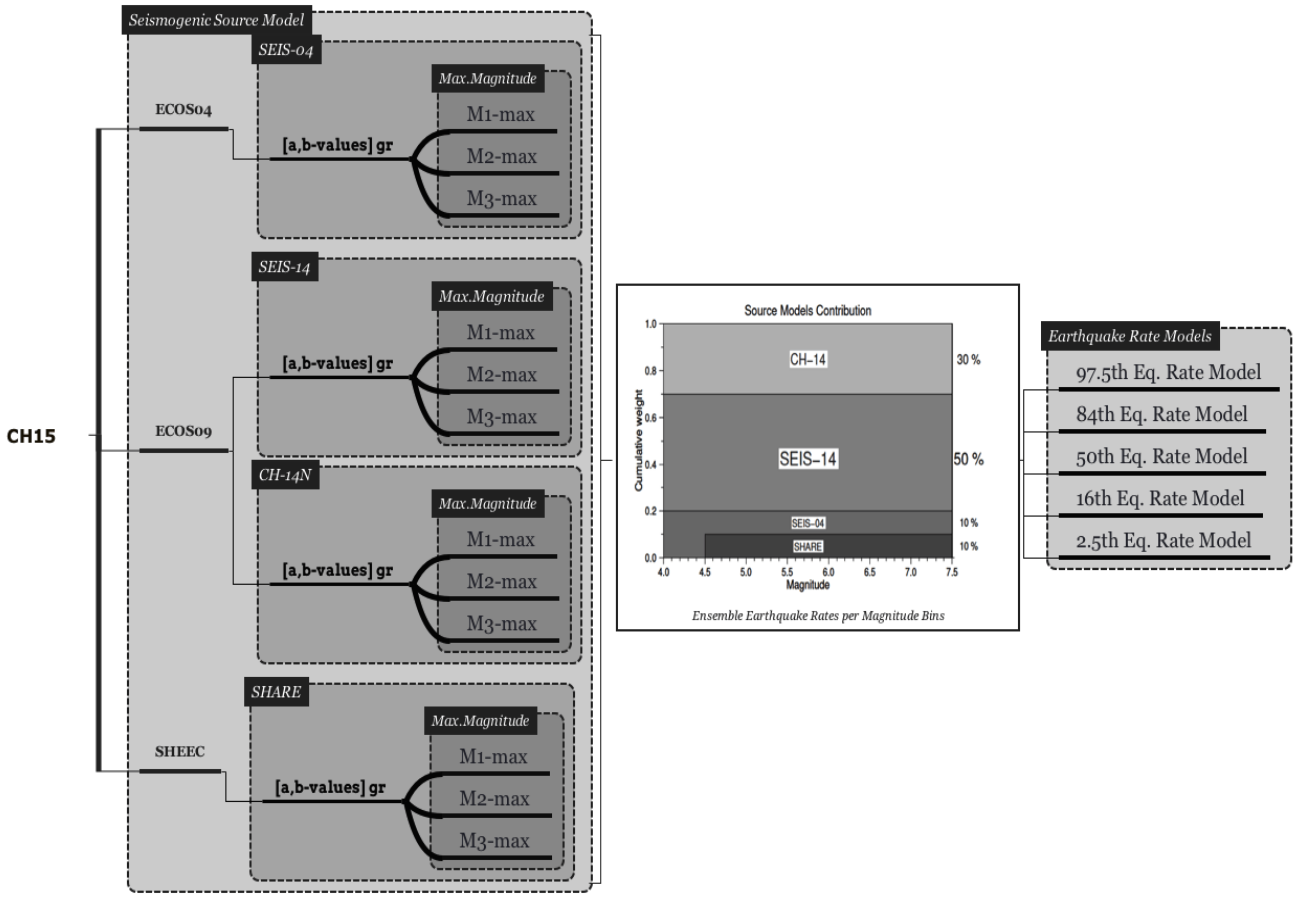

Figure 34: Schematic illustration of the seismogenic source logic tree.

4.8 SEIS-15 model

Unchanged from the 2004 modelling, all source experts in our team considered the most important contribution to the seismogenic zonation model a classical area source model using ECOS09 as the relevant catalogue for rate estimation. Such a model is driven by both the spatial distribution of past seismicity as well as knowledge on tectonic boundaries, it is thus conceived to be a good balance between the various input sources. The experts also decided that there is no need for a zonation update, since the 2004 SEIS model was not seen as deficient and no major changes occurred in either the distribution of the seismic activity nor in the relevant understanding of the seismotectonic. Therefore, the SEIS-15 uses exactly the zonations of the previous 2004 SEIS model (Wiemer et al., 2009b) and assumes a spatially and temporally homogeneous distribution of earthquake activity within each zone. The zone borders of the 26 zones are show in Figure 35, the geometries and rates per magnitude bin can be retrieved from the online resources and are part of the hazard input file which is also online available.

The experts subsequently decided after extended discussions, and in-line with most PRP source exerts decision, to start the activity rate determination at a minimum magnitude of Mw=3.0. This is a shift from the 2004 model where in some zones also lower completeness was considered. There are two reasons for this assessment:

– It is not clear if the smallest events that are recorded for a rather short period are representative of the long-term rates in a zone. Using small events more extrapolation in magnitude, using Gutenberg-Richter, and could potentially bias the model towards too much weight for the most recent seismicity because the numerous small events add weight to this period.

– Cutting at M_w above magnitude 2.8 avoids the problem of M_w to M_L conversion in ECOS09. Because the scaling between M_L and M_w changes substantially below this magnitude (Chapter 3, Bethmann et al., 2013; Goertz-Allmann et al, 2011), the scaling of either M_w or M_l cannot follow a power-law distribution with one exponent. It is to date unknown which one (or both) of the magnitude scales break down below magnitude 3.0, and why. This problem is avoided if data from M_w3.0 are used, as demonstrated for example by the b-value as a function of cut-off (Figure 30).

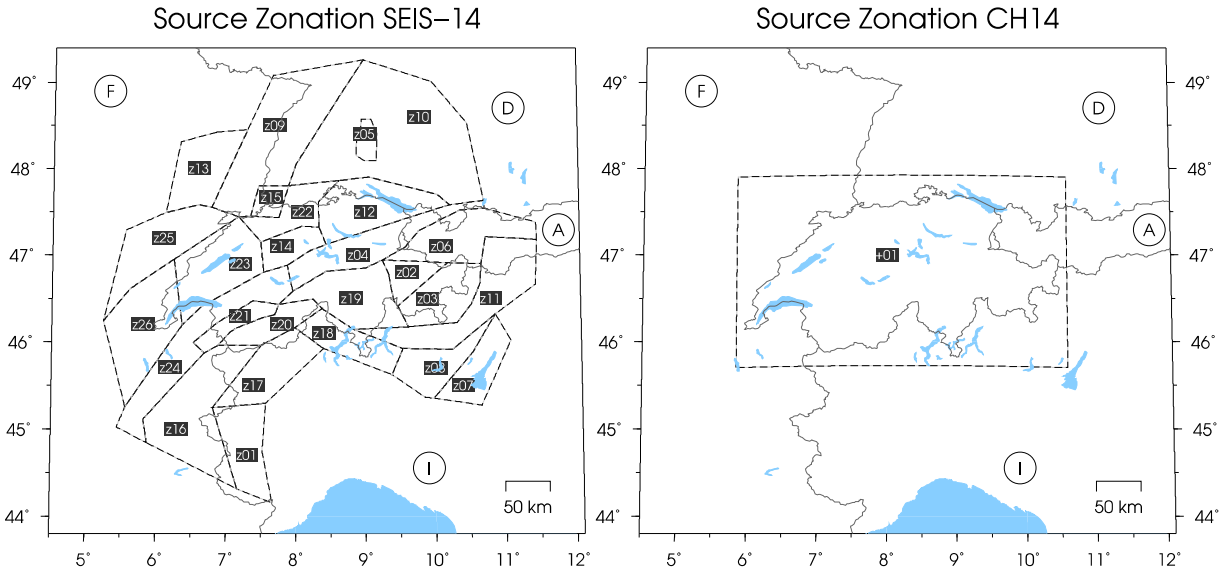

Figure 35: Source zonation model SEIS-15 (composed of 26 source zones) and bounding box of smoothed seismicity model CH14.

For the same reasons, most of the PRP experts adopted a similar cut-off. Note that the final impact on the local rates is in most cases negligible, and not systematic, as can be seen in the com-

parison of the 2004 model and the 2015 model for the same zones (e.g., Figure 31). The activity rate parameters are then determined in each zone using the PML approach (section 4.5) quantifying the uncertainty of the rate estimates. The SEIS-15 model relies on both the historical and instrumental part of the ECOS-09 catalogue, starting in the year 1200. Due to the fact that the 26 area sources cross national borders, we interactively reviewed the normalized cumulative frequency–magnitude distribution of events for each source zone when using the default completeness time history (see Table 1). In some cases, we adjust the completeness threshold (Appendix C). Figure 31 shows an example case for source zone 3 that covers parts of Grisons. Appendix C reports the full list of all resulting a- and b-values.

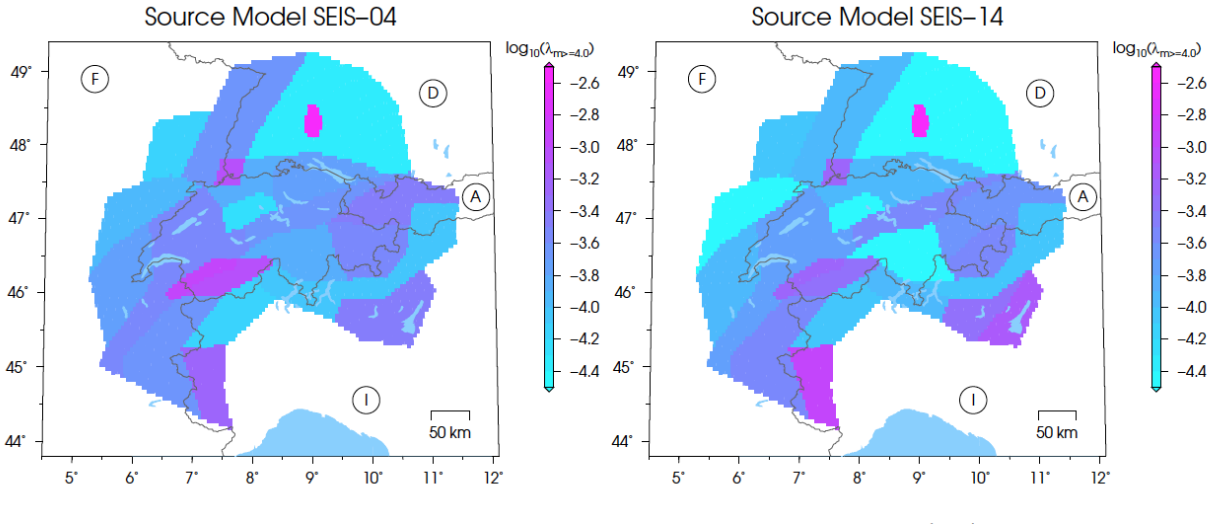

Figure 36: Cumulative annual earthquake rates of magnitude Mw >= 4.0 for area source model SEIS: version 2004 (left) and version 2015 (right).

4.9 SEIS-04 model

We consider the SEIS04 model a viable alternative forecast model with a small weight because it expresses different and still defensible alternative ways to estimate recurrence rates. The differences are 1) in the way M_w is converted to M_L in ECOS09 versus ECOS02 (Fäh et al., 2011); 2) In the way rates are estimated; 3) on the use of smaller magnitudes for rate estimation in individual zones; 4) in the approach taken to estimate M_{max}. The comparison of overall rate of magnitude 4.0 ad larger events between SEIS15 and SEIS04 is shown in Figure 36.

4.10 CH-15 smoothed seismicity model [11]

An alternative to area source models which are based on expert zonation, such as the SEIS-15 model described above, is a zone-free smoothed-seismicity model, also called a smoothed stochastic earthquake rate model. Such models have been increasingly used in a number of contemporary PSHA studies worldwide, and were also used in Switzerland by some of the PEGOSOS experts (Coppersmith et al., 2009). As discussed for example by Hiemer et al., (2014), expert judgment driven areal source models are somewhat subjective, and efforts have been made to introduce more objective, data and algorithm driven models that are fully reproducible. In particular, kernel-smoothed seismicity approaches, starting on a prominent yet experimental attempt to map the seismic hazard within the central and eastern United States (Frankel 1995), have been used as an alternative model branch to address epistemic uncertainties of earthquake occurrence within a PSHA.

[11] Some of the discussion in this chapter has been adopted from Hiemer et al. (2014)

Following the pioneering models of Kagan & Jackson (1994) and Frankel (1995), several other kernel-smoothed seismicity approaches have been proposed (e.g. Cao et al. 1996; Lapajne et al. 2003; Woo 1996; Jackson & Kagan 1999; Stock & Smith 2002; Helmstetter et al. 2007; Zechar et al. 2010a; Werner et al. 2011) which all rely on using only seismicity as input to estimate future earthquake locations and rates, with differences in the shape and functional form of the smoothing kernel. Helmstetter & Werner (2012) used space–time kernels to obtain spatial densities of earthquakes, thereby circumventing the relatively subjective choice of a declustering algorithm. Some efforts were also made to include tectonic knowledge in terms of regionalization schemes (e.g. Burkhard & Grünthal 2009). Pseudo-prospective forecast experiments have been used to optimize the kernel width for a given time period by separating the earthquake catalogue into learning and target periods, finding the optimal kernel width based on likelihood evaluation procedures (e.g. Zechar et al. 2010a). Such data-driven smoothed seismicity models perform well in prospective testing of earthquake forecasts within the framework of the Collaboratory Study for Earthquake Predictability (CSEP, Jordan 2006) for the intermediate-term forecast period of 5 years (e.g. the Regional Earthquake Likelihood Models experiment, RELM, Field 2007; Schorlemmer et al. 2010; Zechar et al. 2013). This is a result of one of the basic assumption of these models: earthquakes occur at or very close to locations of previous seismicity.

Hiemer et al. (2013) introduced a stochastic earthquake source model for California that addresses the lack of integration of geological information criticized in earlier gridded smoothed seismicity models. By combining information on active faulting with a smoothed seismicity approach, they build an alternative source model for California. The model applies in essence the kernel density estimation technique to both past seismicity and fault moment release, with the latter being estimated from slip rates on mapped active fault structures. The resulting forecast relies on data-driven likelihood optimization techniques and is thus less dependent on subjective expert judgments compared to other source model types used in PSHA—though some cannot be avoided. A similar model has been presented for New Zealand (Rhoades & Stirling 2012) pointing out shortcomings within the New Zealand national seismic hazard assessment (Stirling et al. 2012).

Hiemer et al. (2014) adopted this stochastic earthquake source model class to Europe (Figure 37), again integrating in a data-driven approach both seismicity and fault information. The kernel bandwidths and density weighting function are optimized using retrospective likelihood-based forecast experiments. Retrospective and pseudo-prospective likelihood consistency tests underlined the reliability of this model when compared to the classical area source model using the testing algorithms applied in CSEP. When testing the forecasting skill of both models, Hiemer at al. (2014) reports a statistically significant better performance of the stochastic smooth seismicity model for testing periods of 10–20 yr.

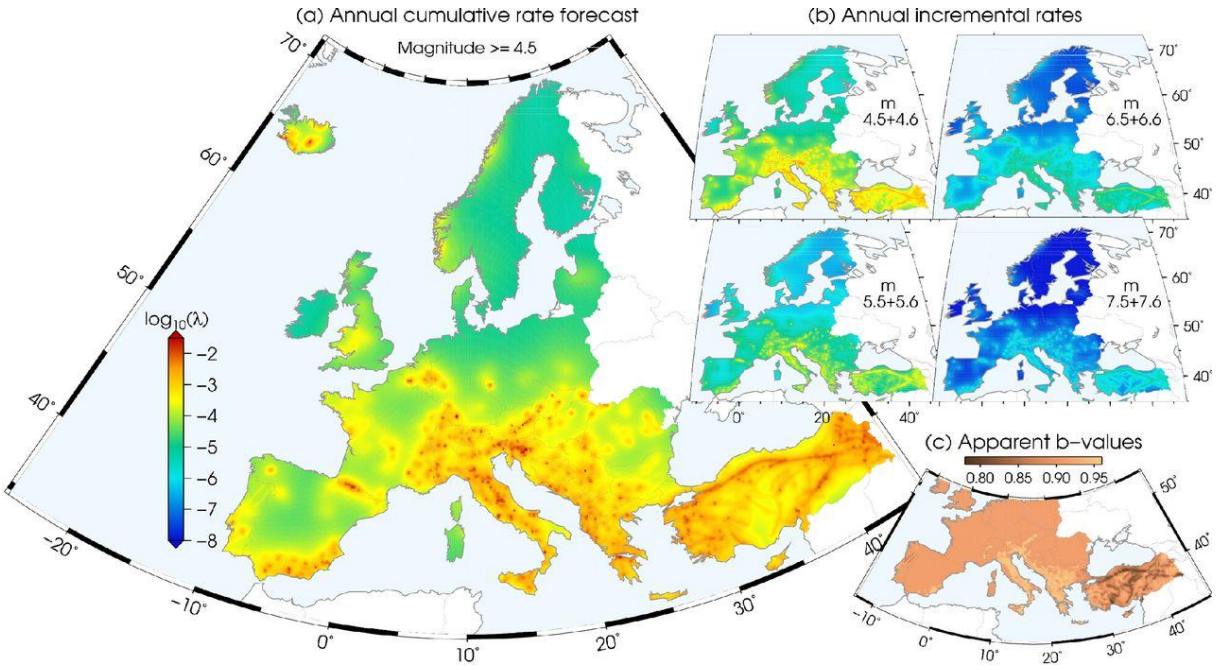

Figure 37: (a) Spatial distribution of cumulative annual earthquake rates (4.5 ≤ m ≤ 8.6) for Europe. The total annual rate is 65.6 events yr−1 (b) Spatial rate distribution for selected incremental magnitudes. Note the increasing imprint of the fault contribution with increasing magnitude (c) Resulting local departures from overall Gutenberg–Richter magnitude distribution (b = 0.9). From Hiemer et al., 2014.

For the SUIhaz2015 project, we also decided to include a stochastic smooth seismicity model as one of the seismogenic source models, because such models are nowadays a viable alternative to areal source models and thus represent one of the views present in the informed technical community. Our model is built under the following assumptions:

– Because too little information on active faults and their respective slip rates is known, our model will only use past seismicity as an input.

– We decouple the kernel and seismicity rate estimation in order to maximize the amount of available information.

– For optimizing the kernel, we used the approach developed by Hiemer et al. (2013) and Hiemer at al. (2014).

The so-called CH15 model is a zone-free smoothed-seismicity model. The model's dimensions correspond to a rectangular box that includes all of Switzerland and is extended by 0.1◦ in all four directions (Figure 35, right frame). Our model will combine a spatial grid of the kernel density with an independently determined overall seismicity rate function, with a b-value of 0.95 (see Figure 30). We modelled the overall magnitude rate distribution solely based on the instrumental part of the ECOS-09 catalogue (that are all events with m ≥ 3.0 and t ≥ 1977). The reasoning for the cut-off magnitude is equivalent to the one used for the SEIS15 model. The time-frame was selected because the model then expresses the alternative view that the past 40 years are the most relevant period of seismicity for forecasting the next 50 years. This is also appropriate because as shown in Figure 30, despite the short length of that part of the catalogue, we found that the estimated recurrence parameters are in good agreement with the rates of all historical m ≥ 5.5 events.

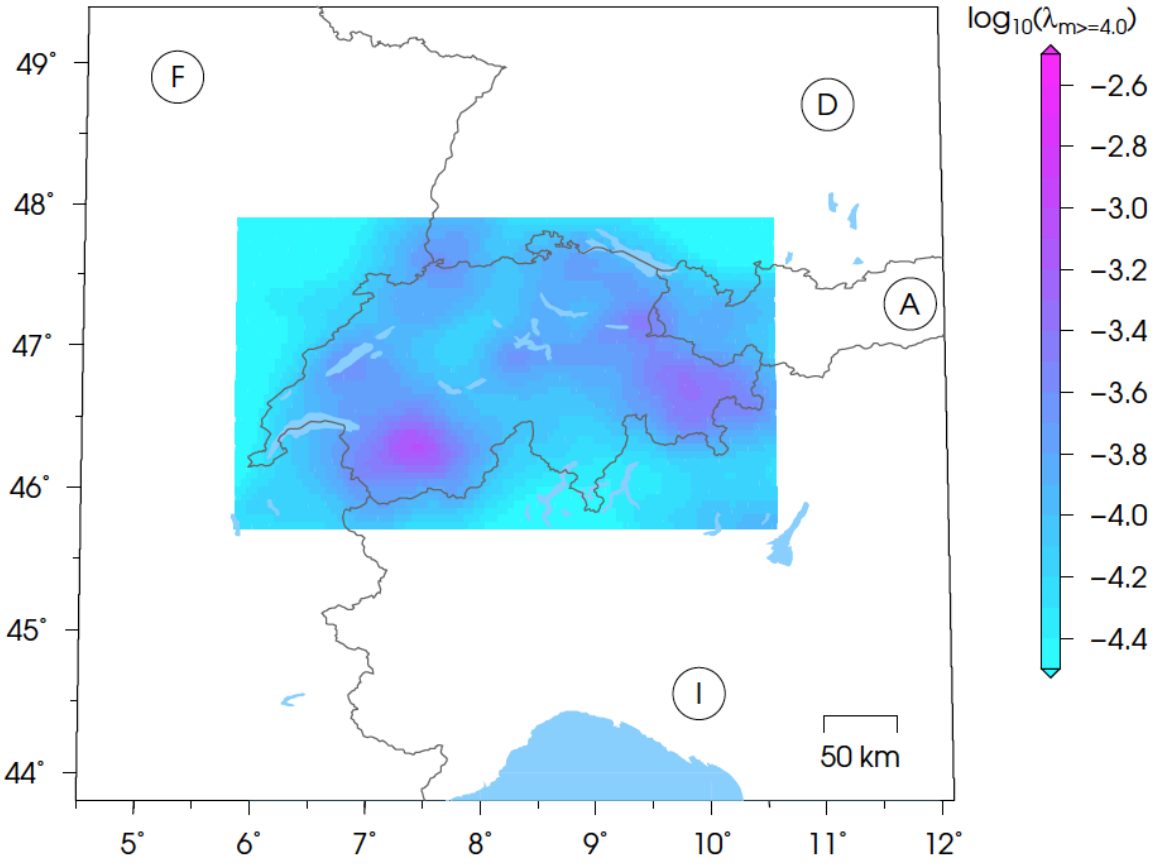

Figure 38: Cumulative annual earthquake rates of magnitude Mw >= 4.0 for the smoothed seismicity model CH15. Note that outside of Switzerland and its immediate vicinity, the model is not defined.

The spatial rate distribution is determined with an adaptive kernel-smoothing approach using a Gaussian kernel with a width of 10 km for pilot density estimation (Silverman, 1986). This adaptive technique avoids the disadvantage of sharp kernel size jumps associated with variable kernel approaches (Kagan and Jackson, 2012; Hiemer et al., 2014), where the smoothing distance associated with an event is derived from the horizontal distance between the event and its n-th closest neighbour (e.g. Helmstetter et al., 2006; Werner et al., 2011).

As input for modelling the spatial seismicity distribution we strove to maximize the available data by: (i) using all complete events (according to the default completeness time Table 1 using the adjustments m ≥ 3.0 for ≥ 1880 and m ≥ 2.5 for ≥ 1977, Wiemer et al., 2009a, c.f. their Table 4) and (ii) extending the ECOS-09 catalogue to 1/Jan/2014. This results in a total number of 1550 events.

4.11 SHARE combined earthquake rate model

The 2013 European Seismic Hazard Model (ESHM13) results from a community-based probabilistic seismic hazard assessment supported by the EU-FP7 project "Seismic Hazard Harmonization in Europe" (SHARE, 2009–2013). The ESHM13 is a consistent seismic hazard model for Europe and Turkey which overcomes the limitation of national borders and includes a through quantification of the uncertainties. It is the first completed regional effort contributing to the "Global Earthquake Model" initiative. The SHARE seismogenic source model as documented in Wössner et al. (2015) is in our assessment state of the art, developed by European experts and a viable alternative to the SEIS15 and CH15 models to be considered. Note that it is not fully independent of the other models: ESHM13 uses as input data from ECOS09, although somewhat reprocessed within the development of the SHEEC catalogue (Stucchi et al 2012). It also uses as a starting point for the areal

sources the TECTO04 model and a similar methodology to develop a stochastic smooth seismicity model. The ESHM rate forecast for the study region is shown in Figure 39.

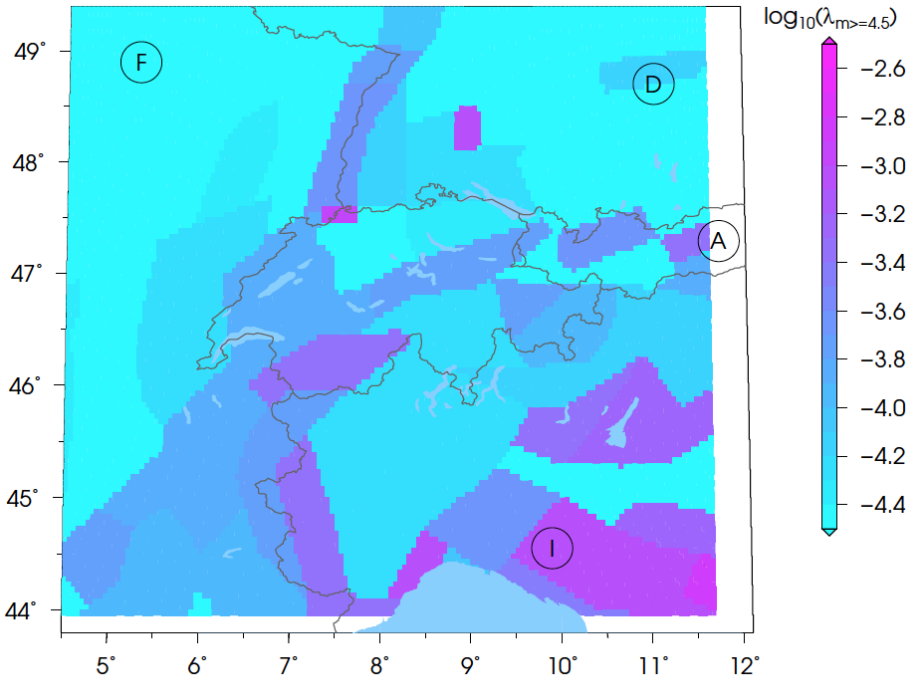

Figure 39: Cumulative annual earthquake rates of magnitude Mw >= 4.5 for the SHARE model.

4.12 Rate forecast comparison and model weights

We present the resulting forecasts in terms of their spatial rate distributions (Figure 36, Figure 38 and Figure 39) and their total annual productivity as a function of magnitude (Figure 40). The CH15 model exhibits the lowest overall rates, which is expected because it uses the most recent, instrumental seismicity as input, resulting in lower rates and a higher b-value (Figure 30). The SEIS15 model is in terms of the rates somewhat lower than the SEIS04 model, which can be seen in both the rate plots but also the density plots of rates. This is partially a consequence of the reduced magnitudes for many of the historical earthquakes in ECOS09 (Fäh et al., 2011). The SHARE model is somewhat in between these two models, but with a different, steeper b-value.

The four different models are within their respective standard deviations and they express a range of different catalogues, differed methods to estimate rates, different approaches to M_{max}, different seismogenic zonation approaches, and last but not least different expert's views. In our assessment, these four models are well suited to capture the epistemic uncertainties that exist in seismogenic source zonation in Switzerland.

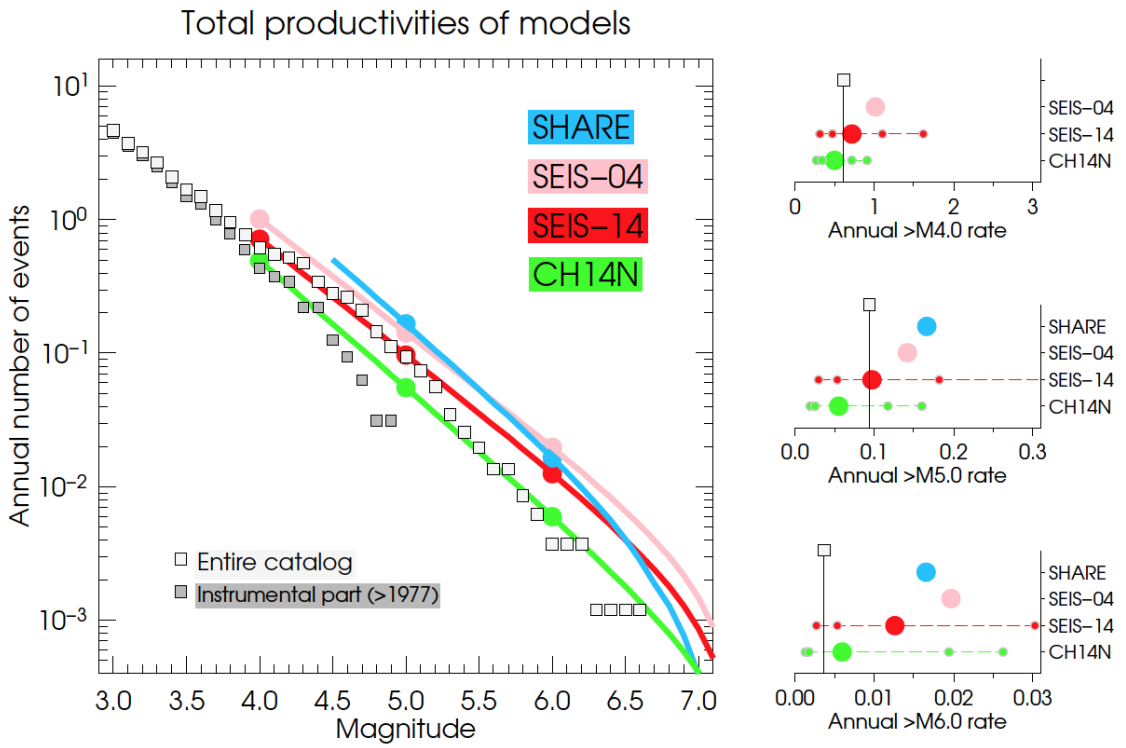

Figure 40: Frequency-magnitude distributions for data (light and dark gray squares, compare Figure 30) and models (coloured lines). Black line shows median values for the ensemble model. Dashed black lines correspond to 2.5, 16, 84 and 97.5 quartiles, respectively.

In a final step, we defined a weighting scheme of the four seismogenic models. These weights were based on the extensive discussion within the SED expert group and represent a consensus view of the experts involved. The weighting scheme applies to the entire region and it is magnitude dependent. That is, at any location of the map the following weights were applied to the recurrence rates of specific magnitude bins. The classical zonation using the most recent data, SEIS-15, receives the largest weight (50%). A small (10% weight is given to the alternative view on earthquakes rates estimates given in SEIS04. The smoothed seismicity model CH15 received 30% of the weight, as it expresses an important alternative to zonation and to the relevance of the most recent data. The SHARE model, finally receives also only a small (10%) weight, since it is not specifically developed for Switzerland. Weights are shown schematically in Figure 41; note that while the expert weighting applied by us is by definition subjective, the influence on the final hazard results is not large, because the differences in the models are not very strong.

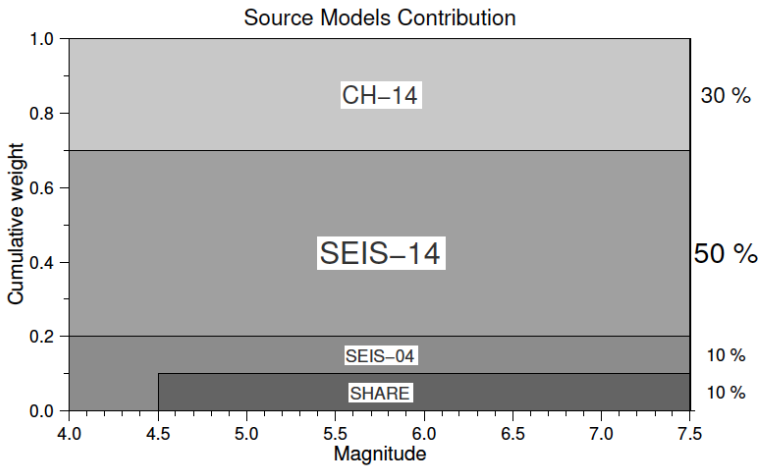

Figure 41: Source model weights. Note that for 4:0 <= m < 4:5 the SEIS-04 source model receives a 20% weight that is due to SHARE's minimum magnitude of m = 4.5.

Given these weights, we are now able to construct an ensemble earthquake rate model spatially distributed, which is shown in Figure 42. This ensemble earthquake rate model shows that the fractiles around the median seismicity rate forecast span the observed seismicity well. The forecasted rate of magnitude 6.0 – 7.0 is somewhat higher than the actual one observed, but well within the uncertainty of both the forecasted rates and the historical event rate. The final spatial footprint of the rate forecast (Figure 42b) still shows a dominance of the SEIS zonation, of course, but clearly smoothed down to the influence of the CH15 model.

The distribution of earthquake rates per magnitude model was assumed to be normal, and five percentiles of the earthquake rate models were retained for hazard calculation. The five percentiles describe the centre body (50th) and ranges (2.5th, 16th, 84th and 97.5th) of the ensemble rates. They are weighted in the subsequent hazard calculation accordingly to the corresponding area of a normal distribution, i.e. 68% for 50th earthquake rate model, 13.5% for 16th and 84th earthquake rate models, and 2.5% for 2.5th and 97.5th earthquake rate models.

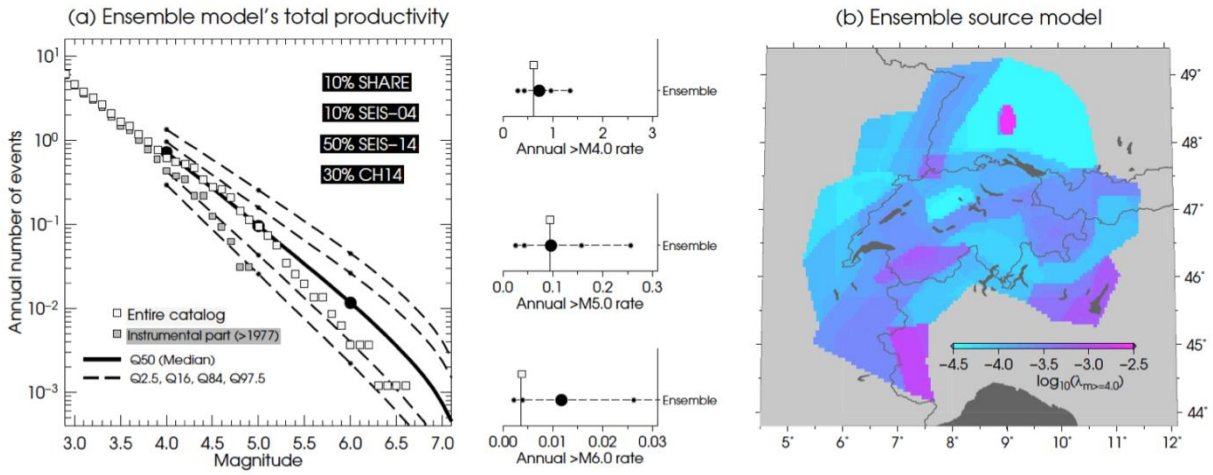

Figure 42: (a) Magnitude rate and (b) spatial rate distribution for the ensemble source model using the weighting scheme given in the inset. Map shows median values and the model's bounding polygon stems from the SEIS models.

4.13 Consistency checks and adjustment for Basle

We perform a visual consistency check for all SEIS source zones that are within the political boundaries of Switzerland. Examples for eight zones are shown Figure 43. We find that in all zones the observed seismicity fits generally well within the forecasted ones, considering the uncertainty ranges. Note that in the areas of higher activity, and with historically larger events (e.g., Valais, Basle, the median forecasted rates and observations are in good agreement. The fact that the overall forecasted rate is somewhat higher than the observed historical rate of M6 events (Figure 42) is therefore mostly a consequence of the summed-up contributions of sources where larger events are forecasted with a small rate, but have historically not yet occurred (e.g., SEIS-4, eastern Alpine Foreland).

Visual inspection of the seismicity in the Basle region (area source Figure 43) reveals that this is the one and only zone where the observed seismicity falls outside of the 97.5% upper confidence limit of the ensemble model. This mismatch triggered a re-analysis of our model in this region. There are at least two hypotheses that explain the mismatch between model and observation:

1. The occurrence of the Basle 1356 Mw=6.7 event outside of the model range could be interpreted as anomalous in the sense that while the natural recurrence of such events is only every 5,000, 10,000 or more years, we just happened to have had such event in the past 800 years. In this case the model would be correct on forecasting a lower rate and hazard.

2. Alternatively, the seismicity of smaller (M3.0 - M5.5) events in this zone may be inconsistent with the large event rate, because the Basle controlling fault may behave characteristically moving primarily in large events, or because the seismicity of the recent past was by chance below average. Characteristic behaviour as well as intermittent quiescence are documented for some fault segments, such as the segment of the San Andrea Fault South of the Creeping segment and Parkfield, that moved last in a large event in 1857. Geodesy shows that the segment today is fully locked an accumulating strain, but the seismicity of the past 30 and more years has been very low. If assuming such a scenario for the Basle region, our model would be biased towards too low rates and hazard and would need to be adjusted.

Fortunately, the Basle region is at the same time the one region where the most reliable paleoseismic information is known (see also Chapter 3 and references therein). The combined evidence from rock-falls, subaqueous landslides, trenching, quaternary despites, geodetic evidence and historical earthquakes (Lemeille et al., 1999; Rodŕiguez-Pascua et al., 2000; Meghraoui, 2001; Becker et al., 2002; Monecke et al., 2004; Becker et al., 2005; Ferry et al., 2005; Monecke et al., 2006; Strasser et al., 2006; Strasser et al., 2013; Kremer et al., 2015; Reusch et al., 2016) is consistent with a return period of a M6.5 'Basle 1356 type' event in the region about every 1,500 – 5,000 years. Ferry et al. (2005) report five events on the Reinach fault in the past 1,200 or so years, or a recurrence of 2400 years, but not all of these are undisputed fault ruptures in large events. This recurrence was also the assessment of most of the PRP source experts in a late-stage elicitation by ENSI in spring 2015. Therefore, independent evidence suggests that hypothesis 1 can be rejected, while the alternative hypothesis 2 is consistent with the data. It is also the conservative choice.

We therefore decided to adjust our rate model in this one area such that the model is consistent with the paleo-seismic recurrence rates. We manually re-assigned the weights to ensemble model, in essence moving to the mean ensemble to the 84th percentile. Therefore, all grid nodes within the areal source zones 15 are assigned the following weights: The 84th percentile is assigned a weight of 68%, 13.5% weight are assigned to the 16th and 50th percentiles and 2.5% for the 2.5th and 97.5th percentiles.

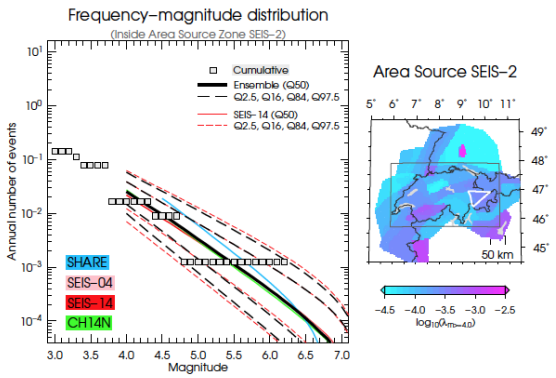

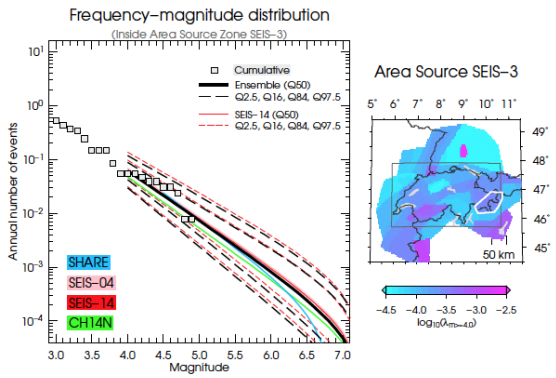

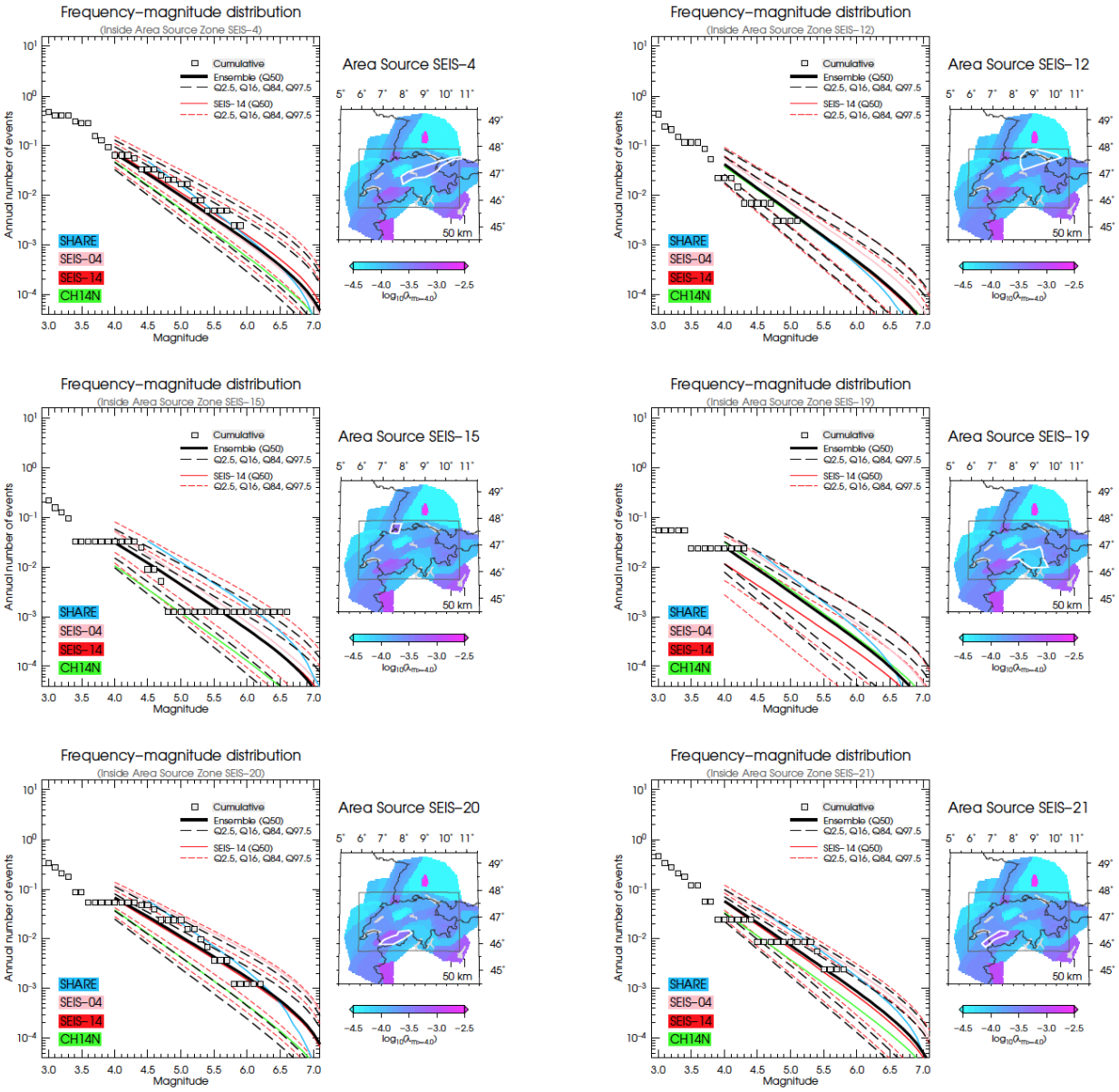

Figure 43: Magnitude rate distribution for selected area source zones. Maps show rate distribution of the median ensemble model and white polygons delineate respective area source zone.

To check the impact of this adjustment, and as an additional consistency check, we map out the average return period (in years) of very large events (M6.5 and larger, Figure 44). To do so, we sum up the rates of all grid nodes within a 50 km radius around every location on the map. The resulting map shows that such large events are expected at most about every 1500 years or so in the Valais, which is consistent with the historical record – the largest event recorded so far reached a M6.2 in 1852 near Visp. In the Basle area Figure 44 suggest that such an earthquake should occur about every 3,000 – 4,000 years, which is again consistent with the paleoseismic record.

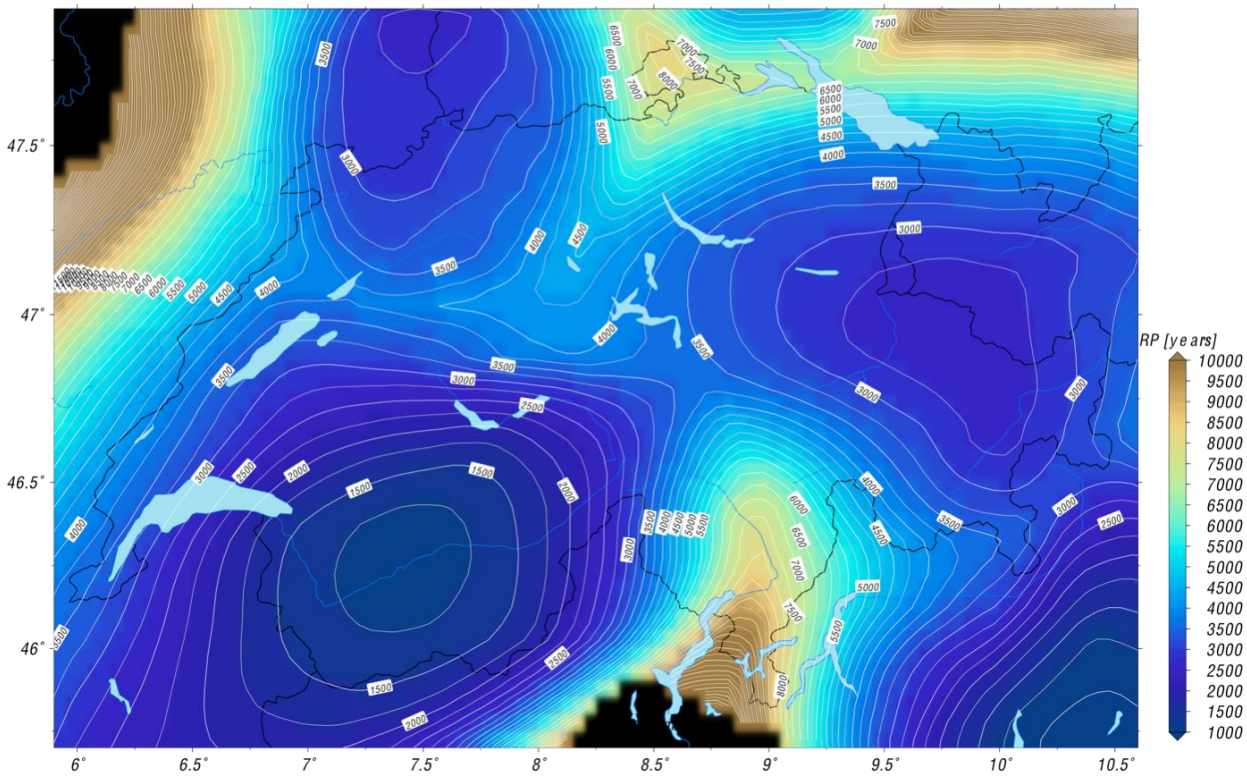

Figure 44: Average return period of a Magnitude 6.5 or larger earthquake within 50 km radius for any point in Switzerland. In the Basle area, this value is around 3000 years.

The SED model in the Basle region varies substantially from the PRP models that forecast a repeat of an M6.5 or larger event in the Basle source ranging between 8,400 years and 25,000 years, resulting in a combined mean of 15,000 years. The fact that the PRP model forecast diverges by a factor of 5 and more from the observed paleoseismic record was one of the primary criticisms raised by the ENSI review team[12]. Figure 44 serves also as a reminder that Switzerland is an earthquake country: No place in Switzerland is safe from being near to a magnitude 6.5 or larger earthquake, but in some places the recurrence times of such events is 3-4 times longer than in others.

We performed one additional consistency check by computing a so-called composite b-value map (Figure 45). This map analyzes the final rate forecast across all branches of the earthquake rates model within 50 km of each grid-node for the slope of the earthquake-size distribution. Because the composite b-value is influenced by many choices along the way (models, weight, Mmax etc.), it is not at all a given that the composite values are close to the original input. In our case (Figure 45), values range from about 0.82 to 0.95, with the lowest values near Basle and in the Valais and the highest in northeastern Switzerland. The distribution of values looks reasonable and may in fact offer some insights into tectonic processes, something to be investigated in future studies.

[12] ENSI Final Report: Review Approach and Comments Concerning the PEGASOS Refinement Project (PRP) and the PRP Summary Report. https://www.ensi.ch/en/documents/ensi-final-report-review-approach-and-comments-concerning-the-pegasos-refinement-project-prp-and-the-prp-summary-report/

This final earthquake rate model is then used as the input for hazard computations (Chapter 6).

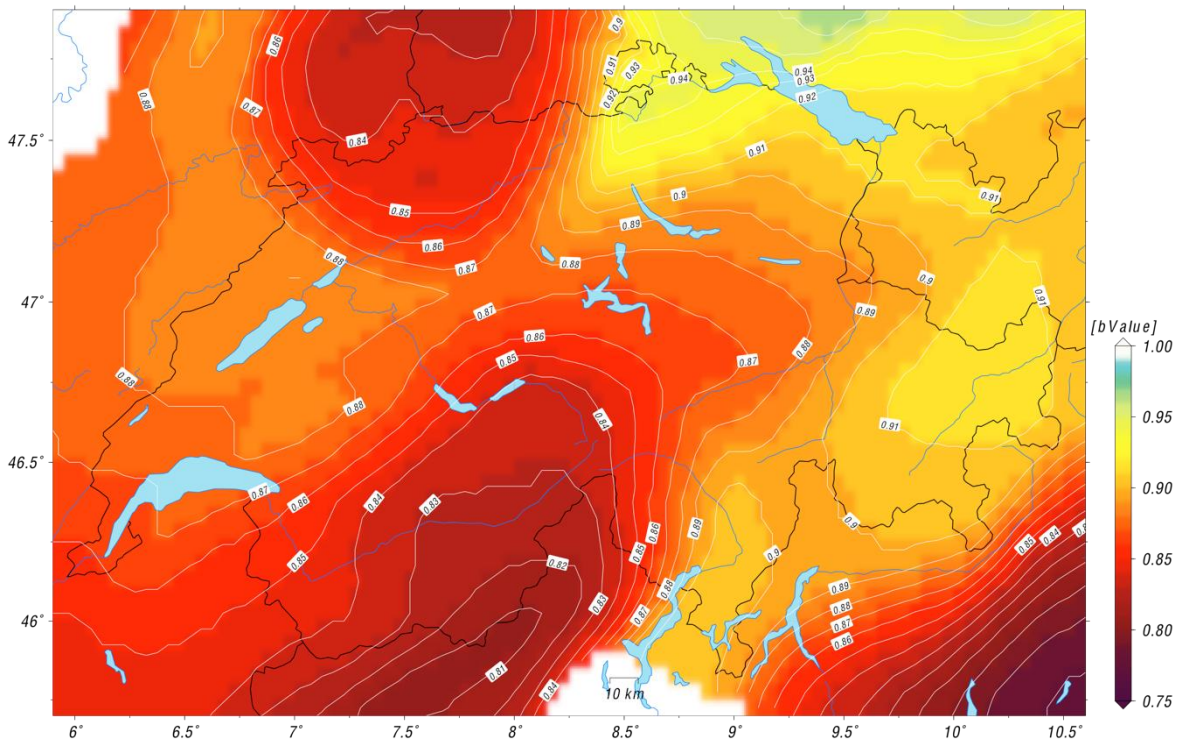

Figure 45: Composite b-value map of Switzerland, resulting from evaluating the resulting frequency-magnitude distribution of final combined model within 50 km of every grid node.

4.14 References

Baer, M., Deichmann, N., Braunmiller, J., Husen, S., Fäh, D., Giardini, D., Kästli, P., Kradolfer, U., and Wiemer, S. (2005). Earthquakes in Switzerland and surrounding regions during 2004. Eclogae Geologicae Helvetiae, 98(3): 407-418.

Becker, A., et al., (2002). Palaeoseismicity studies on end-Pleistocene and Holocene lake deposits around Basle, Switzerland. Geophysical Journal International 149, 659-678.

Becker, A., Ferry, M., Monecke, K., Schnellmann, M., Giardini, D., (2005). Multiarchive paleoseismic record of late Pleistocene and Holocene strong earthquakes in Switzerland. Tectonophysics 400, 153-177.

Bethmann, F., Deichmann, N., and Mai, P. M., 2011, Scaling Relations of Local Magnitude versus Moment Magnitude for Sequences of Similar Earthquakes in Switzerland: Bulletin of the Seismological Society of America, v. 101, no. 2, p. 515-534.

Bommer, J. J., Coppersmith, K. J., Coppersmith, R. T., Hanson, K. L., Mangongolo,A., Neveling, J., Rathje, E. M., Rodriguez-Marek, A., Scherbaum, F., Shelembe, R., Stafford, P. J., and Strasser, F. O. (2013). A SSHAC Level 3 Probabilistic Seismic Hazard Analysis for a New-Build Nuclear Site in South Africa. Earthquake Spectra.

Burkhard, M. and Grünthal, G. (2009). Seismic source zone characterization for the seismic hazard assessment project PEGASOS by the Expert Group 2 (EG1b). Swiss.

Cao, T., Petersen, M. & Reichle, M., 1996. Seismic hazard estimate from background seismicity in southern California, Bull. seism. Soc. Am.,

Coppersmith, K. J., Youngs, R. R., and Sprecher, C. (2009). Methodology and main results of seismic source characterization for the PEGASOS Project, Switzerland. Swiss Journal of Geosciences, 102(1):91-105.

Cornell, C. (1968). Engineering seismic risk analysis. Bulletin of the Seismological Society of America, 58(5):1583-1606.

Deichmann, N. (1992). Structural and rheological implications of lower-crustal earthquakes below northern Switzerland. Physics of the Earth and Planetary Interiors, 432 69(3-4):270-280.

Deichmann, N. and Giardini, D. (2009). Earthquakes Induced by the Stimulation of an Enhanced Geothermal System below Basel (Switzerland). Seismological Research Letters, 80(5):784-798.

Deichmann, N., Baer, M., Braunmiller, J., and Ballarin Dol_n, D. (2000). Earthquakes in Switzerland and surrounding regions during 1999. Eclogae Geologicae Helvetiae, 93(395).

Diehl, T., Deichmann, N., Clinton, J., Husen, S., Kraft, T., Plenkers, K., Edwards, B., Cauzzi, C., Michel, C., Kaestli, P., Wiemer, S., Haslinger, F., Fäh, D., Kradolfer, U., and Wössner, J. (2013). Earthquakes in Switzerland and surrounding regions during 2012. Swiss Journal of Geosciences, 106(3):543-558.

Edwards, B. and Fäh, D. (2013). A Stochastic Ground-Motion Model for Switzerland. Bulletin of the Seismological Society of America, 103(1):78-98. Fäh, D., Giardini, D., Bay, F., Braunmiller, J., Deichmann, N., Furrer, M., Gantner, L.,

Fäh, D., Giardini, D., Deichmann, N., Gisler, M., Schwarz-Zanetti, G., Alvarez-Rubio, S., Sellami, S., Edwards, B., Allmann, B., Bethmann, F., Wössner, J., Gassner-Stamm, G., Fritsche, S., and Eberhard, D. A. J. (2011). ECOS-09 earthquake catalogue of Switzerland release 2011 report and database. Report Swiss Seismological Service ETH Zurich, pages 1-42.

Ferry, M., Meghraoui, M., Delouis, B., Giardini, D., 2005. Evidence for Holocene palaeoseismicity along the Basel—Reinach active normal fault (Switzerland): a seismic source for the 1356 earthquake in the Upper Rhine graben. Geophysical Journal International 160, 554-572.

Frankel, A. D. (1995). Mapping seismic hazard in the central and eastern United States. Seismological Research Letters, 66(4):8-21.

Gardner, J. and Knopoff, L. (1974). Is the sequence of earthquakes in southern California, with aftershocks removed, Poissonian Bull. Seismol. Soc. Am, 64(5):1363-1367.

Giardini, D., Gruenthal, G., Shedlock, K., and Zhang, P. (1999). The GSHAP Global Seismic Hazard Map. Annals of Geophysics, 42(6):1225-1230.

Giardini, D., Wiemer, S., Faeh, D., and Deichmann, N., 2004, Seismic hazard assessment of Switzerland, 2004: SED internal report.

Giardini, D., Wössner, J., Danciu, L., Crowley, H., Cotton, F., Gruuenthal, G., Pinho, R., Valensise, G., Akkar, S., Arvidsson, R., Basili, R., Camelbeeck, T., Campos-Costa, A., Douglas, J., Demircioglu, M. B., Erdik, M., Fonseca, J., Glavatovic, B., Lindholm, C., Makropoulos, K., Meletti, F., Musson, R., Pitilakis, K., Sesetyan, K., Stromeyer, D., Stucchi, M., and Rovida, A. (2014). Seismic Hazard Harmonization in Europe (SHARE): Online Data Resource.

Gisler, M., Isenegger, D., Jimenez, M. J., Kästli, P., Koglin, R., Masciadri, V., Rutz, M., Scheidegger, C., Schibler, R., Schorlemmer, D., Schwarz-Zanetti, G., Steimen, S., Sellami, S., Wiemer, S., andWössner, J. (2003). Earthquake catalogue of Switzerland (ECOS) and the related macroseismic database. Eclogae geol. Helv., 96:219-236.

Grünthal, G. (1999). Seismic hazard assessment for Central, North and Northwest Europe: GSHAP Region 3. Annals of Geophysics, 42(6): 999-1011.

Grünthal, G., Mayer-Rosa, D., and Lenhardt, W. A. (1998). Abschätzung der Erdbebengefährdung für die D-A-CH- Staaten - Deutschland, Österreich, Schweiz.Bautechnik, 75(10):753-767.

Goertz-Allmann, B. P., Edwards, B., Bethmann, F., Deichmann, N., Clinton, J., Fah, D., and Giardini, D., 2011, A New Empirical Magnitude Scaling Relation for Switzerland: Bulletin of the Seismological Society of America, v. 101, no. 6, p. 3088-3095.

Hardebeck, J. L. and Hauksson, E. (2001). Stress Orientations Obtained from Earthquake Focal Mechanisms: What Are Appropriate Uncertainty Estimates? Bulletin of the Seismological Society of America, 91(2):250-262.

Häring, M. O., Schanz, U., Ladner, F., and Dyer, B. C. (2008). Characterisation of the Basel enhanced geothermal system. Geothermics, 37(5):469-495.

Helmstetter, A., Kagan, Y. Y., and Jackson, D. D. (2006). Comparison of Short-Term and Time-Independent Earthquake Forecast Models for Southern California. Bulletin of the Seismological Society of America, 96(1):90-106.

Helmstetter, A., Kagan, Y.Y. & Jackson, D.D., 2007. High-resolution time independent grid-based forecast for M > = 5 earthquakes in California, Seism. Res. Lett., 78(1), 78–86.

Helmstetter, a.&Werner,M.J., 2012. Adaptive spatiotemporal smoothing of seismicity for long-term earthquake forecasts in California, Bull. seism. Soc. Am., 102(6), 2518–2529.

Hiemer, S., J. Woessner,R. Basili, L. Danciu, D. Giardini and S. Wiemer, (2014), A smoothed stochastic earthquake rate model considering seismicity and fault moment release for Europe, Geophys. J. Int., 198, 1159–1172, doi: 10.1093/gji/ggu186.

Hiemer, S., Jackson, D.D.,Wang, Q., Kagan, Y.Y.,Woessner, J., Zechar, J.D. &Wiemer, S., (2013). A stochastic forecast of California earthquakes based on fault slip and smoothed seismicity, Bull. seism. Soc. Am., 103(2A), 799–810.

Husen, S., Kissling, E., Deichmann, N., Wiemer, S., Giardini, D., and Baer, M. (2003). Probabilistic earthquake location in complex three-dimensional velocity models: Application to Switzerland. Journal of Geophysical Research, 108(B2):2077.

Jackson, D.D. & Kagan, Y.Y., 1999. Testable earthquake forecasts for 1999, Seism. Res. Lett., 70(4), 393–403.

Jimenez, M. J., Giardini, D., and Gruenthal, G. (2003). The ESC-SESAME Unified Hazard Model for the European-Mediterranean region. CSEM / EMSC Newsletter,19:2-4.

Johnston, A., Coppersmith, K., Kanter, L., and Cornell, C. (1994). The earthquakes of stable continental regions - Assessment of large earthquake potential. EPRI Report TR-102261-V1, 2-1-98.

Jordan, T.H., 2006. Earthquake predictability, brick by brick, Seism. Res. Lett., 77(1), 3–6.

Journal of Geosciences, 102(1):149-188.

Kagan, Y. Y. and Jackson, D. D. (2012). Whole Earth high-resolution earthquake forecasts. Geophysical Journal International, 190(1):677-686.

Kagan, Y.Y. & Jackson, D.D., (1994). Long-term probabilistic forecasting of earthquakes, J. geophys. Res., 99(B7), 13 685–13 700.

Kastrup, U., Zoback, M. L., Deichmann, N., Evans, K. F., Giardini, D., and Michael, A. J. (2004). Stress field variations in the Swiss Alps and the northern Alpine foreland derived from inversion of fault plane solutions. Journal of Geophysical Research,109(B1):B01402.

Kremer et al., Lake sediment records as earthquake catlogue : limitations and perscpectives, submitted to Quaternary Science Reviews

Kremer, K., Hilbe, M., Simpson, G., Decrouy, L., Wildi, W., Girardclos, S., 2015. Reconstructing 4000 years of mass movement and tsunami history in a deep peri-Alpine lake (Lake Geneva, France-Switzerland). Sedimentology 62, 1305-1327.

Lapajne, J., Motnikar, B.S. & Zupancic, P., 2003. Probabilistic seismic hazard assessment methodology for distributed seismicity, Bull. seism. Soc. Am., 93(6), 2502–2515.

Lemeille, F., Cushing, M., Carbon, D., Grellet, B., Bitterli, T., Flehoc, C., Innocent, C., 1999. Co-seismic ruptures and deformations recorded by speleothems in the epicentral zone of the Basel earthquake. Geodinamica Acta 12, 179-191.

Marschall, I., Deichmann, N., and Marone, F. (2013). Earthquake focal mechanisms and stress orientations in the eastern Swiss Alps. Swiss Journal of Geosciences, 106(1):79-90.

Meghraoui, M., 2001. Active normal faulting in the Upper Rhine Graben and paleoseismic identification of the 1356 Basel earthquake (vol 293, pg 2070, 2001). Science 294, 57-57.

Michael, A. J. (1984). Determination of Stress from Slip Data: Faults and Folds. Journal of Geophysical Research, 89:517-526.

Michael, A. J. (1987). Use of focal mechanisms to determine stress: A control study. Journal of Geophysical Research, 92(B1):357.

Monecke, K., Anselmetti, F.S., Becker, A., Schnellmann, M., Sturm, M., Giardini, D., 2006. Earthquake-induced deformation structures in lake deposits: A late Pleistocene to holocene paleoseismic record for central Switzerland. Eclogae Geologicae Helvetiae 99, 343-362.

Monecke, K., Anselmetti, F.S., Becker, A., Sturm, M., Giardini, D., 2004. The record of historic earthquakes in lake sediments of Central Switzerland. Tectonophysics 394, 21-40.

Musson, R. (2000). The use of Monte Carlo simulations for seismic hazard assessment in the UK. Annals of Geophysics, 43(1).

Musson, R. M. W., Sellami, S., and Bruestle, W. (2009). Preparing a seismic hazard model for Switzerland: the view from PEGASOS Expert Group 3 (EG1c). Swiss Journal of Geosciences, 102(1):107-120.

NAGRA (2004). Probabilistic Seismic Hazard Analysis for Swiss Nuclear Power Plant Sites (PEGASOS Project), Final Report. Technical report.

Pavoni, N., Maurer, H. R., Roth, P., and Deichmann, N. (1997). Seismicity and seismotectonics of the Swiss Alps, deep structures of the Swiss Alps, results of NRP 20. Birkhaeuser, Basel, Switzerland, pages 241-250.

Reinecker, J., Tingay, M., Mueller, B., and Heidbach, O. (2010). Present-day stress orientation in the Molasse Basin. Tectonophysics, 482(1-4):129-138.

Reiter, L. (1990). Earthquake hazard analysis: Issues and insights. Columbia University Press (New York).

Renault, P., Heuberger, S., and Abrahamson, N. A. (2010). PEGASOS Refinement Project: An improved PSHA for Swiss nuclear power plants. Proceedings of 14ECEE5 European Conference of Earthquake Engineering, page Paper ID 991.

Reusch, A., Moernaut, J., Anselmetti, F.S., Strasser, M., 2016. Sediment mobilization deposits from episodic subsurface fluid flow—A new tool to reveal long-term earthquake records? Geology 44, 243-246.

Rhoades, D.A. & Stirling, M.W., 2012. An earthquake likelihood model based on proximity to mapped faults and cataloged earthquakes, Bull. seism. Soc. Am., 102(4), 1593–1599.

Rodŕiguez-Pascua, M.A., Calvo, J.P., De Vicente, G., Gómez-Gras, D., 2000. Soft-sediment deformation structures interpreted as seismites in lacustrine sediments of the Prebetic Zone, SE Spain, and their potential use as indicators of earthquake magnitudes during the Late Miocene. Sedimentary Geology 135, 117-135.

Ruettener, E. (1995). Earthquake hazard evaluation for Switzerland. Matériaux pour la Géologie de la Suisse, Géophysique No 29 publié par la Commission Suisse de Geophysique. Schweizerischer Erdbebendienst, Zuerich, page 106.

Ruettener, E., Egozcue, J. J., Mayer-Rosa, D., and Mueller, S. (1996). Bayesian estimation of seismic hazard for two sites in Switzerland. Natural Hazards, 14(2-3):165-178.

Saegesser, R. and Mayer-Rosa, D. (1978). ErdbebengeFährdung in der Schweiz. Schweizerische Bauzeitung SIA, 78:3-18.

Schmid, S. M. and Slejko, D. (2009). Seismic source characterization of the Alpine foreland in the context of a probabilistic seismic hazard analysis by PEGASOS Expert Group 1 (EG1a). Swiss Journal of Geosciences, 102(1):121-148.

Schorlemmer, D., Zechar, J.D., Werner, M.J., Field, E.H., Jackson, D.D. & Jordan, T.H., 2010. First results of the regional earthquake likelihood models experiment, Pure appl. Geophys., 167(8-9), 859–876.

Silverman, B. W. (1986). Density Estimation for Statistics and Data Analysis. Monographs on Statistics and Applied Probability, Chapman and Hall, London.

Stirling, M.W. et al., 2012. National seismic hazard model for New Zealand: 2010 update, Bull. seism. Soc. Am., 102(4), 1514–1542.

Strasser, M., Anselmetti, F.S., Fäh, D., Giardini, D., Schnellmann, M., 2006. Magnitudes and source areas of large prehistoric northern Alpine earthquakes revealed by slope failures in lakes. Geology 34, 1005-1008.

Strasser, M., Monecke, K., Schnellmann, M., Anselmetti, F.S., 2013. Lake sediments as natural seismographs: A compiled record of Late Quaternary earthquakes in Central Switzerland and its implication for Alpine deformation. Sedimentology 60, 319-341.

Stucchi, M., Rovida, A., Gomez Capera, a. a., Alexandre, P., Camelbeeck, T., Demircioglu, M. B., Gasperini, P., Kouskouna, V., Musson, R. M. W., Radulian, M., Sesetyan, K., Vilanova, S., Baumont, D., Bungum, H., Fäh, D., Lenhardt, W., Makropoulos, K., Martinez Solares, J. M., Scotti, O., Z_iv_ci_c, M., Albini, P., Batllo,J., Papaioannou, C., Tatevossian, R., Locati, M., Meletti, C., Vigano_, D., and Giardini, D. (2012). The SHARE European Earthquake Catalogue (SHEEC) 1000-1899.Journal of Seismology, 17(2):523-544.

van Stiphout, T., Zhuang, J., and Marsan, D. (2012). Models and Techniques for Analyzing Seismicity: Seismicity Declustering. Community Online Resource for Statistical Seismicity Analysis, pages 1-25.

Wagner, M., Kissling, E., and Husen, S. (2012). Combining controlled-source seismology and local earthquake tomography to derive a 3-D crustal model of the western Alpine region. Geophysical Journal International, 191(2):789-802.

Weichert, D. (1980). Estimation of the earthquake recurrence parameters for unequal observation periods for different magnitudes. Bulletin of the Seismological Society of America, 70(4):1337-1346

Werner, M. J., Helmstetter, A., Jackson, D. D., and Kagan, Y. Y. (2011). High-Resolution Long-Term and Short-Term Earthquake Forecasts for California. Bulletin of the Seismological Society of America, 101(4):1630-1648.

Werner, M.J., Helmstetter, A., Jackson, D.D. & Kagan, Y.Y., 2011. High resolution long-term and short-term earthquake forecasts for California, Bull. seism. Soc. Am., 101(4), 1630–1648.

Wheeler RL (2009) Methods of Mmax estimation east of the Rocky Mountains: U.S. Geological Survey Open-File Report 2009–1018, 43 p., accessed on November 15, 2015, at http://pubs.usgs.gov/of/2009/1018/.

Wiemer, S., and Baer, M., 2000, Mapping and removing quarry blast events from seismicity catalogs: Bulletin of the Seismological Society of America, v. 90, p. 525-530.

Wiemer, S. and Wyss, M. (2000). Minimum Magnitude of Completeness in Earthquake Catalogs: Examples from Alaska, the Western United States, and Japan. Bulletin of the Seismological Society of America, 90(4):859-869.

Wiemer, S., Garcia-Fernandez, M., and Burg, J.-P. (2009a). Development of a seismic source model for probabilistic seismic hazard assessment of nuclear power plant sites in Switzerland: the view from PEGASOS Expert Group 4 (EG1d). Swiss Journal of Geosciences, 102(1):189-209.

Wiemer, S., Giardini, D., Fäh, D., Deichmann, N., and Sellami, S. (2009b). Probabilistic seismic hazard assessment of Switzerland: best estimates and uncertainties. Journal of Seismology, 13(4):449-478.

Woo, G., 1996. Kernel estimation methods for seismic hazard area source modelling, Bull. seism. Soc. Am., 86(2), 353–362.

Wössner, J. and Wiemer, S. (2005). Assessing the Quality of Earthquake Catalogues: Estimating the Magnitude of Completeness and Its Uncertainty. Bulletin of the Seismological Society of America, 95(2):684-698.

Wössner, J., Danciu, L., Crowley, H., Cotton, F., Gruenthal, G., Valensise, G., Arvidsson, R., Basili, R., Demircioglu, M. B., Hiemer, S., Meletti, C., Musson, R. M. W., Rovida, A., Sesetyan, K., and Stucchi, M. (2014). The 2013 European Seismic Hazard Model - Key Components and Results (in prep.). Journal of Seismology.

Zechar, J.D., Gerstenberger, M.C. & Rhoades, D.A., (2010). Likelihood- Based Tests for Evaluating Space-Rate-Magnitude Earthquake Forecasts, Bull. seism. Soc. Am., 100(3), 1184–1195.

Zechar, J.D., Schorlemmer,D.,Werner, M.J.,Gerstenberger,M.C., Rhoades, D.a. & Jordan, T.H., (2013). Regional earthquake likelihood models I: first order results, Bull. seism. Soc. Am., 103(2A), 787–798.

5. Assessment, adjustment and weighting of ground motion prediction models

5.1 Introduction

Lying between the seismically active region of Italy to the south, and the low-seismicity regions of northern Europe, earthquake activity in Switzerland can be described as moderate (Giardini *et al.*, 2014). Over the entire region earthquakes with moment magnitude M_W 5 are expected approximately every 10 years, and M_W 6 every 100 years. The most recent significant event, with M_W 5.8 (Earthquake Catalogue of Switzerland, ECOS09; Fäh *et al.*, 2011), occurred in Sierre, Canton Valais, on the 25th January, 1946. The epicentral intensity reached degree VIII on the European Macroseismic Scale (EMS-98), corresponding to moderate to significant damage within a radius of about 25 km. A strong aftershock (M_W ~ 5.5) with significant secondary effects (landslides, rockfalls, *etc.*) followed closely afterwards on the 30th May. This is by no means unusual for the region of Valais, which dominates the national seismic hazard (Wiemer *et al.*, 2009), with significant events (around M_W 6 or greater) having occurred in 1524, 1584, 1685, 1755, 1855 and 1946 (Fritsche and Fäh, 2009). The strongest documented earthquake (M_W 6.6, EMS-98 epicentral intensity IX) to have occurred in central Europe was located in the region of Basle (at the border among Switzerland, France and Germany) in 1356, with significant destruction to the city (Fäh *et al.*, 2009).

Based on well documented historical seismicity in Switzerland (Gisler *et al.*, 2003, Schwarz-Zanetti *et al.*, 2003, Gisler *et al.*, 2004a, Gisler *et al.*, 2004b, Gisler *et al.*, 2004c, Schwarz-Zanetti *et al.*, 2004, Fritsche *et al.*, 2006, Gisler *et al.*, 2007, e.g., Fäh *et al.*, 2009, Fritsche *et al.*, 2009, Fritsche *et al.*, 2012), seismic hazard is clearly an important issue to address. The topic has seen significant focus and progress in the last 15 years. Between 2000 and 2004 a multi-national research project (Probabilistic Seismic Hazard Analysis for Swiss Nuclear Power Plant Sites, PEGASOS) was undertaken by *swissnuclear,* the nuclear energy section of the *swisselectric* group (Abrahamson *et al.*, 2002). In parallel the Swiss Seismological Service (SED) undertook a national seismic hazard assessment (Wiemer *et al.*, 2009), leading to the previous national seismic hazard map to be delivered in 2004. In follow up to the PEGASOS project, *swissnuclear* undertook a Senior Seismic Hazard Analysis Committee (SSHAC) Level 4 seismic hazard assessment project (PEGASOS Refinement) from 2008 to 2014 (Renault, 2014). On a wider scale, the EU project Seismic Hazard Harmonization in Europe (SHARE), which began in 2009, resulted in Europe-wide seismic hazard maps, published in 2013 (Woessner *et al.*, 2015).

This paper forms part of the scientific documentation of the most recent assessment of the national seismic hazard by the SED, with the final national seismic hazard maps delivered in 2015 (see section: Data and Resources). The national seismic hazard is assessed using the probabilistic approach originally developed by Cornell (1968). This approach integrates possible earthquake sources and their resulting ground-motion fields over time. This paper focuses on the latter component, *i.e.*, the definition of ground-motion fields for prescribed earthquake sources. However, a brief summary of the earthquake source model used as input to the 2015 Swiss seismic hazard maps is given here for completeness. The earthquake source model combines four components: the original area source model of the 2004 Swiss Hazard Model (Giardini *et al.*, 2004), the relevant area sources of the 2013 European Seismic Hazard (SHARE) Model (Woessner *et al.*, 2015), an updated version of the 2004 area sources and a newly developed smoothed-seismicity model conceptually similar to that presented by Hiemer *et al.* (2014). The first two models were inherited entirely without modification from the original seismic source models. The latter two are newly developed to reflect the latest seismicity observations and harmonization of the earthquake catalogue (ECOS-09, Fäh *et al.* (2011)). A penalized-maximum likelihood method was used for recurrence rate parameter estimation and the EPRI approach for estimating the maximum magnitude, as described by (Johnston *et al.*, 1994, Hiemer *et al.*, 2014). The four seismic source models are

weighted per magnitude bins in an ensemble earthquake rate forecast. Each model is characterized by a recurrence rate distribution for each magnitude and five branches are sampled to represent the uncertainties of the earthquake recurrence rates for each magnitude bin. The five earthquake rate branches (Figure 46) are spatially distributed over a grid of point sources that covers Switzerland and border regions. The resulting earthquake scenarios, accounting for uncertainties of seismicity patterns, earthquake completeness in time and space, style-of faulting, seismicity depth-distribution, maximum magnitude and earthquake recurrence parameters are then used as input to the ground motion prediction equations in order to estimate probabilities of exceedance for different ground motion levels.

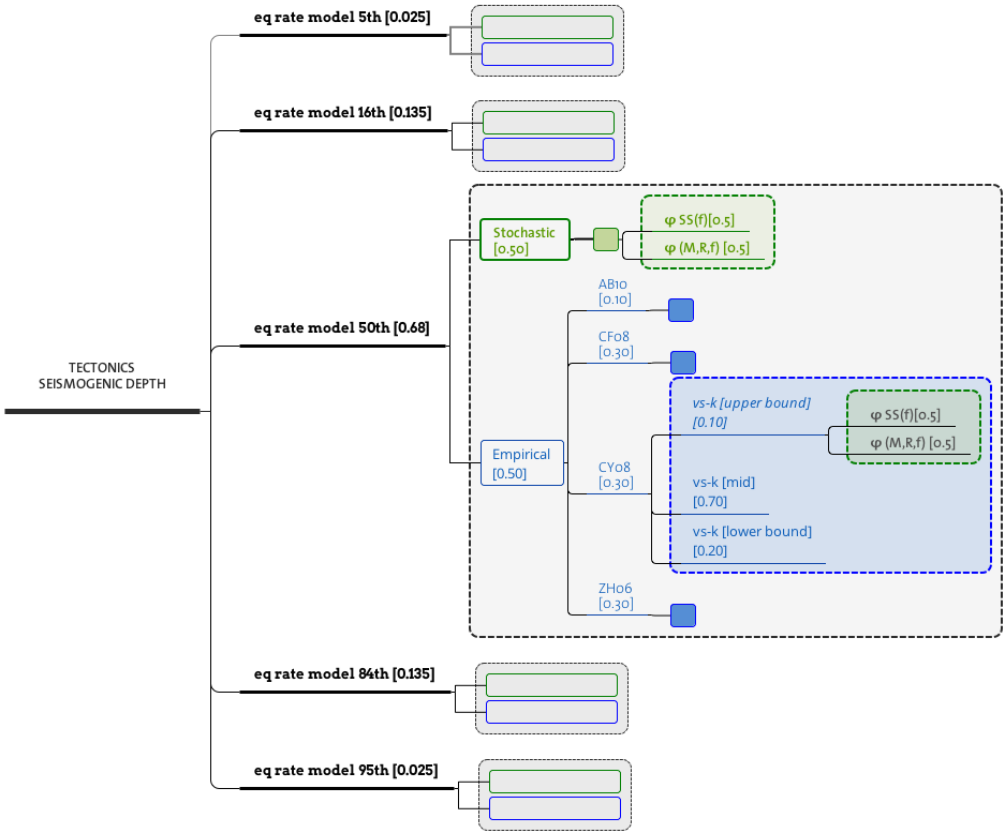

Figure 46: Master logic tree depicting the earthquake rate forecast models and the ground motion models. Empty branches indicate a repetition of the ground motion branches (stochastic and empirical). Abbreviations are described in the text.

The prediction of earthquake ground-motions is non-trivial due to the complex nature of earthquake sources and wave-propagation through complex media. While deterministic models using either kinematic or dynamic rupture representations are produced for well-studied earthquakes and/or active faults (e.g., Graves and Pitarka, 2010, Dalguer *et al.*, 2008), the significant uncertainty of input parameters for future earthquakes means that simplifications and assumptions have to be made. In practice this is done through the development of ground-motion prediction equations (GMPEs), which act as a statistical tool to provide the expected mean and standard deviation of (logarithmically transformed) ground-motions for a given set of simplified earthquake descriptors (predictors, explanatory variables). The main predictor variables in current GMPEs are earthquake magnitude, a measure of source-to-site distance, style of faulting (*i.e.,* normal, reverse or strike-slip) and one or more terms to describe the local site classification (upper 30 m time-averaged shear-wave velocity, depth to bedrock, *etc.*). GMPEs are calibrated based on either empirical data or simulated data. Different authors have developed models for global mixtures of events (*e.g.*, the Next Generation Attenuation database (Chiou *et al.*, 2008), only regional events (*e.g.*, the European and Middle East database (Akkar *et al.*, 2014)), or only local events (*e.g.*, Japanese database (Zhao *et al.*, 2006)). Differences in GMPEs arise from using different datasets, raising an open question as to the regional effects on ground-motion (Stafford, 2014).

5.2 GMPE selection

Despite the recent development of a modern and dense seismic network (Clinton *et al.*, 2011, Michel *et al.*, 2014, Cauzzi and Clinton, 2013, Diehl *et al.*, 2013, Diehl *et al.*, 2014) the availability of GMPEs specifically developed for Switzerland is significantly limited due to a recent quiescence in seismicity. In fact, the largest events recorded on modern instrumentation have all occurred outside Swiss borders: for example, the St. Dié, France, earthquake with M_L 5.3 (M_W 4.6); the 1999 Bormio, Italy, event with M_L 4.9 (M_W 4.9); and the 2004 Garda, Italy, event with M_L 5.0 (M_W 5.0). The largest event to have recently occurred within Swiss borders was the 1991 Vaz earthquake with M_L 5.0 (M_W 4.7). This lack of strong-motion data leaves two main options for the development of regional GMPEs: the use of data from other, more seismically active regions of the world; or the simulation of ground-motion data.

Availability and selection of empirical models

Due to the high number of available GMPEs developed around the world, strict selection criteria are often used to limit our choice to the required number of models (Bommer *et al.*, 2010). Previous GMPEs selected for use in Switzerland in the recent SHARE project and the two PEGASOS projects are given in Table 2. The SHARE project segregated Switzerland into two broad tectonic regions, stable continental to the north, and shallow active to the south. Such a distinction is strongly debated, however GMPEs used for the two regions present a great deal of overlap (Table 2).

Since the end of the SHARE and PEGASOS PSHA projects, and during the course of the current national seismic hazard project, several high-quality new GMPEs became available. Notably the Next Generation Attenuation (NGA) West 2 dataset (Ancheta *et al.*, 2014) based models (Gregor *et al.*, 2014), the European and Middle East RESORCE dataset (Akkar *et al.*, 2014) based models (Douglas *et al.*, 2014) and a major update of the broadband prediction model of the Cauzzi and Faccioli (2008) GMPE (Cauzzi *et al.*, 2015b). Despite the availability of these equations arising during the current project, which began in 2013, it was decided not to implement them. The reason for this was primarily due to the fact that significant testing and verification had been carried out on the existing GMPEs over the course of other recent hazard projects. This was not the case for the newly published equations: *errata* to any of the models would prove extremely costly due to the numerous stages of conversion required for implementation in Switzerland. Based on their implementation and testing in previous projects we therefore decided to select the following four empirical GMPEs: Akkar and Bommer (2010), Chiou and Youngs (2008), Cauzzi and Faccioli (2008) and Zhao *et al.* (2006) (Table 2). Hereinafter the models are referred to as AB10, CY08, CF08 and ZETAL06 respectively. The chosen predictive models are the same used in project SHARE for regions with active shallow crustal seismicity. AB10 is generally considered to be representative of Euro-Mediterranean seismicity, since it is based on data from the European and Middle East strong ground motion database (Ambraseys *et al.*, 2004). A significant limitation of this model is the use of simple site classification (rock, stiff soil, soft soil, very soft soil), which introduces large uncertainties if site amplification and attenuation adjustments are implemented. Despite being based on worldwide data (the NGA database) with primarily Californian events for moderate magnitudes, CY08 was found to be suitable for ground motion prediction in the greater European region by Delavaud *et al.* (2012). CY08 use a more sophisticated ground type classification based on $V_{S,30}$, making host to site adjustments somewhat easier. $V_{S,30}$ is used also by CF08, a global model dominated by Japanese data, with a significant contribution from Italian data at small-to-moderate magnitudes. Notable in CF08 is the use of digital recordings only and a careful characterisation of the geophysical properties of the recording sites. ZETAL06 uses exclusively Japanese data, with site classification based on natural period. A comprehensive overview of the functional forms, prediction variables and recommended magnitude and distance application ranges for the aforementioned empirical GMPEs is given in Douglas (2015) (see Data and Resources).

Cua and Heaton (2008) developed a model for predicting peak ground acceleration (*PGA*) and velocity (*PGV*) by combining weak motion recordings from Switzerland with strong-motion recordings from the Next Generation Attenuation (NGA) (Power *et al.*, 2008) database (Chiou *et al.*, 2008). The Cua and Heaton (2008) equations have been the basis for the *ShakeMap* (Worden *et al.*, 2010) implementation at the Swiss Seismological Service until their recent revision in 2014 (Cauzzi *et al.*, 2015a). The model is, however, not used in the Swiss national seismic hazard assessment since it does not cover response spectral ordinates (elastic 5 %-damped pseudo-spectral acceleration) over a broad vibration period range, which will form the basis of the hazard analyses.

	SHARE (stable continental regions)	SHARE (active shallow crustal regions)	PEGASOS Refinement	Swiss Hazard 2014	Reference
AB06 *			(•)		(Atkinson and Boore, 2006)
AB10	•	•	•	•	(Akkar and Bommer, 2010)
AC10			•		(Akkar and Cagnan, 2010)
AS08			•		(Abrahamson and Silva, 2008)
BA08			•		(Boore and Atkinson, 2008)
BETAL11			(•)		(Bindi *et al.*, 2011)
CA03 *	•				(Campbell, 2003)
CB08			•		(Campbell and Bozorgnia, 2008)
CF08	•	•		•	(Cauzzi and Faccioli, 2008)
CY08	•	•	•	•	(Chiou and Youngs, 2008)
TO02 *	•		(•)		(Toro *et al.*, 1997)
ZETAL06		•	•	•	(Zhao *et al.*, 2006)
EF13 *			•	•	(Edwards and Fäh, 2013b)

* indicates simulation based models. • = GMPEs that were used; (•) = GMPEs that were evaluated but not used.

Table 2: Overview of GMPEs used in recent seismic hazard projects in Switzerland.

Available simulation based models

In order to overcome the issue of limited strong motion data in Switzerland, Bay *et al.* (2005) built on their earlier work (Bay *et al.*, 2003) by implementing the stochastic point-source ground-motion simulation method, as described in detail by Boore (2003). The stochastic simulation approach and related random-vibration theory techniques (e.g., Cartwright and Longuet-Higgins, 1956, Hanks and Mcguire, 1981) rely on the observation that high-frequency earthquake acceleration time-series can be approximated by duration-limited random-phase signal, with frequency content modulated by a simple representation of the earthquake source, path and site effects. The synthetic GMPE of Bay *et al.* (2005) was used for the 2004 Swiss national hazard maps (Wiemer *et al.*, 2009), providing predictions at vibration frequencies between 1 Hz and 15 Hz.

A significant issue related to point source models is their applicability for larger earthquakes, where finite-ruptures tend to spread the radiated energy over a wider source region. Point source simulation models therefore significantly over-estimate ground-motions from large earthquakes in the near-field region. Recent improvements to stochastic simulation methods have introduced either finite sources composed of numerous sub-faults (Motazedian and Atkinson, 2005), or geometrical effects to account for near-source saturation effects (Atkinson and Silva, 2000, Rietbrock *et al.*, 2013). While the sub-fault solution is more flexible, it also requires more input parameters, including knowledge of the hypocentre location. For the purposes of ground-motion prediction in Switzerland this is not known *a priori*. In contrast, Boore (2009) showed that for randomised hypocentre locations the so called effective distance measure (R_{EFF}), in practice a geometrical adjustment, produces saturation effects (which are magnitude–, distance–, and period-dependent) comparable to sub-fault models and to the observations of real earthquakes.

With this background, Edwards and Fäh (2013b) developed a stochastic ground-motion simulation model for Switzerland based on their and others' earlier work characterising attenuation (Edwards

et al., 2011) and crustal amplification (Poggi *et al.*, 2011) in the greater Swiss region. The model was based on the spectral analysis of Swiss earthquakes recorded on the broadband seismic network, and was calibrated at high magnitudes to historical macroseismic observations (Fäh *et al.*, 2011). Their model provides elastic 5 %-damped pseudo-spectral acceleration *PSA* at vibration periods between *PGA* (0 s) and 2 s, and *PGV*. The predictions are for a well-defined reference rock profile (Poggi *et al.*, 2011), with differentiation between Foreland and Alpine motions. The use of a reference rock velocity profile marked a significant improvement on previous empirical and simulation-based models, which left the reference rock profile unknown (only defined, for example by a site class, or $V_{S,30}$ range). The model of Edwards and Fäh (2013b) for the Swiss Foreland was used in the PEGASOS Refinement project and has recently been integrated into the *ShakeMap* implementation at the SED (Cauzzi *et al.*, 2015a, Cauzzi *et al.*, 2014) through parameterisation into a functional form allowing its implementation into the OpenQuake hazard engine (Silva *et al.*, 2014). As part of the comprehensive quality assurance process the model was tested against free-field surface accelerometer data from Japan (KiKNet), where it was found to provide – after adjustment for regional effects – predictions comparable with existing GMPEs for the region for magnitudes up to M_w 7. For this project we therefore implement the parameterized version (Cauzzi *et al.*, 2015a) of the model of Edwards and Fäh (2013b). The regional components (Alpine and Foreland) are used, however rather than the fixed stress parameter of 6 MPa suggested by Edwards and Fäh (2013b), we use a variable source stress-parameter to account for epistemic uncertainty in the model (e.g., Douglas *et al.*, 2013, Edwards and Douglas, 2013, Bommer *et al.*, 2016). This is calibrated based on testing against macroseismic intensity data points [as discussed in Cauzzi *et al.* (2015a)]. The previously developed model by Bay *et al.* (2005), as implemented in the previous national seismic hazard maps, is not used due to the fact that it is entirely point-source based and therefore does not provide reasonable predictions in the near-field of large earthquakes, nor does it refer to a well-constrained velocity profile.

5.3 Empirical GMPEs: calibration and adjustment

Following the approaches of the SHARE and PEGASOS Refinement projects, the selected empirical GMPEs were adjusted to account for Swiss rock reference conditions and extension to smaller magnitudes.

V_S-κ_0 adjustments

Two principal elements make up the site component of ground motion predictions as input to PSHA: elastic amplification, and near surface site-specific attenuation. Elastic amplification and to some extent the associated attenuation can be considered a direct consequence of the local velocity profile beneath the site. Non-linearity (*e.g.* soil plasticity) also plays a role at high levels of shaking at particular soil sites. However, this is generally assumed to be regionally independent (*i.e.* a property only of the soil, and therefore $V_{s,30}$) and described either implicitly or explicitly by individual GMPEs. Also, non-linearity is of comparably lesser importance for shaking predictions at rock sites.

Kappa (κ) controls the high-frequency decay of the Fourier amplitude spectrum (FAS) of earthquake ground-motion (Anderson and Hough, 1984) and has a significant impact on the results of PHSA at high vibration frequencies (Renault, 2014). Its site-specific zero-distance component (κ_0) represents the attenuation of shear waves below and near a given site due to the mechanical and geophysical properties of the subsurface geo-materials. The host-to-target adjustment, often referred to as V_S-κ_0 adjustment, aims at mapping changes in the velocity profiles from the host region (implicitly defined in the GMPE) to the target region: in this case, Switzerland.

The target velocity profile forms part of the definition of the hazard model. In this study we use the velocity model of Poggi *et al.* (2011) and associated amplification. By design, therefore, there

is no epistemic uncertainty associated to the reference rock profile in the target region. Epistemic uncertainty in the near surface attenuation for this reference velocity profile is considered to be captured by the alternative use of (a) the model by Anderson and Hough (1984) with $\kappa_0 = 0.0159\,s$ (Edwards *et al.*, 2011) and (b) $\kappa_0 = 0.0260\,s$ (Poggi *et al.*, 2013), the former being consistent with the simulation model of Edwards and Fäh (2013b).

We employ a systematic approach to account for the differences in host (GMPE based) velocity profiles, as detailed in (Al Atik *et al.*, 2014). This approach has the advantage that, unlike other approaches for determining κ_0 from response spectra, no assumption of the background seismological model (e.g., *Q*, Δσ, etc.) is required. Frequency-dependent adjustment functions $C_{FAS,Vs-\kappa_0}$ are initially determined based on the ratio of the predicted FAS at rock reference sites in the host and target region for a given scenario:

$$C_{FAS,Vs-\kappa_0}(f) = \frac{A_{target}(f)}{A_{host}(f)} e^{-\pi f(\kappa_{0,target}-\kappa_{0,host})} \approx \frac{\mathrm{FAS_{target}}}{\mathrm{FAS_{GMPE}}}(f) \quad (1)$$

with A describing amplification and κ_0 attenuation in the GMPE (host) and target regions. Using the host and target velocity profiles, amplification, *A,* was determined through 1D-SH wave propagation for both the GMPE and target regions (Knopoff, 1964). Since the chosen predictive models provide only response spectra and peak ground motions, response spectrum compatible $\mathrm{FAS_{GMPE}}$ were obtained through inverse random vibration theory (iRVT) (Rathje *et al.*, 2005) using the computer program STRATA (Kottke and Rathje, 2008). The iRVT method takes the input GMPE response spectrum ($\mathrm{PSA_{GMPE}}$) and provides a best fit spectrum ($\mathrm{PSA_{GMPE,iRVT}}$) and corresponding FAS ($\mathrm{FAS_{GMPE}}$). $\mathrm{FAS_{GMPE}}$ is then directly adjusted using $C_{FAS,Vs-\kappa_0}$ (Equation (1)), which is calculated based on A and κ_0, before being restored to the response spectral domain ($\mathrm{PSA_{target}}$) through RVT. The PSA based adjustment can then be defined as:

$$C_{PSA,Vs-\kappa_0}(T) = \frac{\mathrm{PSA_{target}}}{\mathrm{PSA_{GMPE,iRVT}}}(T) \quad , \quad (2)$$

which is averaged over different scenarios and can be used to directly adjust GMPEs for prediction at the target site. Initially we used nine scenarios (M_W = 4, 5, 6 and R_{JB} = 5, 10, 20 km), however we found that there was limited sensitivity to the selected scenario, and therefore used a single scenario to define $C_{PSA,Vs-\kappa_0}$. Note that although Al Atik *et al.* (2014) suggest to use $\mathrm{PSA_{GMPE}}$ directly in Equation (2), we found that the $\mathrm{PSA_{GMPE}}$ could not always be matched with $\mathrm{PSA_{GMPE,iRVT}}$. In our implementation, we therefore use $\mathrm{PSA_{GMPE,iRVT}}$ to define the final PSA based adjustment factors. As a cross check, we found that this approach is consistent with that of (Campbell, 2003), which uses GMPE compatible stochastic models to make the adjustment to the response spectrum. We detail here the V_S-κ_0 adjustment procedure for CY08, while the adjustments operated on the other empirical models are given in Tables S1 to S4 of the Electronic Supplement to this manuscript. The host and target parameters defining A and κ_0 are as follows:

(a) Our target V_S profile for Swiss rock sites is always that of Poggi *et al.* (2011);

(b) the V_S profile of CY08 in our study is either that of Boore and Joyner (1997) or an adjusted version of Poggi *et al.* (2011), both with $V_{S,30}$ = 620 $\mathrm{ms^{-1}}$ (Figure 47);

(c) κ_0 at rock sites in the host region (Western United States) is estimated either based on Edwards *et al.* (2011): κ_0 = 0.0218 s; Poggi *et al.* (2013): κ_0 = 0.0345 s; or the iRVT technique: 0.0356 s;

(d) κ_0 at hard rock sites in the target region (Switzerland) is estimated either based on Edwards *et al.* (2011): κ_0 = 0.0159 or Poggi *et al.* (2013): κ_0 = 0.0260.

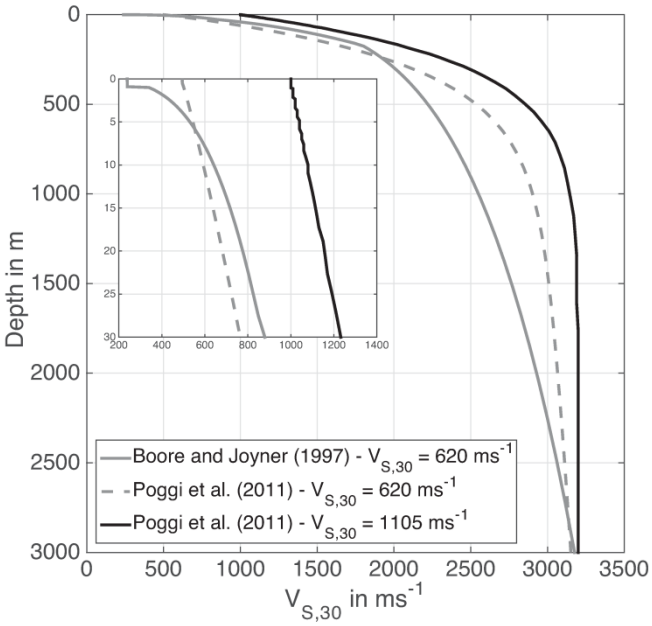

Figure 47: Host rock V_S profiles used for adjusting the CY08 GMPE, as described in the text. The onset shows the V_S profiles in the uppermost 30 m.

(b), (c) and (d) are designed to capture the epistemic uncertainty associated with assessing κ_0 in Switzerland and in the Western United States and defining the reference V_S profile at rock sites in the Western United States. The host V_S profile for CH08 is based on Boore and Joyner (1997) since the majority of data used for the GMPE is from recording stations in the Western United States and California. For predictions in the host region we used a $V_{S,30}$ = 620 ms^{-1} corresponding to the majority of the rock sites in Boore and Joyner (1997). This was assessed as part of the SSHAC Level 4 PEGASOS Refinement Project and largely based on personal communications with the authors of the predictive model. To cover the epistemic uncertainty related to this selection, we also used another generic rock profile, namely that of Poggi *et al.* (2011), adjusted to $V_{S,30}$ = 620 ms^{-1}.

Several methods can be used to define κ_0. One option is to use the value determined from directly fitting the FAS_{GMPE} from the iRVT approach described above. Alternatively one can use empirical relations between $V_{S,30}$ and κ_0 (e.g., Chandler *et al.*, 2006, Silva *et al.*, 1998, Edwards and Fäh, 2013a) to define κ_0 or, alternatively to directly define $\Delta\kappa_0 = \kappa_{0,target} - \kappa_{0,host}$ accounting for the host-target conversion. The latter approach, defining $\Delta\kappa_0$, avoids mixing different $V_{S,30}$ – κ_0 relations, which may have methodological (Edwards *et al.*, 2015) or regional biases, and instead shows the expected change due to the host to target conversion. Using the iRVT approach means including a directly measured estimate for the host, which may be more reliable than $V_{S,30}$ – κ_0 relations. Without mixing different $V_{S,30}$ - κ_0 relations, (c) and (d) yield four different values of $\Delta\kappa_0$, as listed in Table 3. Both the iRVT and $V_{S,30}$ - κ_0 based $\Delta\kappa_0$ approaches are independent of background seismological models, as required when performing a full host-to-target conversion (Campbell, 2003, Scherbaum *et al.*, 2006).

The resulting suite of V_S-κ_0 adjustments (8 in total, based on two amplification functions and four $\Delta\kappa_0$ values) is shown by the shaded area in Figure 48 for CY08. Amongst all the possible adjustments, only three, representative of the mean, lower- and upper-bound adjustments, were retained to build the PSHA logic tree in order to avoid too many branches. The adjustments are implemented as period-dependent multiplicative factors ($C_{PSA,Vs-\kappa_0}(T)$) to be applied to the original GMPEs. For vibration periods T > 0.2 s, the adjustments result into a decrease of the original spectral levels, irrespective of the V_S profile and $\Delta\kappa_0$ values.

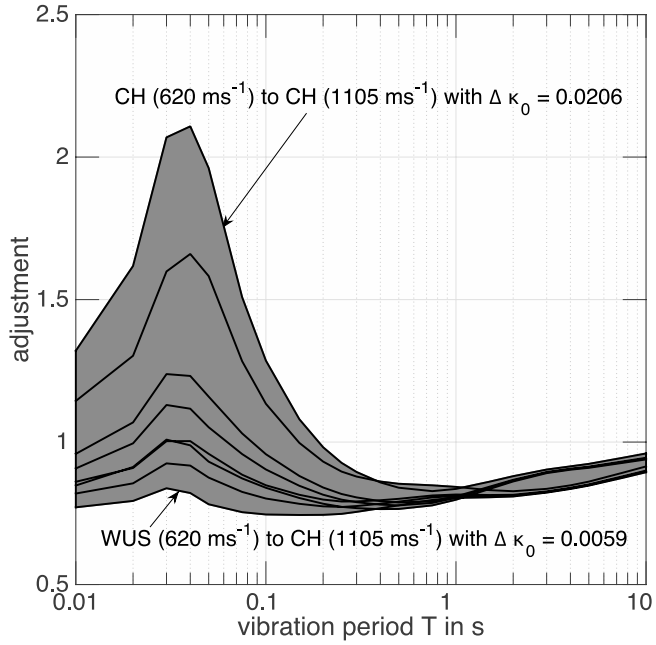

Figure 48: Summary of the V_S-κ_0 adjustments for the CY08 GMPE. WUS = Western United States rock profile; CH = Swiss reference rock profile.

Source		Values		
Host κ₀	***Target κ₀***	***Host κ₀***	***Target κ₀***	***Δκ₀***
EETAL11	EETAL11	0.0218	0.0159	-0.0059
PETAL13	PETAL13	0.0345	0.0260	-0.0085
iRVT	EETAL11	0.0365	0.0159	-0.0206
iRVT	PETAL13	0.0365	0.0260	-0.0105

EETAL11: (Edwards *et al.*, 2011); PETAL13: (Poggi *et al.*, 2013); iRVT: inverse Random Vibration Theory.

Table 3: Host and target κ_0 along with $\Delta\kappa_0$ used to adjust CY08 to Swiss rock conditions.

Small magnitude adjustments

Empirical GMPEs are often derived from datasets with moderate-to-large events, typically with M_W larger than ~ 5 mainly because such events are likely to cause damage to the built environment and are therefore of primary interest for engineering applications. Additionally, the metadata (magnitude, depth, distance to fault, etc.) for moderate and larger events are reasonably well known. For smaller events this information is more uncertain. Authors that have included small magnitude data in GMPE development (e.g., Chiou *et al.*, 2010, Bommer *et al.*, 2007) have concluded that: (1) GMPEs should be derived using data at least one magnitude unit below that required for their target application and (2) the aleatory variability significantly increases as a result of including small magnitude data.

Since the PSHA for the new Swiss National Seismic Hazard Maps uses a rather low minimum magnitude of 4, we had to ensure all the selected empirical GMPEs to be valid at this magnitude. To this end, we followed the methodology developed during the PEGASOS Refinement Project (Stafford, 2011) and subsequently used elsewhere (e.g., Bourne *et al.*, 2015) where the small magnitude adjusted (SMA) GMPE Y_{SMA} is given by:

$$Y_{SMA} = Y - \delta(M,R|T) \quad (3)$$

with

$$\delta(M,R|T) = \left(\frac{M_{ref}-M}{a}\right)^b \left(c + d\ ln\left(\frac{\max(\min(R,R_{max}),R_{min})}{R_{ref}}\right)\right), \quad M \le M_{ref} \quad (4)$$

and

$$\delta(M,R|T) = 0, \quad M > M_{ref} \quad (5)$$

Y is the original GMPE prediction (in terms of natural logarithms). M_{ref} is chosen based on the magnitude above which the GMPE is trusted (we set $M_{ref} = 5.5$). $R_{ref} = 20$ km is a generic distance chosen as a reference while the coefficients *(a…d)* are determined through regressions on the residual misfit of a specific GMPE to the locally recorded small magnitude data. $R_{min} = 10$ km and R_{max} (determined through regression) are the minimum and maximum distances used for the correction, respectively. An example of small magnitude adjustment applied to the model AB10 is shown in Figure 49 and the coefficients shown in

Table 3. The adjustments applied to the other empirical models are provided in Tables S5 to S12 of the Electronic Supplement to this manuscript. Recorded Swiss foreland and alpine data for events with magnitude ranging between 3.3 and 3.7 are shown as symbols in Figure 49. The original (non-adjusted) GMPE for M_W = 3.5 clearly over-predicts the median observations. The fully adjusted GMPE (SMA and V_S-κ_0) is shown to reasonably match the data distribution and the Swiss model of Edwards and Fäh (2013b: EF13). It is apparent from Figure 49, that the SMA is much stronger than the V_S-κ_0 adjustment for small magnitude events, to the extent that uncertainties involved in defining the SMA would make any V_S-κ_0 adjustment statistically insignificant. However, it is important to put these corrections into the context of seismic hazard. From hazard disaggregation we know that tectonic hazard is dominated by moderate-to-large earthquakes (e.g., M ~ 6 – 7) at short distances (e.g., R_{JB} ~ 30 km). For such events the SMA is zero, while the V_S-κ_0 leads to changes in the rock (Vs30 ~ 620 m/s) motions, in the case of CY08, of up to a factor of 2 at 20 Hz (Figure 48). While the SMA is therefore clearly more dramatic for the smallest events considered in PSHA, it is the combined effect of both SMA and any V_S-κ_0 adjustment that will affect the final hazard. Due to the limited influence of small magnitude events on ground motion exceedance (particularly when the predicted motions are reduced by the SMA), it is therefore the V_S-κ_0 adjustment that has the biggest impact on the final hazard estimates.

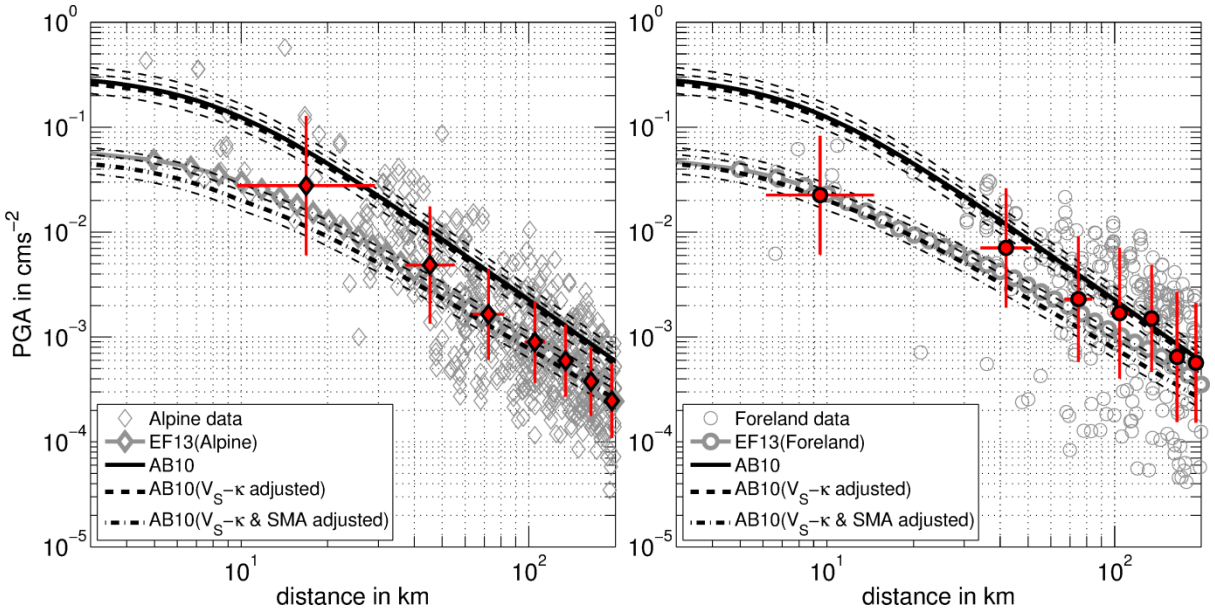

Figure 49: V_S-κ_0 and small magnitude adjustment (SMA) for the AB10 predictive model for PGA at M_w=3.5, compared with recorded Swiss small magnitude data (3.3≤M_w≤3.7) and the stochastic model of EF13. For the adjusted models, thin lines indicate the individual adjustments used in the logic tree, thick lines indicate the uniform average. Left panel: Alpine data and EF13 model; right panel: foreland data and EF13 model. Filled symbols with error bars indicate bin-averages and standard deviation.

Period (s)	a	b	c	d	R_{max} (km)	R_{min} (km)	R_{ref} (km)	M_{ref}
0.010	1.415563	1.239239	0.995590	-.216847	1972.3	10.0	20.0	5.50
0.020	1.258943	1.000000	0.994693	-.245797	1144.3	10.0	20.0	5.50
0.030	1.278509	1.000000	0.996465	-.237767	1322.2	10.0	20.0	5.50
0.040	1.277566	1.042382	0.996425	-.277362	868.9	10.0	20.0	5.50
0.050	1.276418	1.077745	0.996358	-.309346	501.0	10.0	20.0	5.50
0.100	1.433038	1.222753	0.996372	-.400643	240.5	10.0	20.0	5.50
0.150	1.384642	1.250938	0.996417	-.319041	631.1	10.0	20.0	5.50
0.200	1.350304	1.271328	0.996450	-.261144	908.2	10.0	20.0	5.50
0.250	1.517877	1.262536	0.996806	-.275018	766.5	10.0	20.0	5.50
0.300	1.654794	1.255398	0.997098	-.286355	650.7	10.0	20.0	5.50
0.350	1.855761	1.322266	0.996444	-.328013	467.2	10.0	20.0	5.50
0.400	2.030328	1.383505	0.995872	-.364282	307.8	10.0	20.0	5.50
1.000	-5.169560	1.000000	1.010650	0.622190	1.0E+09	10.0	20.0	5.50
1.050	-6.821261	1.000000	1.016859	0.833713	1.0E+09	10.0	20.0	5.50
1.100	-8.396109	1.000000	1.022780	1.035395	1.0E+09	10.0	20.0	5.50
1.150	-9.900941	1.000000	1.028437	1.228109	1.0E+09	10.0	20.0	5.50
1.200	-1.341718	1.000000	1.033854	1.412621	1.0E+09	10.0	20.0	5.50
1.250	-2.723671	1.000000	1.039049	1.589599	1.0E+09	10.0	20.0	5.50
1.300	-4.051415	1.000000	1.044041	1.759635	1.0E+09	10.0	20.0	5.50
1.350	-5.329044	1.000000	1.048844	1.923254	1.0E+09	10.0	20.0	5.50
1.400	-6.560203	1.000000	1.053472	2.080921	1.0E+09	10.0	20.0	5.50
1.450	-7.748154	1.000000	1.057938	2.233055	1.0E+09	10.0	20.0	5.50
1.500	-8.895828	1.000000	1.062253	2.380030	1.0E+09	10.0	20.0	5.50
1.550	-0.005867	1.000000	1.066426	2.522186	1.0E+09	10.0	20.0	5.50
1.600	-1.080660	1.000000	1.070467	2.659828	1.0E+09	10.0	20.0	5.50
1.650	-2.122377	1.000000	1.074383	2.793235	1.0E+09	10.0	20.0	5.50
1.700	-3.132994	1.000000	1.078182	2.922658	1.0E+09	10.0	20.0	5.50
1.750	-4.114313	1.000000	1.081872	3.048330	1.0E+09	10.0	20.0	5.50
1.800	-5.067986	1.000000	1.085457	3.170461	1.0E+09	10.0	20.0	5.50
1.850	-5.995527	1.000000	1.088944	3.289246	1.0E+09	10.0	20.0	5.50
1.900	-6.898331	1.000000	1.092338	3.404863	1.0E+09	10.0	20.0	5.50
1.950	-7.777683	1.000000	1.095644	3.517476	1.0E+09	10.0	20.0	5.50
2.000	-8.634770	1.000000	1.098866	3.627238	1.0E+09	10.0	20.0	5.50
2.050	-8.634770	1.000000	1.098866	3.627238	1.0E+09	10.0	20.0	5.50
2.100	-8.634770	1.000000	1.098866	3.627238	1.0E+09	10.0	20.0	5.50
2.150	-8.634770	1.000000	1.098866	3.627238	1.0E+09	10.0	20.0	5.50
2.200	-8.634770	1.000000	1.098866	3.627238	1.0E+09	10.0	20.0	5.50
2.250	-8.634770	1.000000	1.098866	3.627238	1.0E+09	10.0	20.0	5.50
2.300	-8.634770	1.000000	1.098866	3.627238	1.0E+09	10.0	20.0	5.50
2.350	-8.634770	1.000000	1.098866	3.627238	1.0E+09	10.0	20.0	5.50
2.400	-8.634770	1.000000	1.098866	3.627238	1.0E+09	10.0	20.0	5.50
2.450	-8.634770	1.000000	1.098866	3.627238	1.0E+09	10.0	20.0	5.50
2.500	-8.634770	1.000000	1.098866	3.627238	1.0E+09	10.0	20.0	5.50
2.550	-8.634770	1.000000	1.098866	3.627238	1.0E+09	10.0	20.0	5.50
2.600	-8.634770	1.000000	1.098866	3.627238	1.0E+09	10.0	20.0	5.50
2.650	-8.634770	1.000000	1.098866	3.627238	1.0E+09	10.0	20.0	5.50
2.700	-8.634770	1.000000	1.098866	3.627238	1.0E+09	10.0	20.0	5.50
2.750	-8.634770	1.000000	1.098866	3.627238	1.0E+09	10.0	20.0	5.50
2.800	-8.634770	1.000000	1.098866	3.627238	1.0E+09	10.0	20.0	5.50
2.850	-8.634770	1.000000	1.098866	3.627238	1.0E+09	10.0	20.0	5.50
2.900	-8.634770	1.000000	1.098866	3.627238	1.0E+09	10.0	20.0	5.50
2.950	-8.634770	1.000000	1.098866	3.627238	1.0E+09	10.0	20.0	5.50
3.000	-8.634770	1.000000	1.098866	3.627238	1.0E+09	10.0	20.0	5.50
4.000	-8.634770	1.000000	1.098866	3.627238	1.0E+09	10.0	20.0	5.50

Table 4: Coefficients used for Equation 4 with the model of Akkar and Bommer (2010).

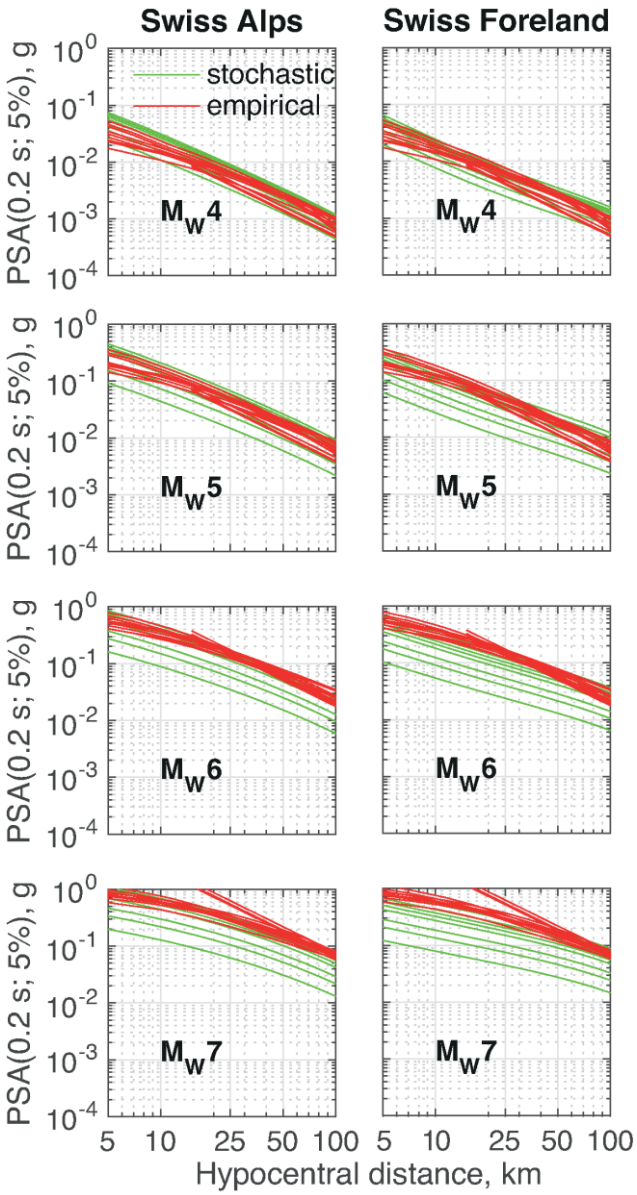

Figure 50: Median predictions of the simulation-based and empirical GMPEs adopted in this study at 0.2 s, as a function of the hypocentral distance and moment magnitude. For each empirical model, three curves corresponding to alternative V_S-κ_0 adjustments are plotted in the picture.

Figure 50 shows the median *PSA(T = 0.2 s; ζ = 5 %)* predictions of the simulation-based and empirical GMPEs adopted in this study as a function of the hypocentral distance and moment magnitude. The different curves shown for the simulation-based stochastic model correspond to different values of the stress parameter $\Delta\sigma$ as explained in Section Adopted logic tree. Note the different amplitude and shape of attenuation with distance of the Swiss stochastic models in the Swiss Alps and foreland (Edwards and Fäh, 2013b, Cauzzi *et al.*, 2015a). For each empirical model, three curves corresponding to alternative V_S-κ_0 adjustments are plotted. The straight lines correspond to the model CF08 that does not implement a saturation term as it is calibrated for hypocentral distances larger than 15 km. As apparent from Figure 50, without considering any weighting the entire set of empirical and stochastic median predictions spans roughly one order of magnitude in *PSA(T = 0.2 s; ζ = 5 %)* over a broad distance range. For $M_W \geq 6$, the lower bound of the median predictions is given by the model EF13 for $\Delta\sigma$ = 1 MPa [considered valid for shallow (depth < 6 km) crustal events], while the upper bound is the model of CF08. At lower magnitudes, the upper bound of the median predictions is the model EF13 for $\Delta\sigma$ = 12 MPa. As shown in Figure 50, for the higher values of $\Delta\sigma$ ($\geq 5\ MPa$) the stochastic and empirical models are broadly comparable. Only the lowest three models ($\Delta\sigma \leq 3\ MPa$), considered valid for shallow seismicity, show significantly different predictions. While GMPEs are known to provide robust predictions throughout

the magnitude range of interest, none have been developed specifically in Switzerland. Furthermore, they are likely dominated by deeper focus (and therefore higher stress-parameter (e.g., Hough, 2014) events, which our logic tree aims to specifically separate. We therefore feel that while these models do predict relatively low amplitudes compared to global GMPEs, their inclusion within the logic tree-framework is justified due to their consistency with both small magnitude weak-motion data, and large-magnitude macroseismic data in the specific setting of the shallow (depth < 6 km) crust.

5.4 Prediction uncertainties

GMPEs are multi-degree-of-freedom models that require careful fitting in order to derive robust coefficients and avoid trade-offs between the source, path and site effects. Typically the fitting of the GMPE to the data is done using a multi-stage maximum-likelihood approach (Joyner and Boore, 1993) or more commonly for recent GMPEs, the random-effects approach (Abrahamson and Youngs, 1992). The misfit of a GMPE to the data used to derive it (represented as the standard deviation of log-space residuals, σ_T) is considered as total uncertainty. σ_T is then split into at least a between-event (also called inter-event), τ, and a within-event (or intra-event) uncertainty component, φ, in order to isolate event-specific and path-site specific aleatory variability (randomness):

$$\sigma_T = \sqrt{\tau^2 + \varphi^2} \tag{6}$$

This is an important feature used in seismic hazard analysis to appropriately incorporate the lower variability ground-motion expected from a single event (φ), with respect to the average variability over many events (σ_T). Recent work has shown the importance of further decoupling uncertainty in GMPEs and the subsequent (partial) removal of the ergodic assumption (Rodriguez-Marek *et al.*, 2013). The ergodic assumption used to develop GMPEs is that the ground-motion observed in the spatial domain (*i.e.*, over numerous recording sites) is reflective of the ground-motion observed in the time-domain (*i.e.*, at one site). A problem with this approach is that site-to-site variability is mapped into the within-event uncertainty measure of GMPEs. However, when computing hazard, or simply examining scenario events, we use a reference site (in our case Poggi *et al.*, 2011). Including site-to-site variability in predictions therefore unjustifiably increases the overall prediction uncertainty for this application.

The reality is that in many cases we know the expected site response behaviour and its uncertainty. In this case the so-called single-site sigma (σ_{SS}) can significantly reduce the predicted ground-motion variability and the resultant hazard at long return periods (Atkinson, 2006). Single-site sigma is given by:

$$\sigma_{SS} = \sqrt{\tau^2 + \varphi_{SS}{}^2}) \tag{7}$$

where φ_{SS} is the within-event uncertainty for a single site: the standard deviation of ground-motions observed if we were to record a single earthquake on multiple clones of a given site (at various azimuths, distances, etc.). Rodriguez-Marek *et al.* (2013) determined φ_{SS} for a variety of regions (including Switzerland) and found that it appears, on average, to be regionally independent. They proposed four models to describe φ_{SS}: period dependent, distance-period dependent, magnitude-period dependent and magnitude-distance-period dependent. Physical reasons for magnitude and distance dependence of ground-motion variability do support a higher variability of ground-motion in the near-field ($R \lesssim 30\,km$), where complex and highly variable source effects are often observed (*e.g.*, directivity), and for smaller earthquakes which tend to exhibit more variability than larger events (*e.g.*, in terms of source depth, stress-drop, *etc.*).

In this study we adopted two alternative approaches to model φ_{SS}, namely: *(i)* the magnitude-, distance- and period-dependent model by Rodriguez-Marek *et al.* (2013) and (ii) the period-dependent average across Switzerland of Edwards and Fäh (2013b), as shown in Figure 51. Note how φ_{SS} decreases with distance for low magnitudes ($M_W \sim 4.5$) while it is independent of distance at high magnitudes ($M_W \sim 7$). We defined the total uncertainty using Equation (7) with τ taken from the corresponding GMPEs. The variation of σ_T as a function of magnitude and distance for the different empirical and stochastic models used in this study, along with *trellis* plots for all the ground motion prediction models, is shown in Figures S1 to S15 of the Electronic Supplement to this manuscript.

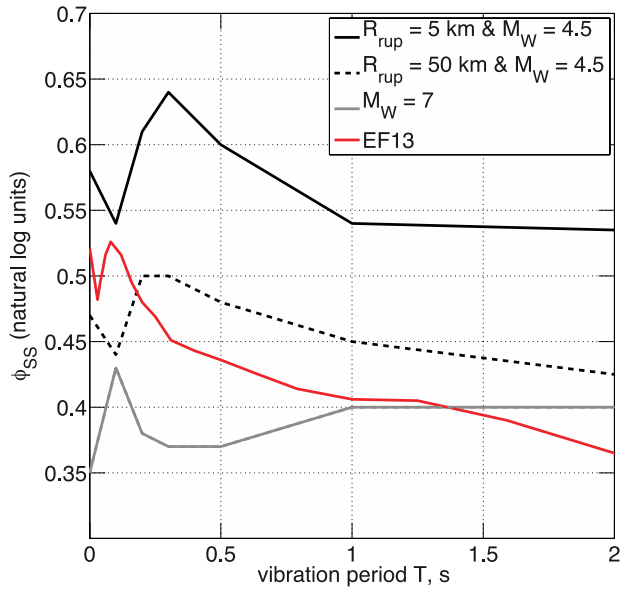

Figure 51: Comparison of the different models of single station sigma φ_{ss} used in this study. The curves for specific magnitude and distances represent the model of Rodriguez-Marek et al. (2013). Note that for M ≥ 7 the model is distance independent. The φ_{ss} model of Edwards and Fäh (2013b) (EF13) is also shown and is a function of vibration period only.

5.5 Adopted logic tree

Critical in the Swiss context is the implementation of region-specific ground-motion models (Edwards and Fäh, 2013b) and corresponding predictive equations (Cauzzi *et al.*, 2015a). The main reasons are that: (a) the attenuation of shear wave energy is regionally dependent (Edwards *et al.*, 2011); (b) the earthquakes located in the alpine region typically occur at shallower depths than those located in the Swiss foreland (Fäh *et al.*, 2011, Diehl *et al.*, 2013, Diehl *et al.*, 2014); (c) the shallow (depth < 6 km) and deep earthquakes exhibit different stress parameter values, typically increasing with depth (Cauzzi *et al.*, 2015a, Goertz-Allmann and Edwards, 2014).

The logic tree used in this study for shallow seismicity is identical in the Swiss Alps and foreland (Figure 52) while different choices were made for deep seismicity in the two regions (Figure 53 and Figure 54). Within each seismotectonic context (shallow seismicity; deep alpine seismicity; deep foreland seismicity), the first logic tree branching level accounts for the availability of stochastic and empirical prediction models, weighted 0.6 and 0.4 respectively. We assigned more weight to the stochastic predictions because they were specifically derived for Switzerland with separation of shallow and deep, foreland and alpine seismicity that has been calibrated against macroseismic and instrumental data. However, we do not exceed 60 % weight to penalise the synthetic nature of the predictions, which leads to increased epistemic uncertainty at higher magnitudes (e.g., $M_w > 6.5$). Furthermore, we believe that by using the small magnitude and *Vs*-κ_0 corrections, the empirical models present a suitable means for predicting ground motion amplitudes in Switzerland. The empirical prediction models are all weighted 0.3 apart from AB10 that contributes 10 %. This is due to the relatively simplistic ground type classification used by AB10

that resulted in comparatively less effective *Vs*-κ_0 corrections, as shown by a careful scrutiny of the *PSA* spectral shapes obtained after the adjustment.

For each empirical prediction model, the subsequent branching level accounts for the *Vs*-κ_0 adjustments. We picked three *Vs*-κ_0 models representative of the average, minimum and maximum amplification with respect to the target rock profile of Poggi *et al.* (2011), with weights equal to 0.7, 0.2 and 0.1 respectively, thus penalising large amplifications and de-amplifications of the original GMPEs. This is valid for all models apart from CF08 that takes weights 0.4, 0.3 and 0.3 due to comparatively less scattered results of the *Vs*-κ_0 adjustments (more gentle variation of spectral shapes).

The weighting scheme adopted for the stochastic models is consistent with the findings of (Cauzzi *et al.*, 2015a) who tested Edwards and Fäh (2013b) with different values of stress parameter $\Delta\sigma$ against a dataset of ~ 2000 EMS-98 intensity data points available in the earthquake catalogue of Switzerland ECOS-09 (Fäh *et al.*, 2011), generated by events with $4.7 < M_W < 6.6$ and distances within 230 km of the earthquake source. Stochastic predictions of shallow events are based on six different values of $\Delta\sigma$ in EF13, namely 1, 2, 3, 5, 6 and 7.5 MPa, with weights 0.23, 0.24, 0.23, 0.1, 0.1 and 0.1 respectively. For deep events we use $\Delta\sigma$ = 5, 6, 7.5 and 9 MPa in the Swiss foreland and $\Delta\sigma$ = 6, 7, 9 and 12 MPa in the Swiss Alps, with weights equal to 0.35, 0.35, 0.2 and 0.1 respectively.

The last branching level for both empirical and stochastic models accounts for the epistemic uncertainty in modelling single-station sigma, as presented in Section 4. Adopting an equal weight means that we consider both models alternative options. Sensitivity analyses performed on the two alternative models showed a difference of ~ 5 % on the mean ground-shaking estimates

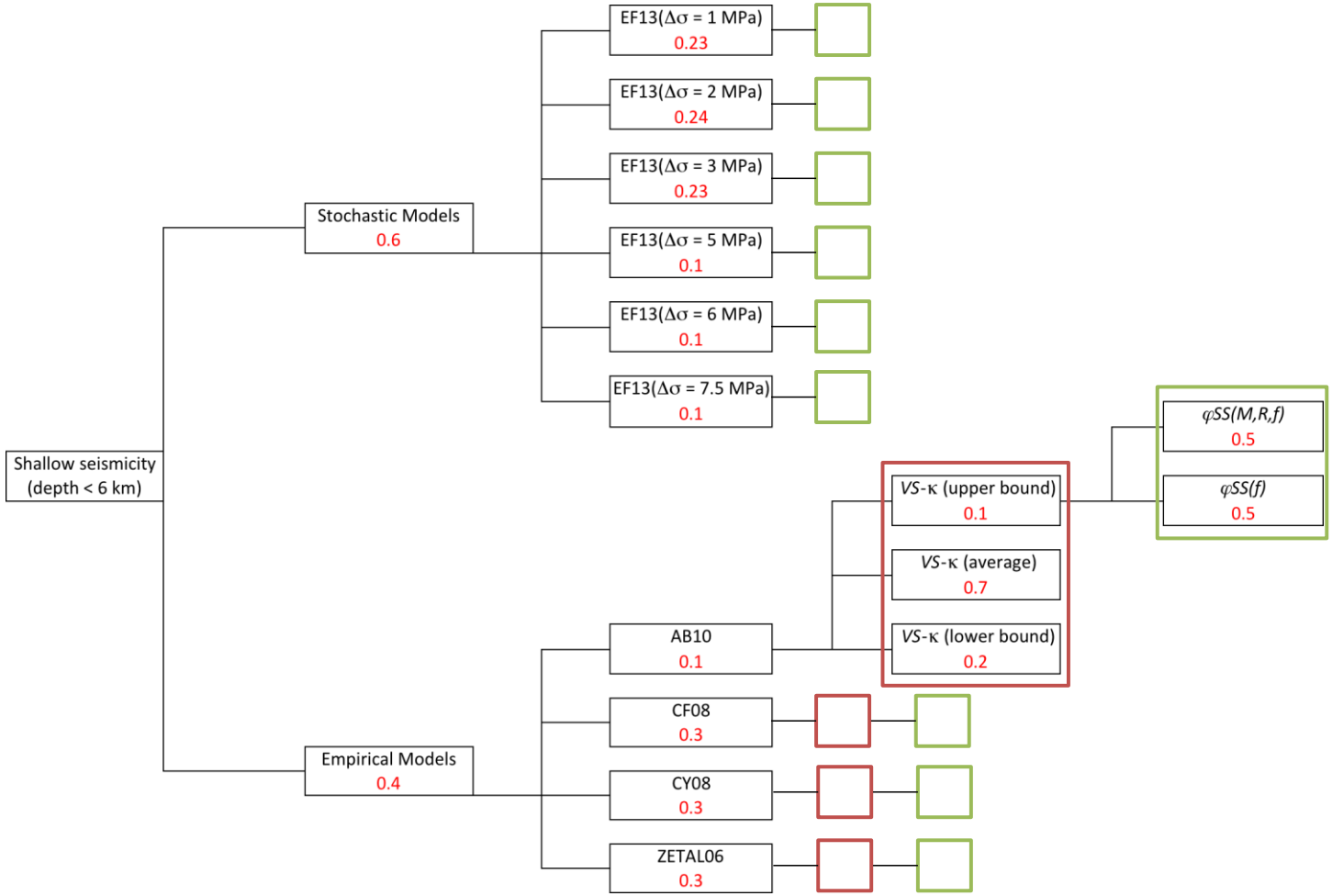

Figure 52: Logic tree for ground motion prediction models and shallow seismicity (depth < 6 km).

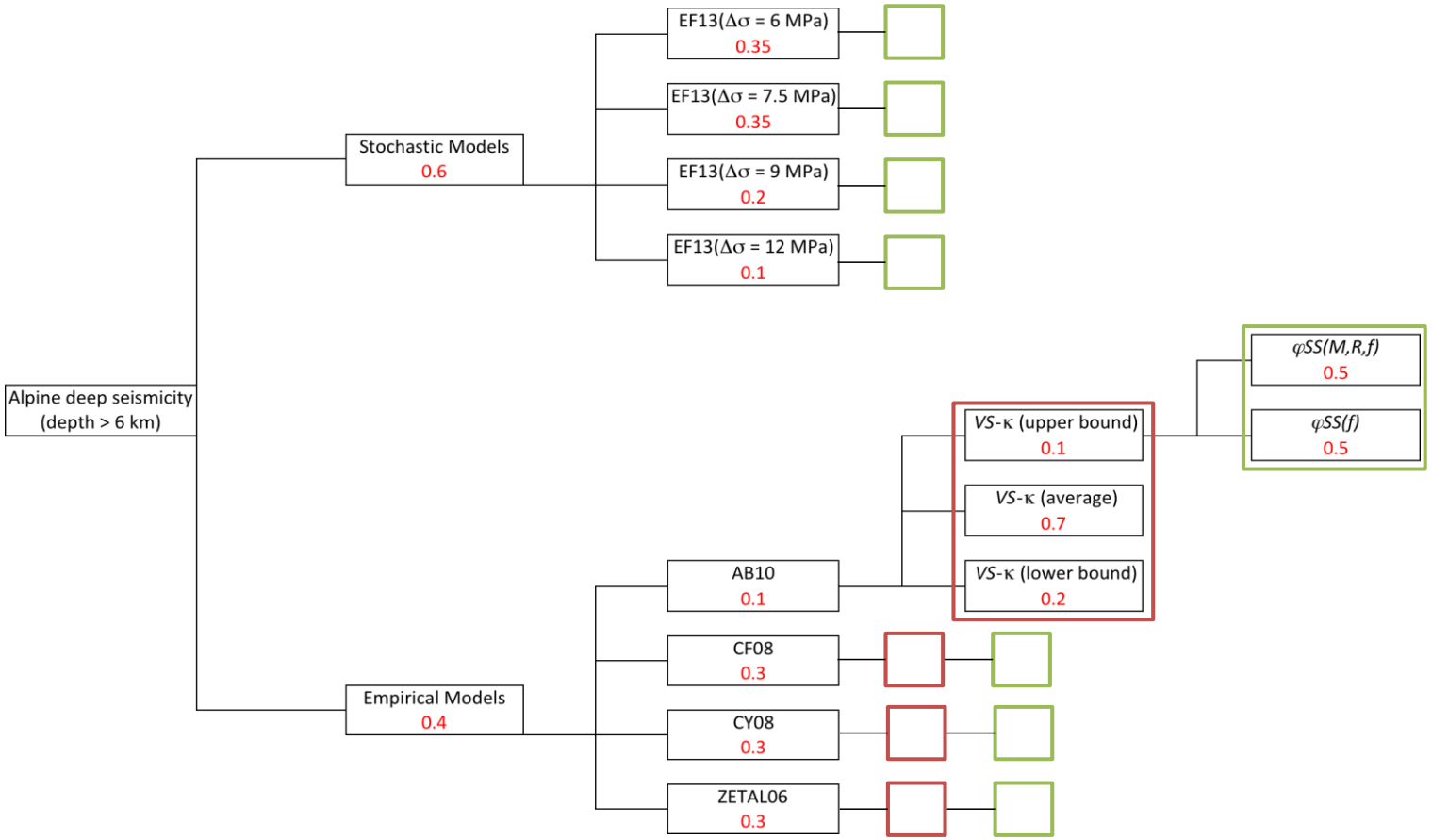

Figure 53: Logic tree for ground motion prediction models for deep (depth > 6 km) Alpine seismicity.

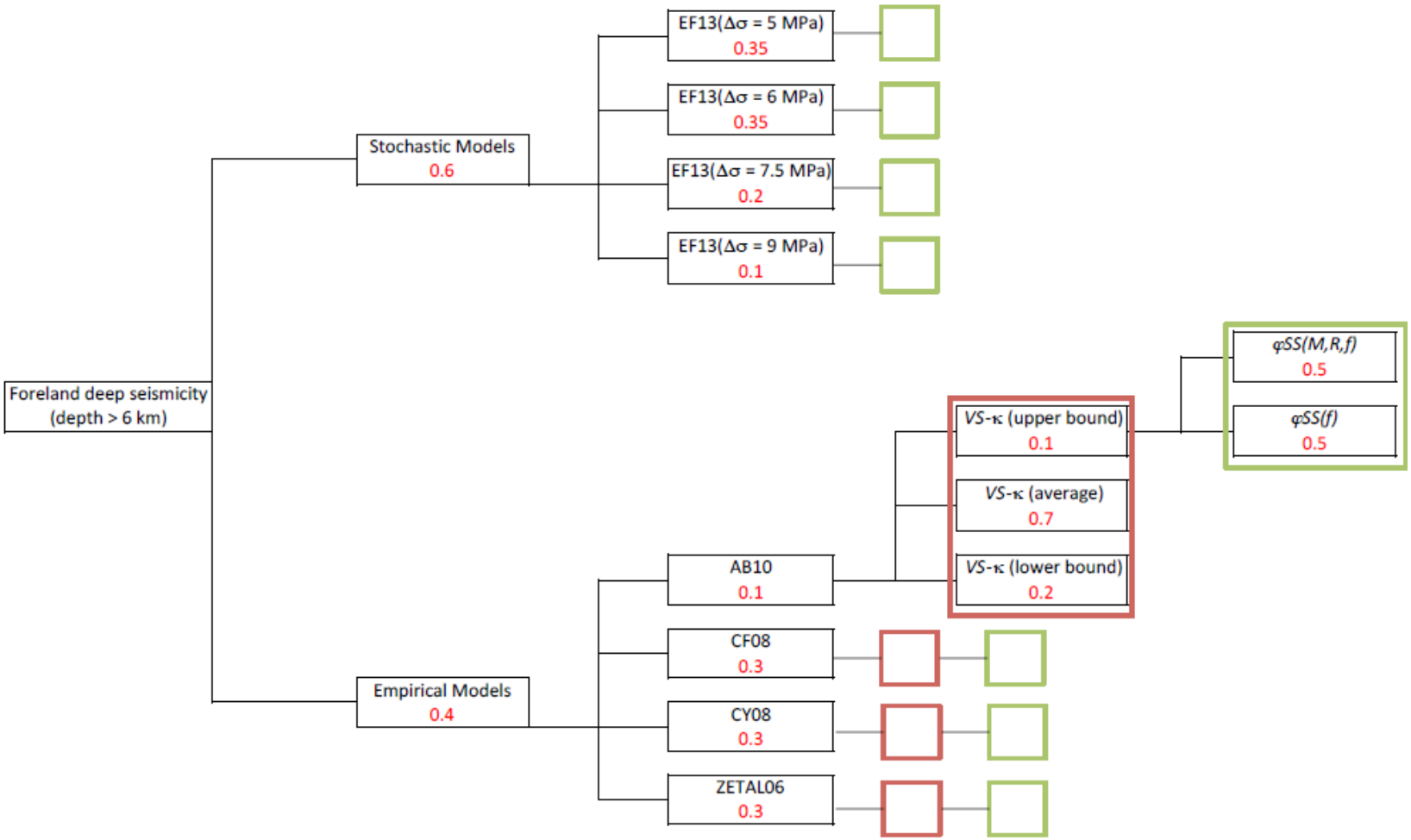

Figure 54: Logic tree for ground motion prediction models for deep (depth > 6 km) events in the Swiss foreland.

Figure 52 shows the hazard curves (5-, 16-, 50-, 84- and 95-percentile levels) for the city of Basle located in the Swiss foreland region (the location of the largest historical central European earthquake on record, with M_w *6.6*), at the border among Switzerland, Germany and France. Hazard is expressed as the probability of exceedance of a given spectral acceleration level in 50 years. Note, how the empirical models yield significantly higher hazard levels than the stochastic models in the Swiss foreland at all vibration periods, even after host-to-target and small magnitude adjustment. The empirical branches are effectively equivalent to 84-percentile levels of the total hazard, while the stochastic models (specifically calibrated for Switzerland) tend to lie within the median and the 16th percentile of the total hazard.

In the Swiss Alps (Figure 53) the average hazard levels yielded by the stochastic model tend to match the median values of the total hazard at all vibration periods for acceleration levels lower than 2 g. The empirical branches contribute with generally slightly higher hazard values, although they never reach or exceed the 84th percentile of the total hazard at short periods. Significant differences are apparent at T = 2 s, where the average hazard produced by the empirical models matches the 84th percentile of the total hazard.

Figure 54 shows uniform hazard spectra for Sion and Basle, and two different return periods, namely T_R = 475 years (used for design and assessment of residential buildings) and 10,000 years (used for design and assessment of special structures and infrastructure such as dams). As anticipated from Figure 54 and Figure 55, the empirical predictions tend to systematically exceed the stochastic predictions over a broad period range both in the Alps and the foreland, the only exception being the case of Sion at T_R = 10,000 years and T ~ 0.05 s. In Sion, the mean predictions yielded by the stochastic models are in good agreement with the mean total hazard. In Basle, the empirical predictions typically match the 84th percentile of the total hazard for T > 0.1 s. Note that, while the peak of the uniform hazard spectrum (UHS) is at 0.1 s for both the stochastic and empirical models (and therefore the total hazard as well), the latter tend to show a different spectral shape with comparatively more energy at 0.15 s and 0.2 s. This reflects part of the epistemic uncertainties of the ground motion models. We note however that the spectral shapes of the empirical models might result as well from poorly constrained host rock conditions, as discussed in the previous sections. The total hazard UHS computed for Sion and Basle would support using T_B = 0.05 s as the lower bound of the constant acceleration branch of the design spectrum. Finally, we note that the full 2015 Swiss National Seismic Hazard model has been implemented within the online European Facility for Earthquake Hazard and Risk (EFEHR), which can be used to easily obtain user defined hazard maps, exceedance curves and uniform hazard spectra at any point in Switzerland.

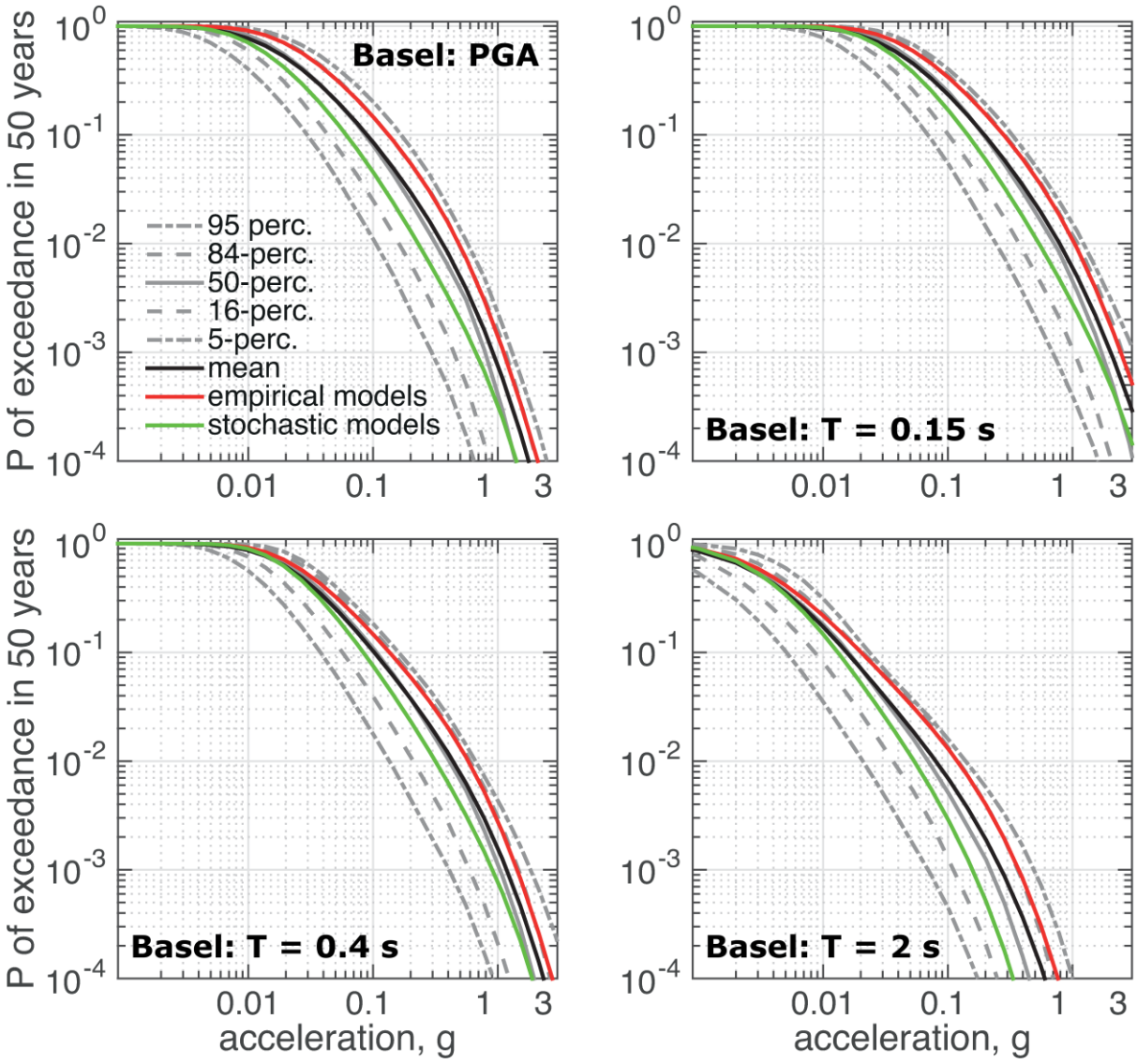

Figure 55: Hazard curves for the city of Basle located in the Swiss foreland region. Total hazard estimates (mean and percentiles) are indicated along with hazard levels obtained considering the empirical or stochastic prediction models only.

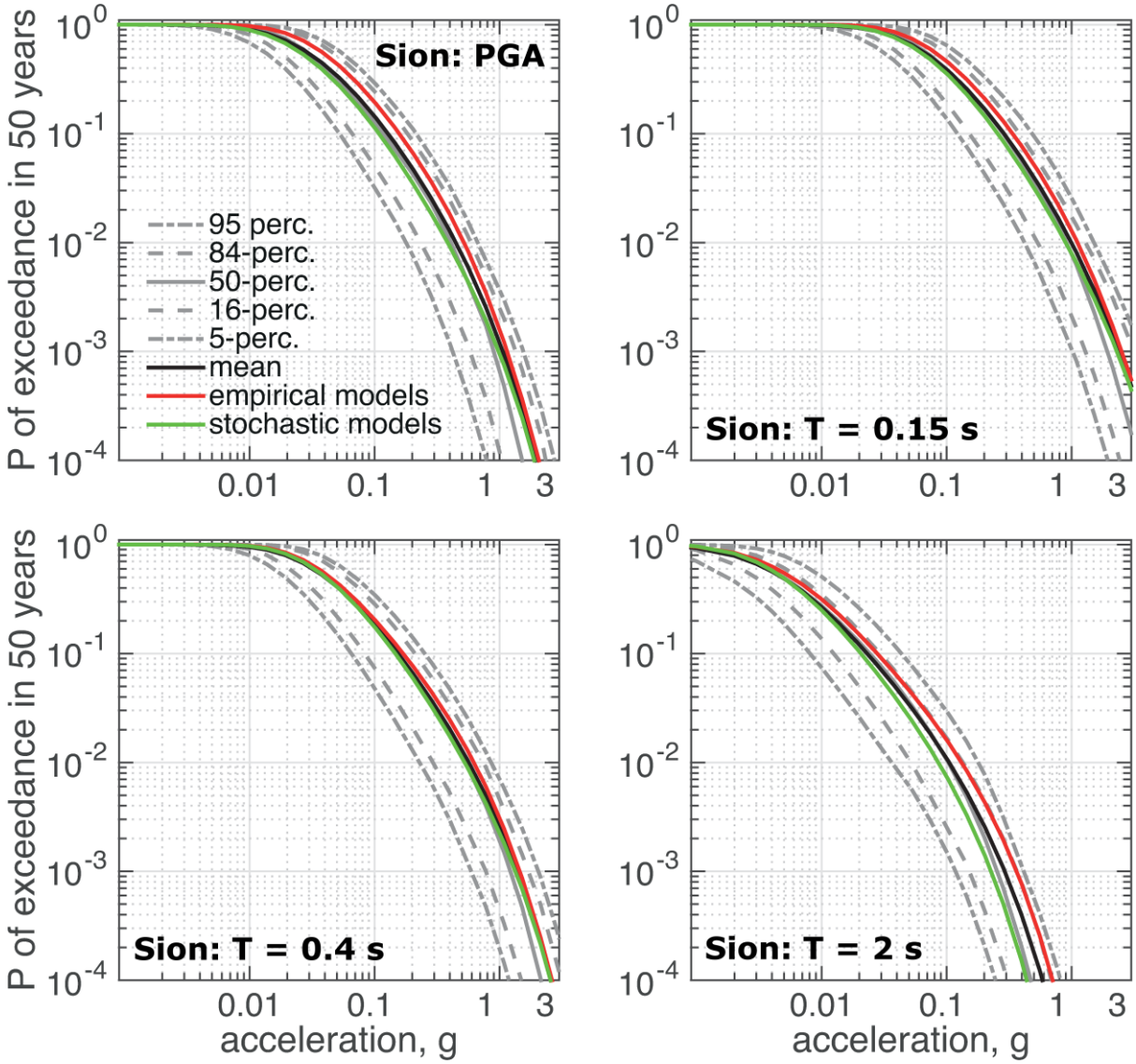

Figure 56: As Figure 10 but for town of Sion, in the Swiss Alps.

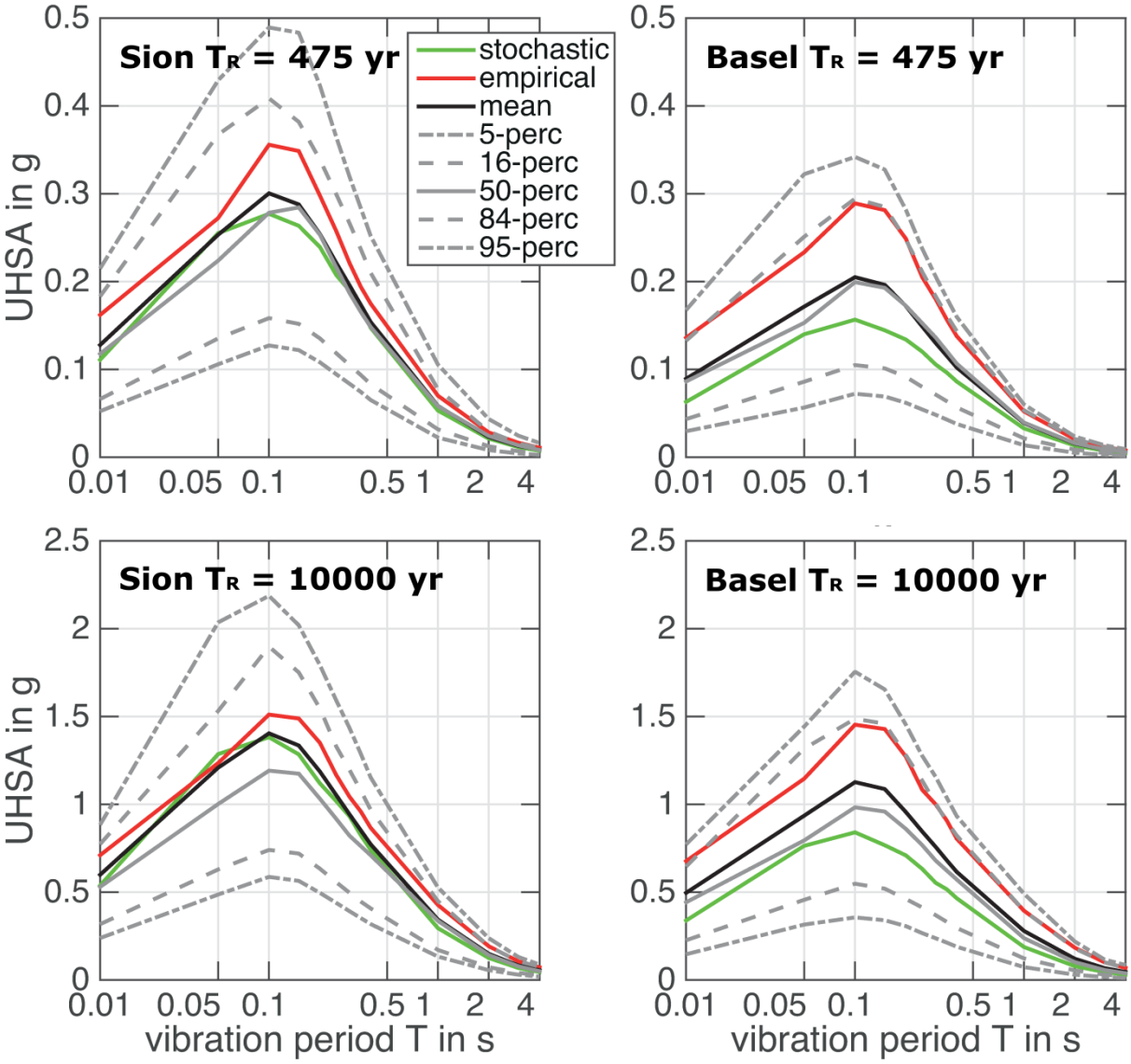

Figure 57: Uniform hazard spectral acceleration (UHSA) as a function of vibration period *T* for Sion (Swiss Alps, LHS panels) and Basle (Swiss Foreland, RHS panels) and two different return periods, namely 475 years (top panels) and 10,000 years (bottom panels). The mean and percentiles of the total hazard are indicated along with the mean acceleration levels obtained using the stochastic or empirical branches only.

5.6 Conclusions

We presented the assessment, adjustment and weighting of ground motion prediction models adopted for the current update of the Swiss national seismic hazard delivered by the Swiss Seismological Service. The hazard estimates are based on bringing together the best elements of both empirical and stochastic ground motion prediction models. We used only consolidated empirical models largely used and tested in Europe and worldwide, namely those of Zhao *et al.* (2006: ZETAL06), Chiou and Youngs (2008: CY08), Cauzzi and Faccioli (2008: CF08) and Akkar and Bommer (2010: AB10). While we are aware that the release of an updated GMPE by the same authors generally supersedes previous models and should therefore be preferred, users' experience shows that potential issues with newly-published GMPEs are generally spotted several months after the release through testing in several applied research projects. We decided not to take this risk in the update of the national Swiss seismic hazard maps and to rely on consolidated models, of which strengths and deficiencies we believe are well informed. As to the stochastic models, we adopted the Swiss-specific prediction of Edwards and Fäh (2013b: EF13) that are based on a well-defined Swiss reference-rock profile by Poggi *et al.* (2011). This marks a significant discontinuity with respect to traditional empirical ground motion prediction studies, where the

definition of the reference rock through ground types determined by the surface geology and $V_{S,30}$ values (often estimated and not measured) can be vague and incomplete. Consistent with the most recent state-of-the-art in ground motion characterisation for PSHA (Renault, 2014, Coppersmith *et al.*, 2014), we adjusted the empirical predictive models to match the amplification and attenuation levels typical of the Swiss reference rock, and made them suitable for predictions at moderate-to-low magnitudes (Stafford, 2011) typical of the instrumentally recorded seismicity of the greater Swiss region. The uncertainty estimates in our updated hazard model are based on single-station sigma values obtained through two alternative approaches; using a regionally independent model for within-event ground motion variability (Rodriguez-Marek et al., (2013), and using Swiss specific within-event ground motion variability (Edwards and Fäh, 2013b).

The update of the Swiss National Seismic Hazard has taken advantage of significant recent advances in ground motion characterisation. The resulting median predictions (and epistemic uncertainty) consequently represent a step-change in quality compared to previous models and reflects state-of –the-art practice typically reserved for PSHA at nuclear power stations. The move towards non-ergodic (single station) sigma leads to a reduction in exceedance levels (and hence seismic hazard) at long return periods. The choices documented in the present study provides a methodological framework for region specific ground motion characterisation within PSHA. While applied to the development of the Swiss National Seismic Hazard Maps, the scope of this manuscript is significantly beyond this application, with usage particularly suited to regions of low to moderate seismicity.

5.7 Data and resources

A summary of the Swiss National Seismic Hazard Maps 2015 can be viewed online: http://www.seismo.ethz.ch/eq_swiss/ErdbebengeFährdung/index_EN (last accessed March 2016), while the European Facility for Earthquake Hazard and Risk (EFHAR) can be used for interactive viewing of the hazard map, exceedance curves and uniform hazard spectra: www.efehr.org (last accessed March 2016). Douglas (2015) provides a summary of the empirical GMPEs used in this study and can be downloaded from: http://www.gmpe.org.uk (last accessed December, 2015). The Swiss specific adjusted GMPEs are available under open-source license at: https://github.com/gem/oq-hazardlib/tree/master/openquake/hazardlib/gsim (last accessed March, 2016). The computer programme STRATA (Kottke and Rathje, 2008) can be downloaded from https://nees.org/resources/strata (last accessed December 2015).

5.8 Acknowledgements

We are indebted to our colleagues Stefan Wiemer, Domenico Giardini, Florian Haslinger, Philipp Kaestli, Edi Kissling, Jochen Wössner (now at Risk Management Solutions), Valerio Poggi (now at the Global Earthquake Model Foundation), Clotaire Michel, Stefan Hiemer and numerous others at the Swiss Seismological Service with whom we have worked together on the updated Swiss seismic hazard maps. We thank associate editor Mark Stirling and two anonymous reviewers who provided useful comments on this manuscript.

5.9 References

Abrahamson, N., P. Birkhauser, M. Koller, D. Mayer-Rosa, P. Smit, C. Sprecher, S. Tinic and R. Graf (2002). Pegasos—a Comprehensive Probabilistic Seismic Hazard Assessment for Nuclear Power Plants in Switzerland. *in Proceedings of the Twelfth European Conference on Earthquake Engineering*,

Abrahamson, N. and W. Silva (2008). Summary of the Abrahamson & Silva Nga Ground-Motion Relations, *Earthq Spectra* 24, 67-97

Abrahamson, N. A. and R. R. Youngs (1992). A Stable Algorithm for Regression-Analyses Using the Random Effects Model, *B Seismol Soc Am* 82, 505-510

Akkar, S. and J. J. Bommer (2010). Empirical Equations for the Prediction of Pga, Pgv, and Spectral Accelerations in Europe, the Mediterranean Region, and the Middle East, *Seismol Res Lett* 81, 195-206

Akkar, S. and Z. Cagnan (2010). A Local Ground-Motion Predictive Model for Turkey, and Its Comparison with Other Regional and Global Ground-Motion Models, *B Seismol Soc Am* 100, 2978-2995

Akkar, S., M. A. Sandikkaya, M. Senyurt, A. A. Sisi, B. O. Ay, P. Traversa, J. Douglas, F. Cotton, L. Luzi, B. Hernandez and S. Godey (2014). Reference Database for Seismic Ground-Motion in Europe (Resorce), *B Earthq Eng* 12, 311-339

Al Atik, L., A. Kottke, N. Abrahamson and J. Hollenback (2014). Kappa (Kappa) Scaling of Ground-Motion Prediction Equations Using an Inverse Random Vibration Theory Approach, *B Seismol Soc Am* 104, 336-346

Ambraseys, N., P. Smit, J. Douglas, B. Margaris, R. Sigbjörnsson, S. Olafsson, P. Suhadolc and G. Costa (2004). Internet Site for European Strong-Motion Data, *B Geofis Teor Appl* 45, 113-129

Ancheta, T. D., R. B. Darragh, J. P. Stewart, E. Seyhan, W. J. Silva, B. S. Chiou, K. E. Wooddell, R. W. Graves, A. R. Kottke and D. M. Boore (2014). Nga-West 2 Database, *Earthq Spectra*

Anderson, J. G. and S. E. Hough (1984). A Model for the Shape of the Fourier Amplitude Spectrum of Acceleration at High-Frequencies, *B Seismol Soc Am* 74, 1969-1993

Atkinson, G. M. (2006). Single-Station Sigma, *B Seismol Soc Am* 96, 446-455

Atkinson, G. M. and D. M. Boore (2006). Earthquake Ground-Motion Prediction Equations for Eastern North America, *B Seismol Soc Am* 96, 2181-2205

Atkinson, G. M. and W. Silva (2000). Stochastic Modeling of California Ground Motions, *B Seismol Soc Am* 90, 255-274

Bay, F., D. Fäh, L. Malagnini and D. Giardini (2003). Spectral Shear-Wave Ground-Motion Scaling in Switzerland, *B Seismol Soc Am* 93, 414-429

Bay, F., S. Wiemer, D. Fäh and D. Giardini (2005). Predictive Ground Motion Scaling in Switzerland: Best Estimates and Uncertainties, *J Seismol* 9, 223-240

Bindi, D., F. Pacor, L. Luzi, R. Puglia, M. Massa, G. Ameri and R. Paolucci (2011). Ground Motion Prediction Equations Derived from the Italian Strong Motion Database, *B Earthq Eng* 9, 1899-1920

Bommer, J. J., B. Dost, B. Edwards, P. J. Stafford, J. v. Elk, D. Doornhof and M. Ntinalexis (2016). Developing an Application-Specific Ground-Motion Model for Induced Seismicity, *B Seismol Soc Am* 106

Bommer, J. J., J. Douglas, F. Scherbaum, F. Cotton, H. Bungum and D. Fäh (2010). On the Selection of Ground-Motion Prediction Equations for Seismic Hazard Analysis, *Seismol Res Lett* 81, 783-793

Bommer, J. J., P. J. Stafford, J. E. Alarcon and S. Akkar (2007). The Influence of Magnitude Range on Empirical Ground-Motion Prediction, *B Seismol Soc Am* 97, 2152-2170

Boore, D. M. (2003). Simulation of Ground Motion Using the Stochastic Method, *Pure Appl Geophys* 160, 635-676

Boore, D. M. (2009). Comparing Stochastic Point-Source and Finite-Source Ground-Motion Simulations: Smsim and Exsim, *B Seismol Soc Am* 99, 3202-3216

Boore, D. M. and G. M. Atkinson (2008). Ground-Motion Prediction Equations for the Average Horizontal Component of Pga, Pgv, and 5%-Damped Psa at Spectral Periods between 0.01 S and 10.0 S, *Earthq Spectra* 24, 99-138

Boore, D. M. and W. B. Joyner (1997). Site Amplifications for Generic Rock Sites, *B Seismol Soc Am* 87, 327-341

Bourne, S., S. Oates, J. Bommer, B. Dost, J. van Elk and D. Doornhof (2015). A Monte Carlo Method for Probabilistic Hazard Assessment of Induced Seismicity Due to Conventional Natural Gas Production, *B Seismol Soc Am*

Campbell, K. W. (2003). Prediction of Strong Ground Motion Using the Hybrid Empirical Method and Its Use in the Development of Ground-Motion (Attenuation) Relations in Eastern North America, *B Seismol Soc Am* 93, 1012-1033

Campbell, K. W. and Y. Bozorgnia (2008). Nga Ground Motion Model for the Geometric Mean Horizontal Component of Pga, Pgv, Pgd and 5% Damped Linear Elastic Response Spectra for Periods Ranging from 0.01 to 10 S, *Earthq Spectra* 24, 139-171

Cartwright, D. E. and M. S. Longuet-Higgins (1956). The Statistical Distribution of the Maxima of a Random Function, *Proc R Soc Lon Ser-A* 237, 212-232

Cauzzi, C. and J. Clinton (2013). A High- and Low-Noise Model for High-Quality Strong-Motion Accelerometer Stations, *Earthq Spectra* 29, 85-102

Cauzzi, C., B. Edwards, D. Fäh, J. Clinton, S. Wiemer, P. Kästli, G. Cua and D. Giardini (2014). New Predictive Equations and Site Amplification Estimates for the Next-Generation Swiss Shakemaps., *submitted to Geophysical Journal International*

Cauzzi, C., B. Edwards, D. Fäh, J. Clinton, S. Wiemer, P. Kästli, G. Cua and D. Giardini (2015a). New Predictive Equations and Site Amplification Estimates for the Next-Generation Swiss Shakemaps., *Geophys J Int* 200, 421–438

Cauzzi, C. and E. Faccioli (2008). Broadband (0.05 to 20 S) Prediction of Displacement Response Spectra Based on Worldwide Digital Records, *J Seismol* 12, 453-475

Cauzzi, C., E. Faccioli, M. Vanini and A. Bianchini (2015b). Updated Predictive Equations for Broadband (0.01-10 S) Horizontal Response Spectra and Peak Ground Motions, Based on a Global Dataset of Digital Acceleration Records, *B Earthq Eng* 13, 1587-1612

Chandler, A. M., N. T. K. Lam and H. H. Tsang (2006). Near-Surface Attenuation Modelling Based on Rock Shear-Wave Velocity Profile, *Soil Dyn Earthq Eng* 26, 1004-1014

Chiou, B., R. Darragh, N. Gregor and W. Silva (2008). Nga Project Strong-Motion Database, *Earthq Spectra* 24, 23-44

Chiou, B., R. Youngs, N. Abrahamson and K. Addo (2010). Ground-Motion Attenuation Model for Small-to-Moderate Shallow Crustal Earthquakes in California and Its Implications on Regionalization of Ground-Motion Prediction Models, *Earthq Spectra* 26, 907-926

Chiou, B. S. J. and R. R. Youngs (2008). An Nga Model for the Average Horizontal Component of Peak Ground Motion and Response Spectra, *Earthq Spectra* 24, 173-215

Clinton, J., C. Cauzzi, D. Fäh, C. Michel, P. Zweifel, M. Olivieri, G. Cua, F. Haslinger and D. Giardini (2011). The Current State of Strong Motion Monitoring in Switzerland, *in Earthquake Data in Engineering Seismology: Predictive Models, Data Management and Networks*, S. Akkar, P. Gülkan and T. v. Eck Editors), Springer, Dordrecht.

Coppersmith, K., J. Bommer, K. Hanson, J. Unruh, R. Coppersmith, L. Wolf, R. Youngs, A. Rodriguez-Marek, L. Al Atik and G. Toro (2014). Hanford Sitewide Probabilistic Seismic Hazard Analysis. Pnnl-23361, *Pacific Northwest National Laboratory, Richland Washington. http://www. hanford. gov/page. cfm/OfficialDocuments/HSPSHA*

Cornell, C. A. (1968). Engineering Seismic Risk Analysis, *B Seismol Soc Am* 58, 1583-&

Cua, G. and T. Heaton (2008). New Ground Motion Prediction Equations Spanning Weak and Strong Motion Levels. *in AGU Fall Meeting Abstracts*, pp. S51A-0230,

Dalguer, L. A., H. Miyake, S. M. Day and K. Irikura (2008). Surface Rupturing and Buried Dynamic-Rupture Models Calibrated with Statistical Observations of Past Earthquakes, *B Seismol Soc Am* 98, 1147-1161

Delavaud, E., F. Cotton, S. Akkar, F. Scherbaum, L. Danciu, C. Beauval, S. Drouet, J. Douglas, R. Basili, M. A. Sandikkaya, M. Segou, E. Faccioli and N. Theodoulidis (2012). Toward a Ground-Motion Logic Tree for Probabilistic Seismic Hazard Assessment in Europe, *J Seismol* 16, 451-473

Diehl, T., J. Clinton, T. Kraft, S. Husen, K. Plenkers, A. Guilhelm, Y. Behr, C. Cauzzi, P. Kastli, F. Haslinger, D. Fäh, C. Michel and S. Wiemer (2014). Earthquakes in Switzerland and Surrounding Regions During 2013, *Swiss Journal of Geosciences* 107, 359-375

Diehl, T., N. Deichmann, J. Clinton, S. Husen, T. Kraft, K. Plenkers, B. Edwards, C. Cauzzi, C. Michel, P. Kastli, S. Wiemer, F. Haslinger, D. Fäh, U. Kradolfer and J. Wössner (2013). Earthquakes in Switzerland and Surrounding Regions During 2012, *Swiss Journal of Geosciences* 106, 543-558

Douglas, J., S. Akkar, G. Ameri, P. Y. Bard, D. Bindi, J. J. Bommer, S. S. Bora, F. Cotton, B. Derras, M. Hermkes, N. M. Kuehn, L. Luzi, M. Massa, F. Pacor, C. Riggelsen, M. A. Sandikkaya, F. Scherbaum, P. J. Stafford and P. Traversa (2014). Comparisons among the Five Ground-Motion Models Developed Using Resorce for the Prediction of Response Spectral Accelerations Due to Earthquakes in Europe and the Middle East, *B Earthq Eng* 12, 341-358

Douglas, J., B. Edwards, V. Convertito, N. Sharma, A. Tramelli, D. Kraaijpoel, B. M. Cabrera, N. Maercklin and C. Troise (2013). Predicting Ground Motion from Induced Earthquakes in Geothermal Areas, *B Seismol Soc Am* 103, 1875-1897

Edwards, B. and J. Douglas (2013). Selecting Ground-Motion Models Developed for Induced Seismicity in Geothermal Areas, *Geophys J Int* 195, 1314-1322

Edwards, B. and D. Fäh (2013a). Measurements of Stress Parameter and Site Attenuation from Recordings of Moderate to Large Earthquakes in Europe and the Middle East, *Geophys J Int* 194, 1190-1202

Edwards, B. and D. Fäh (2013b). A Stochastic Ground-Motion Model for Switzerland, *B Seismol Soc Am* 103, 78-98

Edwards, B., D. Fäh and D. Giardini (2011). Attenuation of Seismic Shear Wave Energy in Switzerland, *Geophys J Int* 185, 967-984

Edwards, B., O.-J. Ktenidou, F. Cotton, N. Abrahamson, C. V. Houtte and D. Fäh (2015). Epistemic Uncertainty and Limitations of the Kappa0 Model for near-Surface Attenuation at Hard Rock Sites, *Geophys J Int*

Fäh, D., D. Giardini, P. Kästli, N. Deichmann, M. Gisler, G. Schwarz-Zanetti, S. Alvarez-Rubio, S. Sellami, B. Edwards and B. Allmann (2011). Ecos-09 Earthquake Catalogue of Switzerland Release 2011 Report and Database. Public Catalogue, 17. 4. 2011. Swiss Seismological Service Eth Zurich, pp. 42,

Fäh, D., M. Gisler, B. Jaggi, P. Kastli, T. Lutz, V. Masciadri, C. Matt, D. Mayer-Rosa, D. Rippmann, G. Schwarz-Zanetti, J. Tauber and T. Wenk (2009). The 1356 Basel Earthquake: An Interdisciplinary Revision, *Geophys J Int* 178, 351-374

Fritsche, S. and D. Fäh (2009). The 1946 Magnitude 6.1 Earthquake in the Valais: Site-Effects as Contributor to the Damage, *Swiss Journal of Geosciences* 102, 423-439

Fritsche, S., D. Fäh, M. Gisler and D. Giardini (2006). Reconstructing the Damage Field of the 1855 Earthquake in Switzerland: Historical Investigations on a Well-Documented Event, *Geophys J Int* 166, 719-731

Fritsche, S., D. Fäh and G. Schwarz-Zanetti (2012). Historical Intensity Viii Earthquakes Along the Rhone Valley (Valais, Switzerland): Primary and Secondary Effects, *Swiss Journal of Geosciences* 105, 1-18

Fritsche, S., D. Fäh, B. Steiner and D. Giardini (2009). Damage Field and Site Effects: Multidisciplinary Studies of the 1964 Earthquake Series in Central Switzerland, *Nat Hazards* 48, 203-227

Giardini, D., D. Giardini, D. Giardini and S. Erdbebendienst (2004). *Seismic Hazard Assessment of Switzerland, 2004*, Swiss Seismological Service, Swiss Federal Institute (ETH) Zürich.

Giardini, D., J. Wössner and L. Danciu (2014). Mapping Europe's Seismic Hazard, *Eos, Transactions American Geophysical Union* 95, 261-262

Gisler, M., D. Fäh and N. Deichmann (2004a). The Valais Earthquake of December 9, 1755, *Eclogae Geol Helv* 97, 411-422

Gisler, M., D. Fäh and P. Kastli (2004b). Historical Seismicity in Central Switzerland, *Eclogae Geol Helv* 97, 221-236

Gisler, M., D. Fäh and V. Masciadri (2007). "Terrae Motus Factus Est": Earthquakes in Switzerland before A.D. 1000. A Critical Approach, *Nat Hazards* 43, 63-79

Gisler, M., D. Fäh and R. Schibler (2003). Two Significant Earthquakes in the Rhine Valley at the End of the 18(Th) Century: The Events of December 6, 1795 and April 20, 1796, *Eclogae Geol Helv* 96, 357-366

Gisler, M., D. Fäh and R. Schibler (2004c). Revising Macroseismic Data in Switzerland: The December 20, 1720 Earthquake in the Region of Lake Constance, *J Seismol* 8, 179-192

Goertz-Allmann, B. P. and B. Edwards (2014). Constraints on Crustal Attenuation and Three-Dimensional Spatial Distribution of Stress Drop in Switzerland, *Geophys J Int* 196, 493-509

Graves, R. W. and A. Pitarka (2010). Broadband Ground-Motion Simulation Using a Hybrid Approach, *B Seismol Soc Am* 100, 2095-2123

Gregor, N., N. A. Abrahamson, G. M. Atkinson, D. M. Boore, Y. Bozorgnia, K. W. Campbell, B. S. J. Chiou, I. M. Idriss, R. Kamai, E. Seyhan, W. Silva, J. P. Stewart and R. Youngs (2014). Comparison of Nga-West2 Gmpes, *Earthq Spectra* 30, 1179-1197

Hanks, T. C. and R. K. Mcguire (1981). The Character of High-Frequency Strong Ground Motion, *B Seismol Soc Am* 71, 2071-2095

Hiemer, S., J. Wössner, R. Basili, L. Danciu, D. Giardini and S. Wiemer (2014). A Smoothed Stochastic Earthquake Rate Model Considering Seismicity and Fault Moment Release for Europe, *Geophys J Int* 198, 1157-1170

Hough, S. E. (2014). Shaking from Injection-Induced Earthquakes in the Central and Eastern United States, *B Seismol Soc Am*

Johnston, A. C., K. Coppersmith, L. Kanter and C. Cornell (1994). The Earthquakes of Stable Continental Regions. – Assessment of Large Earthquake Potential. Epri Report Tr-102261-V1, 2–1-98., Palo Alto, California, United States.

Joyner, W. B. and D. M. Boore (1993). Methods for Regression-Analysis of Strong-Motion Data, *B Seismol Soc Am* 83, 469-487

Knopoff, L. (1964). A Matrix Method for Elastic Wave Problems, *B Seismol Soc Am* 54, 431-438

Kottke, A. R. and E. M. Rathje (2008). Technical Manual for Strata, *University of California, Berkeley*

Michel, C., B. Edwards, V. Poggi, J. Burjanek, D. Roten, C. Cauzzi and D. Fäh (2014). Assessment of Site Effects in Alpine Regions through Systematic Site Characterization of Seismic Stations, *B Seismol Soc Am* 104

Motazedian, D. and G. M. Atkinson (2005). Stochastic Finite-Fault Modeling Based on a Dynamic Corner Frequency, *B Seismol Soc Am* 95, 995-1010

Poggi, V., B. Edwards and D. Fäh (2011). Derivation of a Reference Shear-Wave Velocity Model from Empirical Site Amplification, *B Seismol Soc Am* 101, 258-274

Poggi, V., B. Edwards and D. Fäh (2013). Reference S-Wave Velocity Profile and Attenuation Models for Ground-Motion Prediction Equations: Application to Japan, *B Seismol Soc Am* 103, 2645-2656

Power, M., B. Chiou, N. Abrahamson, Y. Bozorgnia, T. Shantz and C. Roblee (2008). An Overview of the Nga Project, *Earthq Spectra* 24, 3-21

Rathje, E., A. Kottke and C. Ozbey (2005). Using Inverse Random Vibration Theory to Develop Input Fourier Amplitude Spectra for Use in Site Response, *16th International Conference on Soil Mechanics and Geotechnical Eningeering: TC4 Earthquake Geotechnical Engineering Satellite Conference*, 160-166

Renault, P. (2014). Approach and Challenges for the Seismic Hazard Assessment of Nuclear Power Plants: The Swiss Experience, *B Geofis Teor Appl* 55, 149-164

Rietbrock, A., F. Strasser and B. Edwards (2013). A Stochastic Earthquake Ground-Motion Prediction Model for the United Kingdom, *B Seismol Soc Am* 103, 57-77

Rodriguez-Marek, A., F. Cotton, N. A. Abrahamson, S. Akkar, L. Al Atik, B. Edwards, G. A. Montalva and H. M. Dawood (2013). A Model for Single-Station Standard Deviation Using Data from Various Tectonic Regions, *B Seismol Soc Am* 103, 3149-3163

Scherbaum, F., F. Cotton and H. Staedtke (2006). The Estimation of Minimum-Misfit Stochastic Models from Empirical Ground-Motion Prediction Equations, *B Seismol Soc Am* 96, 427-445

Schwarz-Zanetti, G., N. Deichmann, D. Fäh, D. Giardini, M. J. Jimenez, V. Masciadri, R. Schibler and M. Schnellman (2003). The Earthquake in Unterwalden on September 18, 1601: A Historico-Critical Macroseismic Evaluation, *Eclogae Geol Helv* 96, 441-450

Schwarz-Zanetti, G., N. Deichmann, D. Fäh, V. Masciadri and J. Goll (2004). The Earthquake in Churwalden (Ch) of September 3,1295, *Eclogae Geol Helv* 97, 255-264

Silva, V., H. Crowley, M. Pagani, D. Monelli and R. Pinho (2014). Development of the Openquake Engine, the Global Earthquake Model's Open-Source Software for Seismic Risk Assessment, *Nat Hazards* 72, 1409-1427

Silva, W., R. Darragh, N. Gregor, G. Martin, N. Abrahamson and C. Kircher (1998). Reassessment of Site Coefficients and near-Fault Factors for Building Code Provisions, Technical Report Program Element Ii: 98-Hqgr-1010Pacific Engineering and Analysis, El Cerrito, USA.

Stafford, P. (2011). Procedure for Small-Magnitude Extension of Gmpes, pp. 25, Imperial College London,

Stafford, P. J. (2014). Crossed and Nested Mixed-Effects Approaches for Enhanced Model Development and Removal of the Ergodic Assumption in Empirical Ground-Motion Models, *B Seismol Soc Am* 104, 702-719

Stucchi, M. et al., (2012). The SHARE European Earthquake Catalogue (SHEEC) 1000–1899, J. Seismol., 17(2), 523–544.

Toro, G. R., N. A. Abrahamson and J. F. Schneider (1997). Model of Strong Ground Motions from Earthquakes in Central and Eastern North America: Best Estimates and Uncertainties, *Seismol Res Lett* 68, 41-57

Wiemer, S., D. Giardini, D. Fäh, N. Deichmann and S. Sellami (2009). Probabilistic Seismic Hazard Assessment of Switzerland: Best Estimates and Uncertainties, *J Seismol* 13, 449-478

Wössner, J., D. Laurentiu, D. Giardini, H. Crowley, F. Cotton, G. Grünthal, G. Valensise, R. Arvidsson, R. Basili and M. B. Demircioglu (2015). The 2013 European Seismic Hazard Model: Key Components and Results, *B Earthq Eng* 13, 3553-3596

Worden, C., D. Wald, T. Allen, K. Lin, D. Garcia and G. Cua (2010). A Revised Ground-Motion and Intensity Interpolation Scheme for Shakemap, *B Seismol Soc Am* 100, 3083-3096

Zhao, J. X., J. Zhang, A. Asano, Y. Ohno, T. Oouchi, T. Takahashi, H. Ogawa, K. Irikura, H. K. Thio, P. G. Somerville, Y. Fukushima and Y. Fukushima (2006). Attenuation Relations of Strong Ground Motion in Japan Using Site Classification Based on Predominant Period, *B Seismol Soc Am* 96, 898-913.

6. Hazard integration and computational aspects

6.1 Computational Aspects of PSHA

Probabilistic Seismic Hazard Assessment (PSHA) - short introduction

Probabilistic seismic hazard analysis (PSHA) as originally proposed by Cornel (1968) allows computation of the probability of predefined levels of ground motion at a site being exceeded. During the last few decades, PSHA has become the generally preferred state-of-the art procedure for regional and site-specific seismic hazard analyses; it was also applied for the 2004 Hazard Model (Wiemer et al., 2009a), the PEGASOS projects (Coppersmith, 2009; Wiemer et al., 2009b, Musson et al., 2009), the SHARE model (Wössner et al, 2014) and for all contemporary hazard models of countries neighbouring Switzerland (e.g., Gruenthal, 2009). A key aspect of PSHA is the integration of all sources of hazard and allowance of uncertainty handling. Assuming that earthquake incidents follows a stationary Poisson process (earthquake occurrence is time-independent) the probability that a ground motion parameter exceeds a specific value in a given observation time, t, can be estimated as:

$$P\,(Q\ >\ q)\ =\ 1\ -\ e^{-\lambda(q)\mathrm{t}} \qquad (1)$$

-where $\lambda(q)$ is the annual mean number of earthquakes in which the ground motion parameter "Q" (peak or response spectral accelerations) exceeds the value "q" at a site. A priori, the levels of ground motion must be defined together with the observational time. The average frequency $\lambda(q)$ combines the variability in time, size and location of future earthquakes with the variability (aleatory and epistemic) in the level of ground motions. The pair - probabilities of exceedence and ground motion levels is usually referred as *hazard curve*. From hazard curves of a spatial site distribution, equal probabilities maps might be extracted to construct *hazard maps*. The procedure described by Equation 1 is implemented in various seismic hazard software packages, among the most used being FRISK88M (McGuire 1996) and OpenQuake (Pagani et al., 2014). Note that the Monte Carlo approach implemented in the 2004 national hazard models (Wiemer et al., 2009) is in principle fully equivalent to the hazard integration performed in the 2015 model using OpenQuake.

6.2 Software framework used for the hazard integration

In an internal vetting process, the SED selected the software Framework OpenQuake for the national hazard computations (Figure 58). OpenQuake originated at SED – ETH Zurich within the Global Earthquake Model (GEM) – pilot project in 2009. Since then, OpenQuake has become mature and gained in popularity within the scientific community, due to its unique set of features of computing both seismic hazard and risk. We chose OpenQuake because it is the most modern software available, multi-processor capable, it is open-source, well documented and freely available on GEM's public repositories (https://github.com/gem). An important argument was also that the SED has considerable expertise and experience in operating and developing OpenQuake, a relevant factor for ensuring efficiency and the integrity of the computations. Hazard integration using complex logic trees requires strict quality control procedures in order to ensure the numerical integrity of the computations. Last but not least, the Global Earthquake Model and OpenQuake continues to be supported by the Swiss Federal Government through its support to GEM.

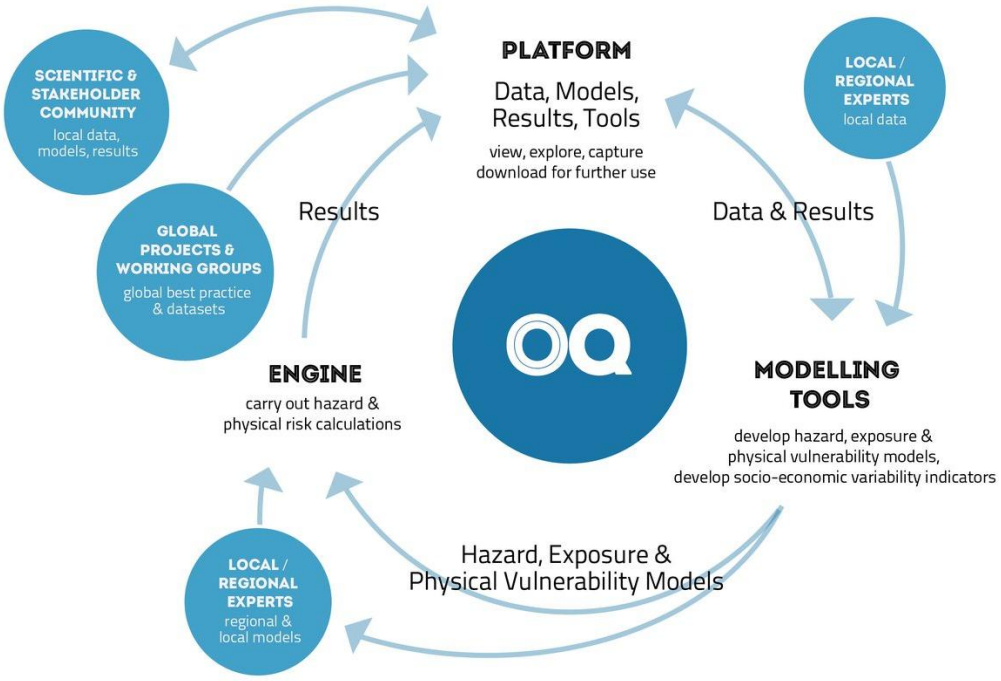

Figure 58: Schematic view of the OpenQuake Platform (source: www.globalequakemodel.org).

OpenQuake is fully supported and under continuous development by the GEM IT team, to which the SED maintains close links. Scientifically, the hazard-calculator integrates the probabilistic algorithms described by Field et al (2003). A key feature of OpenQuake is the use of state-of-the art seismic source representation combined with logic tree options for accounting the input uncertainties. The hazard calculator went through an extensive public validation process (The PEER-Lifelines Validation of Software used in Probabilistic Seismic Hazard Analysis) and thus far, it has been successfully applied to calculate the hazard for large-scale regions such as Europe (Wössner et al., 2015), Middle East or Central Asia (Danciu and Giardini 2015). More information on OpenQuake can be found in Pagani et al. (2013) and Silva et al. (2013).

The use of OpenQuake hazard calculation in Switzerland required a number of adaptations, particularly because the selected ground-motion prediction equations (GMPEs) were not available in the OpenQuake core-hazard library. Thus, we first implemented the selected GMPEs (as described in Chapter 5) following the test-driven development (TDD) paradigm adopted by the GEM IT developing team. This procedure is described at [Implementing-a-new-GSIM-in-the-OpenQuake][13] and source code is available at OpenQuake-GMPEs[14].

6.3 Validation against FRISK88[15]

One important verification of the numerical engine OpenQuake against FRISK88 is performed by PROSEIS and the SED as part of a mandate by ENSI for creating a hybrid SED-PRP model. Test computations were carried out at SED with OpenQuake and at PROSEIS with FRISK88m. On both sides the respective implementation of the full SED source model was combined with a single

[13] https://github.com/gem/oq-hazardlib/wiki/Implementing-a-new-GSIM-in-the-OpenQuake-hazard-library-%5Bprovisional%5D
[14] https://github.com/gem/oq-hazardlib/tree/master/openquake/hazardlib/gsim
[15] This section has been adopted from the Hazard Input Document for the SED-PRP Hybrid model, prepared by PROSEIS (P. Roth; Sept. 15 2015)

GMPE branch, where the Zhao et al. (2006) GMPE was used with a reference VS30 velocity of 700 m/s. The native sigma without truncation was applied for a site located in the canton of Thurgau (9°/47.553°), near the centre of a large source zone of the seismo model.
The computed hazard curves shown in Figure 59 are almost identical up to annual probability of exceedance of 1E-4, with differences in mean spectral acceleration for 100 Hz up to 1.5%. From there, below where the SED model is validated, the curves start to diverge more starkly. We believe that these differences at low annual probabilities of exceedance are to be assigned to the different hazard integration algorithms implemented within the software codes used, and that the observed discrepancies are due to:

- different algorithms for aggregating the total hazard (Field et al. (2003) in OpenQuake vs. Cornell (1968) and McGuire (1976) in Frisk88m)
- differences in the approaches on generating the extended ruptures that are magnitude dependent
- differences in the algorithms for the nucleation of these ruptures along strike and dip
- differences in the algorithms for the source-to-site distance computation
- differences in the implementations of ground motion truncation algorithms
- possible slightly different GMPE implementations
- possible different definitions of magnitude-scaling equations (Wells and Coppersmith 1994) or point-like scaling relationship)

Such differences between existing seismic hazard codes have long been known about and have been the subject of extensive studies (e.g. Thomas et al., 2010). We consider an agreement of up to 1.5% at the very longest return periods considered an excellent and fully satisfactory agreement, and a verification that the OpenQuake-based computations of the SED hazard model are correctly implemented.

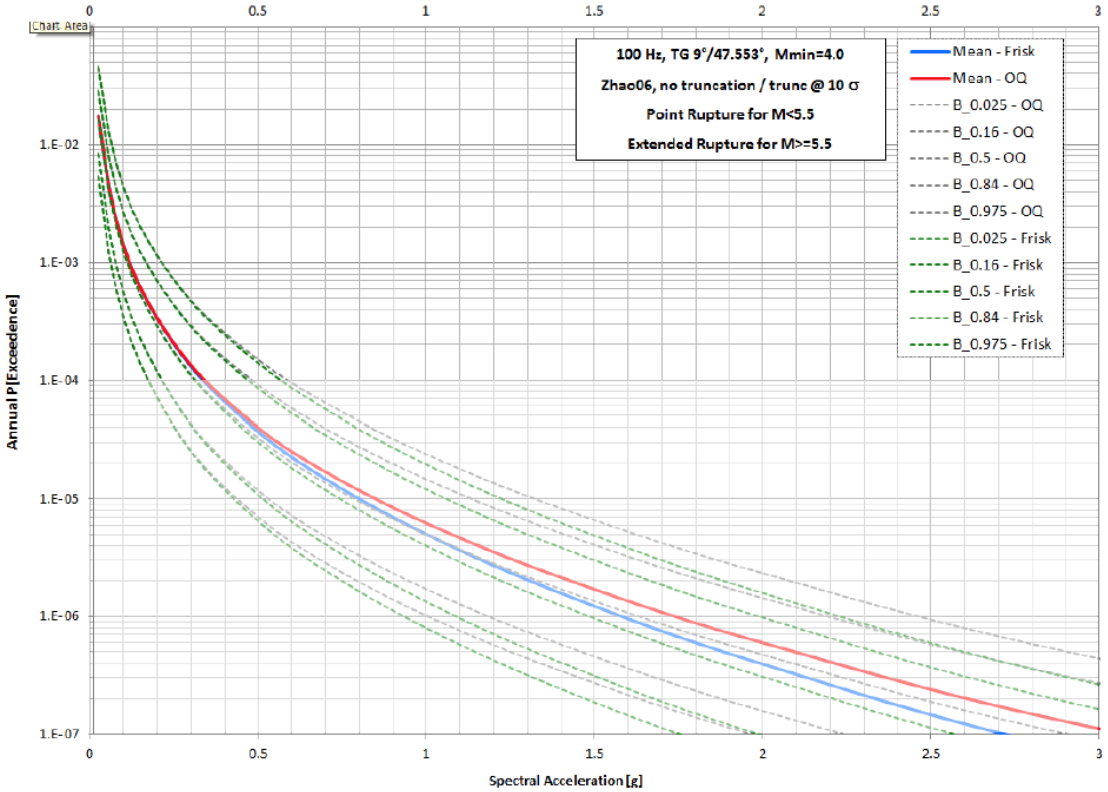

Figure 59: Hazard obtained with OpenQuake at SED (red and green curves) and with frisk88 at PROSEIS (blue and grey curves), combining the SED source characterization model with a single GMPE branch (see text). For both sites the curves start to diverge

at approx. 0.4g. The greyed-out area below an annual probability of 1E-04 is the area for which the SED model has not been validated (source: PROSEIS, P. Roth).

6.4 Single source parameterization

A key aspect of the hazard calculation is always the parameterization of seismic sources, which generally conforms to the software requirements. In the Swiss 2015 model case, each seismogenic source is modelled as a point source following the taxonomy and blueprints defined by OpenQuake User's manual. A point source as featured by OpenQuake is an earthquake source capable of nucleating finite ruptures as extended surfaces, sometimes also called an extended rupture. These extended surfaces are magnitude-dependent controlled by empirical magnitude-scaling relationships (i.e. Wells and Coppersmith 1994) and rupture aspect ratio. Their shape is constrained to extend within a lower and upper seismogenic depth; hence avoiding uncontrolled extension over the surface. An example, extracted from OpenQuake of such extensive ruptures controlled is presented in Figure 60.

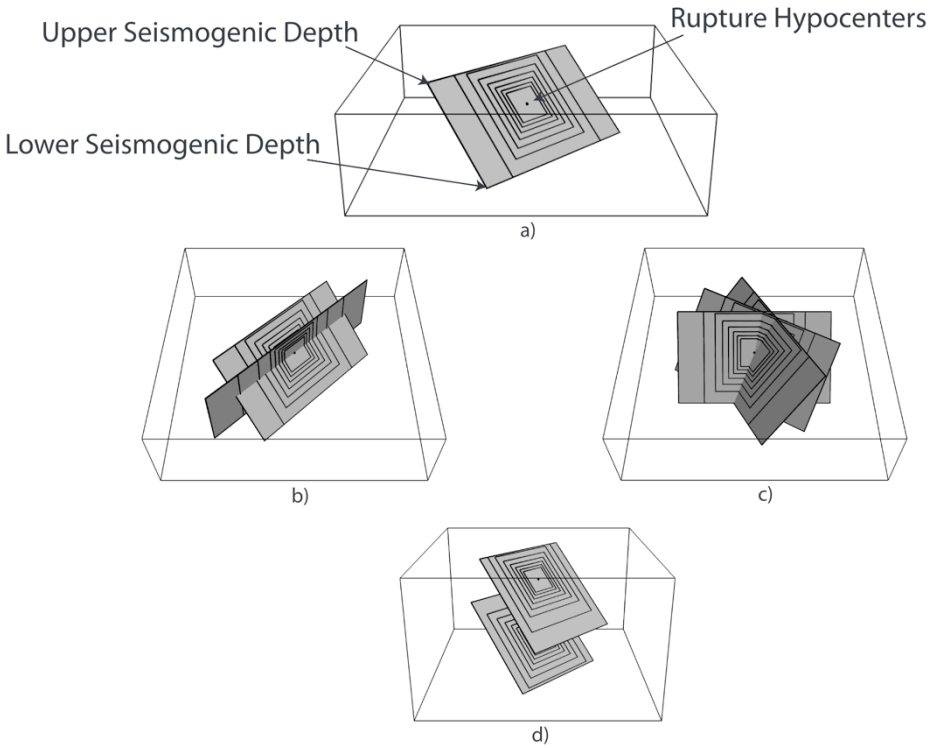

Figure 60: Examples of various types of extensive earthquake ruptures as generated by a point source. For a single location on Earth surface, extensive ruptures are nucleating underneath, with their size controlled by a magnitude-scaling relationship and shape controlled by aspect ratio value. Ruptures can be distributed over multiple dips b), strikes c) and hypocentral depths d). All ruptures forced to not exceed the upper and lower seismogenic depths. Figure extracted with permission from *The OpenQuake-engine Book: Hazard* (Pagani et al 2014).

The use of complex point sources is a major difference of the 2015 model when compared to the 2004 Swiss seismic hazard model (Wiemer et al., 2009) that used for simplicity, a single point source representation even for the largest-scale events. While the point source approximation is appropriate for small magnitude earthquakes (e.g., magnitude 5 or smaller) it is clearly an over-simplification for extended rupture of magnitudes exceeding 6.0. Considering rupture finiteness with respect to the point-rupture leads to a significant increase in the probabilities of exceedence for a given level of motion (Monelli et al., 2014) even if the orientation of the fault is unknown and assumed to be random. In the Swiss hazard model, we assume that the seismogenic sources are capable of generating extensive ruptures above Mw5.5. Below this magnitude value, the earthquake ruptures are approximated as a point. We consider the point approximation as suitable for small magnitude ruptures given that earthquake events of small magnitude almost never reveal

themselves at the Earth surface. This aspect introduces additional uncertainties into the magnitude-scaling relationships that are calibrated to larger-scale events with well-identified fault traces. We will term the seismogenic sources modelling earthquake magnitudes less than or equal to M_w5.5 as "point sources" and those of magnitudes greater then M_w 5.5 as "extensive-point sources".

Style-of-faulting is another important feature to be defined, particularly to extensive point sources. Style-of-faulting links the seismogenic source with the median ground motion corresponding to that particular style-of-faulting. Three styles of faulting, namely normal, reverse and strike-slip are defined for each extensive-point source. The average strike, dip and rake angles are parameterized to define the style-of-faulting. Seismogenic depth is yet another key parameter to be assigned to each seismogenic source. The distribution of the seismogenic depth values follows the observations of the seismicity with depth summarized in Chapter 4.

6.5 Master logic tree

A logic tree structure is used to reflect alternative data, models, and methods, and incorporating the centre, body, and range of technically defensible interpretations into the final hazard model. A logic tree is ideally built in such a way that the branches are mutually exclusive and cumulatively exhaustive (see Marzocchi et al., 2015, for an extensive discussion and drawbacks). In this sense, the final logic tree is optimized to include only those elements that capture current knowledge and uncertainties which are believed to be significant to hazard. The main elements of the logic tree combine the ground motion models with the regional seismotectonic settings, i.e. Foreland and Alpine, as a function of seismogenic depth. The *shallow* logic tree describes the modelling uncertainties of the shallow seismicity down to 9km, above this value the *deep* logic tree modelling the observed deep seismicity. Four logic trees result for the following combinations of seismotectonic regions: Alpine Shallow, Alpine Deep, Foreland Shallow and Foreland Deep. The final configuration of each logic-tree consists of two major branching levels one for the earthquake rate models and one for the ground motion.

Aleatory uncertainty of ground motion was directly integrated in the hazard calculation via two equally weighted models of "*sigma"*. The "s*igma"* is the standard deviation of the regression residuals about the median prediction equation, and it is generally separated in two parts: inter- and intra-event. Incorporation of the "*sigma*" in the hazard calculation results in an increase of the median hazard particularly at low probabilities. We use an inter-event (single-station) "*sigma"*, and the choice of the "*sigma*" models is described in Chapter 5 and is not repeated here. The aleatory uncertainty is also captured in all the percentiles of the hazard estimates.

In addition to the ground motion logic tree, the uncertainty of the seismogenic sources depicts five branches of earthquake rates. The earthquake rate branches represent all information related to earthquake occurrence systematically addressed to forecast the long-term seismicity rates as described in Chapter 3. The earthquake rate branches are the basis for computing the probabilities of exceedence of ground motion as described in turn by the stochastic and empirical GMPEs models. The final logic tree for seismic hazard calculation consists of four main GMPEs logic trees and five earthquakes rate models as shown in Figure 61.

The resulting number of end-branches for a site is about 1 million. The total number of seismogenic source representations is about 154,000. The large number of end-branches combined with the number of seismogenic source greatly affect how the seismic hazard is calculated and decisions were taken to simplify the procedure without losing the accuracy of the final hazard results. Consequently, for computational efficiency we used the option of random-sampling the entire logic tree. OpenQuake features a sampling technique for trimming large logic trees, which is

computationally efficient for reducing the total distribution of the end-branches realizations. The random sampling technique implies sampling of mutually exclusive models, and the resulting samples are correlated. Nonetheless, one needs to estimate beforehand the number of simulations required to obtain stable results, which might be time consuming. After several trials we have stabilized the number to 100,000 samples. This still captures the range of uncertainty acceptably well, and has lower computational requirements.

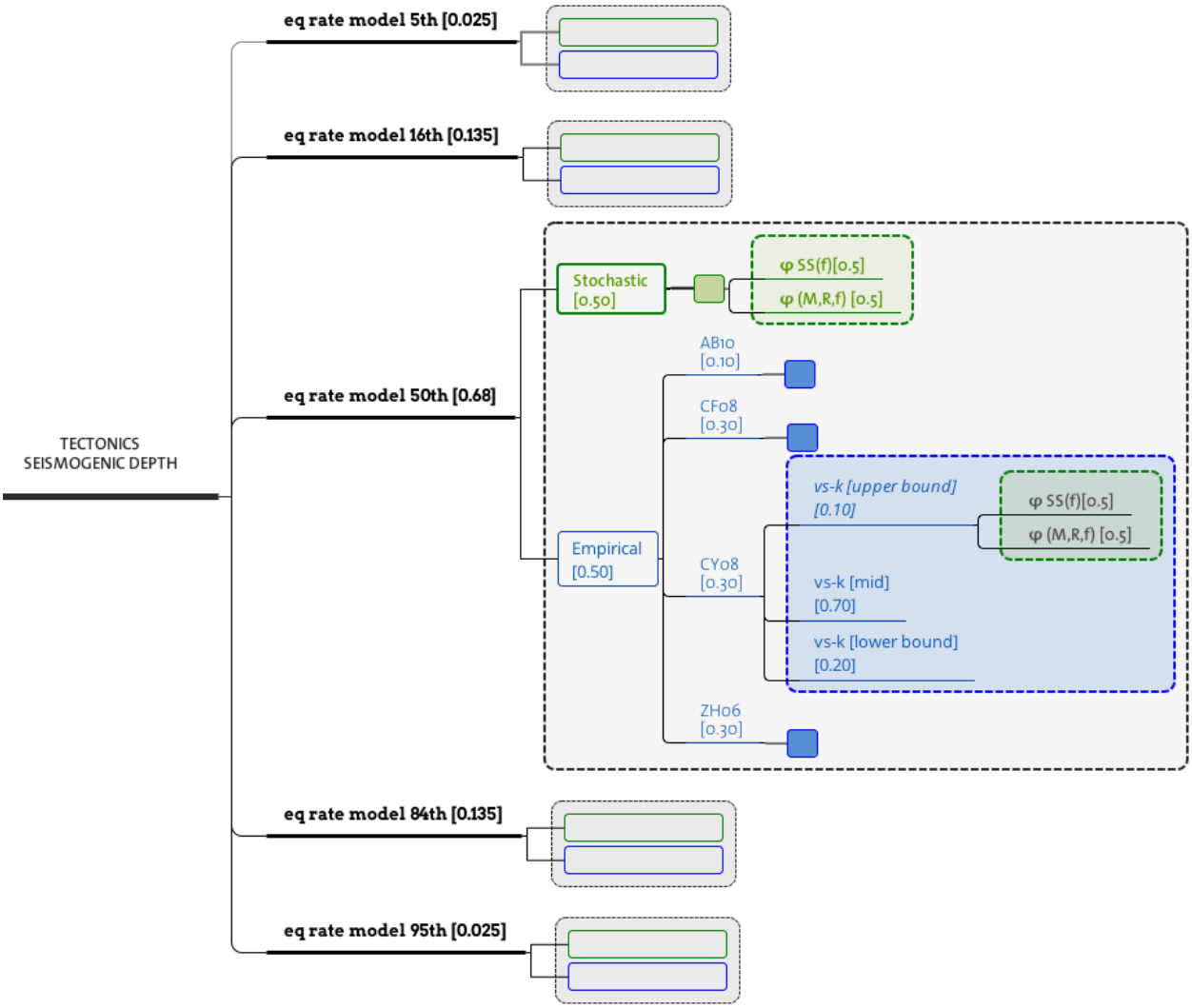

Figure 61: Master logic tree depicting the earthquake rate forecast models and the ground motion models. The stochastic models are illustrated in green and correspond to their definition in Figures 5 to 7, Chapter 3. The blue branches represent the empirical ground motion models. The empty branches indicate a repetition of the ground motion branches (stochastic and empirical). See Figure 34 for the breakdown of the source logic tree.

6.6 Computational settings

The computational grid is retained identical to the computational grid used to generate the maps of the 2004 Swiss seismic hazard (Giardini et al. 2004; Wiemer et al., 2009). This will facilitate comparison between the two models without spatial interpolation. The seismic hazard model aggregates the contribution of earthquakes greater than magnitude $M_w \geq 4.00$, the minimum magnitude of engineering significance. Also, contributions from distant-source zones (more than 200 km) were excluded, because their hazard contributions are negligible.

Input files are prepared for OpenQuake following the NRML standardization. The NRML stands for Natural hazards and Risk Mark-up Language adopted by GEM as the default file formats. The use

of a standardized file will provide the unique possibility of replicating the computational paths entirely or partially, reviewing the input models and re-computing the hazard. Sample input files for OpenQuake are given in Appendix B. The analysis is performed for a reference (base rock) site condition with an average V_{s30} (the average shear-velocity down to 30 m) of 1100 m/s (see Chapter 5).

The ground motion is described by peak ground acceleration (PGA) and pseudo-acceleration spectra of 5-percent damping (hereafter SA) at various fundamental periods. The former describes the dynamic properties of a simplified oscilloscope of different masses, in the frequency (periods) ranges of engineering interest throughout the Swiss built environment. The values (in seconds) of the fundamental periods are: 0.05, 0.01, 0.1, 0.2, 0.25, 0.3, 0.4, 1.0, 2.0, 3.0 and 4.0.

Hazard results consist of median (50^{th}) values, mean and pairs of *one- sigma* (16^{th} and 84^{th}) percentiles and of *two-sigma* (5^{th} and 95^{th}) percentiles; the latter includes a measure of epistemic uncertainties incorporated into the hazard model. Either median or mean might be used as basis for engineering design; we recommend the median (50^{th}). Statistically speaking, the median represents the central value of a distribution, and divides the distribution in equal number of data values which are above it and bellow it. Median values were also reported in the 2004 Swiss hazard model (Giardini et al 2004).

The current results are valid for the geometrical mean of the two horizontal components of the ground shaking. Vertical ground shaking was not modelled, mainly due to limitation of available ground motion models for vertical ground motion.

To ensure an understanding in the changes of the results with respect to the ground motion input, we provide results of sensitivity analyses. Also, we investigate the comparison in the hazard estimates between the 2004 (Giardini et al., 2004) and the present study. Of significant importance is the comparison between the new results and the Swiss Standard for seismic design SIA 261. We also compare results to the PRP site-specific hazard results.

7. Swiss hazard 2015: main results

This chapter presents selected results of the seismic hazard for Switzerland and its uncertainties. We illustrate here only a limited number of hazard outputs. The full collection of the hazard results (390 hazard maps, 23220 uniform hazard spectra and 50310 hazard curves) is online and open-for-access at European Facilities for Earthquake Hazard and Risk (www.efehr.org).

The following hazard outputs are described in this chapter:

- Hazard Curves
- Hazard maps
- Uniform Hazard Spectra
- Disaggregation

7.1 Seismic hazard curves

Results are presented for the reference rock only, in the form of hazard curves, for the 5th, 16th, 15th, 50th (median), 85th, 95th percentiles and mean estimates of the geometric mean of the two horizontal components of the ground motion. All hazard curves hereinafter are defined as probabilities of exceedance in a 50-year observational period (y-axis) of various ground motion levels (x-axis). The latter is defined either by PGA or spectral acceleration (5% damping) in units of gravitational acceleration [g]. The hazard curves are presented for the four densely populated cities, Zurich, Geneva, Basle and Lausanne. The corresponding plots for 5% damping spectrum acceleration at a reference period of 0.2 sec (hereafter SA [0.2 sec]) also corresponding to an equivalent frequency of 5Hz is shown in Figure 62. The hazard curves are displayed for probabilities of about 10^{-4}. As expected, hazard estimates are higher for Basle, whereas the values for Zurich and Geneva are comparable. Hazard estimates for Lausanne lie in between the values estimated for Basle and Geneva.

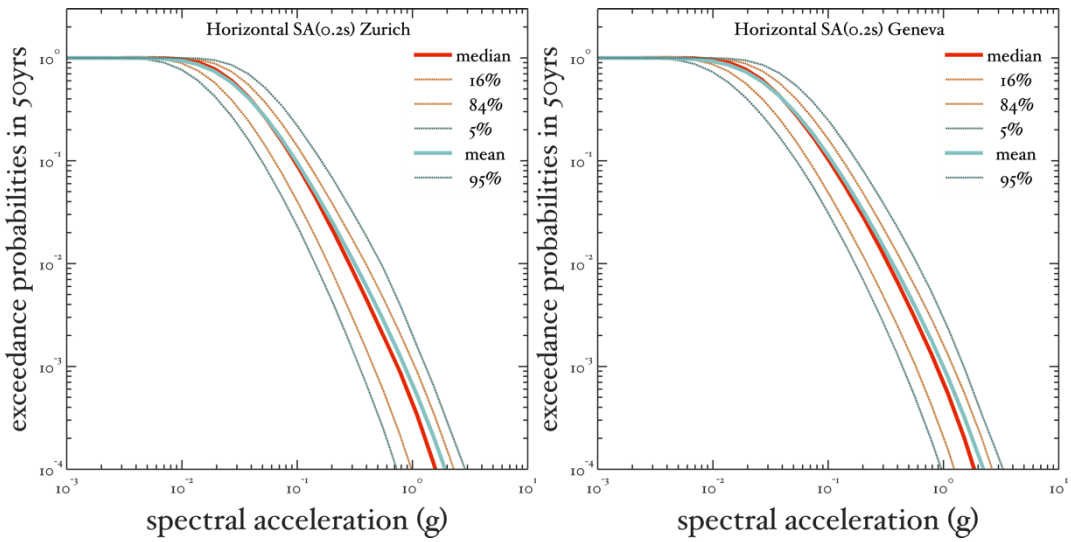

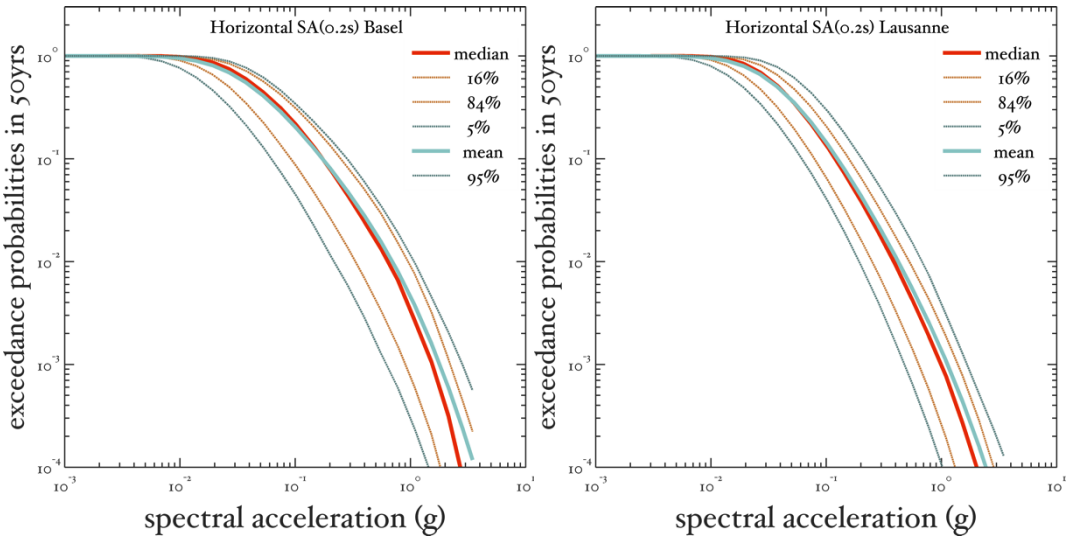

Figure 62: Horizontal - 5% damping - SA [0.2s] hazard curves for six densely populated cities, Zurich, Geneva, Basle and Lausanne. Curves are median (red) mean (blue), *one-sigma percentiles* (orange) and *two-sigma percentiles* (light blue).

7.2 Seismic hazard maps

Typically, a hazard map consists of spatial distribution of ground motion values corresponding to a fixed probability of exceedance reported for each computational grid point. In other words, a hazard map shows the values of all hazard curves at just one exceedance probability or return period. Often the hazard maps are reported in literature as values of a mean annual frequency of exceedence or else by mean return periods. For example, a 10% in 50 years will correspond to a mean annual frequency of exceedence of about 0.002107, and to a mean return period of 475 years (1/0.002107 ~ 475 years, Appendix A). Note, that these terms are to be used only in a statistical sense. A return period of 475 years does not imply an expected hazard in the *next* 475 years; it rather indicates that the hazard level in the next one year has a very low probability (i.e. 0.002107 per annum) of occurring (Musson and Winter 1997).

Figure 63 shows the reference seismic hazard map for SA[0.2s] (i.e., 5Hz) as obtained for a reference rock of 1100m/s corresponding to a mean return period of 475 years (or 10% probability of exceedance in 50years). The reference hazard map incorporates the weighted earthquake rate models combined with the tectonically dependent ground motion models. As might be expected, the contours of equal probabilistic ground motion follow the patterns of the areas where earthquakes were observed in the past *().* Geographically, the maximum ground shaking values are reached in the Valais with the SA [0.2s] values in the range of 0.20-0.25g. The second highest hazard values are obtained in Basle region. Third ranking in terms of ground shaking is Grisons. The regions of lowest hazard are the Ticino and parts of the Molasse basin.

As one can see already from the fractiles hazard curves in Figure 62, there is considerable uncertainty around the median hazard estimate. This is typical for hazard assessments. This uncertainty results partly from the fact that there is a natural variability in the underlying processes:

- The following time periods may see (by chance) fewer or more earthquakes than in the long term average (aleatory variability).
- The estimated rates may be systematically biased, too low or too high, in a certain region, or overall (epistemic uncertainty).
- The events in the next time period may (by chance) produce higher or lower than average ground motions (e.g., because of their stress drops; aleatory variability).
- The ground motions forecast may be systemically too low or too high (epistemic uncertainty).

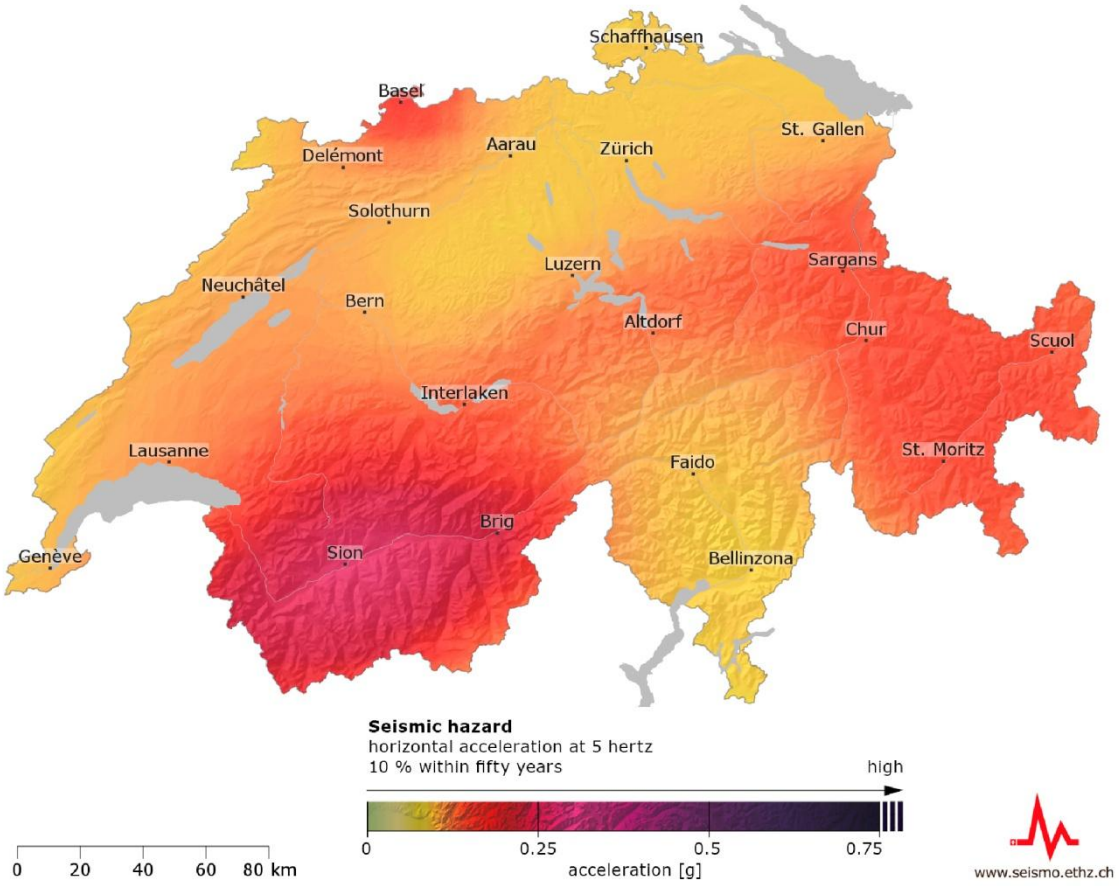

Figure 63: Reference ground motions maps of SA[0.2s] with equal probability level of 10% in 50years estimated on reference (base rock) site condition Vs30 = 1100m/s for Switzerland. This map is also available in poster size.

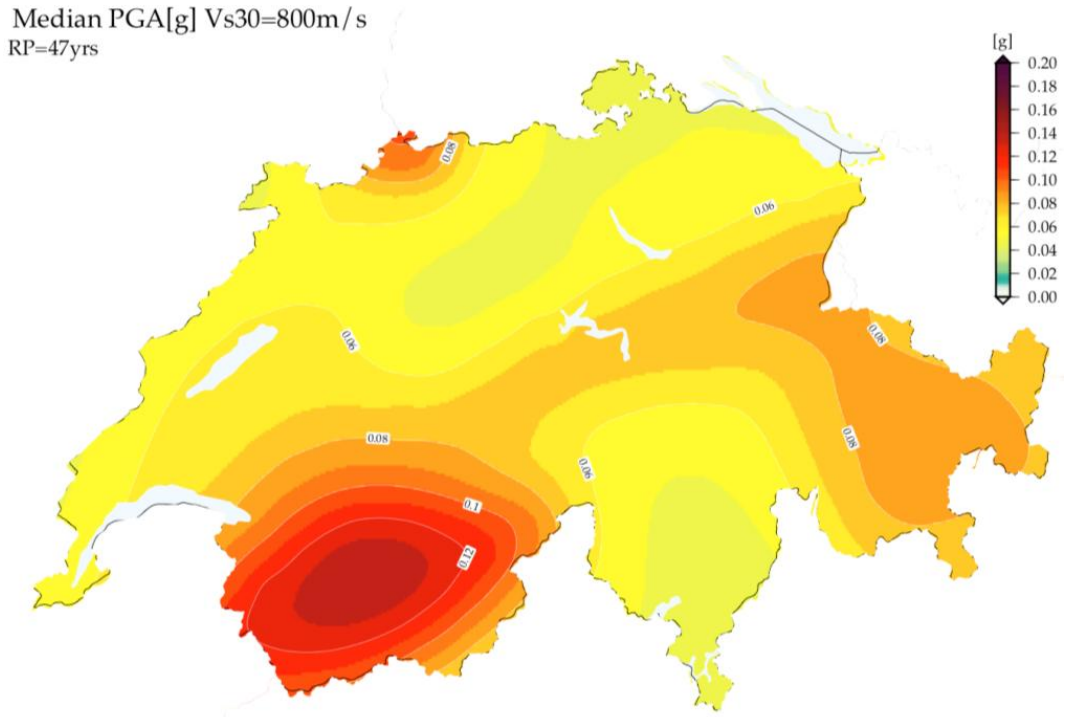

Figure 64: Map of Peak Ground Acceleration (PGA) based on SUIhaz2015 for a return period of 475 years and a reference rock with an assumed shear wave velocity in the top 30 meters of 800 m/s.

These sources of variability and uncertainty are represented in the model and explain the width of the fractiles around the median hazard. Another way to illustrate the uncertainty is depicted in Figure 65, where we show the uncertainty maps corresponding to one standard deviation (16th an 84th percentiles) and two standard deviations (5th and 95th percentiles) of SA[0.2s] and a mean return period of 475 years. The pattern of the percentile seismic hazard maps is preserved when compared with the reference map, as expected. This indicates a statistically stable distribution of results. However, the absolute level of hazard varies substantially, of course: Between the 5th and 95th fractiles, the hazard values change by a factor 3 to 4, which is a typical values found for most contemporary PSHA studies. Additional set of maps (median and percentiles) for different ground motion parameters and different return periods are available online at www.efehr.org.

For engineering purposes, an important map is also the Peak Ground Acceleration (PGA), which is shown in Figure 64 for a reference site of SIA class A, with an assumed 800m/s Vs30 velocity. See Chapter 7.6 for information on the conversion between different site conditions.

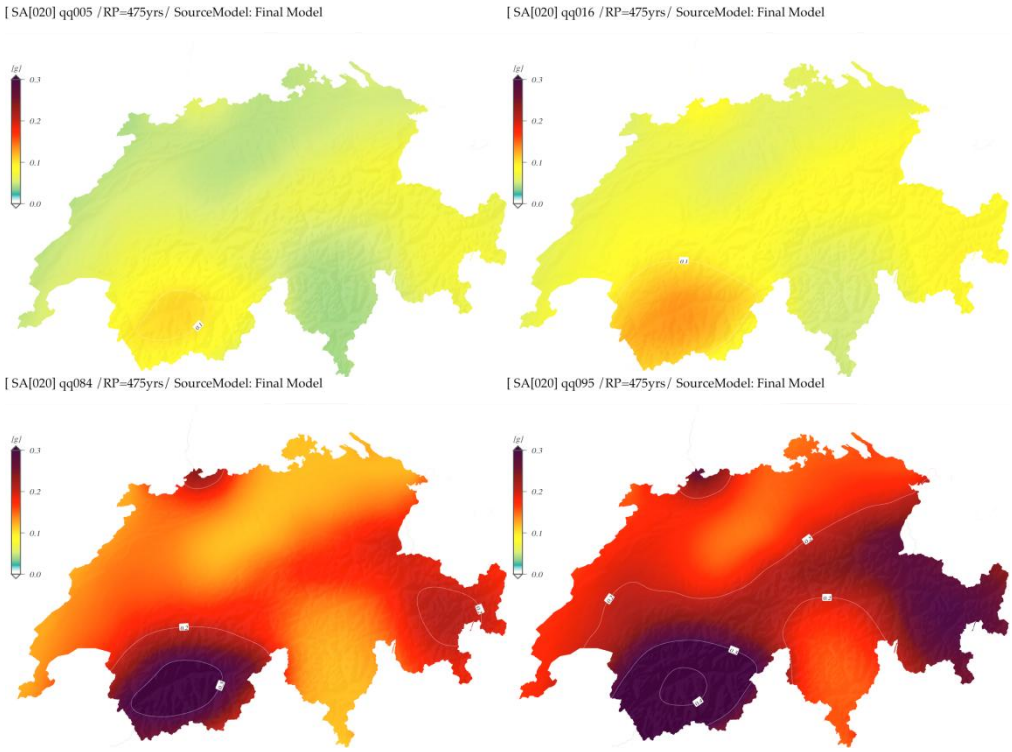

Figure 65: Lower 5th (top-left) and 16th (top-right) quantiles and the upper 84th (bottom-left) and 95th (bottom-right) quantiles maps. All maps represent SA[0.2s] with equal probability level of 10% in 50years estimated on reference (base rock) site condition Vs30 = 1100m/s for Switzerland.

To illustrate the influence of the return period on the overall hazard level, we show in Figure 66 the change of hazard level for different ground motions. Note that we intentionally choose for the published hazard maps one colour scale and range for all return periods and frequencies, so that these first order differences can be appreciated and seen in perspective to spatial variation across the map.

Figure 66 illustrates one of the major consequences of our current understanding of the seismogenesis of Switzerland's consequent hazard: All of Switzerland is earthquake country! Large earthquakes can occur everywhere Switzerland, albeit at a different rate of occurrence. As a consequence, the hazard differences between regions such as the Valais and Zurich, a factor 2-3, is minor when compared to the increase of hazard for longer return periods (a factor 10 – 30). For return periods of 2,500 years, the hazard in the Ticino is about as high as the one for a return period of 500 years in the Valais. In other words:

➔ If one waits long enough, or considers low probabilities, strong shaking will happen everywhere in Switzerland, there are no inherently safe places.

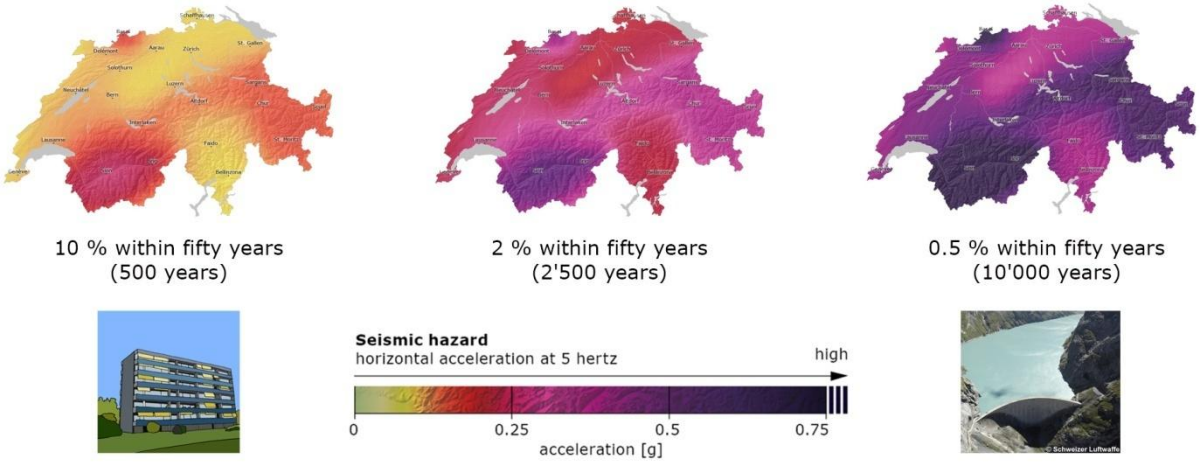

Figure 66: Hazard maps for different exceedance levels: from 50% in 50 years to 0.5% in 50 years. All maps represent SA[0.2s] estimated on reference (base rock) site condition Vs30 = 1100m/s for Switzerland.

7.3 Intensity probability maps for Switzerland, including indicative local site amplification

There is a strong additional effect on hazard due to the local site conditions that a reference-rock maps will not show. Because local site conditions can vary dramatically, on the scale of tens of meters, local site amplifications are only known in few selected places so far that were studied in microzonation projects or specific site effect investigations[16]. It is well known that local site amplification can reach factors of 3 to 5 and more at sediment sites, thus again being equal to the relative spatial difference between regions such as the Valais and the Foreland.

To illustrate the relative importance of local site conditions, we prepared a selection of indicative hazard maps on approximate local site conditions. Examples of these maps are shown in Figure 67. The effects of an earthquake are measured by intensity according to the European Macroseismic Scale (EMS-98). The maps show the probability of intensity VII or larger and the associated effects within the next 50 years. Note that because the foreland generally enhanced in hazard, due to the fact that most sites in the foreland are in relatively soft soil conditions rather than on hard rock. These maps are only indicative and should not be applied for site-specific hazard assessments, which is why we do not provide access to the numerical value of these maps on our online platform.

Intensity probability maps for macroseismic intensities of IV, VII and VII for return periods of 1, 50 and 100 years were calculated starting from the mean hazard curves for reference rock conditions with a vs30 of 1105m/s. For the conversion, the ground motion to intensity conversion equation (GMICE) of Faenza & Michelini (2010) (FM10) was used. Although defined in MCS intensity and derived from Italian data, the Faenza & Michelini GMICE is within one sigma of the Swiss EMS-98 based Kaestli & Fäh (2006) GMICE (KF06), as far as the PGA range of their base data overlap. However, FM10 extends further towards stronger motion and is thus preferred here. Faenza & Michelini do not define their reference soil conditions – we followed the estimation of Fäh et al (2010) for KF06 and assumed a medium stiff soil with a vs30 of 600m/s. In order to correct the converted hazard curves in EMS-98 intensity for the weaker standard soil, we followed Edwards et al. (2009) and Cauzzi et al. (2015) and shifted them by 0.47 intensity units towards higher intensities.

[16] The BAFU and SED are currently proposing a national earthquake risk assessment project, which would substantially improve the existing knowledge base.

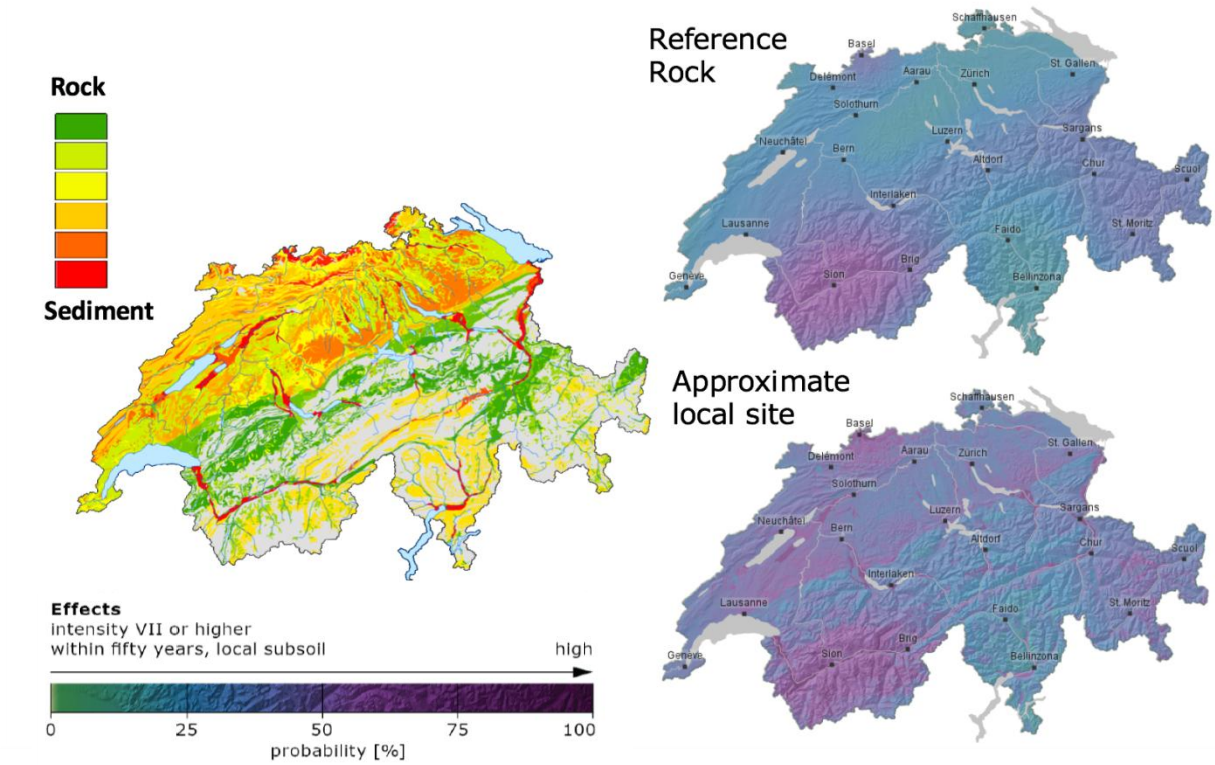

Figure 67: Left: Map of Switzerland, colour-coded is the indicative site amplification between a typical rock and soft sediment site, Right: Effects map: the probability of experiencing shaking on local subsoil with a macroseismic intensity VII or higher within fifty years on reference rock (top) and with indicative local site amplification (bottom).

In order to convert the intensity hazard curves back to a probability of exceedance map for a specific, ordinal intensity of n, the PoE of each curve was read at an intensity of n-0.5, i. e., e.g. at intensity = 6.5 for the intensity 7 map. This takes into account that a continuous/probabilistic intensity of 6.5+δ is more probable to be consistent with the intensity 7 class than with any other, and is a bias-free inversion of the interpolation done when deriving the GMICE from ordinal intensity and continuous PGA.

For these intensity probability maps, which take into account actual soil condition rather than a reference soil (thus include site amplification), we used the site amplification map of Kaestli & Fäh (2006, Figure 67). Following the method described in Alvarez-Rubio et al. (2010), this map starts from the same intensity data set as the KF06 GMICE and derives relative intensity amplifications specific to soil classes of the geological and geotechnical maps of Switzerland at a scale of 1:500'000. Given the consistency of the CF10 and KF06 GMICEs, it is assumed to be applicable also to KF06 converted intensities. For each point of Switzerland, the local site amplification/deamplification was used to add a further shift to the mean hazard curve in intensity of the nearest SUIHAZ-15 grid point, before reading the PoE corresponding to the shifted intensity. Given the fact that the small scale heterogeneity of the rock hazard is considerably lower than the heterogeneity of the amplification and the amplified ground motions, this technique allowed to approximate the resolution of the resulting intensity probability map to the resolution of the geological and geotechnical maps (few 100 meters) rather than the grid of the hazard model (0.05° ≈ 5 km).

The resulting intensity probability maps (Figure 68) report expected values only. While no full error analysis was conducted, it is clear that the uncertainty of the hazard model is notably increased by contributions from the vs30 reference shift, the GMICE (±σ ≈ 0.5 intensity unit ≈ a factor of 2.2 in ground motion), and the fact that the site amplification map disregards the influence of layer thickness, 2D and 3D effects. It is known e.g. from Edwards & Fäh (2013) that spectral acceleration would be a better proxy for earthquake damage and thus intensity than PGA.

However, for spectral acceleration no locally calibrated or confirmed GMICE is available for Switzerland.

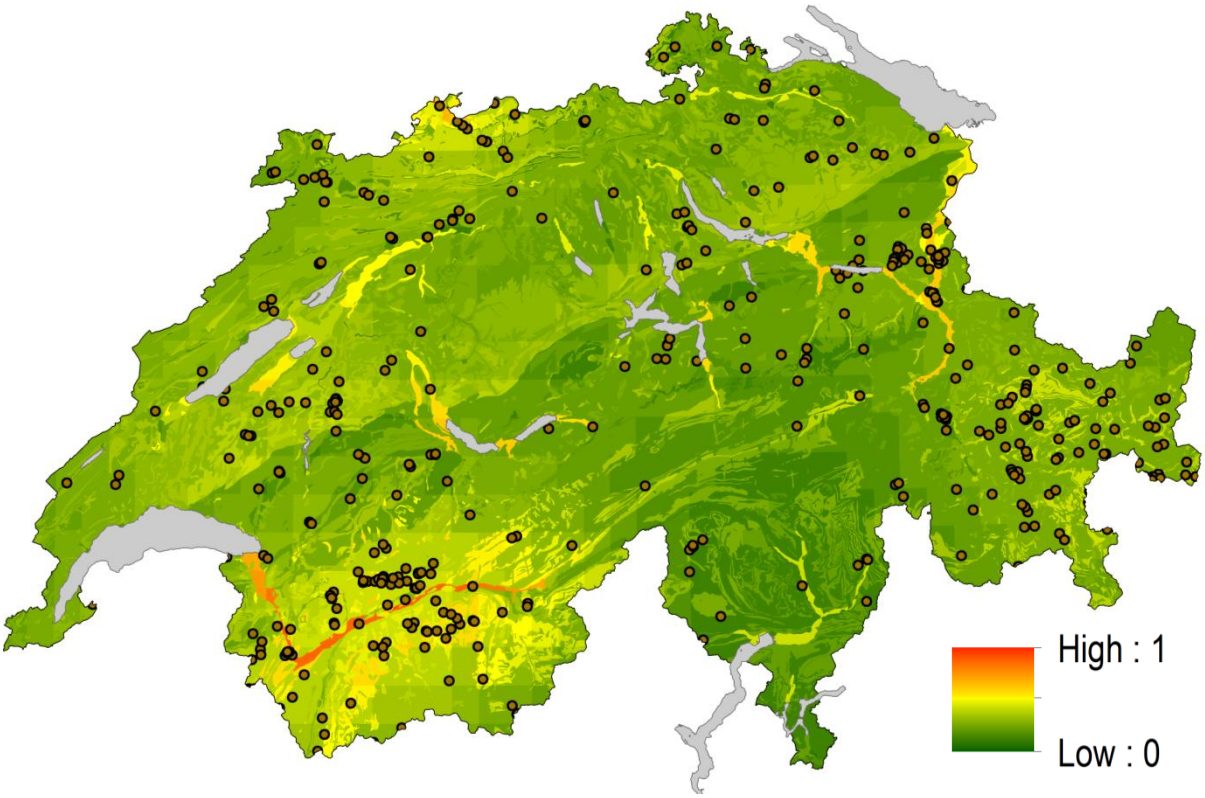

Figure 68: Example of an intensity probability map, colour-coded is the probability of exceedance of an intensity VII within 50 years at local soil conditions. Probabilities of exceedance vary between 3% and 39%. Dots are earthquakes of magnitude M2.5 or larger for the period 1975 - 2015.

7.4 Uniform Hazard Spectra (UHS)

Different building or infrastructure types respond in characteristic ways to different excitation frequencies. Therefore, it is important to compute earthquake ground motions for a wide range of ground motions. This is typically done using an uniform hazard spectra that provide spectral acceleration values of uniform probability levels for a range of spectral periods. Uniform hazard spectra are generally the basis for defining the seismic design level applicable to new buildings. Median (50^{th}) or different percentiles are used to shape these design spectra according to the importance of the structure under design.

Figure 69 illustrates the UHS for the city of Martigny in the Valais. Median (50^{th}), mean value, and four percentiles (5^{th}, 16^{th}, 84^{th} and 95^{th}) are presented for a mean return period of 475 years. In addition, we show the related hazard maps at these frequencies, in order to allow for a comparison of the relative impact of frequency versus location. Figure 70 illustrates the UHS for two cities (i.e. Basle and Vernier) located in regions of relatively high ground-motion hazard. Median (50^{th}), mean, and four percentiles (5^{th}, 16^{th}, 84^{th} and 95^{th}) are presented for different mean return periods of 475, 2,475 and 9,975-years respectively. As expected, the values increase with the increase of return period given the increase of recurrence rates of larger magnitude events that will result in greater ground motion at a site. Most peak horizontal acceleration values occur at ground-motion periods of 10 cycles per second (0.1s). We note that within the PGA and SA (0.05s) there are no intermediate periods used for calculation, hence not plotted. The PGA is plotted as a dots corresponding to different statistical units (mean and percentiles), whereas the remaining spectral periods of the UHS are linked.

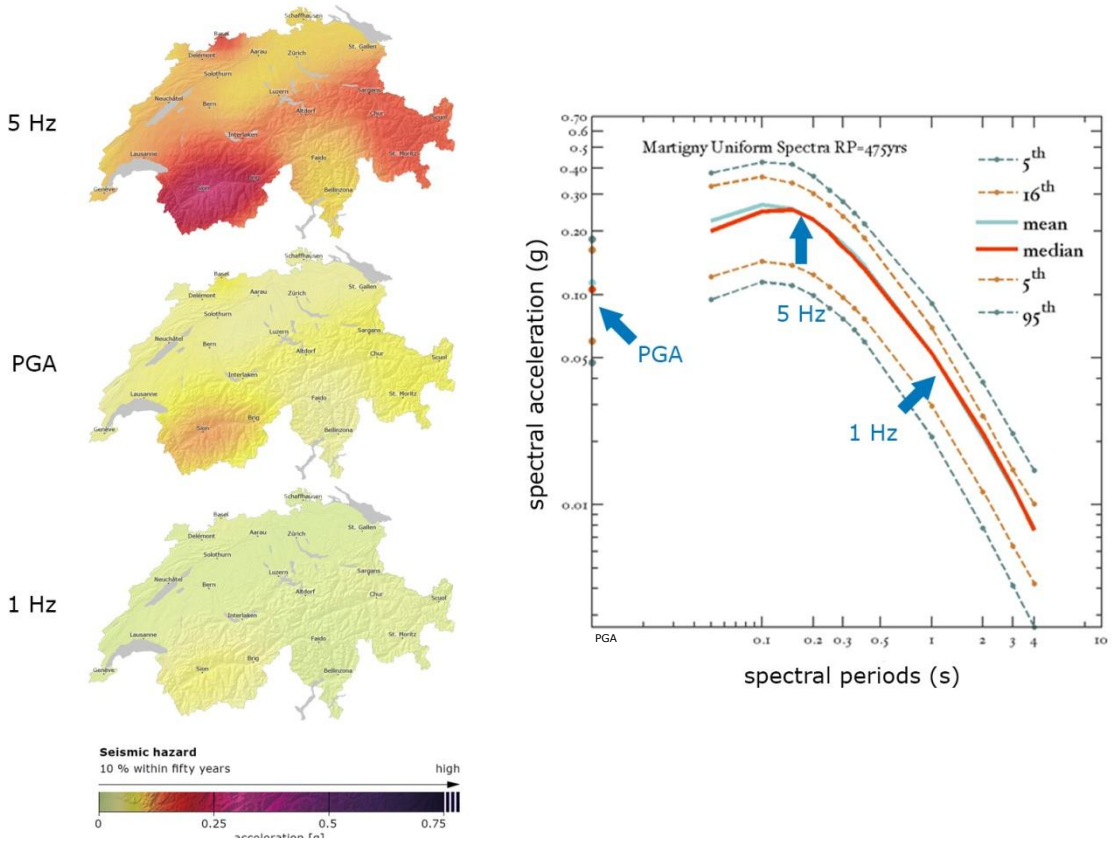

Figure 69: Right: Uniform hazard spectrum for the site 'Martigny' for a return period of 475 year for a reference rock. Arrows indicate the spectral periods for which on the left selected hazard maps are shown.

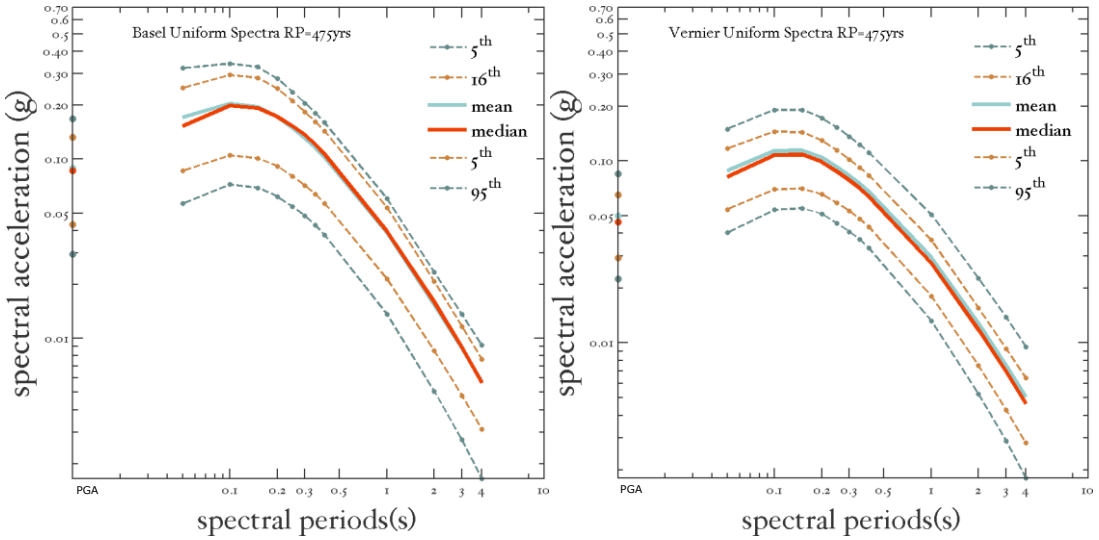

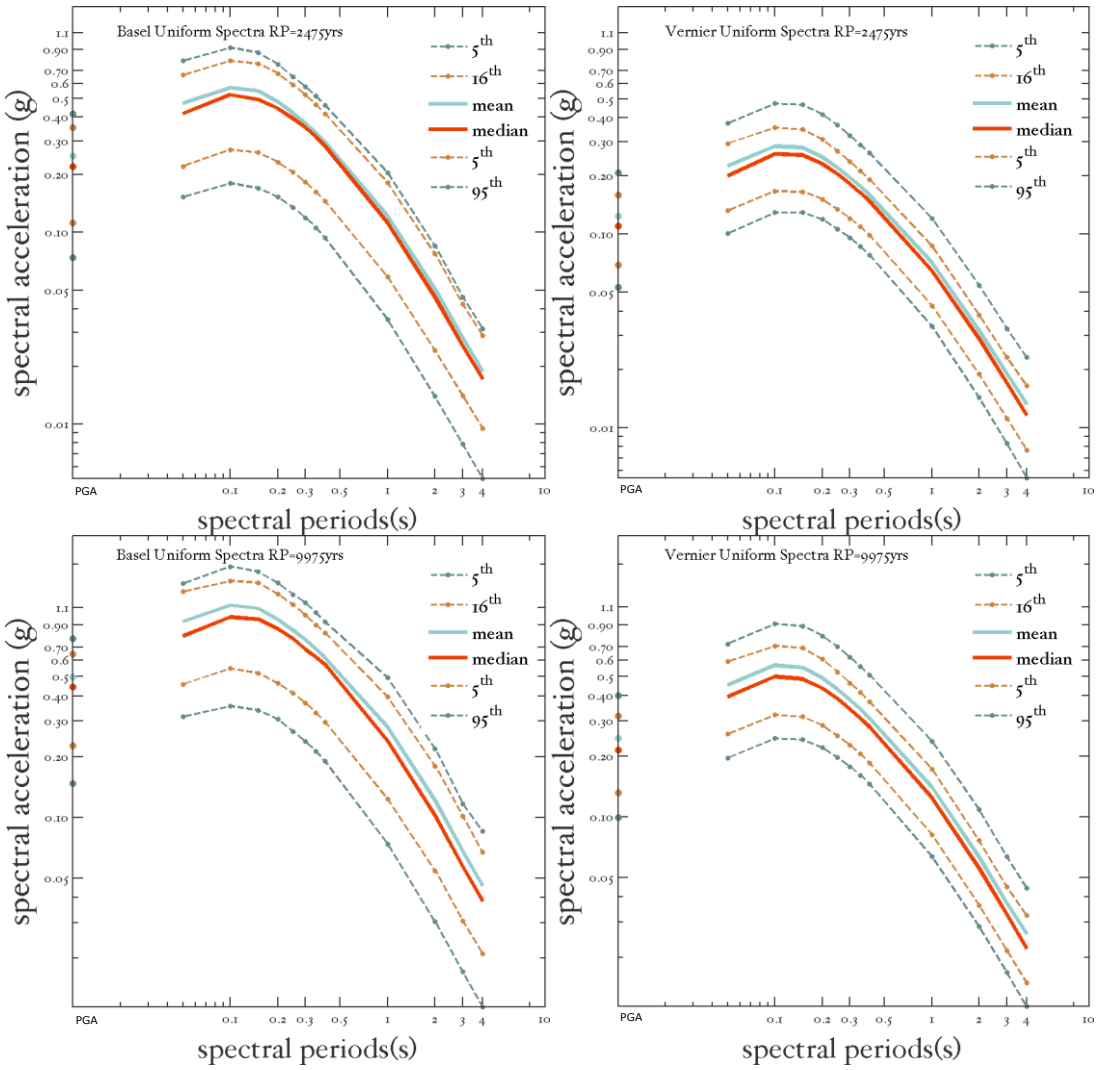

Figure 70: Complete set of Uniform Hazard Spectra for Basle and Vernier. Plots are organized for different mean return periods of 475 years (top), 2,475 years (center) and 9,975 years (bottom).

7.5 Disaggregation results

Disaggregation of the total seismic hazard allows examining the spatial and magnitude dependence of ground-shaking hazard estimates. The aim of the disaggregation procedure is to identify the predominant sources (magnitude-distance pairs), which can be used to generate a predominant earthquake scenario. This forms the basis for two main applications: 1. selection of earthquake recorded time-histories for use in advanced design of critical structures or detailed site effects (i.e. slope stability, liquefaction) analyses; 2. input to seismic risk assessment, as it permits the simulation of scenario earthquakes that are representative for the damage at the site of interest.

The total median reference rock-site hazard estimates were disaggregated for the mean hazard corresponding to the entire spectral periods. The disaggregation is performed for 0.2 bins of magnitude, 5 bins of distance and 3 bins of epsilon. A graphical illustration of the percentile contributions for a hazard level described by SA[0.2s] and two mean return period of 475 years and 2,475 years in Basle is given in Figure 71. These two plots highlight the expected contribution trend: lower magnitude bins contribute to median hazard estimates of mean return periods of 475 years, and larger magnitude bins for the mean return periods of 2,475 years. The distance and epsilon bins are similar, with major contribution of neighbouring distance bins of 0 to 10km within the one-epsilon bin. Note that the 'controlling event' for 475 years in this site is a magnitude 5.6

events within 10 km distance; for longer return periods, this event is a magnitude 6.5 in the same distance range, but with a more unusual ground motions (i.e., higher epsilon).

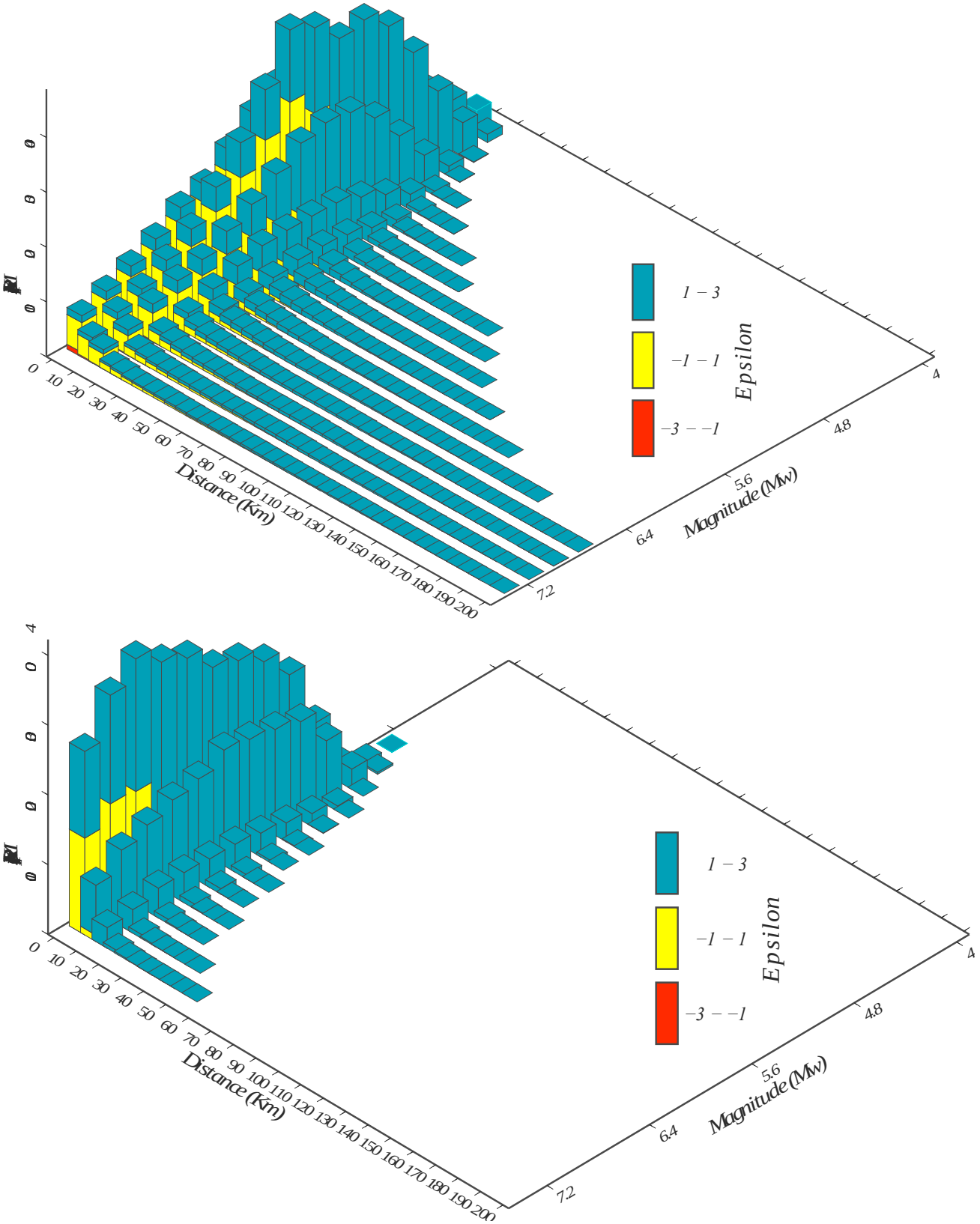

Figure 71: Disaggregation results for Basle: contribution of magnitude, distance and epsilon bins to the median SA[0.2s] of mean return period of 475years (left) and 2,475years (right)

7.6 Comparison with the 2004 national hazard model

Reference rock conversion assumptions

One important benchmark for many users is a comparison of the 2015 PSHA model with the one from 2004, which is what we explore in this section. One drawback of the 2004 model was that due to the limitations in the available data and knowledge (→ Chapter 5), the reference rock site was poorly delineated, as in most existing hazard maps, as "hard rock with an estimated Vs30 for 1500 m/s". The 2015 model on the other hand is based on a well-defined rock condition, defined by a rock profile (Chapter 5). In order to compare the two models, or to compare to other references site conditions, it is necessary to adjust both models to the same reference rock. Doing so is non-trivial, and requires a number of assumptions. The correction factor is may be kappa and frequency, distance and magnitude dependent, and also is coupled with the choice of spectral attention (Chapter 5).

We opt here for an approximate but simple conversion that is not frequency or explicitly kappa dependent, to allow for an approximate comparison. The conversion is defined as *sqrt(host vs30/target vs30)*. We assumed that reference rock of the 2004 seismic hazard estimates is Vs30 = 1500m/s, hence we have correction factor defined as a *sqrt(1500/1100);* where *host* is the reference rock of each hazard model, and target is the reference rock (Vs30=1100m/s) = 1.17, we thus increase the 2005 UHS by increasing them by 17%. To convert from our reference rock to a rock with assumed vs30 of 800 m/s, as required for the comparison with the SIA design spectra, would likewise result in a factor of *sqrt(1100/800) = 1.17.*

Hazard curve comparison

Figure 72 compares the site-condition adjusted median (50^{th}) and one-sigma percentile (16^{th} and 84^{th}) from the CH2004 superimposed with the results of 2015 model (hereafter CH2015) for four cities (i.e. Basle, Sion, Chur and Berne) in terms of horizontal SA[0.2s]. Overall when the median values are compared, we observe an increase of the ground-motion hazard values in respect with the 2004 results, especially for the longest return periods. The increase remains well within the +/- one sigma of either model.

Of significance is the uncertainty range, illustrated in Figure 72 by the area between the lower and the upper percentiles. The 2015 uncertainties estimates are substantially narrower with respect to the CH2004 estimates. The reduction of the sigma is an important element, in four respects:

- A reduced uncertainty range suggests progress in understanding the underlying processes and in reducing the variability of the data.
- The reduction of sigma results in a reduced uncertainty dispersion around the center values of the hazard distribution. In turn, a reduced hazard will result in a more accurate earthquake risk assessment. In addition, because earthquake risk assessment is often driven by the tails of the distributions, the rarest and most extreme scenarios. If risk and hazard are related in non-linear way, then a reduced uncertainty range can have a substantial effect on reducing the risk estimates.
- More certain forecasts are a benefit to users who need to decide if taking certain action is beneficial in a cost-risk-benefit context.
- The SED 2015 uncertainty range is in agreement with that observed in other current hazard studies, including PRP.

One reason why the uncertainty range is reduced is the use of single-station sigma as measures of aleatory uncertainty; in addition, the individual GMPE's selected have reduced sigma value themselves, when compared to the 2004 GMPE's, because the improved ability to separate

source-path and site effects contributes to better uncertainty separation. The reduction of the uncertainty range is also linked to the structure of the logic tree and the treatment of some epistemic uncertainty (depth, style-of-faulting, Mmax) as aleatory. The overall reduction of the uncertainty range is a cumulative effect of the above, in which the sigma of the GMPE's play the most significant role.

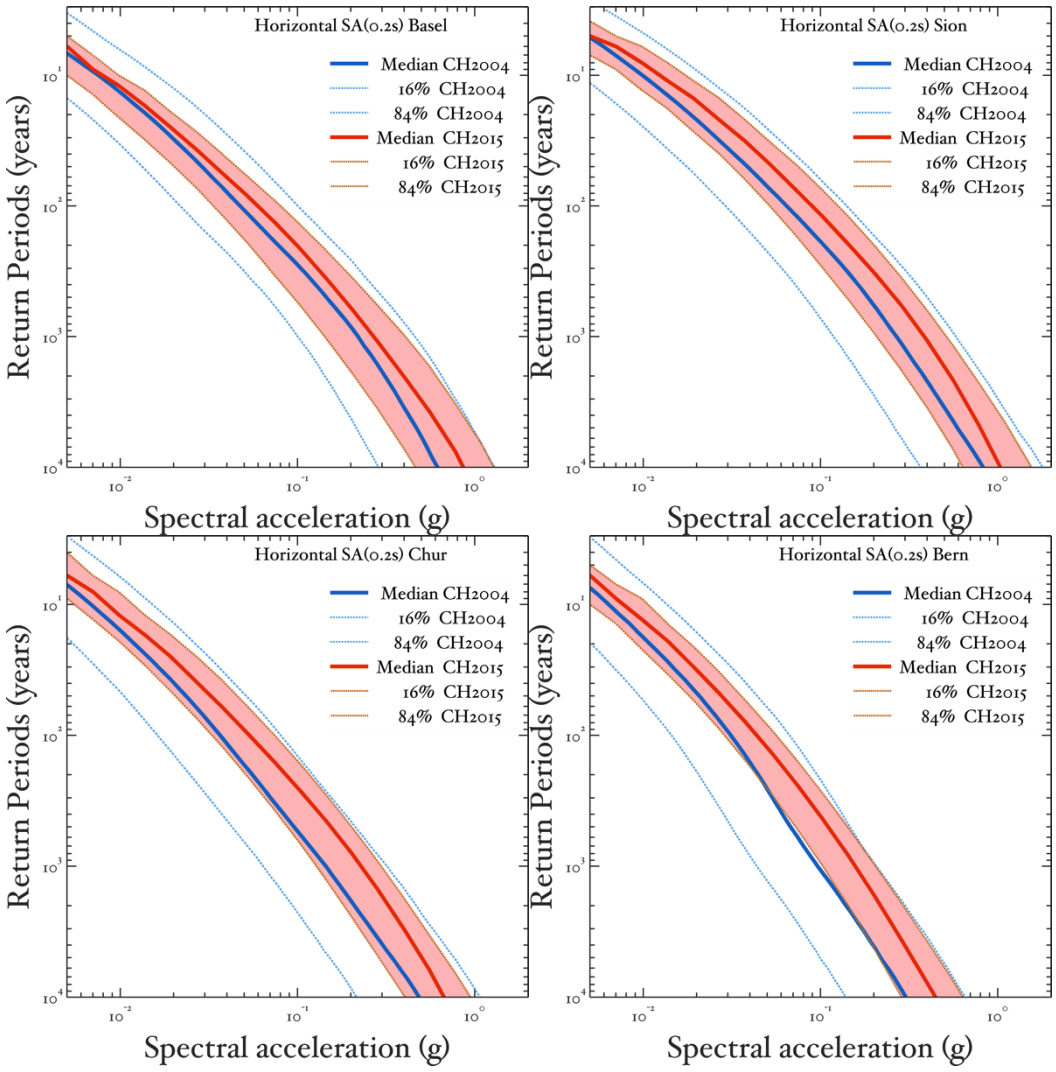

Figure 72: Hazard curves in terms of Sa[0.2s] of the 2015 and 2004 ground motion hazard for the cities of Basle, Sion, Chur and Bern. The median (50th) values are shown with continues lines for 2015 (red) and 2004 (blue). The uncertainty range is illustrated with dashed lines of similar colours.

Uniform Hazard Spectra

This section presents the comparison of the 2015 UHS with the design spectra of SIA261 (REF) and the 2004 uniform hazard spectra. The shape of the design spectrum corresponds to a TYPE 1 spectrum (REF) and the anchoring PGA as defined by the corresponding seismic zonation. The comparison is performed for a reference rock corresponding to class A of 800m/s as defined by SIA261 standard. Median (50th) and one sigma percentile (16th and 84th) are highlighted in Figure 73 together with the design and the UHS as resulted from the 2004 ground-motion hazard for four cites: Basle, Sion, Lucerne and Martigny, respectively.

We observed that 2015 median hazard values (red in Figure 73) are near identical to the 2004 value for spectral periods above 0.5 to 1 seconds. For lower spectral periods, the hazard values are substantially higher for most places, with the exception of Zurich. Note that for the 2004 model, PGA was not directly determined, so it is not shown here.

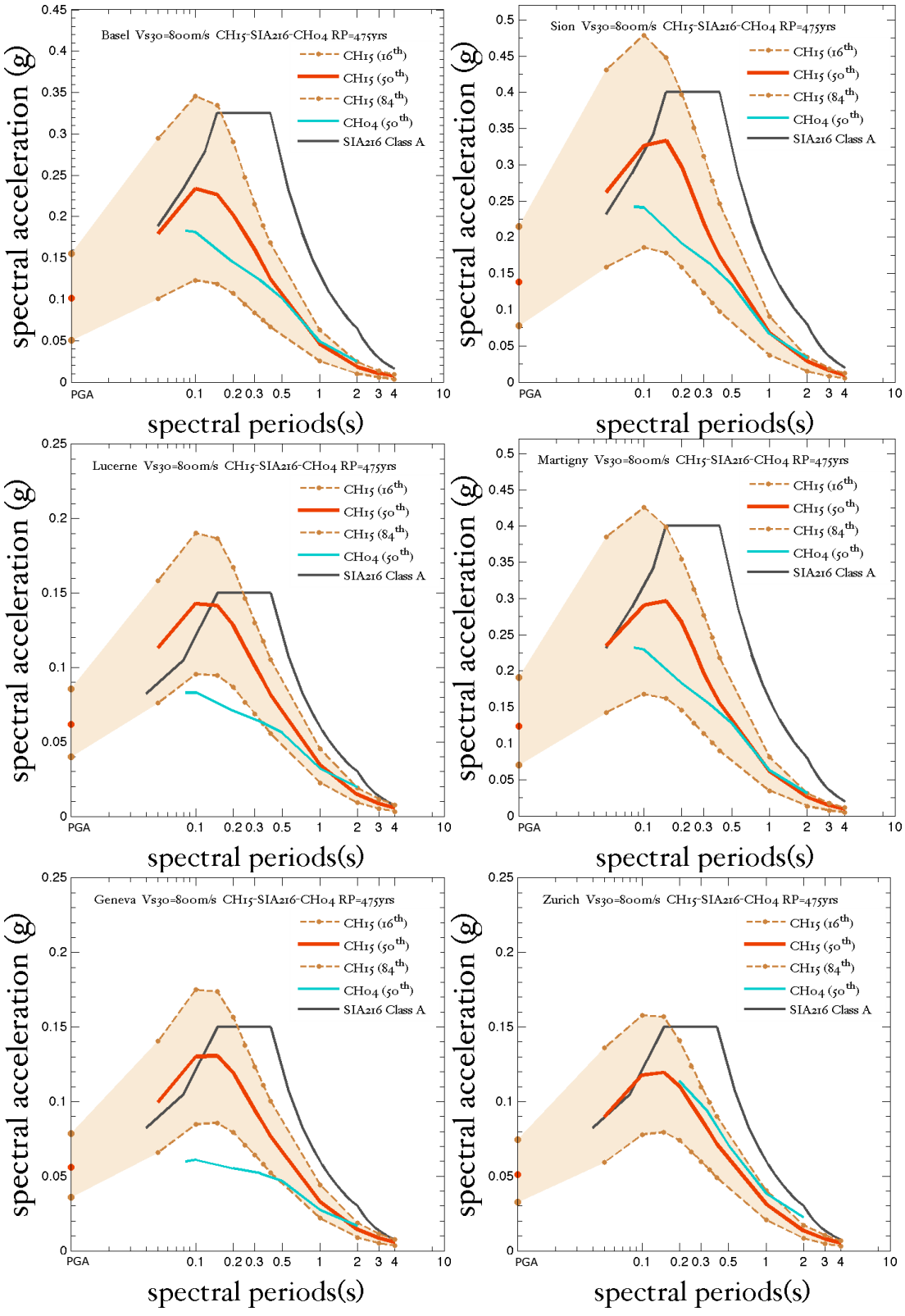

Figure 73: Comparison of uniform hazard spectra for a uniform return period of 475 years as obtained for Basle, Sion, Lucerne, Martigny, Geneva, Zurich. Uncertainty range of the median (50th) values is highlighted when compared with the median values of the 2004 estimates and design spectra of SIA216.

Hazard maps comparison

The 2004 probabilistic hazard map of median SA[0.2s] and SA[1s] for a mean return period of 475 years is reproduced in Figure 74 using a similar colour scale as the 2015 probabilistic hazard map. The 2004 map were again harmonized for comparison purposes to the 2015 reference rock value (Vs30= 1100m/s). The comparison shows:

- The spatial distribution of hazard is very similar, the ranking between regions did not change.
- For longer periods, differences are typically below 20%, and in some regions the hazard values decreased slightly (up to 15%). This is in agreement with the observation from the UHS (Figure 73).
- Near the spectral peak at SA[0.2s], larger differences are observed, ranging from 25% to around 75%, again in agreement with the observation from the UHS (Figure 73).

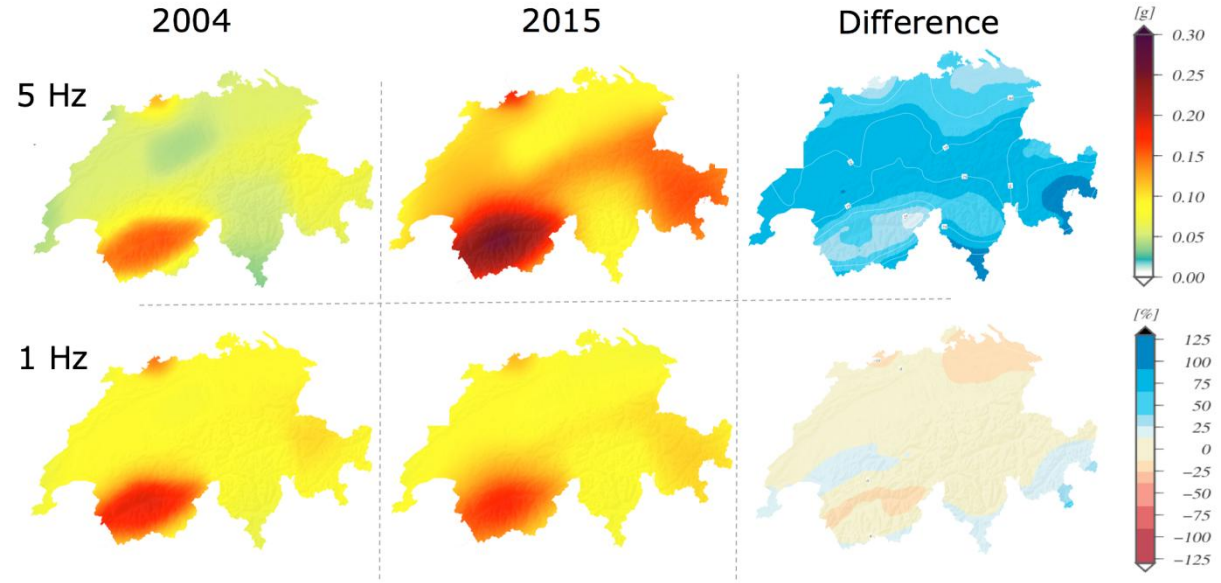

Figure 74: Ground motion hazard map in terms of SA[0.2s] (top row) and SA[1s] (bottom) for mean return maps of 475yrs as obtained in 2004 (left) and in 2015 (middle). The right column indicates the change in percent between the two maps.

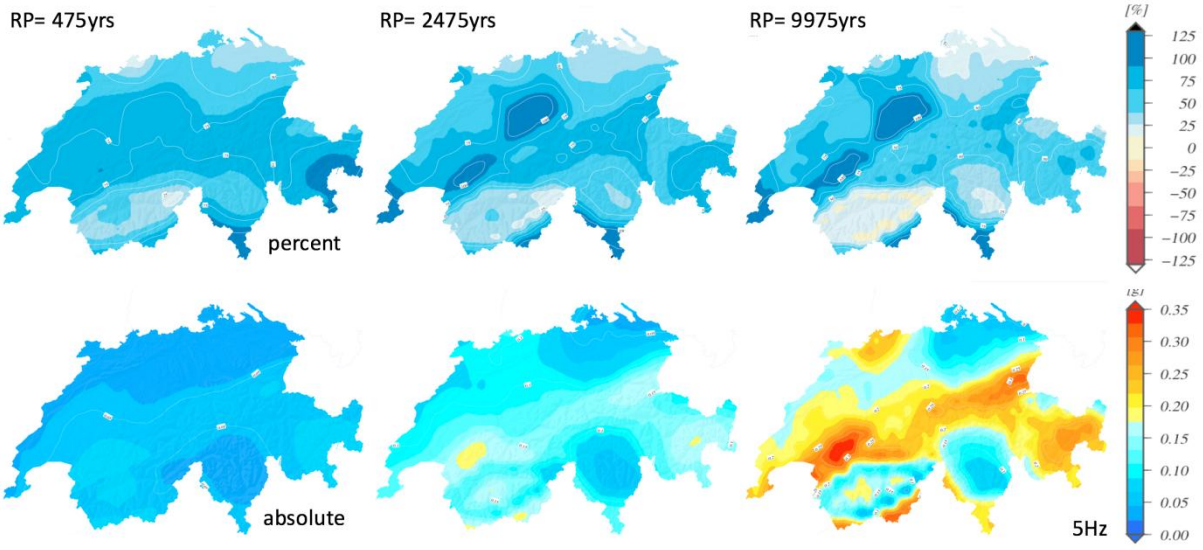

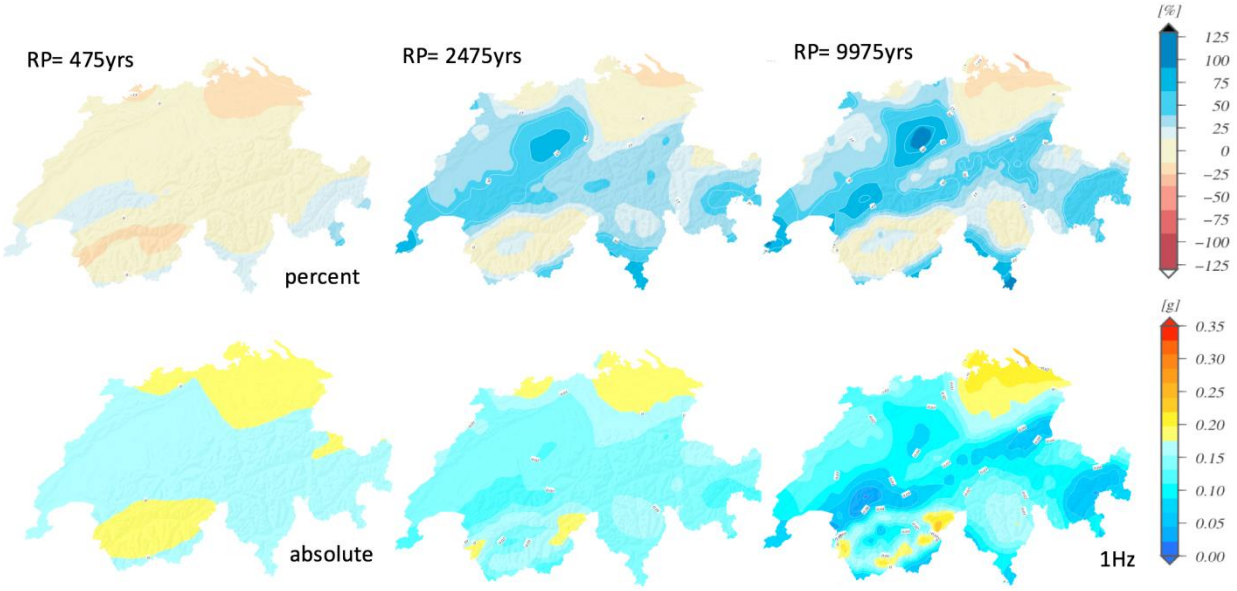

Figure 75: Comparison of the absolute and relative changes in hazard for different return periods and frequencies.

The comparison of hazard maps can also be undertaken for different return periods, and in terms of absolute as well as relative changes. From the maps, shown in Figure 75, we observed somewhat complex patterns of changes depending on region, frequency and return period considered:

- Percentage changes are often high in areas of very low absolute changes. While in Ticino or the Jura the relative changes may exceed 75% at 5Hz, the absolute changes are well below 0.05 g.
- For long return periods, the central Valais shows a small absolute and relative increase only, but the hazard values in the outside to the north and south increase more strongly. This is probably the combined effect of a difference in zonation, a different, more gradual distance decay of the assume GMPE's and the contribution of extended ruptures.
- For longer return periods, the absolute and changes in percent, both positive and negative, are generally more pronounced.

To be able to better pinpoint the reasons for the changes observed, it is helpful to plot the changes in the rate of earthquakes at magnitude 4.5 (Figure 76). This plot shows that the change in overall rate between the two models is rather small, between 0 and a maximum of 10% increase in the 2015 model. However, there are two earthquake-source related factors that will impact the hazard: The changes in the assessment of in the maximum magnitude in the 2015 model, which will a stronger effect for longer spectral periods and long return periods, and the fact that sources are not treated as a point source any longer, increasing the hazard contribution of large-scale events.

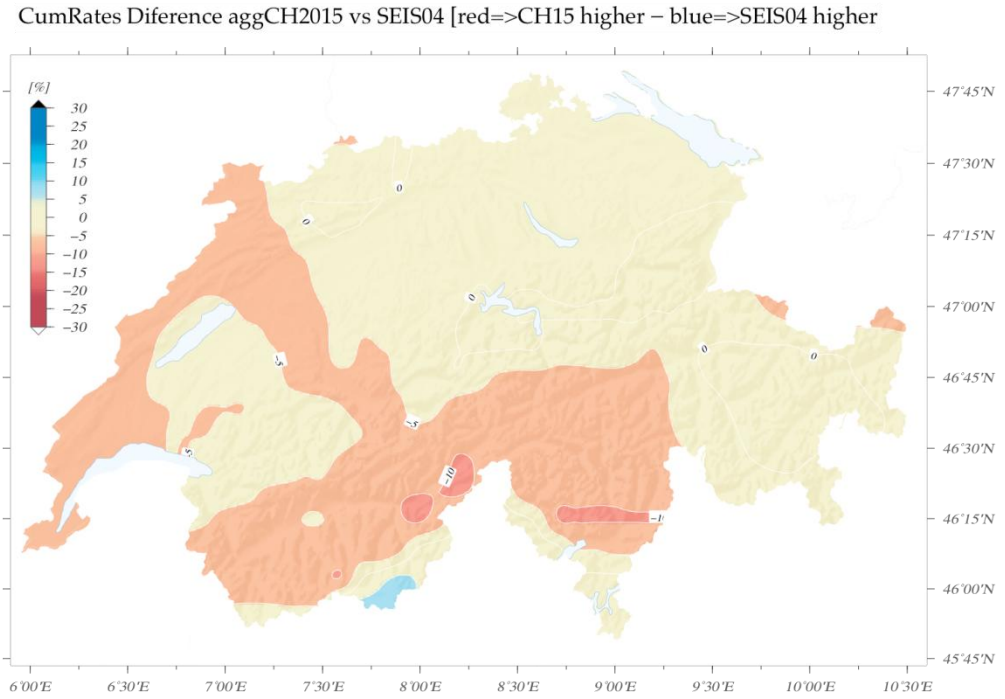

Figure 76: Difference in the annualized cumulative earthquake rates Mw≥4.5 between the SUIhaz2015 and SEIS04 model.

Summary of and reasons for the changes between 2004 and 2015

Switzerland's seismic hazard model 2015 replaces the prior model from 2004. A periodic update reflecting the latest technological and scientific findings forms the basis for adequate protection measures. The seismic hazard model 2015 features numerous changes and improvements, including new data, revised estimates of historical sources, a homogeneous reference rock, and improved predictive models. The uncertainty regarding estimates of likely ground motions has been significantly reduced relative to the 2004 model, meaning the 2015 model provides a more solid estimate of seismic hazard and a good basis for a nationwide risk model.

The estimate of the regional distribution of Switzerland's seismic hazard has not changed substantially over the last ten years: the Valais remains the region with the highest hazard, followed by Basle, Grisons, the St. Gallen Rhine Valley, Central Switzerland and the rest of Switzerland. However when looking into the details, the pattern of changes is somewhat complex and depends on location, frequency and return period under consideration. The implications for users will thus also depend on their respective location and on the type of application.

A hazard model is a complex integration and composite of many types of data, models and expert choices. It is often not uniquely possible (and not needed) to identify the one specific and unique reason why the hazard changes in a certain way, because numerous, partially interrelated factors play a role:

– different earthquake magnitudes and more data in ECOS09
– different zonation approaches, including a zoneless approach
– different ways to determine recurrence parameters
– different ways to determine Mmax

- different depth distributions of seismicity
- the use of extended rather than point sources in hazard integration
- different GMPE models and a more complex GMPE logic tree. This is probably the element with the strongest impact on the overall hazard increase near the spectral peak.
- GMPE dependence on faulting style
- different reference rock conditions. The SUIhaz2015 is referred to a velocity profile derived from measurements at the stations sites. The Vs_{30} of the 2004 hazard is just an estimate.
- the use of single-station sigma in hazard integration
- sundry other reasons

In the next section, we use sensitivity analysis to identify the sensitivity to some of the parameters and choices made in the 2015 hazard model.

7.7 References

Alvarez-Rubio Sonia, Philipp Kästli, Donat Fäh, Souad Sellami (2010): Appendix D - Calibration of historical earthquakes for the earthquake catalogue of Switzerland ECOS-09. In: Fäh, D., Giardini, D., Kästli, P., Deichmann, N., Gisler, M., Schwarz-Zanetti, G., Alvarez-Rubio, S., Sellami, S., Edwards, B., Allmann, B., Bethmann, F., Wössner, J., Gassner-Stamm, G., Fritsche, S., Eberhard, D., 2011. ECOS-09 Earthquake Catalogue of Switzerland Release 2011 Report and Database. Public catalogue, 17. 4. 2011. Swiss Seismological Service ETH Zurich, Report SED/RISK/R/001/20110417

Cauzzi Carlo, Benjamin Edwards, Donat Fäh, John Clinton, Stefan Wiemer, Philipp Kaestli, Georgia Cua, and Domenico Giardini (2014): New predictive equations and site amplification estimates for the next-generation Swiss ShakeMaps. Geophysical Journal International (2015) 200, 421–438

Edwards, B., Fäh, D., Allmann, B. and V. Poggi, 2009. Stochastic Ground Motion Model for Switzerland. Pegasos Refinement Project. Report of the Swiss Seismological Service, ETH Zurich, SED/PRP/R/006/20091130, 30. Nov., 2009.

Edwards, Benjamin ; Fäh, Donat (2013): A stochastic ground-motion model for Switzerland. Bulletin of the Seismological Society of America, 2013, Vol.103(1), pp.78-98.

Edwards, B., Michel, C., Poggi, V., & Fäh, D. (2013). Determination of Site Amplification from Regional Seismicity: Application to the Swiss National Seismic Networks. *Seismological Research Letters*, *84*(4), 611–621. doi:10.1785/0220120176

Joyner, W. B., Warrick, R. E., & Fumal, T. E. (1981). The effect of Quaternary alluvium on strong ground motion in the Coyote Lake, California, earthquake of 1979. *Bulletin of the Seismological Society of America*, *71*(4), 1333–1349.

Fäh Donat, Philipp Kästli, Sonia Alvarez, Valerio Poggi (2010): Intensity data from the MECOS database. Report No. SED/PRP/R/012/20100607 to the Pegasos Refinement project. Zurich: Swiss Seismological Service

Faenza L, and Michelini A (2010)"Regression analysis of MCS intensity and ground motion parameters in Italy and its application in ShakeMap", Geophysical Journal International, 180(3):1138–1152

Kaestli, P., D. Fäh (2006): Rapid estimation of macroseismic effects and shake maps combining macroseismic and instrumental data. Paper 1353 in Proceedings of the First European Conference on Earthquake Engineering and Seismology (ECEES), Genève (CD ROM).

8. Sensitivity analysis and comparison with other models

This section presents a first-order sensitivity analysis of the key elements and parameters in the hazard model. We identify the relative importance of various elements against the total hazard estimates, we also check how much the uncertainty in each parameters influences the hazard. Sensitivity analysis is first of all a tool for quality check ('sanity check'); it also identifies critical dependencies and can help to guide future research directions. Sensitivity analysis can be most readily applied to branching points of the SUIhaz2015 logic tree.

8.1 Seismogenic depth

The first sensitivity analysis aims at assessing the impact of seismogenic depth on the seismic hazard estimates. Seismogenic depth is of particular importance, because it strongly influences the source-to-site distance, which in turn affects the amplitude of the ground motions at a site of interest. The shallower earthquakes are, the higher are the ground motions of an earthquake of a given magnitude, and the higher and more concentrated the hazard.

The SUIhaz2015 logic tree on seismogenic depth distinguishes between two branches: shallow and deep events. We investigate the contribution of seismogenic depth to the total hazard by separately computing the hazard for only the shallow and the deep logic tree branches. The outcome of the sensitivity analysis is illustrated in Figure 77 as a spatial distribution of the percentage difference between the two branches. As expected, the sensitivity results reveal that shallow seismicity estimates are the dominant contributors to the total hazard for both Alpine and Foreland; however, because much of the seismicity in the Valais is within the shallow branch, its relative importance is much higher (>80%) than in the alpine foreland (~50-40-50%).

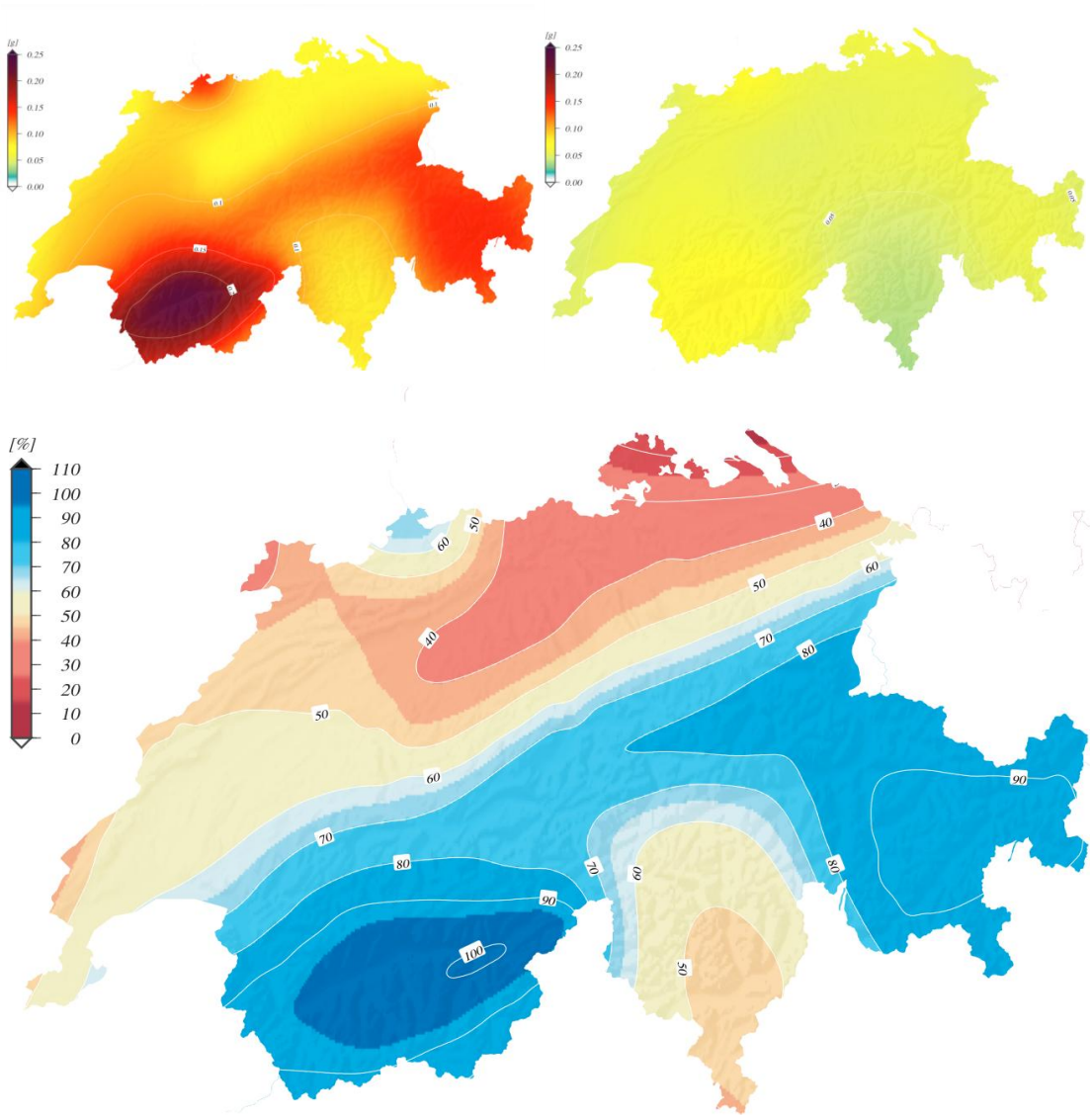

Figure 77: Percentage difference of the two-ground motion hazard map in terms of SA[0.2s] for mean return maps of 475yrs as obtained for the shallow (top left) and the deep sources (top right) and their corresponding ground motion logic tree branches.

8.2 Stochastic versus empirical GMPEs

Sensitivity analysis was also conducted to distinguish the contributions to the total hazard of the stochastic and empirical GMPEs. The sensitivity analysis is carried out for SA[0.2s], reference rock [V_{s30} = 1100m/s] and a mean return period of 475 years. The contribution of each set of GMPEs is estimated as a reference to the weighted mean hazard, and the sensitivity results (Figure 78) shows the difference between the stochastic and empirical GMPEs. The difference in percent between the two branches ranges from 20 to 70%, with the lowest values in the Valais and the highest differences in the Basle region. This difference is expected, given the selected GMPE's explained in Chapter 5. They are also desired to capture the epistemic uncertainty in forecasting strong ground motions in Switzerland, see Chapter 5 for details. The differences between the differences between the stochastic and empirical branches are observed for all ground motion intensity measures (PGA and SA). They increase as the mean return periods increase.

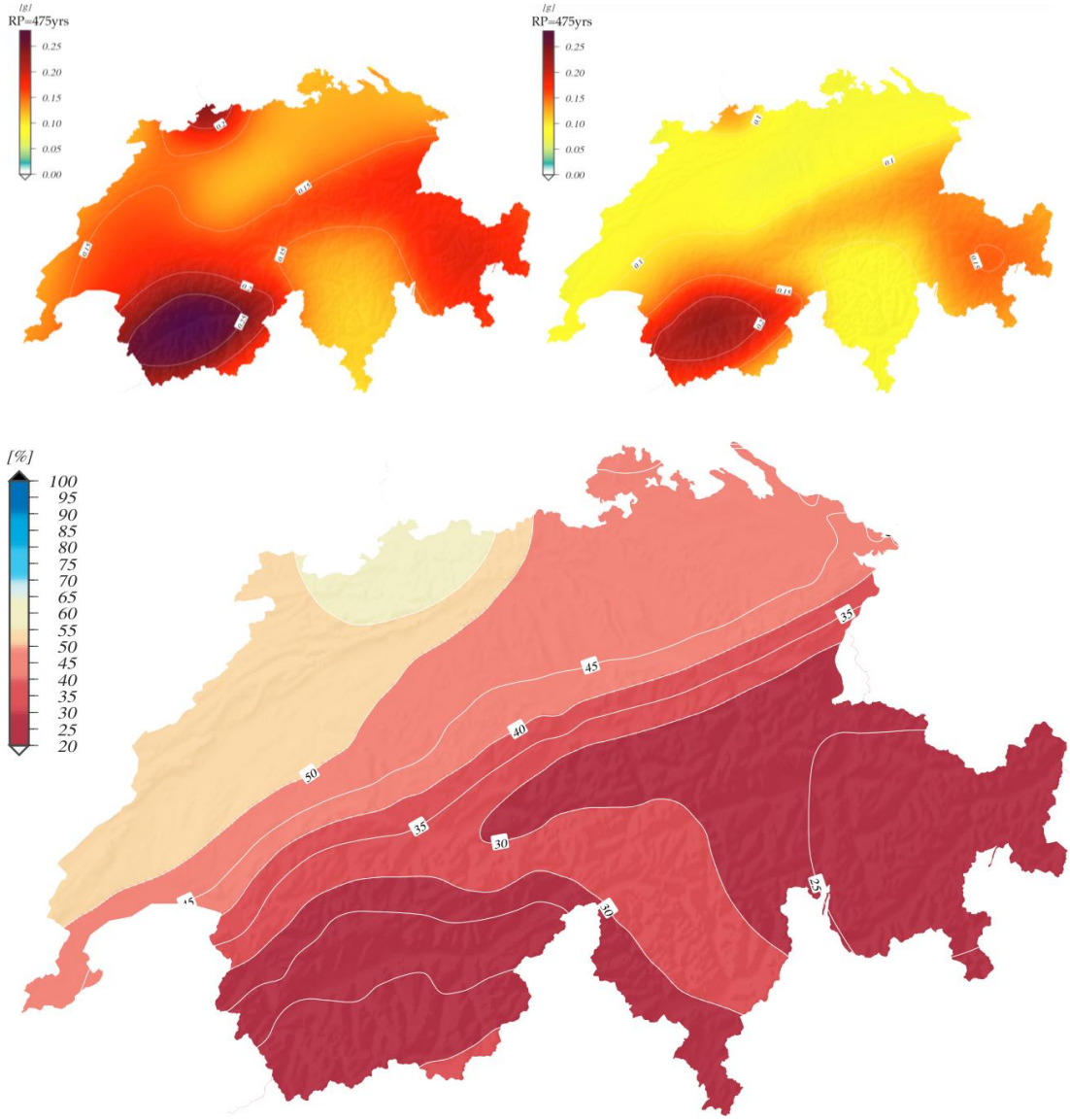

Figure 78: Percentage difference of the two-ground motion hazard map in terms of SA[0.2s] for a mean return period of 475yrs as obtained for the empirical (top left) and the stochastic (top right) GMPEs and their corresponding full source model.

8.3 Individual GMPE contribution

Radar plots are used to represent the sensitivity of the ground motion weighted mean and the individual GMPEs as a function of seismogenic depth and tectonics. The radar plots indicate the GMPEs (listed at the edges of the radar plot) to the mean (the black circle). The ratio GMPE/mean is illustrated as a red polygon; the values outside the black circle indicate a contribution larger than mean value, whereas a value inside the black circle suggests a lower than the mean value. Similar radar plots can be computed for all ground motion intensity measures and various return periods.

Figure 79 presents the GMPE to weighted mean ratio for Basle, for a mean return period of 475yrs, and SA[0.2s]. For Basle, the total hazard is dominated by the Foreland ground motion models and both shallow and deep sources as is anticipated. A visual inspection of the radar plots, clearly indicates a shallow logic tree dominating the Foreland. Empirical models of Akkar and Bommer (2010), in figure labelled as AkB10adj08 (corresponds to upper adjustment bound, see, Chapter 5) and Chiou and Youngs (2008) – CY08adj04 (mid-adjustment bound) show the highest hazard values. The lowest hazard is estimated by the stochastic model of Edwards and Fäh (2013) generated for stress-drop of about 10 bars. Cauzzi and Faccioli (2008) – CF08adj04 (mid adjustment bound) and the 60 bars stochastic model of Edwards and Fäh (2013)- labeled as

EF13f60bars, indicate the same values as the weighted mean. The Foreland Deep radar plot shows a lower contribution to the mean, since the red curves lies entirely inside the mean circle. Yet, the same empirical GMPEs, namely the AkB2010adj08 and CY08adj04 are dominant and a shift in the stochastic models from 60bars to 90bars models of Edwards and Fäh (2013). The remaining radar plots for Shallow and Deep Alpine logic tree, indicate their minor contribution to the hazard estimates in Basle, because epicentres in the Alps are distant to Basle.

Figure 80 presents the radar plots for Sion for SA[0.2s] and a mean return period of 475 years. These plots reveal the Alpine Shallow logic tree as the main contributor to the total hazard, followed by the Alpine Deep. As expected, the Foreland Shallow and Deep models have no impact on the seismic hazard estimates in Sion. The stochastic model EF13a75bar shows a 50% larger value than the weighted mean, whereas the lower value is the 10 bars stochastic model (EF13a10bar). CF08adj04 (mid adjustment bound) and AkB2010adj01 (lower adjustment bound) equal the mean hazard.

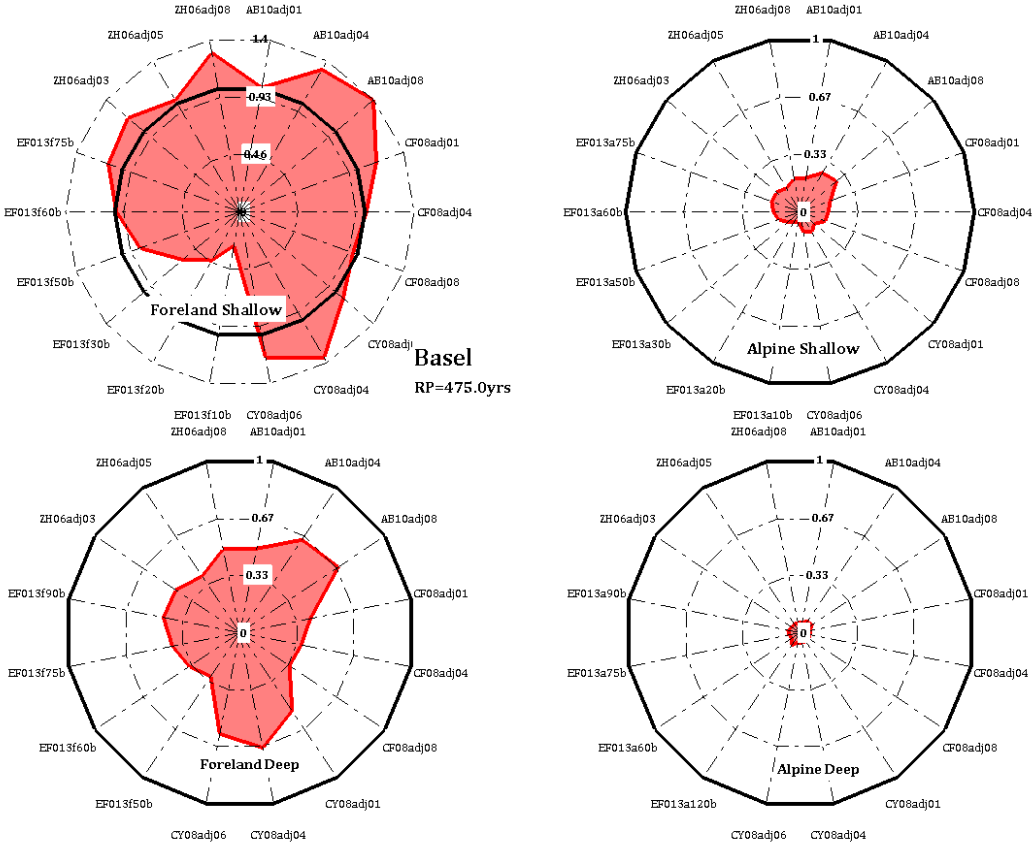

Figure 79: Radar plots for Basle depicting the contribution to the weighted mean of Alpine and Foreland ground motion models and shallow and deep seismogenic sources. The plots are for SA[0.2s] and a mean return period of 475yrs. The red polygon describes the GMPE/mean ratio.

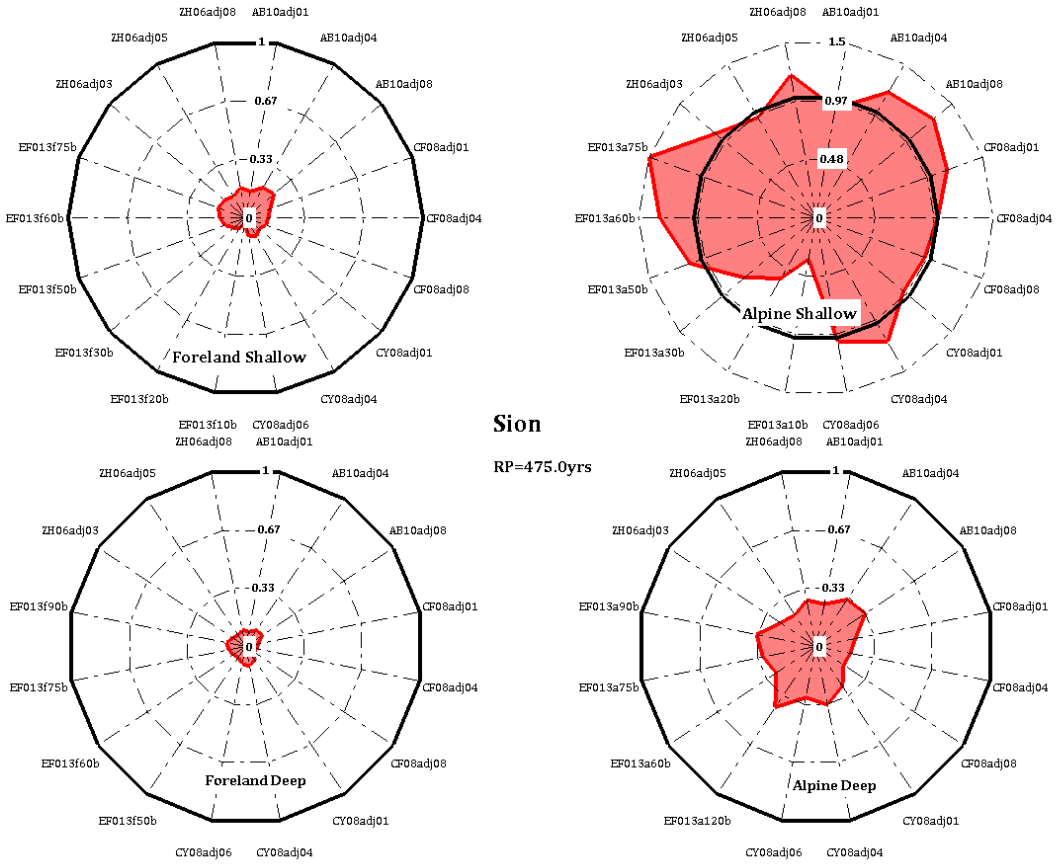

Figure 80: Radar plots for Sion depicting the contribution to the weighted mean of Alpine and Foreland ground motion models and shallow and deep seismogenic sources. The plots are for SA[0.2s] and a mean return period of 475yrs. The red polygon describes the GMPE/mean ratio.

8.4 Mapping the uncertainty ratio

In this section, we analyze the spatial distribution of the uncertainty ratio, as estimated from percentiles maps for SA[0.2s] and a mean return period of 475years. The ratio between the 84th and 16th percentiles is mapped in Figure 81. The uncertainty ratio varies between 2.0 to 2.5. We notice that the largest uncertainty ratio of about 2.5 exists in the Valais, closely followed by the Basle region.

Larger uncertainty ratios can be caused by either more variability in the different branches of the source model and/or by stronger differences between the relative GMPE's. The observed differences in uncertainties are within the range of other contemporary PSHA models; they also vary smoothly and only moderately in space, which is a desirable feature.

Figure 81: Map of the percentile ratio (84^{th}/ 16^{th}) of the ground motion distribution represented by the SA[0.2s] and computed for a mean retunr period of 475years

8.5 Comparison with SIA

This section presents the comparison of the 2015 PGA maps and UHS with the design maps and spectra of SIA261 (REF). The shape of the SIA design spectrum corresponds to a TYPE 1 spectrum (REF) and the anchoring PGA as defined by the corresponding seismic zonation. The comparison is performed for a reference rock corresponding to class A of 800m/s as defined by SIA261 standard.

show the comparison of the SUIhaz2015 map of peak ground accelerations (PGA) for a return period of 475 years and the currently valid zoning map of Switzerland. The maximum PGA is around 0.13 g in the centre of the Valais, and thus slightly below the a_{gd} value of 0.16 in zone 3b. The shape of the hazard contour in the PGA map follows very closely the shape of the SIA zones, a consequence of the fact that between the various updates of the hazard since 1978, little has changed in the assumed spatial distribution of earthquake sources. In very few areas do the PGA values exceed the a_{gd} slightly, for example in the region around Lake Neuchatel.

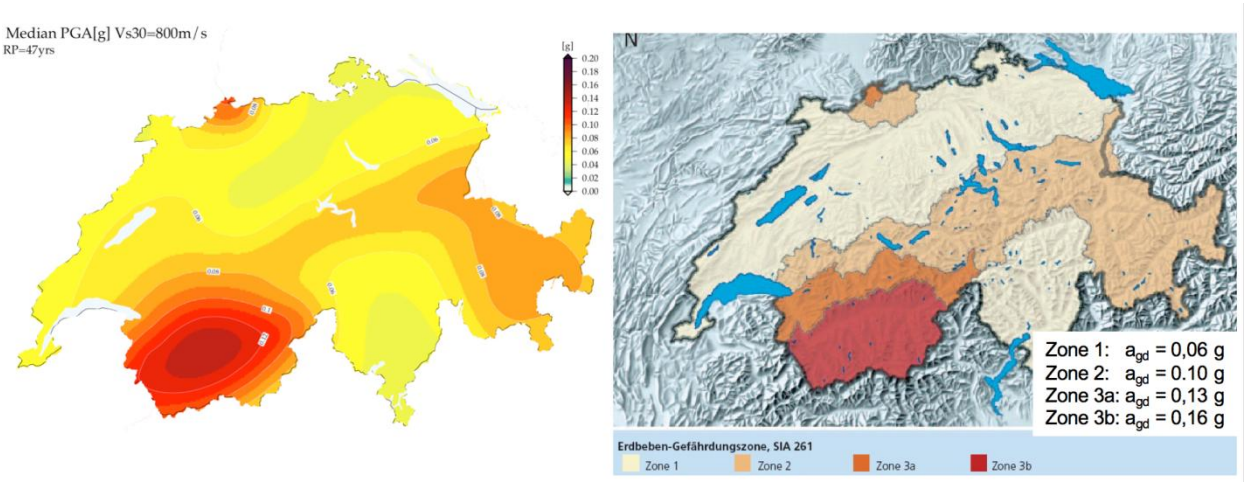

Figure 82: Left: PGA map of SUIhaz2015 for a return period of 475 years. Right: Zoning map of SIA261, contoured is the a_{gd} value, which is equivalent to PGA.

We next compare the SUIhaz2015 UHS for the Median (50th) and one sigma percentile (16th and 84th) with the SIA design spectra for nine cites (Figure 83). With respect to PGA, the UHS conform to the finding from the map comparison (Figure 82): In most regions, the PGA value (red dots) are below the a_{gd} values define in SIA (black dots). Only in Lausanne and Lucerne does the PGA values exceed the a_{gd} value; however, only by a small amount of around 0.01g and always well within the uncertainties of the SUIhaz2015 (brown shading in Figure 83).

With respect to spectral shape: In all places, a spectral shape above 0.2s spectral period (frequencies below 5 Hz), the design spectra are always conservative in the sense that they are always well above the SUIhaz2015 values. This conservatism in the design spectra is well known and a desirable feature. With respect to shorter spectral periods (frequencies from 5Hz upwards), the design spectra are partially conservative; in some places the SUIhaz2015 are higher than the design spectra (e.g., Berne, Lausanne), although always remaining with the uncertainty.

Note that it is not the responsibility of the SED to evaluate the potential impact of the new hazard on building codes in the context of SIA261. This is the task of the SGEB and SIA commissions.

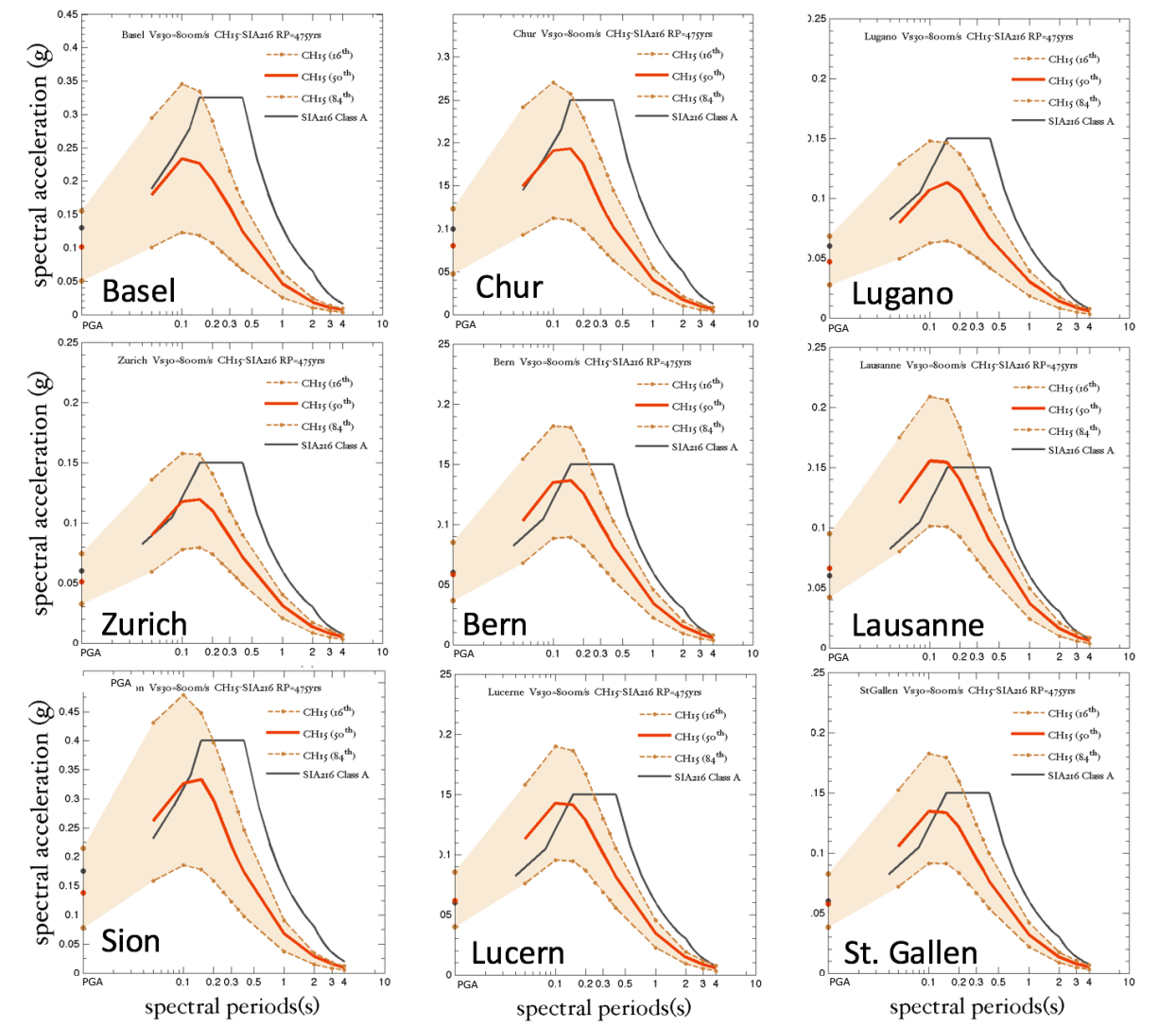

Figure 83: Comparison of the SUIhaz2015 UHS for a return period of 475 years and the SIA 261 design spectra for nine selected cities in Switzerland. PGA values are indicated as dots at the spectral period 0.0. Note that the y-axis scaling varies between graphs.

8.6 Comparison with ESHM13

The ESHM13 (European Seismic Hazard Model 2013; Wössner et al, 2015) was released in 2013 and covers all of Europe including Switzerland. While a harmonized, continent-scale model is designed for different purposes, and not immediately applicable to the national scale, a comparison is interesting. Figure 84 illustrates this comparison for five cities from within Switzerland, the ESHM13/SHARE model shown green. Results show clearly that for all places and most spectral periods, the ESHM13 model is significantly higher than the SUIhaz2015, often by a factor of two around the spectral peak, and in most places outside of the standard variation of the SUIhaz2015 model. This discrepancy of the ESHM13 model has been noted when compared to a number of national hazards, for example Germany and France; it is explained largely by the choice of the GMPE models in the project. This selection is currently being reviewed in the context of the EPOS working group on GMPEs. A full update of the ESHM13 has been proposed to the European Commission; if funded, it will be completed in 2018. For now, we consider the mismatch to ESHM13 an additional indication that the ESHM13 urgently needs to be updated.

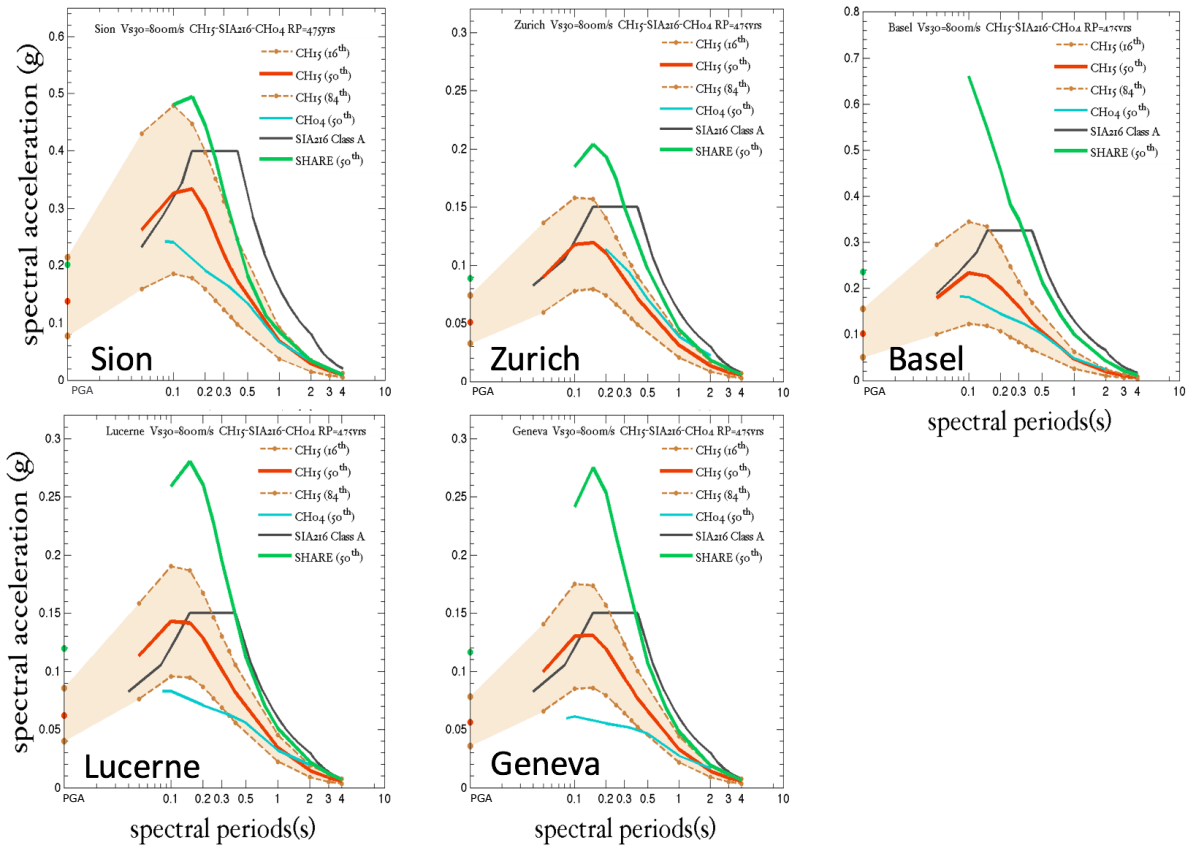

Figure 84: Comparison of the SUIhaz2015 UHS for a return period of 475 years and the SHARE UHS for the some return period.

8.7 Comparison with PRP[17]

The project "Probabilistische Erdbeben-Gefährdungs-Analyse für KKW-Standorte in der Schweiz" (PEGASOS), which was sponsored by swissnuclear, managed by the Swiss National Cooperative for the Disposal of Radioactive Waste (Nagra), and implemented according to the Senior Seismic Hazard Analysis Committee (SSHAC) methodology at Level 4 (SL4), was completed in 2004 {HSK, 2004}. The PEGASOS Refinement Project (PRP) was subsequently conducted to update and improve PEGASOS based on new data and methods, and to address some of HSK's review comments. PRP was funded and managed by swissnuclear, and was independently reviewed by ENSI. PRP planning started prior to 2008, whereas expert participation commenced in September of 2008 with a Project Kick-Off Meeting and first workshop, WS-1. The Project held a Summary Meeting in May 2013 and submitted its summary report and the results to ENSI in December 2013 (swissnuclear, 2013).

The timeline of the SED national hazard 2015 project overlapped in parts with the one of the PRP project, and because the four sites investigated in PRP are located in Switzerland, the two projects used many of the same primary data, such as the earthquake catalogue ECOS09. They both also adopt the PSHA methodology based on Cornell (1968) as their framework, and follow the overall SSHAC ethics of representing the centre, body and range of the informed technical community. However, there are a number of differences between the projects: the two projects are fully independent in their governance and decision processes; there are difference between site-specific and regional PSHA; and in the decisions taken along the way by experts are largely independent. Note also that most of the decisions on the SED model were taken after the completion of PRP, when

[17] This section is adopted from a technical note by swissnuclear, "Post-PRP Comparison of SED Hazard 2015 with PRP 2013 results" (PMT-TN-1295)

PRP was in an internal review phase. The SED did not try to match PRP results at any stage of model building, because PRP results were not open.

A comparison of the final hazard results, therefore, offers an important and at least partially independent check on the influence of expert elucidations of the hazard results, and thus represents also a type of sensitivity study. Because both hazard were supposed to capture the center, body and range of the informed technical community, the expectations would be that the two models should lie within their respective uncertainty bounds.

To perform such a comparison, a few assumptions had to be made (see PMT-TN-1295 for details). Most relevant, the conversion of the SED generic rock to the NPP specific rock was performed by applying a VS_{30} correction to the provided UHS curves. Thus, a correction from 1100 m/s to 1800 m/s for Beznau, 2500 m/s for Gösgen, 2200 m/s for Leibstadt. No rock correction was applied to Mühleberg, since PRP defined for Mühleberg a VS_{30}=1100 m/s, which is the same value as used by SED. The correction is based on taking the ratio of the quarter-wave length amplification function of the NPP site and the generic rock of SED, including a correction for Kappa. Comparison could also be performed for annual probabilities of 1E-4, since this is the only part where the two model overlap. Figure 85 shows the comparison of the Uniform Hazard Spectra for two selected sites, Beznau and Gösgen. Plotted are the mean, the media and the 5% and 95% fractiles. From these comparisons, three important conclusions can be drawn:

1. The two hazard models are largely comparable for all frequencies, differences are typically below 10%, well within the uncertainty of each model and not systematic in the sense that no model is systematically higher or lower for all frequencies.

2. The spectral shapes are highly comparable.

3. The width of the uncertainty ranges are comparable.

Note, however, that while the hazard results are similar, the individual components contributing to the hazard are not necessarily so. The SED hazard forecasts somewhat higher rates of large events as compared to the PRP seismogenic source model. The GMPE logic tree of PRP on the other hand gives on average somewhat higher values than the one of the SED, because the SED model gives a stronger weight to Swiss specific stochastic model. This is partially a consequence of the different application ranges of the models: The SED model targeting annual exceedance probabilities of E--2 to E-4, while PRP targets the range E-4 to 1E-7. For longer return periods the value of Swiss specific information was viewed by PRP experts to be less relevant (i.e., lower weight) compared to global data. One of the consequences of these differences is that the hybrid SED-PRP model (SED source model, plus PRP SP2 and SP3) adopted by ENSI as the relevant reference hazard for the nuclear power plant sites is somewhat higher than the PRP hazard on its own.[18] This difference is strongest for frequencies lower than 2 Hz. For higher frequencies, the SED and hybrid SED-PRP model are within a few percent of each other at annual frequencies of E-4, suggesting that the characteristic sources are quite comparable. For frequencies of 1Hz and lower, for some sites the hazard estimates are 10% or more disparate. At these lower frequencies, the fact that the SED seimogenic source model contains higher rates of large (M6) events than the PRP source model, will take on importance.

[18] see https://www.ensi.ch/de/wp-content/uploads/sites/2/2016/05/Neubestimmung_Erdbebengefaehrdung_KKW_PEGASOS_PRP.pdf

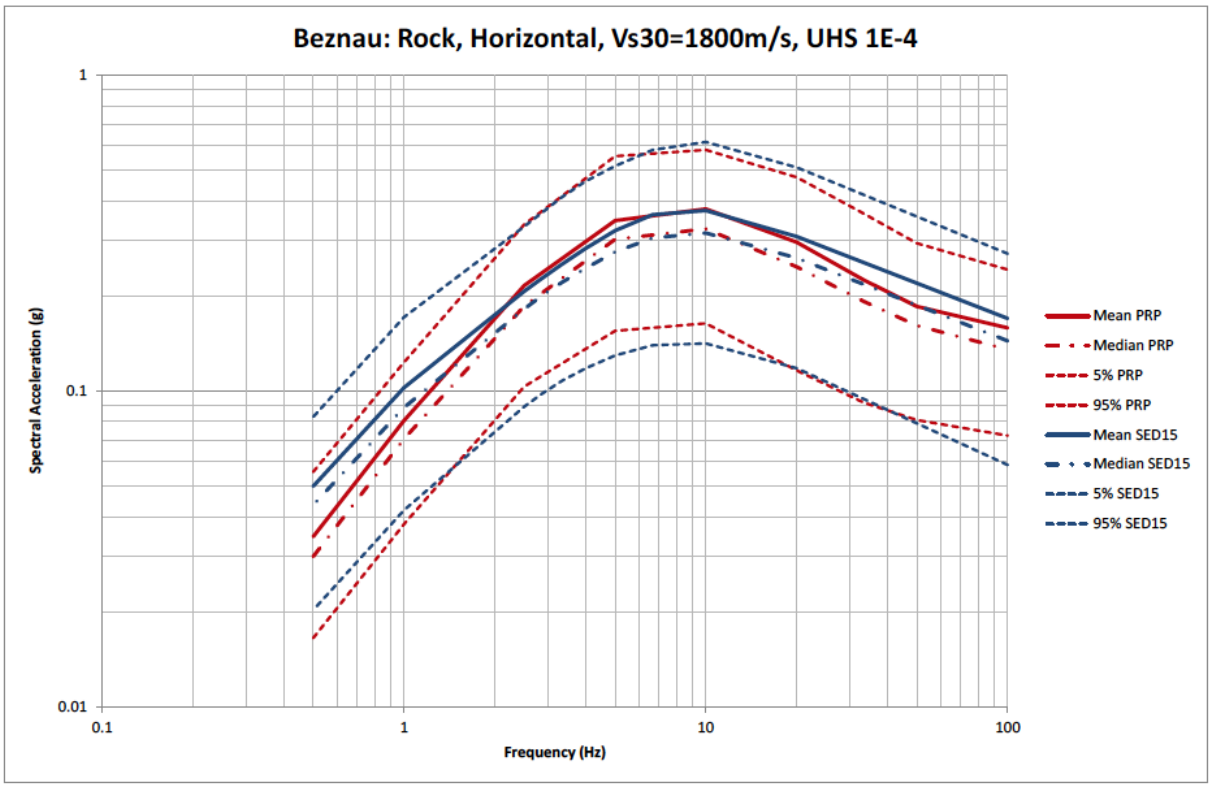

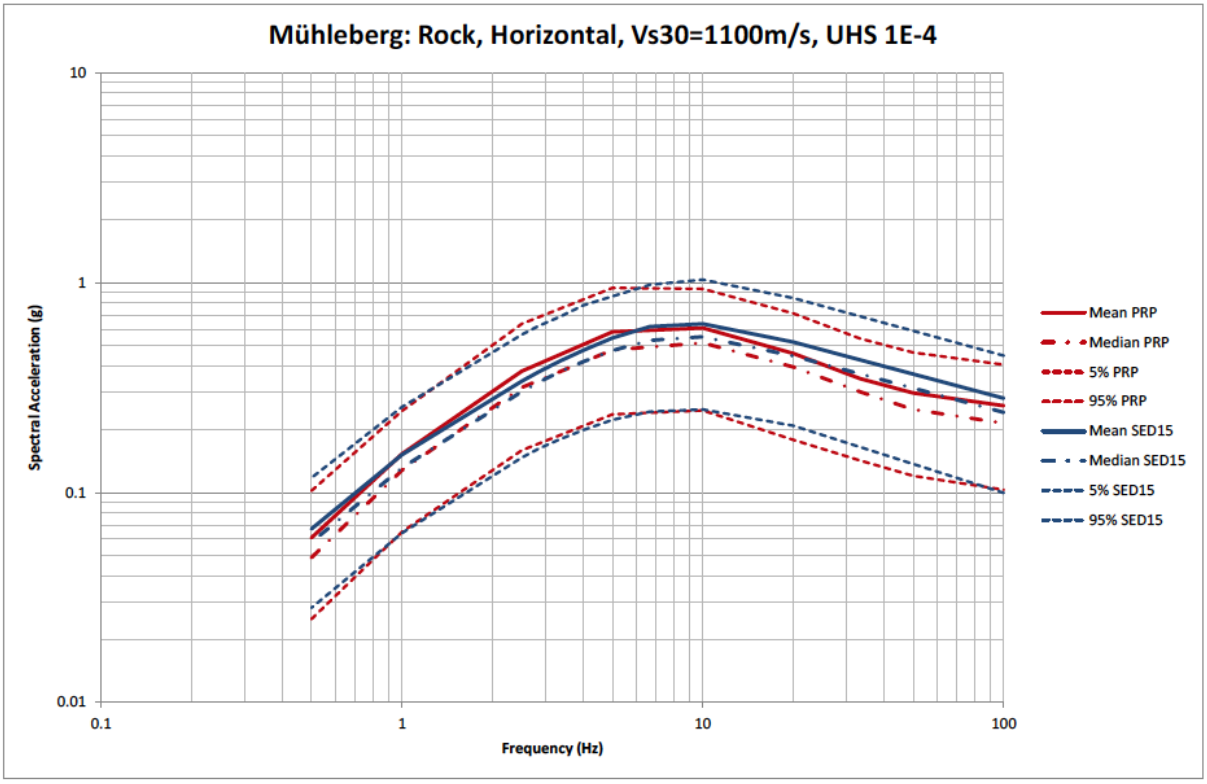

Figure 85: Rock hazard comparison for the site Beznau at an annual probability of exceedance of 1E-4 for PRP and SED 2015.

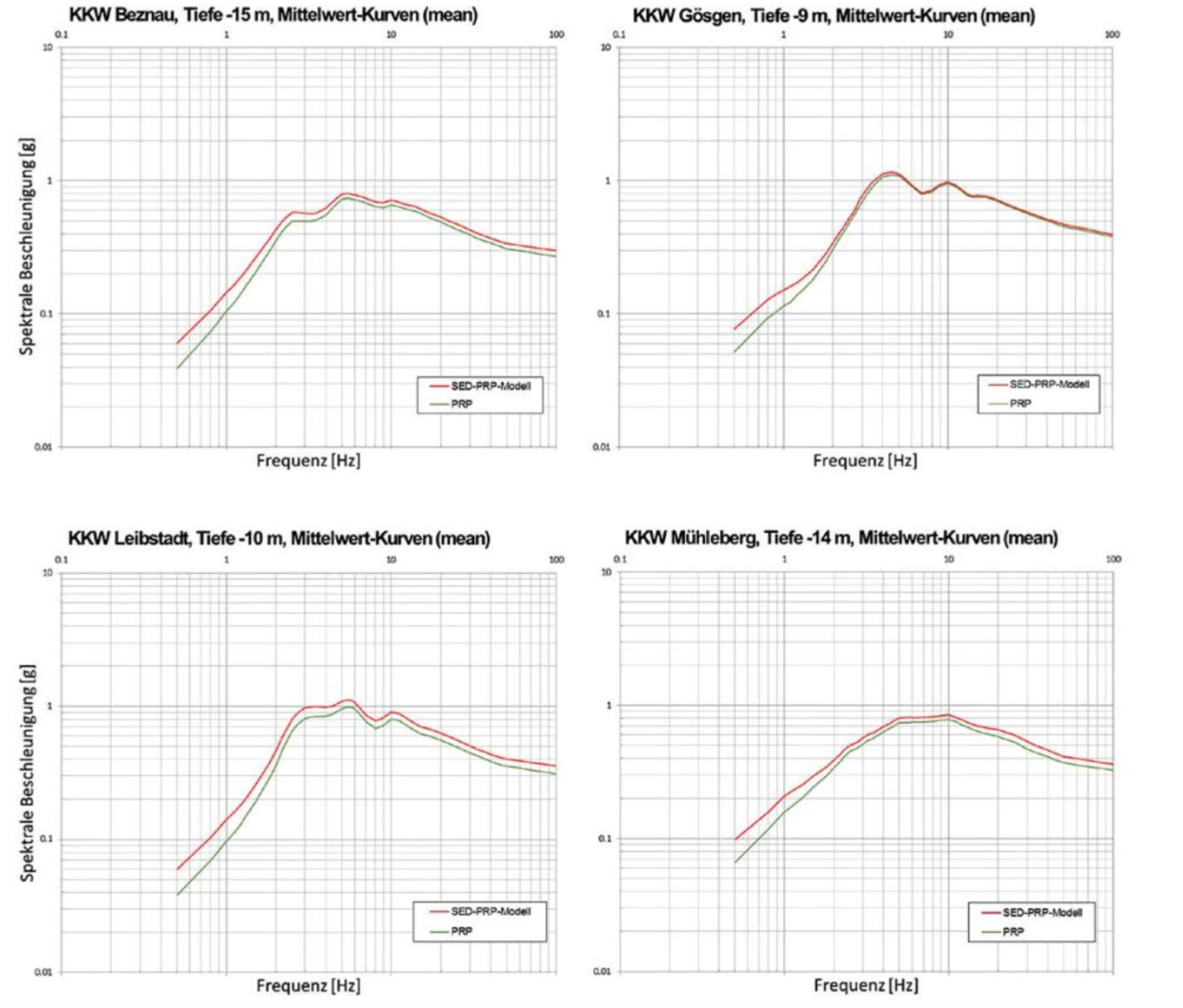

Figure 86: Comparison of the PRP model with the SED-PRP hybrid adopted by ENSI (E-4 annual frequency). Source: ENSI.

8.8 References

Akkar, S. and J. J. Bommer (2010). Empirical equations for the prediction of pga, pgv, and spectral accelerations in europe, the mediterranean region, and the middle east, Seismol Res Lett 81, 195-206

Cauzzi, C. and E. Faccioli (2008). Broadband (0.05 to 20 s) prediction of displacement response spectra based on worldwide digital records, J Seismol 12, 453-475

Chiou BS-J, Youngs RR (2008) An NGA model for the average horizontal component of peak ground mo- tion and response spectra. Earthq Spectra 24:173– 215Cochran W. Sampling Techniques (3rd edn). Wiley: New York, 1977

Cornell C.A. (1968). Engineering Seismic Risk Analysis. "Bulletin of the Seismological Society of America", 58(5):1583-1606.

Crowley, H., V. Silva (2013). OpenQuake Engine Book: Risk v1.0.0. GEM Foundation, Pavia, Italy.

Danciu L., and Giardini D. (2015) Global Seismic Hazard Assessment Program - GSHAP legacy, Annals of Geophysics 58 (1): S0109. doi:10.4401/ag-6734

Field, E. H., T. H. Jordan, and C. A. Cornell (2003). "OpenSHA - A developing Community- Modeling Environment for Seismic Hazard Analysis". In: Seism. Res. Lett. 74, pages 406– 41).

Giardini D., Wiemer S., Fäh D., et al (2004) Seismic Hazard Assessment of Switzerland, Available at http://www.seismo.ethz.ch/prod/haz_map/hazard_report - last accessed December 2015.

McGuire, R.K., FRISK88M: User's Manual, 1996.

Monelli D., M. Pagani, G. Weatherill, L. Danciu, and J. Garcia, (2014), Modeling Distributed Seismicity for Probabilistic Seismic-Hazard Analysis: Implementation and Insights with the OpenQuake Engine, Bulletin of the Seismological Society of America, Vol. 104, No. 4, pp. 1636–1649, August 2014, doi: 10.1785/0120130309

Musson , R.M.W., and Winter , P.W. (1997) Seismic Hazard in UK: source specification problems of intraplate seismicity, Natural Hazards, 15, 105-119

Pagani, M., Monelli, D., Weatherill, G. A. and Garcia, J. (2014). The OpenQuake-engine Book: Hazard. Global Earthquake Model (GEM) Technical Report 2014-08, doi: 10.13117/- GEM.OPENQUAKE.TR2014.08, 67 pages.

SIA 261:2014: Actions on Structures. Swiss Standard SIA 261, Swiss Society of Engineers and Architects, Zurich, 2014.

9. Communicating seismic hazard

9.1 Introduction and context

The new hazard model confirms that earthquakes are a serious threat for Switzerland, being one of the natural hazards with the highest risk potential in terms of both financial losses and casualties (Hohl, Brem, Schulze, & Holthausen, 2015). However, this fact is largely unknown to most inhabitants. Catastrophic earthquakes in Switzerland are fortunately too rare to be remembered or perceived as a threat. In addition, it is generally not well realized that earthquakes, different from other natural hazards such as floods, can occur anywhere in Switzerland and that no warning is possible. Risk reduction through suitable construction design is thus the most powerful mitigation measure available. Fostering the implementation of seismic building codes among other mitigation measures is a challenge concerning a society as a whole. As an important function, a hazard model should therefore permit a wide range of people and parties to be informed about earthquakes and put them in a position to make factual decisions on risk mitigation and management.

The Swiss earthquake hazard model of 2015 (SUIhaz2015), like all contemporary probabilistic seismic hazard models, is in the first instance a complex aggregate of different kinds of inputs, and computational steps leading to a wide range of output products: literally dozens of hazard maps, for different combinations of return periods and frequencies, ground motions measures and fractiles. In addition, hazard curves and uniform hazard for numerous sites as well as spectra for various locations, frequencies and return periods are available. What is very useful for engineers, seismologist and other professionals to work with, is very difficult to understand for the public. For non-scientists, seismic hazard is a rather abstract concept, as it is based on values that are not widely understood. This is true in Switzerland but also around the world: portraying the results of a probabilistic seismic hazard assessment is a serious challenge in science communication, and one that most seismological services, including the SED, have managed poorly in the past.

One could argue that this is not critically important, since the experts working with the seismic hazard model are the primary recipients and understand the given values. Nonetheless, in democratic societies the public and public representatives ultimately decide on mitigation measures, such as building codes or earthquake insurances. Therefore, it is important that authorities, politicians, houseowners etc. understand the implications of seismic hazard for a given region.

With the 2015 release of SUIhaz2015, we are trying a novel approach in communicating seismic hazard results, as detailed in this section. Up to now, surprisingly little is known on the impact of hazard maps and the communication materials related to them. The following chapter summarizes some of the known best practices for communicating hazard information.

9.2 Best practices in communicating seismic hazard

Maps are an established way to illustrate hazards (Gaspar-Escribano & Iturrioz, 2011; Kunz & Hurni, 2011). However, despite widespread use of maps to communicate hazards they often fail to bring home their contents. Especially non-experts in the respective fields often struggle to interpret the maps correctly (Hagemeier-Klose & Wagner, 2009; Kjellgren, 2013; Perry et al., 2016), which prevents them from acting accordingly. Even though seismic hazards maps are mainly tailored to the needs of primarily users like engineers (Perry et al., 2016), they are used likewise to communicate with the public.

Map design critically influences the "correct reception of the seismological message" (Gaspar-Escribano & Iturrioz, 2011). For example, small symbols and light colours seem naturally less alarming than large symbols and dark colours. Red colour hues symbolize danger. The selection of

colour scales should be based on these general principles and offer sufficient contrast to avoid misleading interpretations.

Besides such universal features, specific elements should be tailored to the needs of the various audiences. While engineers prefer precise values in legends to compare them with the building codes, the average houseowner requires a more general statement on the level of danger (such as high, medium, low hazards). Mileti, Nathe, Gori, Greene, & Lemersal (2004) argue that public risk evaluations usually turn into a binary result: dangerous or not dangerous. "Fancy probability estimates for an earthquake on the San Andreas fault will not change that" (Nathe, 2000). Legends should therefore be devised accordingly: compressive, numeric information for professionals and qualitative legends for non-professionals. Another crucial aspect is the definition and number of intervals. It is worthwhile to uncover which interval classes are most likely to be understood, and to categorize the data in three to five classes (Gaspar-Escribano & Iturrioz, 2011).

Apart from map and legend design, the context they are presented in, as well as the compilation of additional information is important. Interactive visualizations offer an additional benefit for users to discover seismic hazard information: "Even with exactly the same presentation, people's understanding of presentation content varies because of differences in interests, experience, intellectual ability, education, or cultural background" (Bostrom, Anselin, & Farris, 2008).Therefore, it is advisable to offer interactive tools with which people can individually investigate the questions they are most interested in. Various options help them to answer the "what if" questions. However, interactive visualizations should not be overloaded or too complex (Dransch, Rotzoll, & Poser, 2010).

Additional information can lead to more accurate beliefs about seismic hazard and a higher tendency to take precautionary measures. However, there are significant differences regarding the impact of information material (Whitney, Lindell, & Nguyen, 2004). Several studies, especially in the field of health communication, examined the effects of different text formats on the understanding of risk information. Even small changes in the informational format help people to better understand statistical information. Bodemer & Gaissmaier (2012) summarized problems and best practices in communicating statistical health information. Nevertheless, they target a different field, the results are transferrable, since the recommendations developed also aim to improve the understanding of the given information:

– Relative risks are more difficult to understand than absolute risks.
  An increase of the seismic hazard by 100 percent in a specific area is difficult to understand, since there is no reference point for lay people. Meanwhile, the chance of an earthquake occurring, increased from one time in 100 years to two times in 100 years, is more comprehensible.

– Natural frequencies are easier to understand than conditional probabilities.
  Statistical judgments based on frequencies compared to probabilities have shown to be more accurate (Peters, Bostrom, & Cutter, 2008). Statistical thinking of experts and non-experts alike improve when statistics are presented as natural frequencies (Hoffrage, Lindsey, Hertwig, & Gigerenzer, 2000). The standard hazard map depicts a probability of exceedance of 10 percent within 50 years. Such conditional probabilities are hard to understand for most people. An explanation such as the following one might aid for a better understanding: The lifetime of a building is approximately fifty years. Within this lifetime, the probability of a residential or office building experiencing a design shaking is ten percent. Earthquake-resistant residential or office buildings in Switzerland are designed to withstand shaking that is expected to occur where the building is located once every 500 years on average (design shaking).

– Single-event probabilities are less intuitive than frequency statements.
  The problem with single-event probabilities is that people often use different reference classes, and consequently may interpret a probability of 3 percent for an earthquake with a magnitude 1 or greater to occur within the next year quite differently. Some might think that an earthquake certainly will occur within the next year, but affect only an area of 3 percent. Others understand that there is always a 3 percent chance for an earthquake to occur anywhere in the country. While the first person refers to the area, the second relates the information to the time frame.

Nevertheless, using an appropriate nomenclature for probabilities will not motivate people to act, but it might raise their awareness of the earthquake hazard. If people recognize that an earthquake might occur in their lifetimes, it is additionally important to illustrate how it might affect them. Most people struggle to understand odds. What they would like to know is the likelihood of an earthquake occurring within a conceivable period of time (Nathe, 2000).

Several studies in the United States focused on the impact of information material regarding earthquake hazard. Summarizing the results, the following aspects seem to be important: Effective hazard communication explains things in non-technical terms. The information should be distributed by various credible sources in a consistent manner. In addition to media reports, people like to have a written document they can refer to and discuss it with their peers. It is important to include information on what has to be done prior to, during and after an earthquake. In principle, people are more willing to act, if they understand what they can do to reduce their risk. In addition, an attractive presentation of the information is helpful. Despite these guidelines, it is important to keep in mind that the public is not uniform (Nathe, 2000). Successful communication measures are tailored to the specific needs of a wide variety of recipients.

9.3 Improvements in the 2015 hazard model communication

Based on scientific evidences and lessons learned from communicating seismic hazards in the past, a number of improvements and innovations have been implemented for SUIhaz2015:

Choice of map colours

In the 2004 model default hazard map, which portrays a probability of exceedance of 10 percent in 50 years, large parts of Switzerland were coloured green or light yellow. Only the Valais and Basle regions were highlighted in red. This colouring scheme illustrated well that the seismic hazard in the Valais and Basle is higher than in other parts of Switzerland. However, the green colour for most other areas is frequently interpreted as “safe”, because green generally means no danger. Besides the scientific evidence for this perception, staff members of the SED often experienced in interaction with the public how misleading these colours were. Many persons pointed on a city in the green part of the country stating “Look, where I live, I have nothing to fear”.

In addition, the 2004 maps used a rather wide dynamic range of colours from green through yellow, orange and red. The intention was to allow users to perceive the fine details of the model differences. However, the side-effect of this choice was that it may have overemphasized the differences between regions, given the uncertainties in the assessment and the fact that site amplification can amplify the ground motions locally by up to a factor of ten.

The updated colouring for the 2015 map retains on the clear characterization of the more endangered areas and uses light colours for low and dark colours for high hazard. In contrary to the previous hazard map, the dynamic range is more constrained and the colour map contains no more shades of green to better emphasize the fact that there are no earthquake free zones in

Switzerland. The colour differences, furthermore, are more distinct, helping to distinguish the different zones even in grey scale print (see Figure 87).

2004	2015
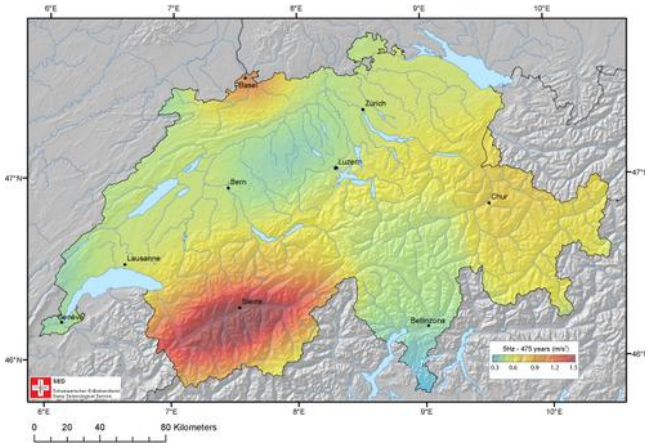	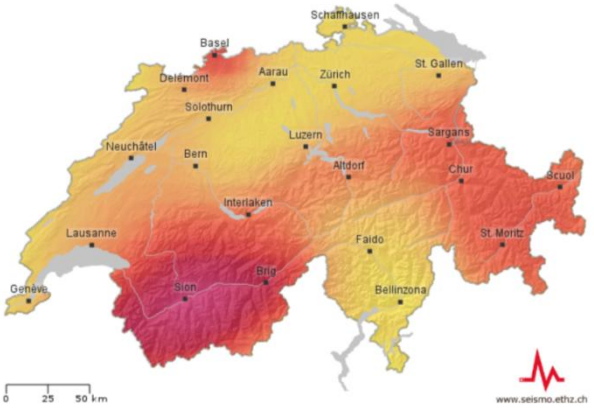
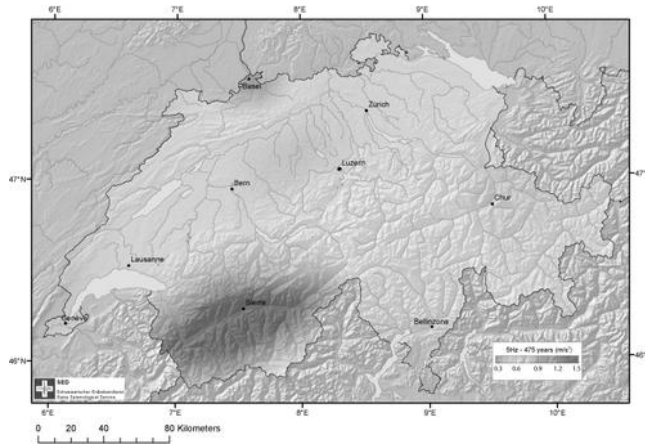	

Figure 87: Colour scales of the Swiss hazard maps in 2004 and 2015 compared.

Comparability of maps

Seismic hazard maps are available for a wide range of relevant return periods and frequencies: from 75 years return period to 10,000 years and from peak ground acceleration to a period of 4 second. The maximum values of the different maps hence range from less than 0.1 to more than 1 g. Therefore, a fundamental decision between the two strategies described below was needed:

- To colour each map individually from the minimum value (or zero) to the maximum value. This maximizes the ability to visualize differences in each map, because the full range of available colours can be used for each map.
- Scale all map colours to the same range, from zero to the overall maximum of all maps. This will ensure that maps can be visually compared with each other.

In 2004, the SED adopted the first strategy, and as a result, hazard maps for different return periods looked nearly the same. This was misinterpreted by many that the hazard actually did not change. In 2015, we decided to adopt the second strategy, in order to assist viewers to appreciate the fact that the hazard values increase everywhere in Switzerland for longer return periods. This

increase (Figure 88) is much more pronounced than the spatial gradients in each of the maps. To permit spatial differences to be visible on each of the maps, we adopted a colour scale that spans a wide range of colours: From white to yellow, orange, red and ending in purple. The same range is used for different frequencies.

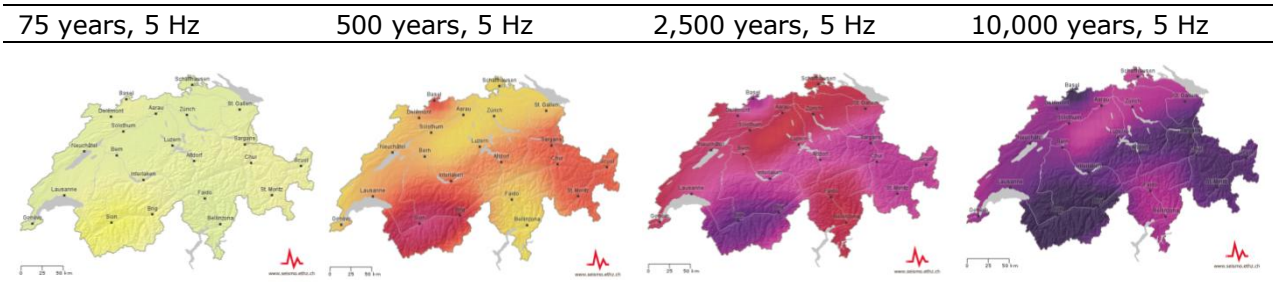

Figure 88: Same colour scale for different return periods.

An interactive web tool permits varying parameters based on users needs to explore their impact (see "interactive web tool" for further information).

Caption annotations

The captions of seismic hazard maps often carry only a colour scale annotated with the respective units shown on the map. Since many people have difficulties in interpreting these technical units, the new hazards maps are also annotated with simplified information, such as an arrow pointing from low to high hazard. This additional annotation should help non-professionals to correctly interpret the information.

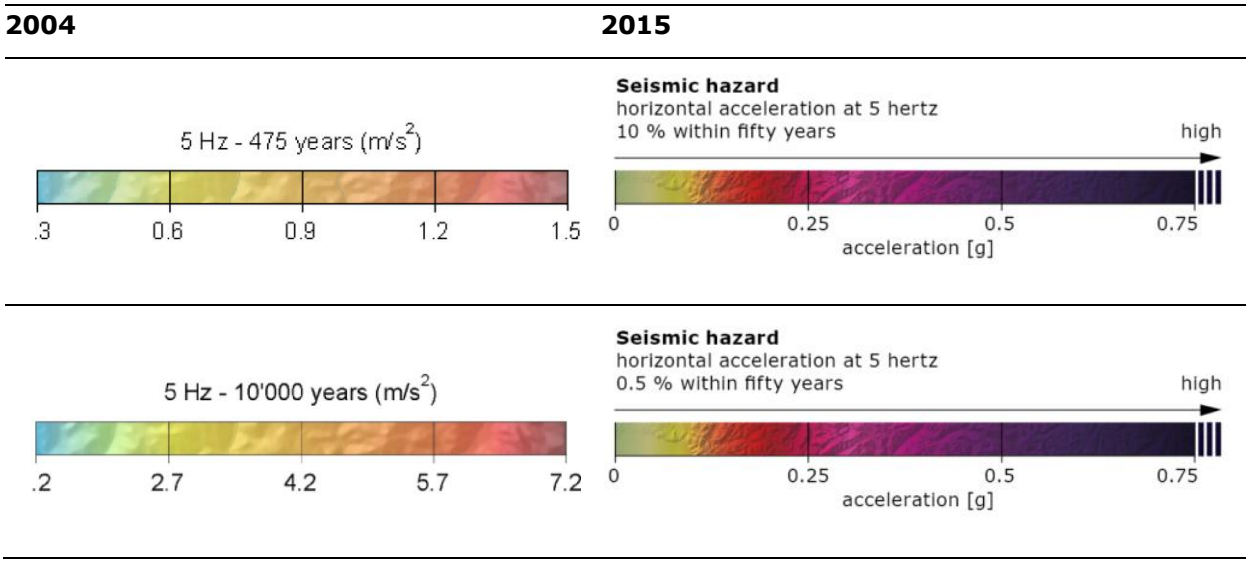

Figure 89: Map legends of the Swiss hazard model 2004 and 2015 compared.

Additional information

A special effort was put into the compilation of additional information explaining seismic hazard and its components for non-experts in an easily comprehensible way. We generally tried, to find meaningful examples to make complex aspects more intuitively accessible. For example, the "probability of exceedance of 10 percent in 50 years (500 years)" is elucidated in connection with building codes:

"Earthquake-resistant residential or office buildings in Switzerland are designed to withstand shaking that is expected to occur where the building is situated once every 500 years on average. The lifetime of a building is approximately fifty years. Within this lifetime, the probability of a residential or office building experiencing the design shaking is ten percent."

In other cases, the meaning of specific units such as intensity or magnitude was explained using illustrative examples:

intensity VIII or higher
In the case of an intensity VIII, major damage and even the collapse of buildings is likely.

magnitude of 6 or higher, within a radius of 50 km
In the case of earthquakes with a magnitude of 6, moderate to major damage is likely over a wide area.

9.4 Products

Besides innovations in the presentation of the hazard information and design characteristics, additional products were launched, in an attempt to offer products for a wider range of users and utilizations. All products are accessible and downloadable on our website.

New map types

People inquiring about earthquake hazard in Switzerland are typically not interested in acceleration values at a certain probability level. They rather would prefer to know when the next earthquake will happen that can be felt or potentially damages their houses. To address these concerns, based on the updated hazard model, two new products were developed: so-called *effect maps* and *magnitude maps*.

Effect maps
The effects maps focus on the likely consequences of an earthquake by depicting intensity values of a certain return period. Like the normal hazard maps, the effects maps are integrated over all possible earthquakes that contribute to the ground motions at a site, but they are computed using an intensity ground motion prediction equation. The effects of an earthquake are in this case measured by intensity according to the European Macroseismic Scale (EMS-98). Minor damage to buildings is likely from intensity VI upward, while intensity VII and above can result in major damage, including building collapse. Intensities below V do not generally cause any damage, although they can still be felt in some cases. The effects of similar-sized earthquakes vary primarily due to distance from the hypocenter, depth of the earthquake, and local subsoil.

The type of subsoil in the uppermost layer, ten to fifty meters directly beneath a location or building has a significant influence on the ground movement likely to occur in that location during an earthquake. Ground movement in two directly adjacent locations, when one is on soft sediment and the other on solid rock, often varies by a factor of ten or more. The ground movement and associated damage can therefore be up to one level of intensity higher. Topography also has an effect. For example, sedimentary basins (often in the vicinity of lakes or riverbanks) strengthen and prolong ground movement, because sediment basins are particularly affected by earthquake waves (resonance vibration).

Because the local subsoil across Switzerland has not been studied in sufficient detail, the SUIhaz2015 maps are based, in accordance with standard practice, on a "reference rock" that behaves in a precisely defined manner. The shear-wave velocity of the ground as a function of depth is an important parameter to consider. In order to determine the level of hazard specific to each particular location, the makeup of the local ground must be taken into account. This necessitates a geotechnical study of the subsoil or a local microzonation. In order to show at least a rough ap-

proximation of the influence of the local subsoil, the SED has included this information on the effects maps as part of SUIhaz2015. The local amplification shown is based on macroseismic data (e.g. from the "Did you feel it?" survey). These macroseismic observations are combined with geological and geotechnical maps to permit typical seismic characteristics to be deduced from particular types of soil. In Figure 90, we show a typical effects map with and without local site amplification.

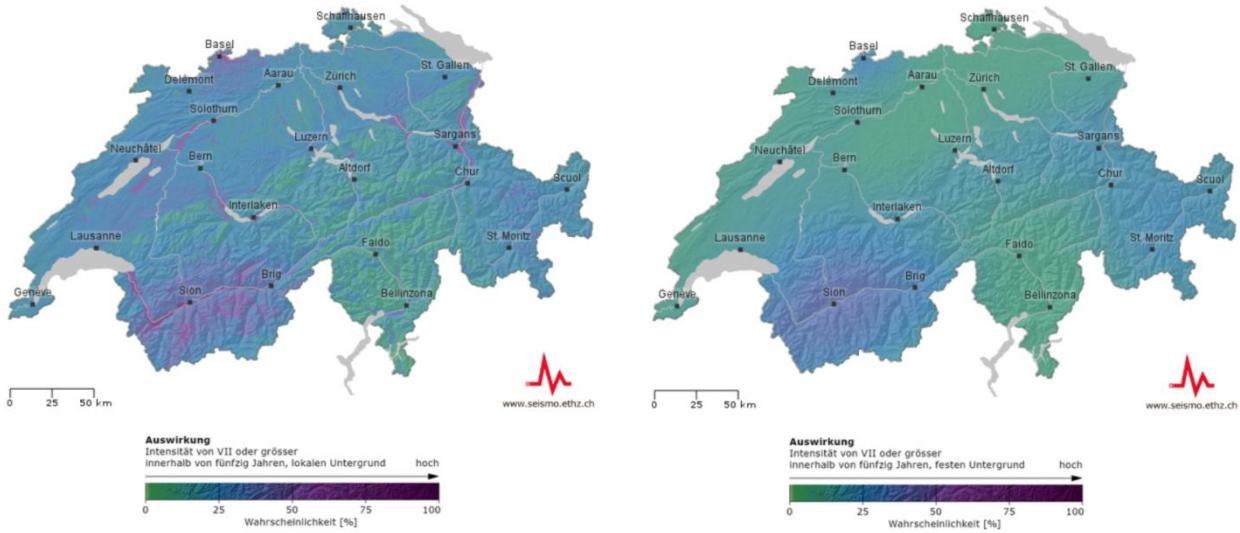

Figure 90: Effects map for intensity VII or higher within fifty years with approximate local soil conditions (left) and reference solid soil that is not locally varying (right).

Magnitude maps

Magnitudes maps show how often an earthquake of, or above, a certain size is expected to occur within a specific radius and during a certain period of time. There is no direct link to the possible effects of an earthquake, since these do not only depend on the magnitude, but also on the distance to the hypocenter, its depth, and the local subsoil. For example, an earthquake with a magnitude of 4.5 in the immediate vicinity will cause similar damage to an earthquake with a magnitude of 6 and with an epicentre 75 km away.

To clearly distinguish between these two types of maps and the hazard maps, distinct colour scales were used for each product (Figure 91).

Hazard	**Effects**	**Magnitudes**

Figure 91: Comparison of the colour scales of the three map types offered for the release of SUIhaz2015. Hazard maps (in units of m/sec^2), Effects maps (in units of EMS Intensity) and Magnitudes.

For maps of effects and magnitude, time periods in the conceivable future of the users were chosen (1, 50 and 100 years).

Web tool

To facilitate the access to the new products and help people to understand the differences between the various kinds of maps, an interactive web tool has been developed. Users can choose between the three map types mentioned above and various displaying options. The tool facilitates the comparison of different elements such as time, unit and soil condition. An introduction explains the map types in detail and all the elements are described in a few words. Every map can be downloaded in high resolution. However, we purposefully do not provide a 'zoom' function, because zooming down to a street address level is not intended for a national product and can in fact be misleading, since the local soil conditions are not known in high enough resolution. In total 45 different maps are accessible via the web tool. The tool is available in four languages: German, French, Italian and English.

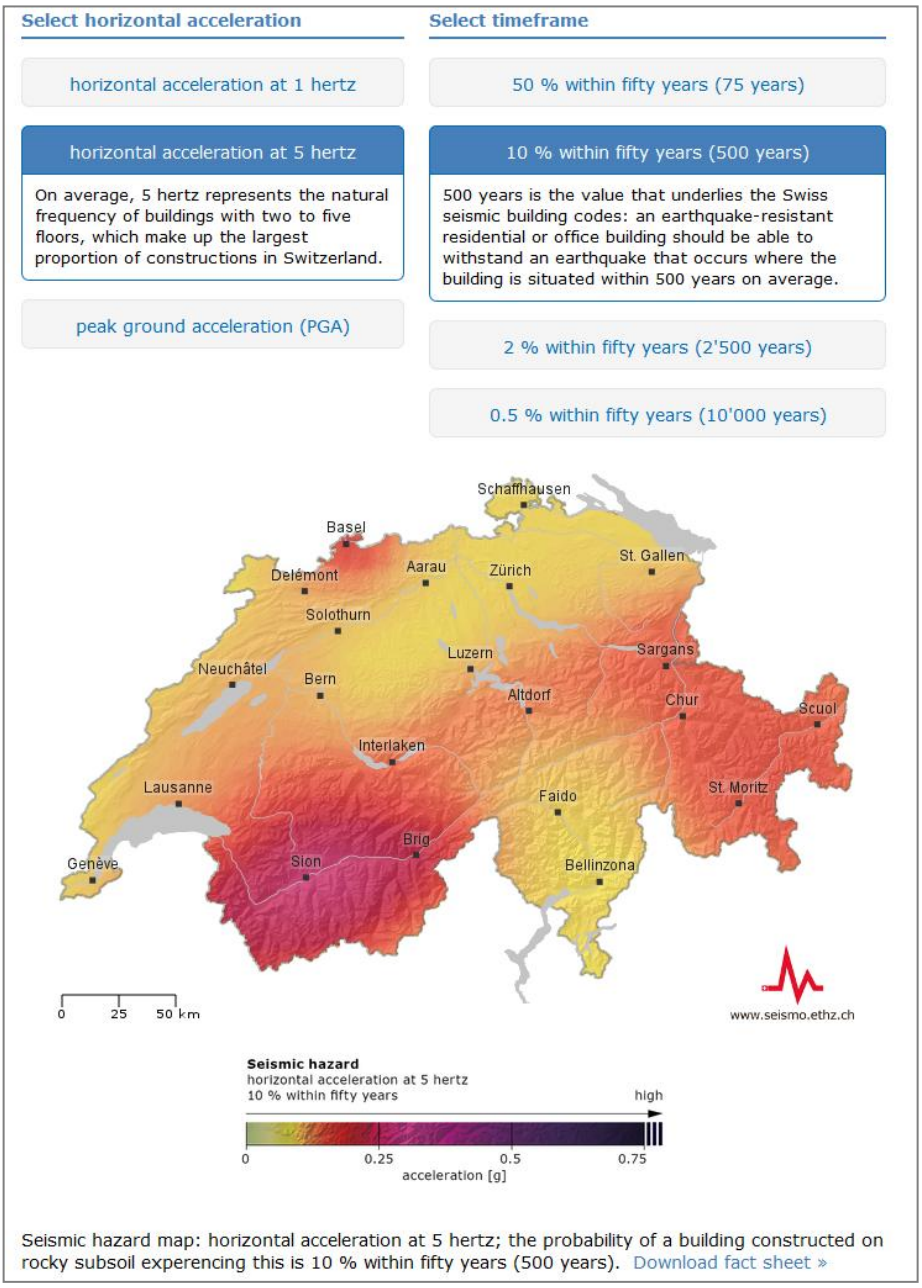

Figure 92: Snapshot of the interactive web tool programmed to facilitate the access to the results of SUIhaz2015.

For professionals

In addition to the general information described above, an additional access for professionals to the hazard data was implemented, in order to overcome a major deficit of the 2004 hazard release. For professionals such as engineers, the SED provides different components of SUIhaz2015 on the data portal of the European Facility for Earthquake Hazard & Risk EFEHR. The portal offers interactive access to the different products of the model (maps, hazard curves, uniform hazard spectra), as well as the option to download data. It also features additional background information and links tailored to professionals needs.

Printed products

A flyer, a factsheet, and a poster were developed to provide a quick overview of the most important elements of SUIhaz2015 The flyer (Figure 93, left). explains the three map types and summarizes the principal facts for an interested public. The fact sheet addresses mainly professionals with a deeper interest explaining (apart from central aspects) the main differences between the 2004 and the 2015 models. In a more visual way a newly developed large scale poster informs about earthquakes in Switzerland and earthquake hazard (Figure 93, right).

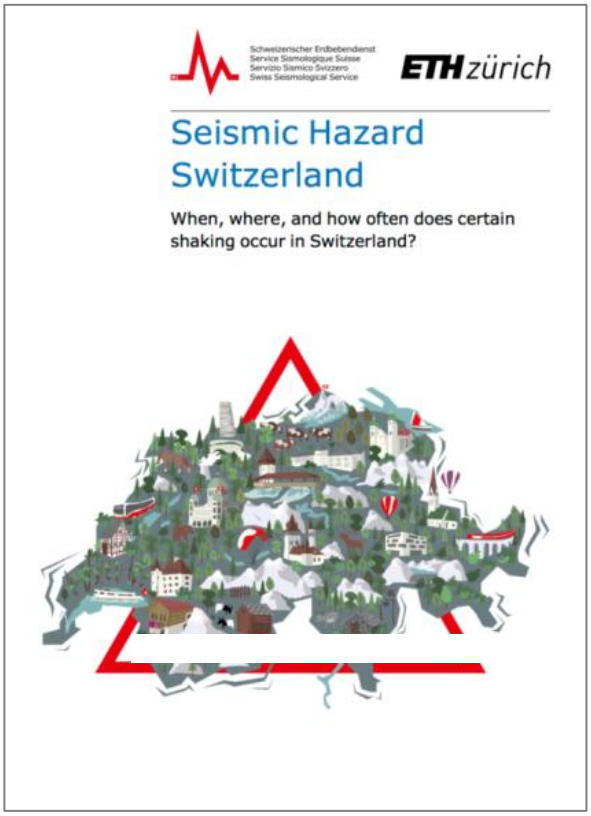

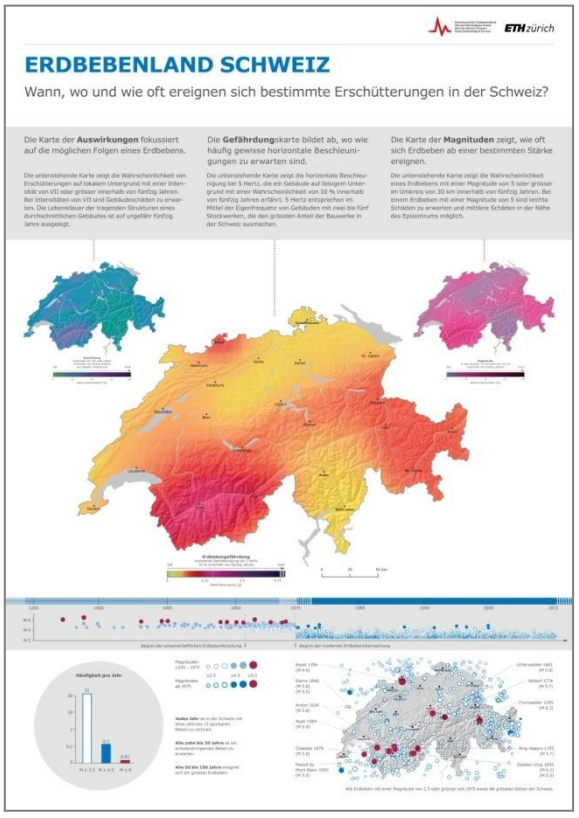

Figure 93: Snapshot of the flyer (left) and poster (right) developed as part of the national seismic hazard release.

Animation of the past and future seismicity

Another way to interactively explain the seismic hazard model is by animating past and assumed future seismicity in Switzerland. The short animation produced for this purpose first shows all major historical earthquakes in Switzerland. It continues into a more detailed presentation of the seismicity in the last 40 years and ends up by depicting simultaneously four scenarios of the assumed future seismicity. With the four scenarios we wanted to illustrate that the seismic hazard does not provide a precise answer on how seismicity will evolve, but presents a good idea on the probabilities for certain events in specific areas.

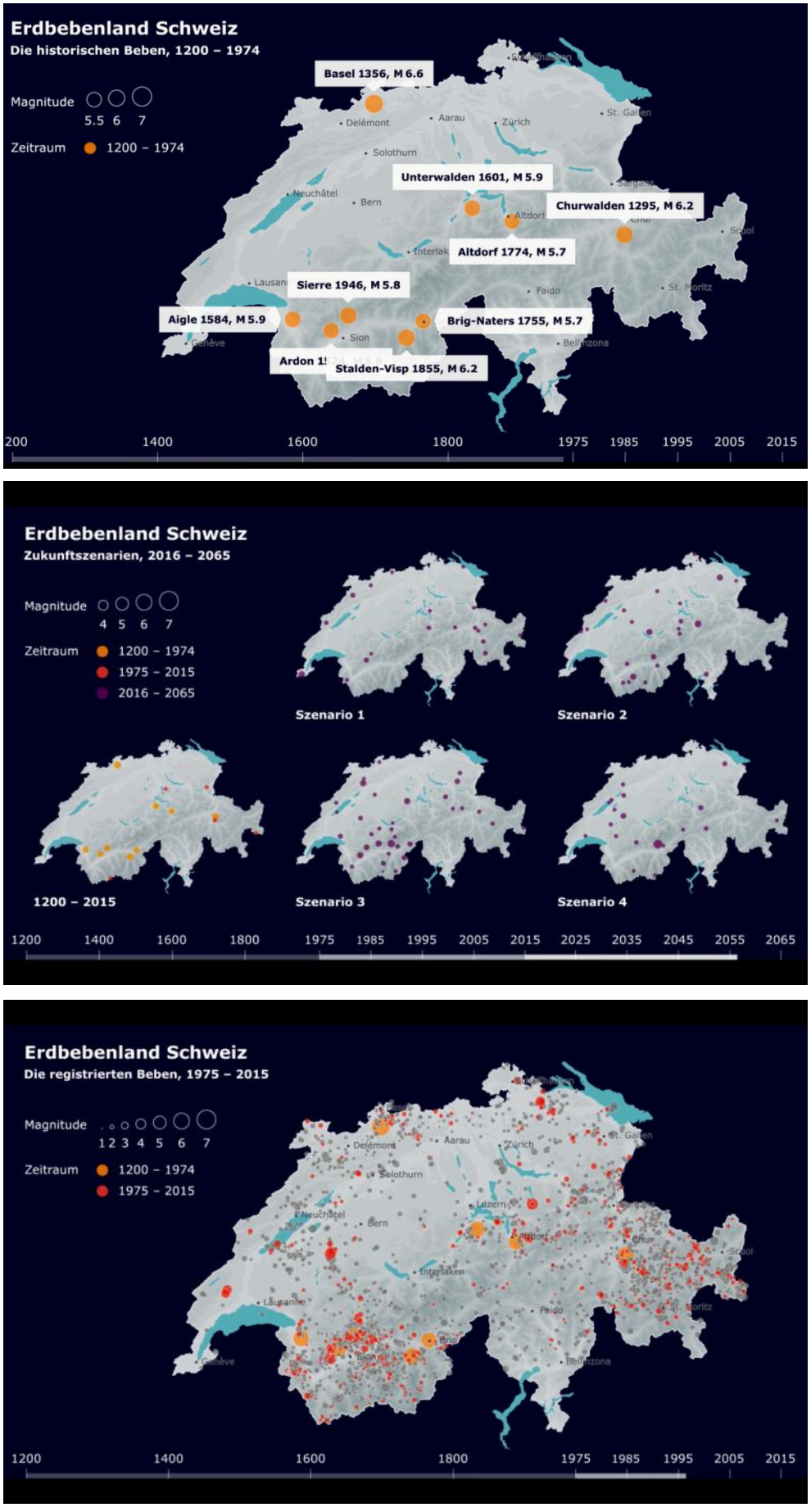

Figure 94: Snapshot of the animation "Earthquake country Switzerland"

9.5 Literature

Bodemer, N., & Gaissmaier, W. (2012). Risk Communication in Health. In S. Roeser, R. Hillerbrand, P. Sandin, & M. Peterson (Eds.), *Handbook of Risk Theory* (pp. 623–660). Springer-Verlag. http://doi.org/10.1007/978-94-007-1433-5

Bostrom, A., Anselin, L., & Farris, J. (2008). Visualizing seismic risk and uncertainty: A review of related research. *Annals of the New York Academy of Sciences*, *1128*, 29–40. http://doi.org/10.1196/annals.1399.005

Dransch, D., Rotzoll, H., & Poser, K. (2010). The contribution of maps to the challenges of risk communication to the public. *International Journal of Digital Earth*, *3*(3), 292–311. http://doi.org/10.1080/17538941003774668

Gaspar-Escribano, J. M., & Iturrioz, T. (2011). Communicating earthquake risk: Mapped parameters and cartographic representation. *Natural Hazards and Earth System Science*, *11*(2), 359–366. http://doi.org/10.5194/nhess-11-359-2011

Hagemeier-Klose, M., & Wagner, K. (2009). Evaluation of flood hazard maps in print and web mapping services as information tools in flood risk communication. *Natural Hazards and Earth System Science*, *9*(2), 563–574. http://doi.org/10.5194/nhess-9-563-2009

Hoffrage, U., Lindsey, S., Hertwig, R., & Gigerenzer, G. (2000). Statistical Communicating Information. *Science*, *290*(December), 2261–2262.

Hohl, M., Brem, S., Schulze, T., & Holthausen, N. (2015). Katastrophen und Notlagen Schweiz - Risikobericht 2012, 58.

Kjellgren, S. (2013). Exploring local risk managers' use of flood hazard maps for risk communication purposes in Baden-Württemberg. *Natural Hazards and Earth System Science*, *13*(7), 1857–1872. http://doi.org/10.5194/nhess-13-1857-2013

Kunz, M., & Hurni, L. (2011). How to Enhance Cartographic Visualisations of Natural Hazards Assessment Results. *Cartographic Journal*, *48*(1), 60–71. http://doi.org/10.1179/1743277411Y.0000000001

Mileti, D., Nathe, S., Gori, P., Greene, M., & Lemersal, E. (2004). Public Hazards Communication and Education: The State of the Art. *Informer*, 1–13.

Nathe, S. K. (2000). Public Education for Earthquake Hazards. *Natural Hazards Review*, *1*(November), 191–196.

Perry, S. C., Blanpied, M. L., Burkett, E. R., Campbell, N. M., Carlson, A., Cox, D. A., … Zarcadoolas, C. (2016). Get Your Science Used — Six Guidelines to Improve Your Products Circular 1419.

Peters, E., Bostrom, A., & Cutter, S. (2008). Preferred Data Visualization Techniques May Not Lead to Comprehension and Use of Hazard Information. In A. Bostom, S. French, & S. Gottlieb (Eds.) (pp. 295–318). Berlin, Heidelberg: Springer-Verlag.

Whitney, D. J., Lindell, M. K., & Nguyen, H.-H. D. (2004). Earthquake beliefs and adoption of seismic hazard adjustments. *Risk Analysis : An Official Publication of the Society for Risk Analysis*, *24*(1), 87–102. http://doi.org/10.1111/j.0272-4332.2004.00414.x

10. Summary and outlook

In Switzerland, earthquakes are the natural hazard with the greatest potential for causing damage. They cannot currently be prevented or reliably predicted. The best protection against earthquake damage persists in implementing adequate mitigation measures for buildings and infrastructures, and this is one of the key areas where a state of the art seismic hazard model is needed.

Switzerland's seismic hazard model is a comprehensive representation of all relevant knowledge on earthquakes. It makes a forecast of potential earthquakes and the resulting ground motions over the next fifty years. The model is based on knowledge of tectonics and geology, information about the history of earthquakes, damage reports, and wave propagation models. Experts and authorities use it as a starting point when making decisions regarding earthquake mitigation and risk management. The Swiss seismic building codes are also based on previous versions of the model, and routinely checked against current model.

Switzerland's seismic hazard model 2015 replaces the previous model from 2004. A periodic update reflecting the latest technological and scientific findings forms the basis for adequate protection measures. The seismic hazard model 2015 features new data, revised estimates of historical sources, a homogeneous reference rock, and improved predictive models. The uncertainty regarding estimates of likely ground motions has been significantly reduced relatively to the 2004 model, meaning the 2015 model provides a more solid estimate of seismic hazard and a good basis for a nationwide risk model. The new model offers a number of improvements when compared to the one in 2004:

- **New measuring data:** High-quality data of the last ten years from the national digital broadband and strong motion measurement network was incorporated in the reassessment of the seismic hazard. Switzerland has one of the most modern and densest seismic measurement networks worldwide. It annually records 500 to 800 earthquakes in Switzerland and its neighbouring countries. Knowledge about the distribution of the small and medium earthquakes is an essential aid for estimating future earthquake activity. The recorded ground accelerations also make it possible to develop improved ground movement forecast models.
- **Newly evaluated historical data:** Numerous data sources were re-evaluated in the scope of the revision of the historical Swiss Earthquake Catalogue. They provide important information about all known damaging earthquakes and their effects up to 1975. Since this time, the seismic network in Switzerland has enabled the nationwide instrumental monitoring of earthquake activity. Historical seismology makes a critical contribution to the hazard analysis by assessing the effects of major earthquakes in the past. Such earthquakes only occur rarely in Switzerland, and, in comparison to their return period, the observation period of instrumental seismology turns out to be very short.
- **Updated and new macroseismic data:** Macroseismology is a classification of the shaking caused by earthquakes based on the effects observed by persons. It makes it possible to reliably estimate the magnitudes and epicentres of historical earthquakes and link these to modern data.
- **Homogeneous reference rock:** Extensive geophysical measurements at different seismometer stations in Switzerland make it possible to determine the influence of the local geology on the recorded seismograms. Effects of the seismic focus, the spread of the seismic waves, and thus the local amplifications can be reliably differentiated this way. This makes it possible to determine the ground acceleration for a rock reference site with a defined shear-wave profile and an average speed of 1,100 m/s. It was not yet possible in 2004 to reliably

calculate the influence of the local amplification. This is an essential advancement in comparison to the seismic hazard model 2004 and makes it possible to reduce the uncertainties in the risk estimate.

- **Improved forecast models:** In the past ten years, extensive high-quality seismic data was recorded worldwide in direct proximity to strong earthquakes. The data thus obtained enables an improved understanding of the influences of the local ground, which leads to clearly more reliable forecast models of the ground movement with the aid of modernized analysis methods. The forecast models now also cover a much broader frequency range, which is important for the implementation of the hazard analysis in the construction engineering sector.
- **Alternative zoning:** The SED has developed alternative approaches in order to statistically analyze and visualize the distribution of earthquakes according to location, time, and magnitude. This alternative to classic seismotectonic zoning is of particular advantage for regions with spatially distributed seismicity without domineering fault zones, such as can be encountered in the Alps.
- **Refined computation approaches:** The open-source software platform OpenQuake, developed in the Global Earthquake Model (GEM) project with participation of the SED, enables a much-improved calculation of the seismic hazard. More complex models make it possible to consider uncertainties to a larger extent and estimate them more precisely. Furthermore, the ground movements are not only modelled for spot sources, but can also be modelled for extensive fissures with varying fissure orientations.
- **Easier access for the public:** In a newly developed web application, the SED visualizes how likely certain shaking is in Switzerland. This makes it possible to answer typical questions such as "How often and how strong does the earth shakes in my neighbourhood?" statistically for any location in Switzerland. The maps can be classified into three types: the *effects* maps focus on the possible consequences of an earthquake; the *hazard* maps show how often buildings are affected by certain incidents of horizontal acceleration; and the *magnitudes* maps show how often an earthquake of, and above, a certain strength occurs. As well as selecting viewing modes, you can also choose between different time periods.
- **Improved access for professionals:** The access to the seismic hazard model is significantly improved for professionals. On a new interactive web portal, construction engineers and geologists can independently view and download answer spectra and hazard curves, as well as deaggregations. The SED is also creating a new peak ground acceleration (PGA) map, which will be used as a basis for zoning in the SIA 261 building standards. This map coincides very well with the present, only indirectly derived and thus approximate PGA map.

The seismic hazard model 2015 confirms first of all that Switzerland is an earthquake-prone country. On average, an earthquake with the magnitude of 5 can be expected to occur every 8 to 15 years, even though the last earthquake of this magnitude dates back roughly 25 years (Vaz GR, 1991). With such an earthquake, extensive damage to buildings is likely, depending on the region and the depth. Earthquakes with a magnitude of 6 or greater, which may cause vast and partially severe damage, occur every 50 to 150 years on average. Earthquakes of this magnitude are principally possible at anytime and anywhere in Switzerland. The last earthquake of this magnitude occurred in upper Valais in 1946 (Sierre VS, 1946).

As expected, the spatial distribution of the seismic hazard has not changed significantly in the past ten years. Valais remains the region with the highest level of hazard in Switzerland, followed by Basle, Grisons, Central Switzerland, the St. Gallen Rhine Valley, and the rest of Switzerland. The hazard estimate for Grisons is now similar to the one for the Basle region. This slightly higher classification of the canton of Grisons can be explained by an adjusted evaluation of previous earthquakes.

Besides the slightly elevated hazard estimation for the canton of Grisons in comparison to other regions, the seismic hazard model 2015 shows higher values for likely ground movements in many frequency ranges compared to 2004. This is primarily due to the evaluation of extensive newly recorded data in proximity to strong earthquakes in Switzerland and abroad. They often turned out to be higher than previously expected.

The relative differences between 2015 and 2004 are approximately 30 percent for a return period of 475 years and a frequency of 5 Hz for a location in Valais. This corresponds to 0.07 g absolute (gravity acceleration). The rise in percent is higher in regions with lower hazard, such as Central Switzerland or Jura: although the values here only increased by 0.03 to 0.05 g in absolute, this corresponds to a relative increase of 50 to 70 percent. As of a frequency of 2 Hz or less, however, the values from 2015 are similar to the values from 2004, or up to 10 percent lower in some regions. In general, the uncertainties in the estimation of likely ground movements are 2015 considerably fewer than in 2004. Less substantial uncertainties are a sign that the numerous work efforts that form the basis of the new seismic hazard model are paying off.

Also in the future, it will remain important to periodically update the seismic hazard assessment of Switzerland in order to integrate new data, new technical and scientific progress as well as emerging requirements of users. It takes typically five to ten years until science and technology have advanced significantly enough to warrant an update of a national PSHA model, and we expect that the SUIhaz2015 model will be stable for at least that period. Meanwhile, in preparing for the need to update the hazard model, the SED is engaging in a number of activities, focused on the most pressing needs and priorities:

- We are monitoring the advances in science and technology around the globe in order to detect if they may have a substantial impact on the validity of SUIhaz2015.
- We continue the seismic monitoring of the seismic activity in Switzerland using the much improved capabilities of the seismic network. The broadband and strong motion networks will continue to collect highly relevant data for future studies, especially since the local site conditions at many stations are much better known today.
- We are filling gaps in the instrumental and macro-seismic record, for example the so-called dark period around 1960.
- We are investigating techniques that will allow to reliably detect earthquakes of smaller magnitudes and located them more precisely. This will facilitate the statistical analysis as well as the seismotectonic analysis and correlation with known faults.
- We are working on ways to improve the consistency of magnitudes across different scales, also hoping to find a way to better understand the Ml - Mw scaling issues.
- We will be investigating alternative, more physics based approaches to forecast the future seismicity, trying to take advantage of emerging computational modelling capabilities of alpine orogeny.
- We are seeking to develop and calibrate the next generation of ground motion prediction models that are capable to separate with even more precision the influence of source, path and local site.

A number of projects and PhD theses have already been started on these topics, more are on the horizon. All of them combine applied research needs and insights into fundamental processes of the earth. Earthquake remain enigmatic and a fascinating and important topic to study, but our primary goal remains to help societies to better cope with the risk earthquakes pose.

11. Acknowledgements

The 2015 hazard model and this hazard report summarize the efforts of numerous people over more than a decade. For many scientist and PhD students, working on seismic hazard related questions was their primary focus, other may have contributed in smaller ways only. Also the technical and administrative staff was fundamental to ensure that we could reach this important milestone, for example by making sure on a daily basis that we are able to record earthquakes with more than 130 stations distributed across Switzerland. I am sincerely grateful to all current and past employees that made SUIhaz2015 possible, the dedication of SED staff is remarkable. Many of the projects and decisions that enabled SUIhaz2015 were taken at the SED before 2012, under the leadership of its former director, Prof. Domenico Giardini, who continued to give important and much appreciated input throughout the project.

The SED is at home in an ideal environment at ETH Zurich, embedded into the thriving research atmosphere at the Department of Earth Science (D-ERDW). We greatly value and critically depend on the continued support of ETH and D-ERDW, and again it is the support by many staff members in across science, administration and support that helped over the years to make SUIhaz2015 possible. Thank you!

Finally, the SED greatly benefitted from the support from external partners that facilitated our work in various ways. We like to thank our neighbouring seismological services for their openness to share data and knowledge across borders. We also depended critically on the financial support of several institutions that funded key projects that made SUIhaz2015 possible: The Swiss Nation Science Foundation (SNF), ETH Rat, EU FP6, FP7 programs, the Federal Office of the Environment (BAFU), the Federal Office of Energy (BFE), the Swiss Federal Nuclear Safety Inspectorate (ENSI), the National Cooperative for the Disposal of Radioactive Waste (NAGRA), swissnuclear and the Global Earthquake Model (GEM).

Appendix A

Exceedance probabilities versus return periods

"The seismic hazard map is for ground motions having a 2% probability of exceedance in 50 years. Are those values the same as those for 10% in 250? (From: http://earthquake.usgs.gov/hazards/about/technical.php)"

A typical seismic hazard map may have the title, "Ground motions having 90 percent probability of not being exceeded in 50 years." The 90 percent is a "non-exceedance probability"; the 50 years is an "exposure time." An equivalent alternative title for the same map would be, "Ground motions having 10 percent probability of being exceeded in 50 years." Typical shorthand to describe these ground motions would be to say that they are 475-year return-period ground motions. This means the same as saying that these ground motions have an annual probability of occurrence of 1/475 per year. "Return period" is thus just the inverse of the annual probability of occurrence (of getting an exceedance of that ground motion).

To get an approximate value of the return period, RP, given the exposure time, T, and exceedance probability, r = 1 - non-exceedance probability, NEP, (expressed as a decimal, rather than a percent), calculate:

RP = T / r* Where r* = r(1 + 0.5r).r* is an approximation to the value -loge (NEP).

In the above case, where r = 0.10, r* = 0.105 which is approximately = -loge (0.90) = 0.10536. Thus, approximately, when r = 0.10, RP = T / 0.105

Consider the following table:

				Rule of Thumb		Exact
NEP	T	r	r*	Calculation	RP	RP
0.90	50	0.10	0.105	50/0.105	476.2	474.6
0.90	100	0.10	0.105	100/0.105	952.4	949.1
0.90	250	0.10	0.105	250/0.105	2381.0	2372.8

In this table, the exceedance probability is constant for different exposure times. Compare the results of the above table with those shown below, all for the same exposure time, with differing exceedance probabilities.

				Rule of Thumb		Exact
NEP	T	r	r*	Calculation	RP	RP
0.90	50	0.10	0.105	50/0.105	476.2	474.6
0.95	50	0.05	0.05125	50/0.05125	975.6	974.8
0.98	50	0.02	0.0202	50/0.0202	2475.2	2475.9

Comparisons of the last entry in each table allows us to see that ground motion values having a 2% probability of exceedance in 50 years should be approximately the same as those having 10% probability of being exceeded in 250 years: The annual exceedance probabilities differ by about 4%. Corresponding ground motions should differ by 2% or less in the EUS and 1 percent or less in the WUS, based upon typical relations between ground motion and return period.

Appendix B

Extract of Input Files for OpenQuake

The main purpose of this appendix is to provide the basic information so that an analyst experienced in PSHA can implement the seismic source model. The appendix summarizes input files for OpenQuake and descriptions of the source specific parameters that define the spatial distribution and frequency of future earthquakes. The reader is referred mainly to Chapter 4 and 5 of the main report for detailed descriptions of procedures and rationale used to develop the model parameters. OpenQuake provides the blueprints for the seismic source representation and OpenQuake –hazard engine book and manual by Pagani et al (2013) shall be consulted for further details.

The seismogenic source model consists of five earthquake rate models corresponding to median, 5^{th}, 16^{th}, 84^{th} and 95^{th} percentiles as illustrated in the master logic tree. Each seismogenic source of each earthquake rate model is represented as a point source following the OpenQuake seismic source taxonomy. In the current source model, we will refer to as *point sources* the seismogenic sources modelling earthquake magnitudes less or equal to M_w5.5 and *extensive-point sources* to those of magnitudes greater then M_w 5.5.

The geometry of these two source typologies is the same, whereas the earthquake magnitude distribution is different. An incremental magnitude distribution is defined between the minimum magnitude 4.00 and upper magnitude equal to 5.45 characterize the point sources without extensive ruptures. In turn, the point ruptures with propagation of the extensive ruptures are characterized by an incremental magnitude distribution that starts at 5.5M_w up to the maximum magnitude defined for each point source. The incremental magnitude frequency distribution is described by a center value of the first magnitude bin, bin size and the number or occurrence rates. In our model, the magnitude bin interval is set to 0.10. Given that the point sources aimed at modelling the small magnitude, a single style of faulting is defined for all type 1-point sources, as described by the nodal plane distribution <*nodalPlaneDist*> field. For point sources that support extensive ruptures propagation, the style of faulting is assigned following the details presented in Chapter 4.

Figures A.2 to A.5 show examples of the two type of sources for the two tectonic Foreland and Alpine. The shallow sources are located at a depth of about 4.5 km, whereas the deep sources are concentrated at a depth of about 13.5 km. The value of the lower and upper seismogenic depths defines the boundaries within which the extensive ruptures are confined to remain. Basically, an earthquake rupture is not allowed to extend above the surface, or below the lower seismogenic depth. When an extensive rupture is generated, its size is controlled by the earthquake magnitude, size scaling geometry model, and the aspect ratio. The later was fixed to unity. The equations of Wells and Coppersmith (1994) are used to control the rupture size for point sources that allow the earthquake rupture propagation.

Three style of faulting, namely normal, reverse and strike-slip are defined for each extensive-point source. The average strike, dip and rake angles are parameterized to define a style-of-faulting as described in Chapter 4. The

```
<pointSource id="57Sp" name="point" tectonicRegion="Alpine Shallow Crust">
    <pointGeometry>
        <gml:Point>
            <gml:pos>5.475 45.025</gml:pos>
        </gml:Point>
        <upperSeismoDepth>0.0</upperSeismoDepth>
        <lowerSeismoDepth>33.7</lowerSeismoDepth>
    </pointGeometry>
    <magScaleRel>PointMSR</magScaleRel>
    <ruptAspectRatio>1.0</ruptAspectRatio>
    <incrementalMFD minMag="4.05" binWidth="0.1">
        <occurRates>
        3.372274E-05 2.776511E-05 2.286263E-05 1.882795E-05 1.550707E-05
        1.409461E-05 1.152286E-05 9.433068E-06 7.719746E-06 6.319887E-06
        5.175709E-06 4.240161E-06 3.474918E-06 2.848749E-06 2.336193E-06
        </occurRates>
    </incrementalMFD>
    <nodalPlaneDist>
        <nodalPlane probability="1.000" strike="0.0" dip="90.0" rake="-90.0"/>
    </nodalPlaneDist>
    <hypoDepthDist>
    <hypoDepth probability="1.000" depth="4.5" />
    </hypoDepthDist>
</pointSource>
```

Figure 95: Extract of the NRML input file for a point source without extensive rupture for Alpine Shallow Crust

```
<pointSource id="57Sf" name="point" tectonicRegion="Alpine Shallow Crust">
    <pointGeometry>
        <gml:Point>
            <gml:pos>5.475 45.025</gml:pos>
        </gml:Point>
        <upperSeismoDepth>0.0</upperSeismoDepth>
        <lowerSeismoDepth>33.7</lowerSeismoDepth>
    </pointGeometry>
    <magScaleRel>WC1994</magScaleRel>
    <ruptAspectRatio>1.0</ruptAspectRatio>
    <incrementalMFD minMag="5.55" binWidth="0.1">
        <occurRates>
        1.916488E-06 1.565758E-06 1.287757E-06 1.060058E-06 8.707086E-07
        7.153958E-07 5.879596E-07 4.833634E-07 3.974866E-07 3.269574E-07
        2.690154E-07 2.213802E-07 1.822432E-07 1.500493E-07 1.235842E-07
        9.578161E-08 7.910467E-08 6.381980E-08 1.813269E-09
         </occurRates>
    </incrementalMFD>
    <nodalPlaneDist>
        <nodalPlane probability="0.166" strike="0.00" dip="90.0" rake="0.00"/>
        <nodalPlane probability="0.166" strike="90.0" dip="90.0" rake="0.00"/>
        <nodalPlane probability="0.166" strike="0.00" dip="90.0" rake="90.0"/>
        <nodalPlane probability="0.166" strike="90.0" dip="90.0" rake="90.0"/>
        <nodalPlane probability="0.166" strike="0.00" dip="90.0" rake="-90.0"/>
        <nodalPlane probability="0.170" strike="90.0" dip="90.0" rake="-90.0"/>
    </nodalPlaneDist>
    <hypoDepthDist>
    <hypoDepth probability="1.000" depth="4.5" />
    </hypoDepthDist>
</pointSource>
```

Figure96: Extract of the NRML input file for an extensive-point source for Alpine Shallow Crust

```
<pointSource id="57Dp" name="point" tectonicRegion="Alpine Deep Crust">
    <pointGeometry>
        <gml:Point>
            <gml:pos>5.475 45.025</gml:pos>
        </gml:Point>
        <upperSeismoDepth>0.0</upperSeismoDepth>
        <lowerSeismoDepth>33.7</lowerSeismoDepth>
    </pointGeometry>
    <magScaleRel>PointMSR</magScaleRel>
    <ruptAspectRatio>1.0</ruptAspectRatio>
    <incrementalMFD minMag="4.05" binWidth="0.1">
        <occurRates>
        5.039030E-06 4.148809E-06 3.416255E-06 2.813372E-06 2.317148E-06
        2.106091E-06 1.721807E-06 1.409539E-06 1.153525E-06 9.443510E-07
        7.733818E-07 6.335872E-07 5.192406E-07 4.256751E-07 3.490864E-07
        </occurRates>
    </incrementalMFD>
    <nodalPlaneDist>
        <nodalPlane probability="1.000" strike="0.0" dip="90.0" rake="-90.0" />
    </nodalPlaneDist>
    <hypoDepthDist>
    <hypoDepth probability="1.000" depth="13.5" />
    </hypoDepthDist>
</pointSource>
```

Figure 97: Extract of the NRML input file for a point source without extensive rupture for Alpine Deep Crust

```
<pointSource id="57Df" name="point" tectonicRegion="Alpine Deep Crust">
    <pointGeometry>
        <gml:Point>
            <gml:pos>5.475 45.025</gml:pos>
        </gml:Point>
        <upperSeismoDepth>0.0</upperSeismoDepth>
        <lowerSeismoDepth>33.7</lowerSeismoDepth>
    </pointGeometry>
    <magScaleRel>WC1994</magScaleRel>
    <ruptAspectRatio>1.0</ruptAspectRatio>
    <incrementalMFD minMag="5.55" binWidth="0.1">
        <occurRates>
        2.863718E-07 2.339639E-07 1.924235E-07 1.583994E-07 1.301059E-07
        1.068982E-07 8.785604E-08 7.222671E-08 5.939454E-08 4.885570E-08
        4.019770E-08 3.307980E-08 2.723175E-08 2.242115E-08 1.846661E-08
        1.431219E-08 1.182024E-08 9.536291E-09 2.709483E-10
        </occurRates>
    </incrementalMFD>
    <nodalPlaneDist>
        <nodalPlane probability="0.166" strike="0.00" dip="90.0" rake="0.00"/>
        <nodalPlane probability="0.166" strike="90.0" dip="90.0" rake="0.00"/>
        <nodalPlane probability="0.166" strike="0.00" dip="90.0" rake="90.00"/>
        <nodalPlane probability="0.166" strike="90.0" dip="90.0" rake="90.00"/>
        <nodalPlane probability="0.166" strike="0.00" dip="90.0" rake="-90.0"/>
        <nodalPlane probability="0.170" strike="90.0" dip="90.0" rake="-90.0"/>
    </nodalPlaneDist>
    <hypoDepthDist>
    <hypoDepth probability="1.000" depth="13.5" />
    </hypoDepthDist>
</pointSource>
```

Figure 98: Extract of the NRML input file for an extensive-point source for Alpine Deep Crust

Appendix C

Seismic source model

Figures for all SEIS source zones listing earthquake recurrence parameters. Left panel: completeness time history (numbers of complete events for each completeness step are given in brackets; blue for using time intervals and gray for using magnitude intervals). Right panel: frequency-magnitude distribution. Solid green line indicates result of PML method using the 2nd EPRI maximum magnitude. The dashed light green line shows PML bootstrapping quantiles using 1st and 3rd EPRI maximum magnitude. Red lines correspond to the a and b-values used in the 2004 hazard model. The thick red line denotes set of recurrence parameters with the highest Akaike-weight (see Wiemer et al., 2009b, for more details)

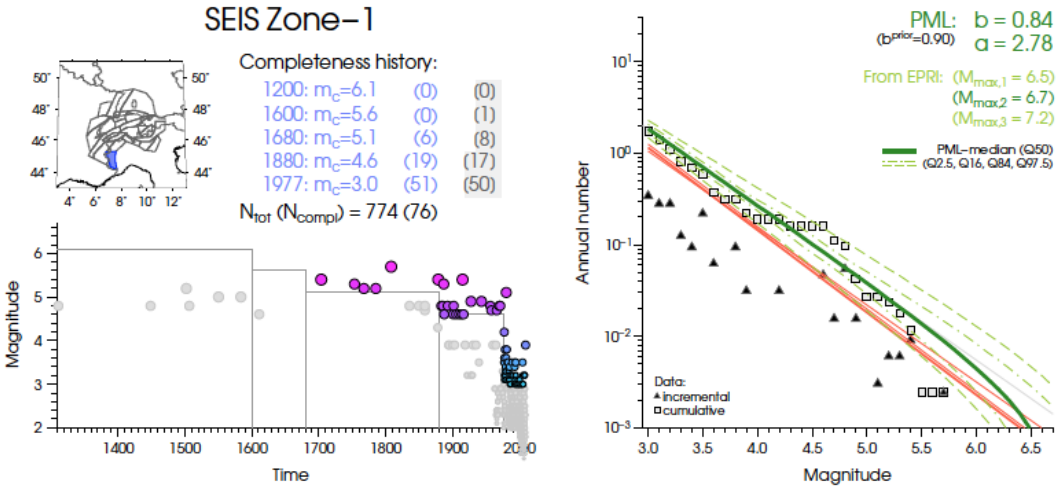

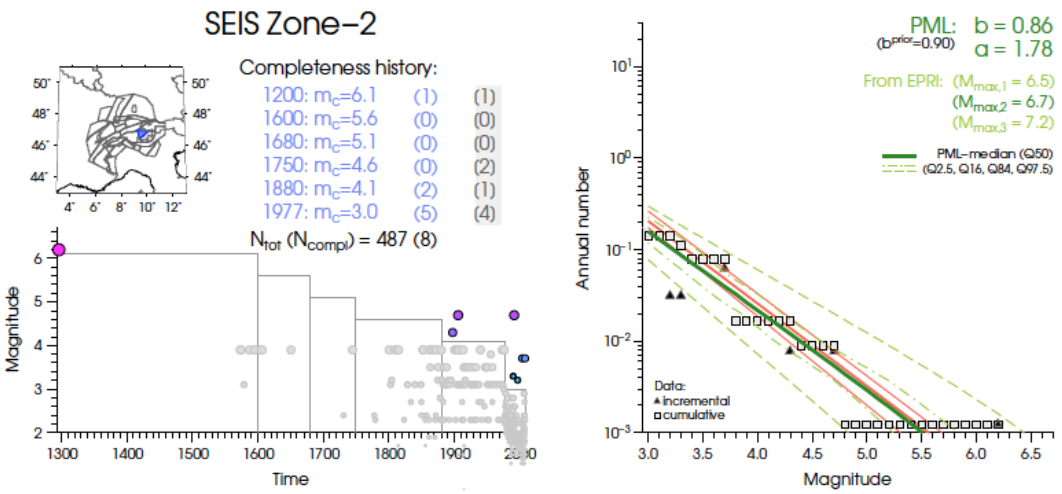

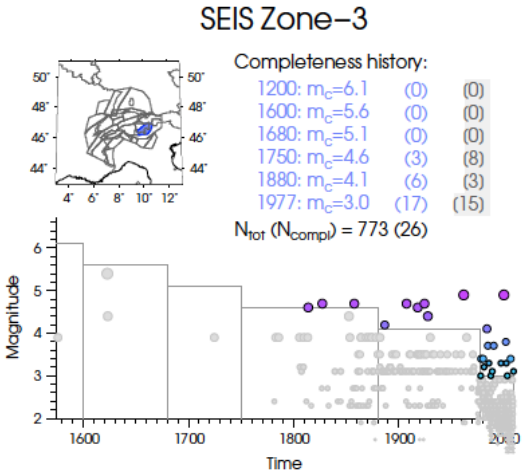
SEIS Zone−3
Completeness history:
1200: mc=6.1 (0) (0)
1600: mc=5.6 (0) (0)
1680: mc=5.1 (0) (0)
1750: mc=4.6 (3) (8)
1880: mc=4.1 (6) (3)
1977: mc=3.0 (17) (15)
Ntot (Ncompl) = 773 (26)
Magnitude
Time

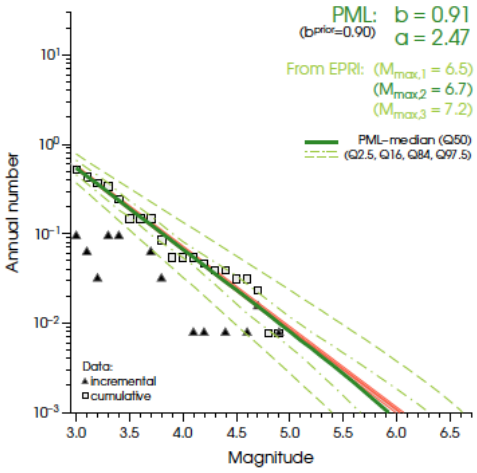
PML: b = 0.91
(bprior=0.90) a = 2.47
From EPRI: (Mmax,1 = 6.5)
(Mmax,2 = 6.7)
(Mmax,3 = 7.2)
PML−median (Q50)
(Q2.5, Q16, Q84, Q97.5)
Data:
incremental
cumulative
Annual number
Magnitude

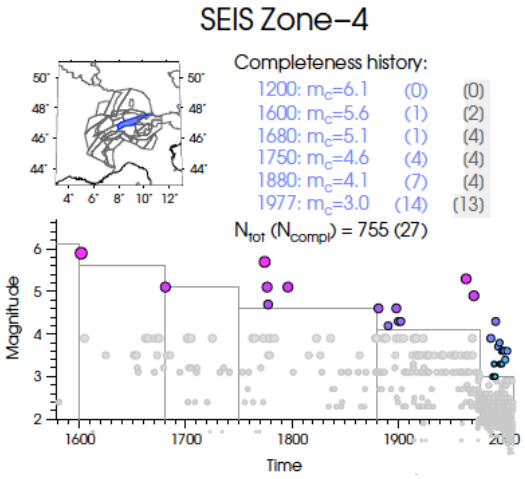
SEIS Zone−4
Completeness history:
1200: mc=6.1 (0) (0)
1600: mc=5.6 (1) (2)
1680: mc=5.1 (1) (4)
1750: mc=4.6 (4) (4)
1880: mc=4.1 (7) (4)
1977: mc=3.0 (14) (13)
Ntot (Ncompl) = 755 (27)
Magnitude
Time

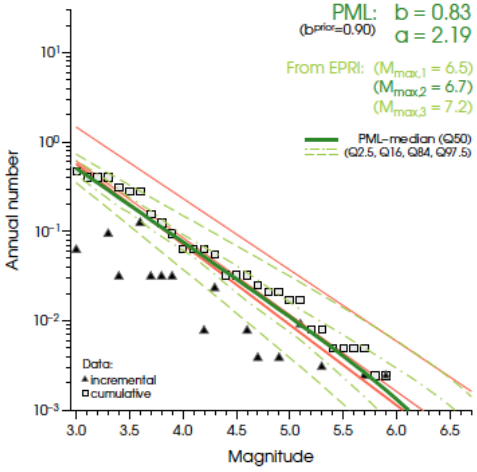
PML: b = 0.83
(bprior=0.90) a = 2.19
From EPRI: (Mmax,1 = 6.5)
(Mmax,2 = 6.7)
(Mmax,3 = 7.2)
PML−median (Q50)
(Q2.5, Q16, Q84, Q97.5)
Data:
incremental
cumulative
Annual number
Magnitude

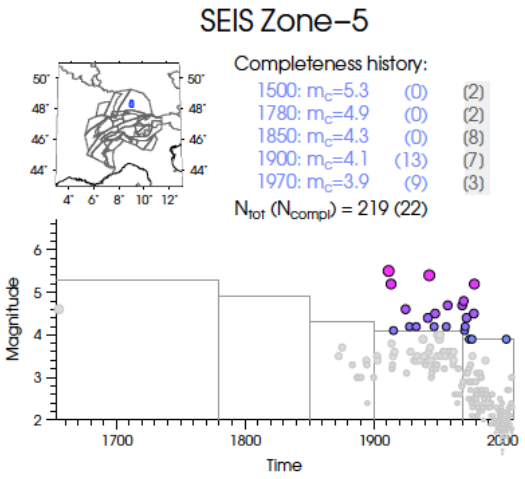
SEIS Zone−5
Completeness history:
1500: mc=5.3 (0) (2)
1780: mc=4.9 (0) (2)
1850: mc=4.3 (0) (8)
1900: mc=4.1 (13) (7)
1970: mc=3.9 (9) (3)
Ntot (Ncompl) = 219 (22)
Magnitude
Time

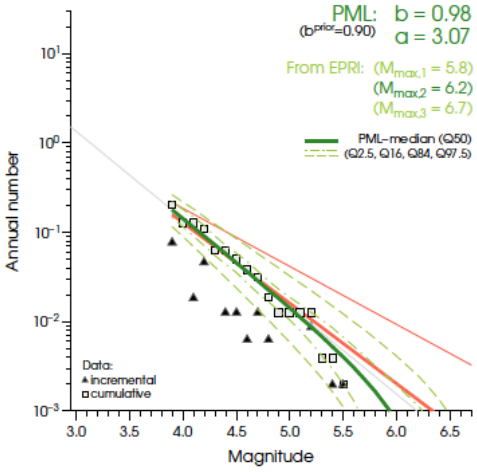
PML: b = 0.98
(bprior=0.90) a = 3.07
From EPRI: (Mmax,1 = 5.8)
(Mmax,2 = 6.2)
(Mmax,3 = 6.7)
PML−median (Q50)
(Q2.5, Q16, Q84, Q97.5)
Data:
incremental
cumulative
Annual number
Magnitude

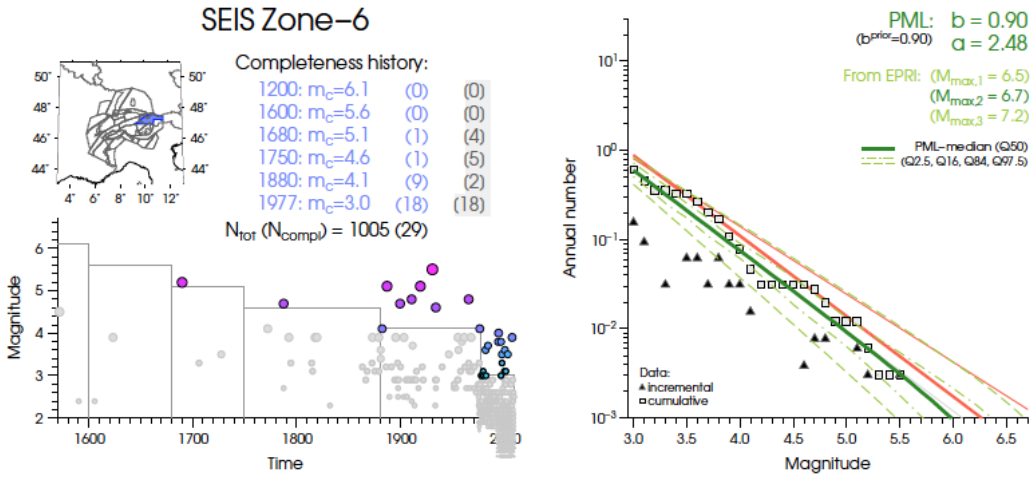
SEIS Zone–6
Completeness history:
1200: m_c=6.1 (0) (0)
1600: m_c=5.6 (0) (0)
1680: m_c=5.1 (1) (4)
1750: m_c=4.6 (1) (5)
1880: m_c=4.1 (9) (2)
1977: m_c=3.0 (18) (18)
N_{tot} (N_{compl}) = 1005 (29)
Magnitude
Time
PML: b = 0.90
(b^{prior}=0.90) a = 2.48
From EPRI: ($M_{max,1}$ = 6.5)
($M_{max,2}$ = 6.7)
($M_{max,3}$ = 7.2)
PML–median (Q50)
(Q2.5, Q16, Q84, Q97.5)
Data:
incremental
cumulative
Annual number
Magnitude

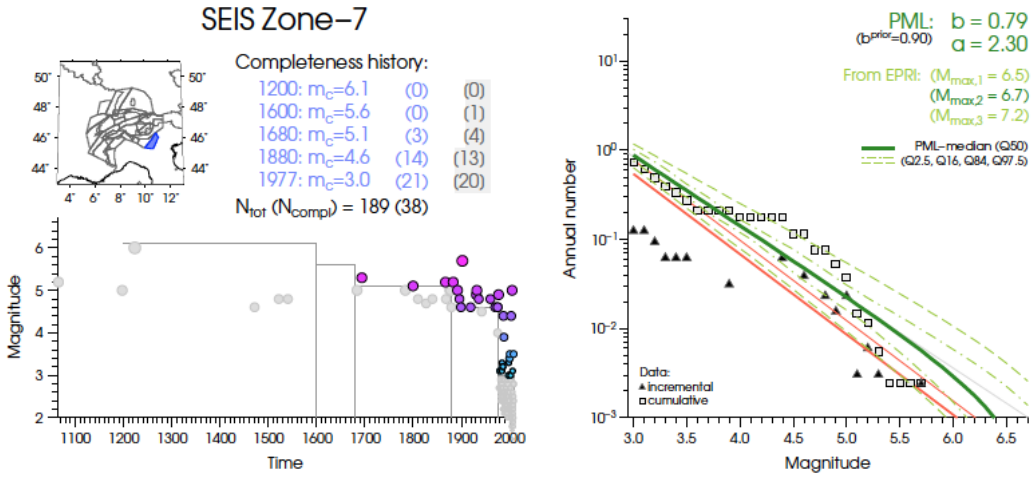
SEIS Zone–7
Completeness history:
1200: m_c=6.1 (0) (0)
1600: m_c=5.6 (0) (1)
1680: m_c=5.1 (3) (4)
1880: m_c=4.6 (14) (13)
1977: m_c=3.0 (21) (20)
N_{tot} (N_{compl}) = 189 (38)
Magnitude
Time
PML: b = 0.79
(b^{prior}=0.90) a = 2.30
From EPRI: ($M_{max,1}$ = 6.5)
($M_{max,2}$ = 6.7)
($M_{max,3}$ = 7.2)
PML–median (Q50)
(Q2.5, Q16, Q84, Q97.5)
Data:
incremental
cumulative
Annual number
Magnitude

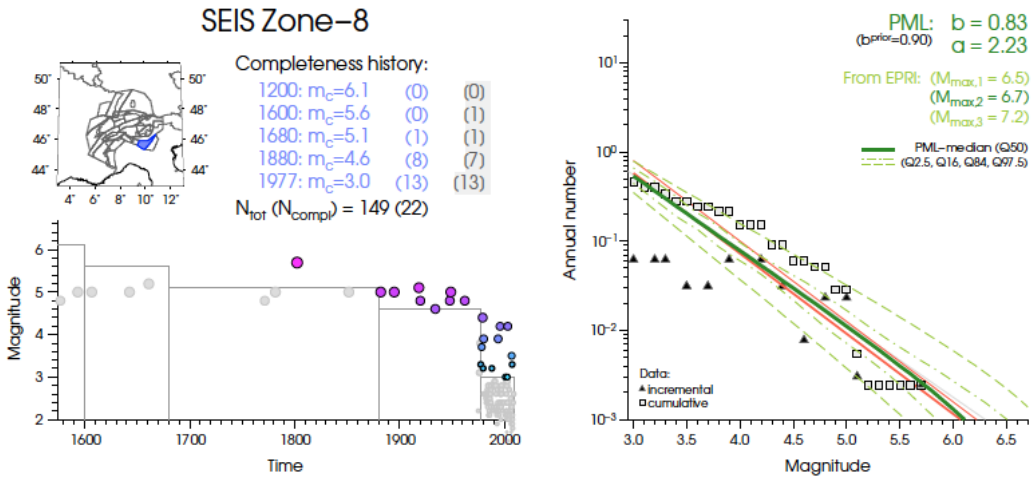
SEIS Zone–8
Completeness history:
1200: m_c=6.1 (0) (0)
1600: m_c=5.6 (0) (1)
1680: m_c=5.1 (1) (1)
1880: m_c=4.6 (8) (7)
1977: m_c=3.0 (13) (13)
N_{tot} (N_{compl}) = 149 (22)
Magnitude
Time
PML: b = 0.83
(b^{prior}=0.90) a = 2.23
From EPRI: ($M_{max,1}$ = 6.5)
($M_{max,2}$ = 6.7)
($M_{max,3}$ = 7.2)
PML–median (Q50)
(Q2.5, Q16, Q84, Q97.5)
Data:
incremental
cumulative
Annual number
Magnitude

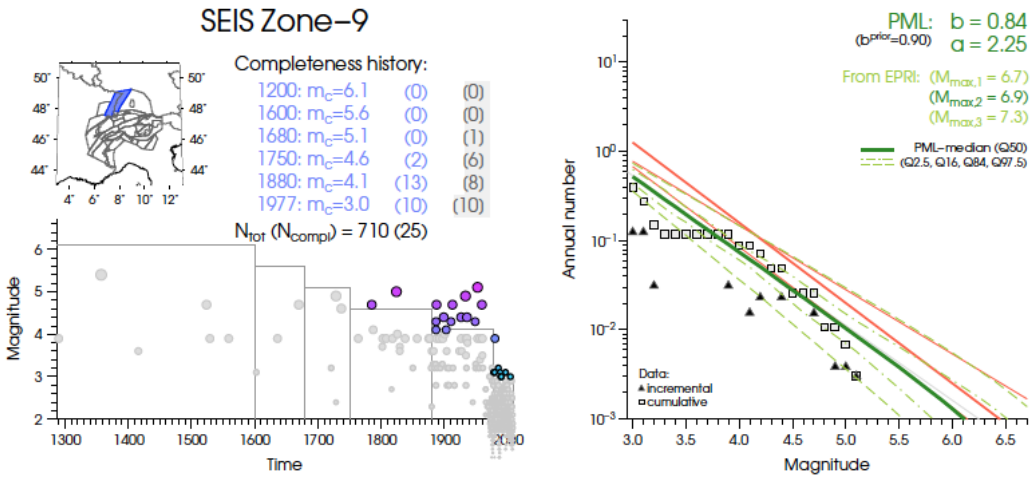
SEIS Zone–9
Completeness history:
1200: m_c=6.1 (0) (0)
1600: m_c=5.6 (0) (0)
1680: m_c=5.1 (0) (1)
1750: m_c=4.6 (2) (6)
1880: m_c=4.1 (13) (8)
1977: m_c=3.0 (10) (10)
N_{tot} (N_{compl}) = 710 (25)
Magnitude
Time
PML: b = 0.84
(b^{prior}=0.90) a = 2.25
From EPRI: ($M_{max,1}$ = 6.7)
($M_{max,2}$ = 6.9)
($M_{max,3}$ = 7.3)
PML–median (Q50)
(Q2.5, Q16, Q84, Q97.5)
Data:
incremental
cumulative
Annual number
Magnitude

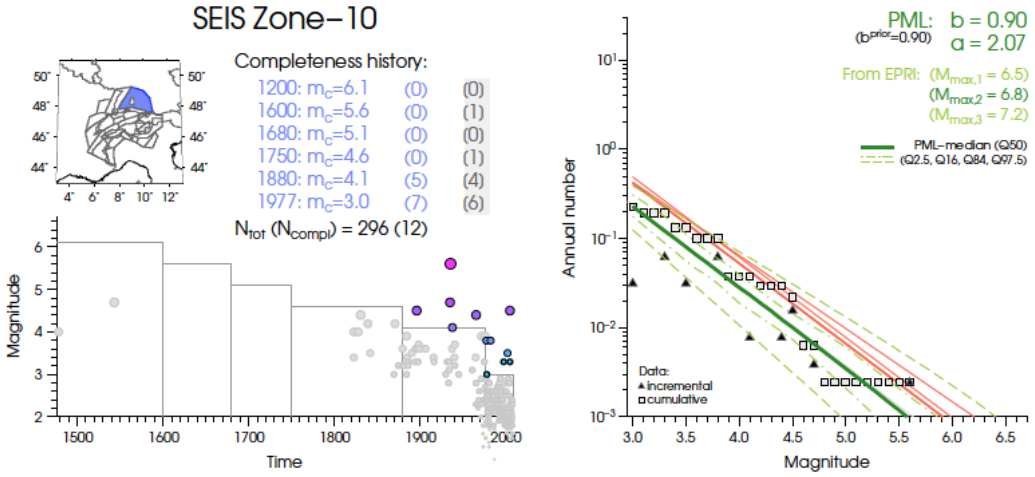
SEIS Zone–10
Completeness history:
1200: m_c=6.1 (0) (0)
1600: m_c=5.6 (0) (1)
1680: m_c=5.1 (0) (0)
1750: m_c=4.6 (0) (1)
1880: m_c=4.1 (5) (4)
1977: m_c=3.0 (7) (6)
N_{tot} (N_{compl}) = 296 (12)
Magnitude
Time
PML: b = 0.90
(b^{prior}=0.90) a = 2.07
From EPRI: ($M_{max,1}$ = 6.5)
($M_{max,2}$ = 6.8)
($M_{max,3}$ = 7.2)
PML–median (Q50)
(Q2.5, Q16, Q84, Q97.5)
Data:
incremental
cumulative
Annual number
Magnitude

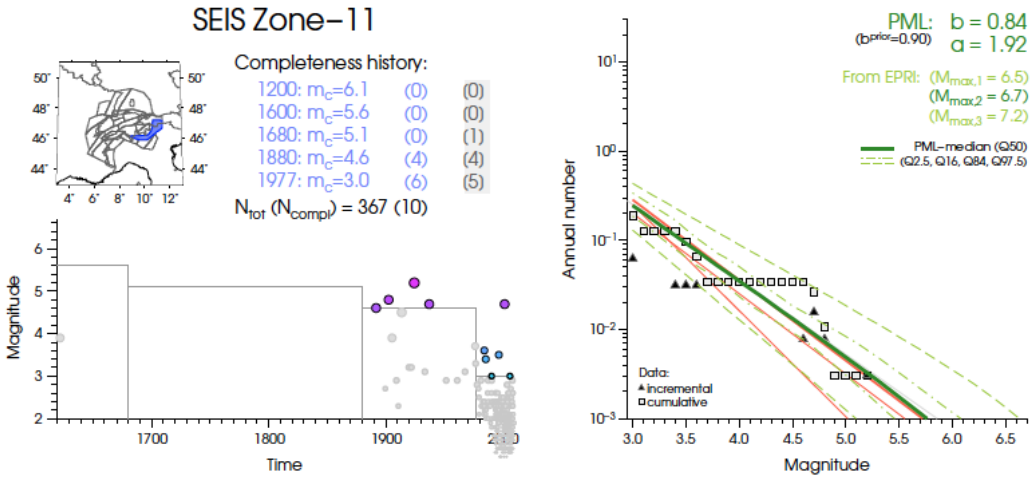
SEIS Zone–11
Completeness history:
1200: m_c=6.1 (0) (0)
1600: m_c=5.6 (0) (0)
1680: m_c=5.1 (0) (1)
1880: m_c=4.6 (4) (4)
1977: m_c=3.0 (6) (5)
N_{tot} (N_{compl}) = 367 (10)
Magnitude
Time
PML: b = 0.84
(b^{prior}=0.90) a = 1.92
From EPRI: ($M_{max,1}$ = 6.5)
($M_{max,2}$ = 6.7)
($M_{max,3}$ = 7.2)
PML–median (Q50)
(Q2.5, Q16, Q84, Q97.5)
Data:
incremental
cumulative
Annual number
Magnitude

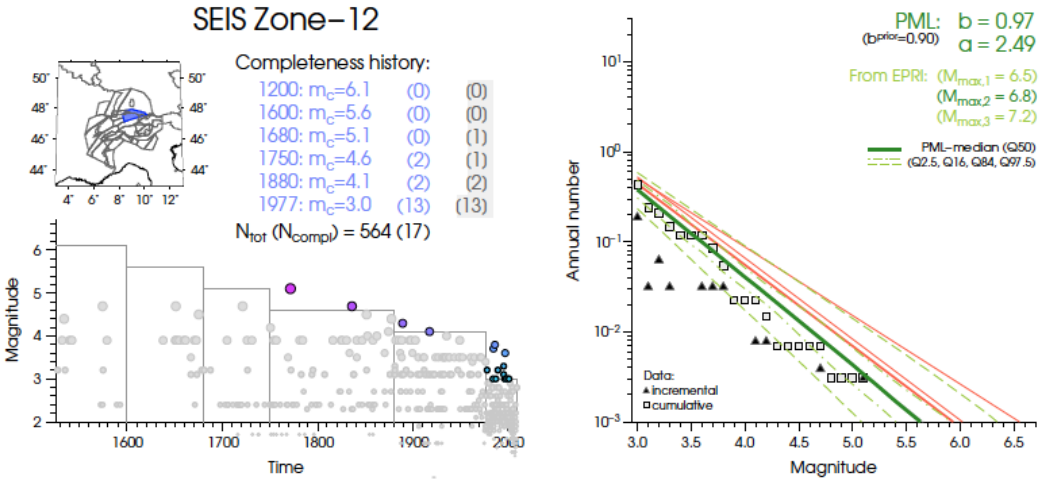
SEIS Zone–12
Completeness history:
1200: mc=6.1 (0) (0)
1600: mc=5.6 (0) (0)
1680: mc=5.1 (0) (1)
1750: mc=4.6 (2) (1)
1880: mc=4.1 (2) (2)
1977: mc=3.0 (13) (13)
Ntot (Ncompl) = 564 (17)
Magnitude
Time
PML: b = 0.97
(bprior=0.90) a = 2.49
From EPRI: (Mmax,1 = 6.5)
(Mmax,2 = 6.8)
(Mmax,3 = 7.2)
PML–median (Q50)
(Q2.5, Q16, Q84, Q97.5)
Data:
incremental
cumulative
Annual number
Magnitude

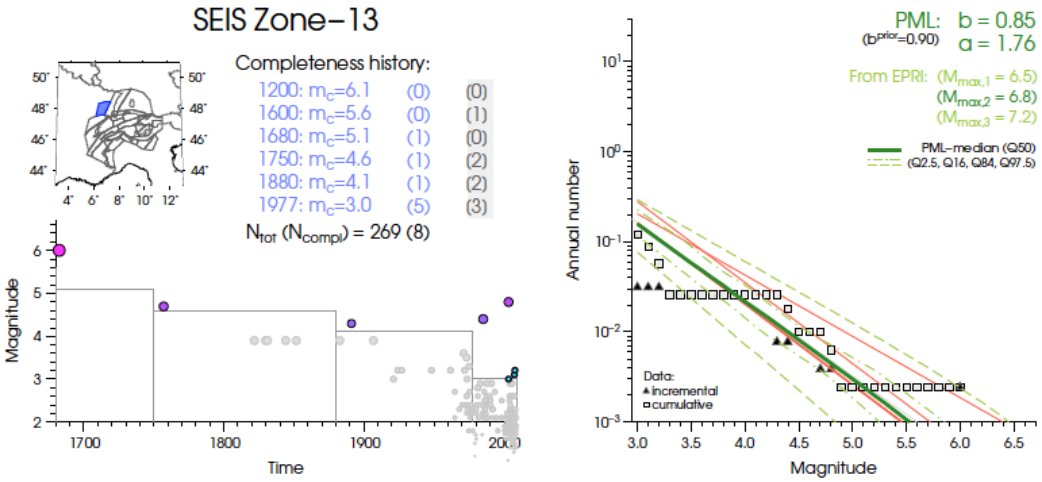
SEIS Zone–13
Completeness history:
1200: mc=6.1 (0) (0)
1600: mc=5.6 (0) (1)
1680: mc=5.1 (1) (0)
1750: mc=4.6 (1) (2)
1880: mc=4.1 (1) (2)
1977: mc=3.0 (5) (3)
Ntot (Ncompl) = 269 (8)
Magnitude
Time
PML: b = 0.85
(bprior=0.90) a = 1.76
From EPRI: (Mmax,1 = 6.5)
(Mmax,2 = 6.8)
(Mmax,3 = 7.2)
PML–median (Q50)
(Q2.5, Q16, Q84, Q97.5)
Data:
incremental
cumulative
Annual number
Magnitude

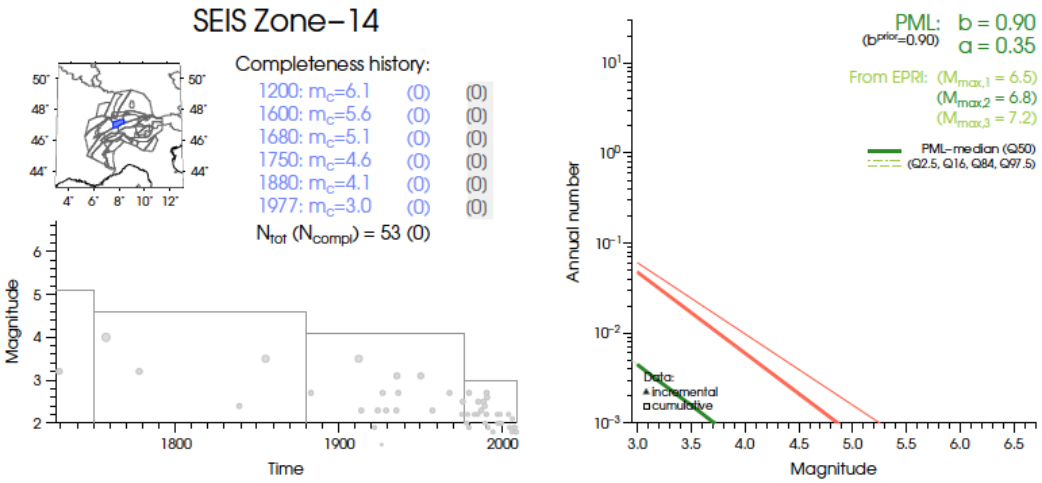
SEIS Zone–14
Completeness history:
1200: mc=6.1 (0) (0)
1600: mc=5.6 (0) (0)
1680: mc=5.1 (0) (0)
1750: mc=4.6 (0) (0)
1880: mc=4.1 (0) (0)
1977: mc=3.0 (0) (0)
Ntot (Ncompl) = 53 (0)
Magnitude
Time
PML: b = 0.90
(bprior=0.90) a = 0.35
From EPRI: (Mmax,1 = 6.5)
(Mmax,2 = 6.8)
(Mmax,3 = 7.2)
PML–median (Q50)
(Q2.5, Q16, Q84, Q97.5)
Data:
incremental
cumulative
Annual number
Magnitude

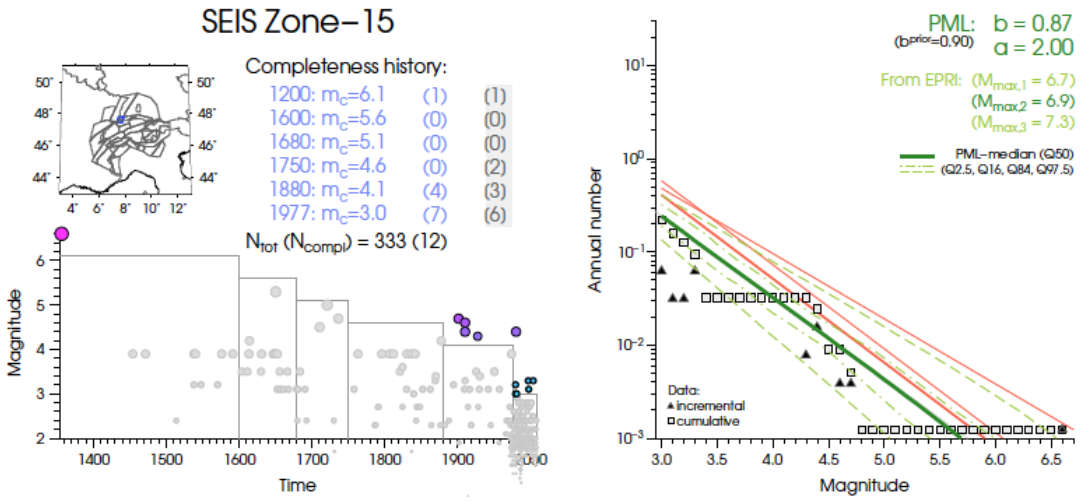
SEIS Zone−15
Completeness history:
1200: m_c=6.1 (1) (1)
1600: m_c=5.6 (0) (0)
1680: m_c=5.1 (0) (0)
1750: m_c=4.6 (0) (2)
1880: m_c=4.1 (4) (3)
1977: m_c=3.0 (7) (6)
N_tot (N_compl) = 333 (12)
Magnitude
Time
PML: b = 0.87
(b^prior=0.90) a = 2.00
From EPRI: (M_max,1 = 6.7)
(M_max,2 = 6.9)
(M_max,3 = 7.3)
PML−median (Q50)
(Q2.5, Q16, Q84, Q97.5)
Annual number
Data:
incremental
cumulative
Magnitude

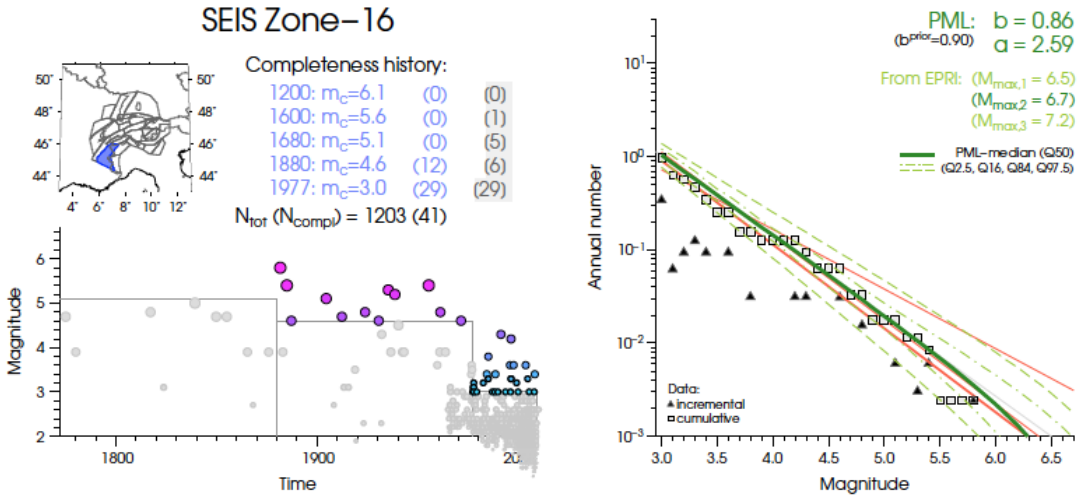
SEIS Zone−16
Completeness history:
1200: m_c=6.1 (0) (0)
1600: m_c=5.6 (0) (1)
1680: m_c=5.1 (0) (5)
1880: m_c=4.6 (12) (6)
1977: m_c=3.0 (29) (29)
N_tot (N_compl) = 1203 (41)
Magnitude
Time
PML: b = 0.86
(b^prior=0.90) a = 2.59
From EPRI: (M_max,1 = 6.5)
(M_max,2 = 6.7)
(M_max,3 = 7.2)
PML−median (Q50)
(Q2.5, Q16, Q84, Q97.5)
Annual number
Data:
incremental
cumulative
Magnitude

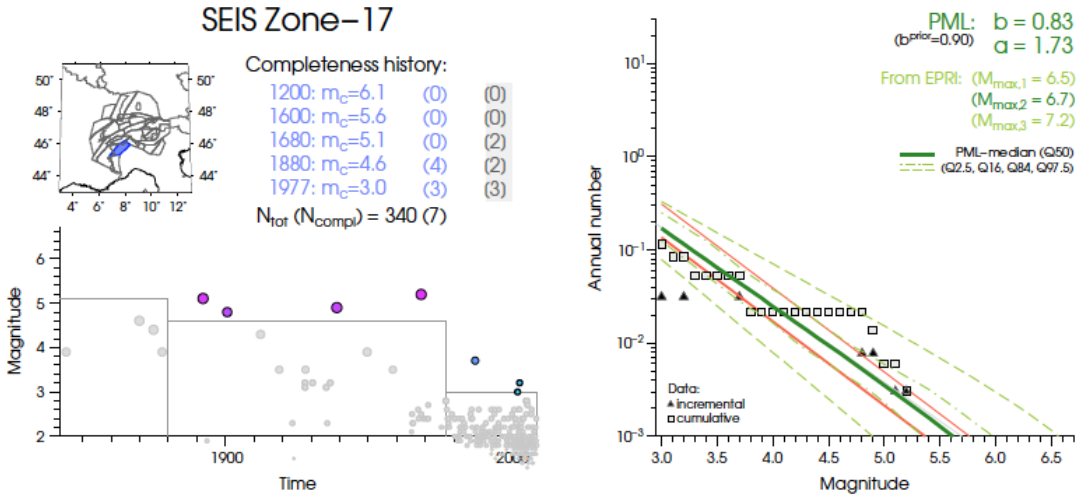
SEIS Zone−17
Completeness history:
1200: m_c=6.1 (0) (0)
1600: m_c=5.6 (0) (0)
1680: m_c=5.1 (0) (2)
1880: m_c=4.6 (4) (2)
1977: m_c=3.0 (3) (3)
N_tot (N_compl) = 340 (7)
Magnitude
Time
PML: b = 0.83
(b^prior=0.90) a = 1.73
From EPRI: (M_max,1 = 6.5)
(M_max,2 = 6.7)
(M_max,3 = 7.2)
PML−median (Q50)
(Q2.5, Q16, Q84, Q97.5)
Annual number
Data:
incremental
cumulative
Magnitude

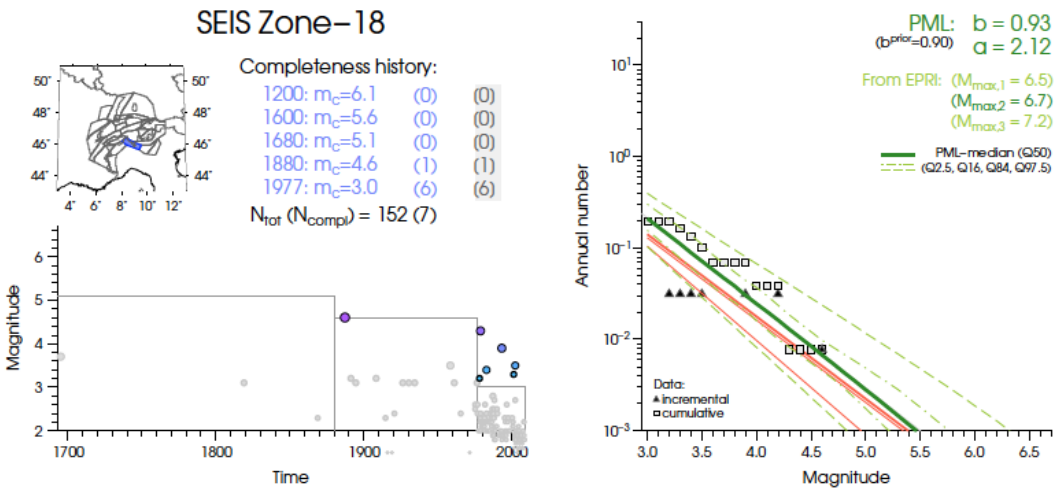
SEIS Zone–18
Completeness history:
1200: mc=6.1 (0) (0)
1600: mc=5.6 (0) (0)
1680: mc=5.1 (0) (0)
1880: mc=4.6 (1) (1)
1977: mc=3.0 (6) (6)
Ntot (Ncompl) = 152 (7)
Magnitude
Time
PML: b = 0.93
(bprior=0.90) a = 2.12
From EPRI: (Mmax,1 = 6.5)
(Mmax,2 = 6.7)
(Mmax,3 = 7.2)
PML–median (Q50)
(Q2.5, Q16, Q84, Q97.5)
Data:
incremental
cumulative
Annual number
Magnitude

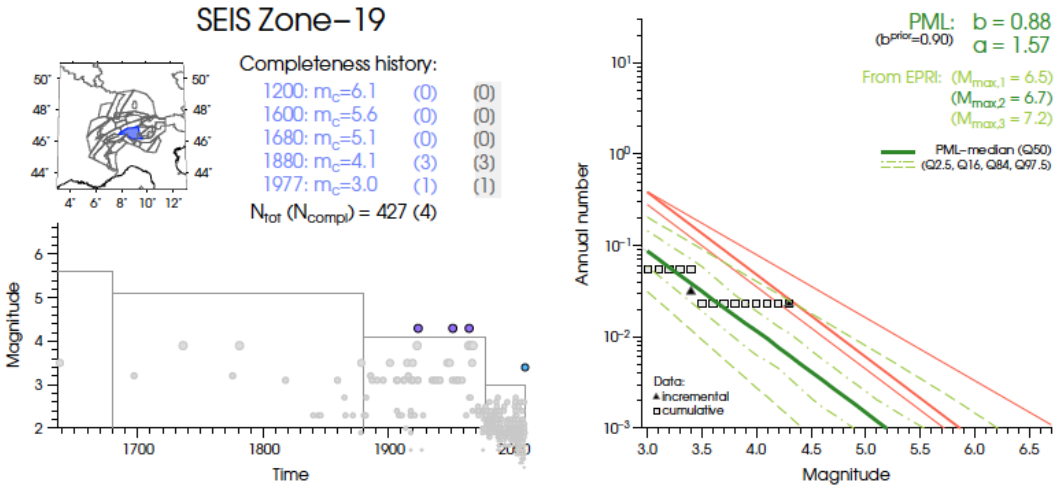
SEIS Zone–19
Completeness history:
1200: mc=6.1 (0) (0)
1600: mc=5.6 (0) (0)
1680: mc=5.1 (0) (0)
1880: mc=4.1 (3) (3)
1977: mc=3.0 (1) (1)
Ntot (Ncompl) = 427 (4)
Magnitude
Time
PML: b = 0.88
(bprior=0.90) a = 1.57
From EPRI: (Mmax,1 = 6.5)
(Mmax,2 = 6.7)
(Mmax,3 = 7.2)
PML–median (Q50)
(Q2.5, Q16, Q84, Q97.5)
Data:
incremental
cumulative
Annual number
Magnitude

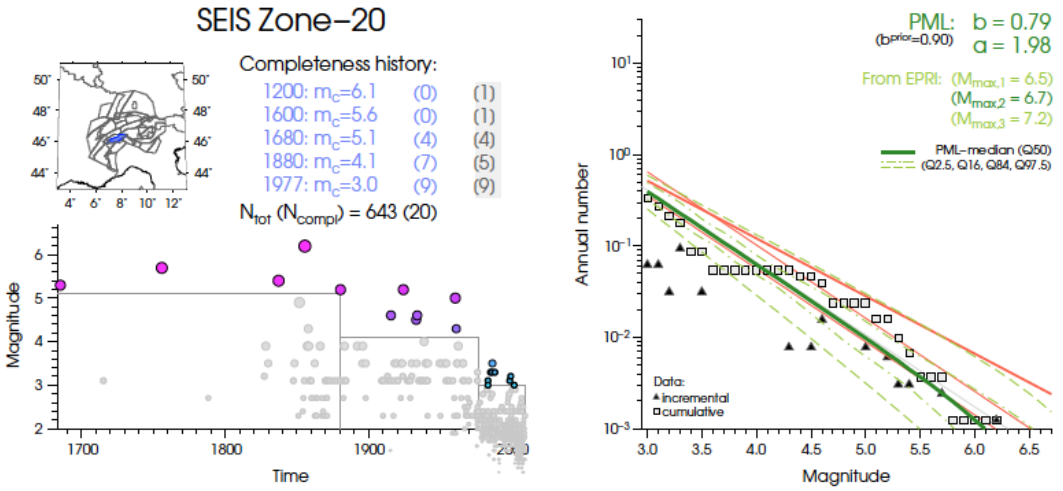
SEIS Zone–20
Completeness history:
1200: mc=6.1 (0) (1)
1600: mc=5.6 (0) (1)
1680: mc=5.1 (4) (4)
1880: mc=4.1 (7) (5)
1977: mc=3.0 (9) (9)
Ntot (Ncompl) = 643 (20)
Magnitude
Time
PML: b = 0.79
(bprior=0.90) a = 1.98
From EPRI: (Mmax,1 = 6.5)
(Mmax,2 = 6.7)
(Mmax,3 = 7.2)
PML–median (Q50)
(Q2.5, Q16, Q84, Q97.5)
Data:
incremental
cumulative
Annual number
Magnitude

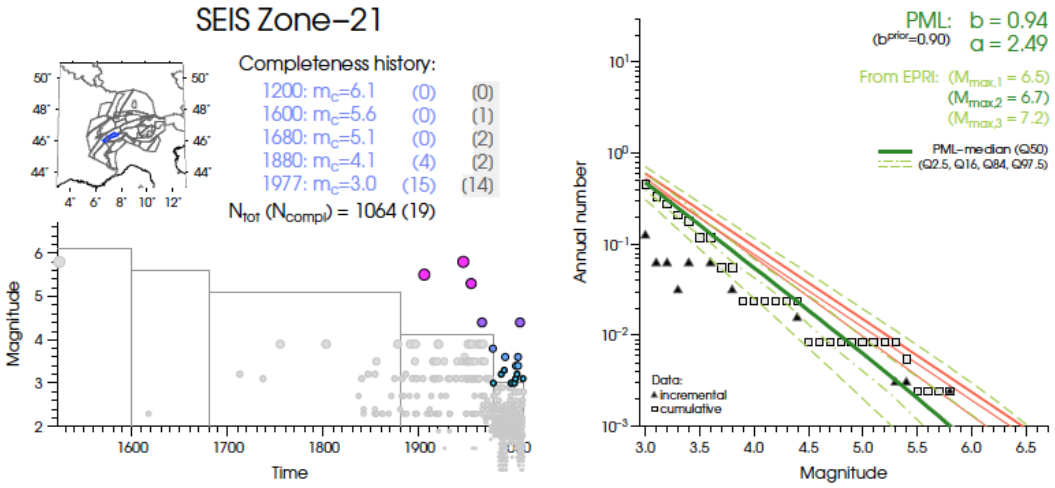
SEIS Zone–21
Completeness history:
1200: mc=6.1 (0) (0)
1600: mc=5.6 (0) (1)
1680: mc=5.1 (0) (2)
1880: mc=4.1 (4) (2)
1977: mc=3.0 (15) (14)
Ntot (Ncompl) = 1064 (19)
Magnitude
Time
PML: b = 0.94
(bprior=0.90) a = 2.49
From EPRI: (Mmax,1 = 6.5)
(Mmax,2 = 6.7)
(Mmax,3 = 7.2)
PML–median (Q50)
(Q2.5, Q16, Q84, Q97.5)
Data:
incremental
cumulative
Annual number
Magnitude

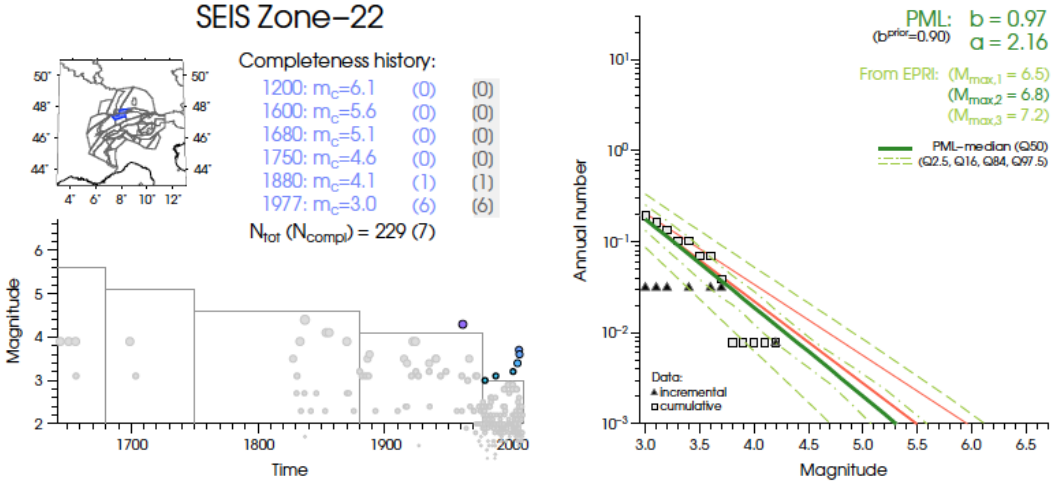
SEIS Zone–22
Completeness history:
1200: mc=6.1 (0) (0)
1600: mc=5.6 (0) (0)
1680: mc=5.1 (0) (0)
1750: mc=4.6 (0) (0)
1880: mc=4.1 (1) (1)
1977: mc=3.0 (6) (6)
Ntot (Ncompl) = 229 (7)
Magnitude
Time
PML: b = 0.97
(bprior=0.90) a = 2.16
From EPRI: (Mmax,1 = 6.5)
(Mmax,2 = 6.8)
(Mmax,3 = 7.2)
PML–median (Q50)
(Q2.5, Q16, Q84, Q97.5)
Data:
incremental
cumulative
Annual number
Magnitude

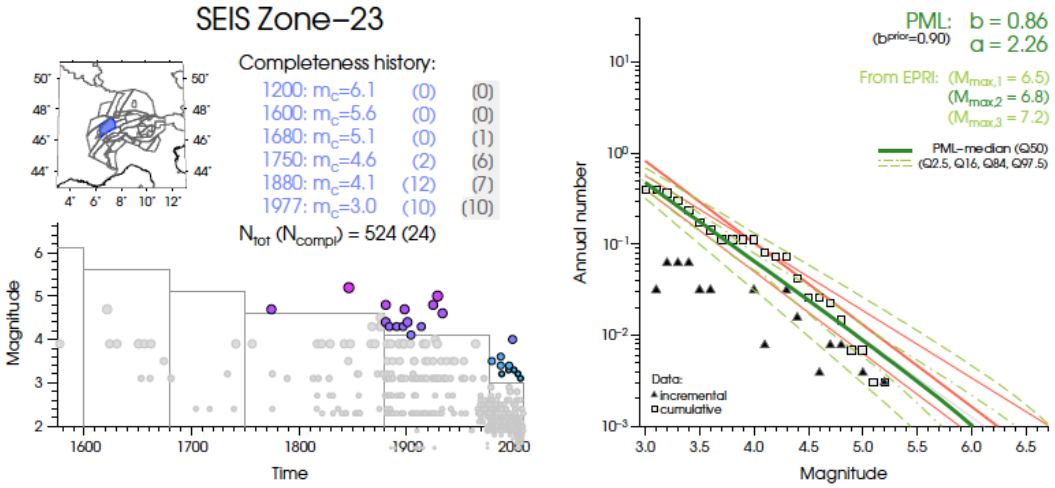
SEIS Zone–23
Completeness history:
1200: mc=6.1 (0) (0)
1600: mc=5.6 (0) (0)
1680: mc=5.1 (0) (1)
1750: mc=4.6 (2) (6)
1880: mc=4.1 (12) (7)
1977: mc=3.0 (10) (10)
Ntot (Ncompl) = 524 (24)
Magnitude
Time
PML: b = 0.86
(bprior=0.90) a = 2.26
From EPRI: (Mmax,1 = 6.5)
(Mmax,2 = 6.8)
(Mmax,3 = 7.2)
PML–median (Q50)
(Q2.5, Q16, Q84, Q97.5)
Data:
incremental
cumulative
Annual number
Magnitude

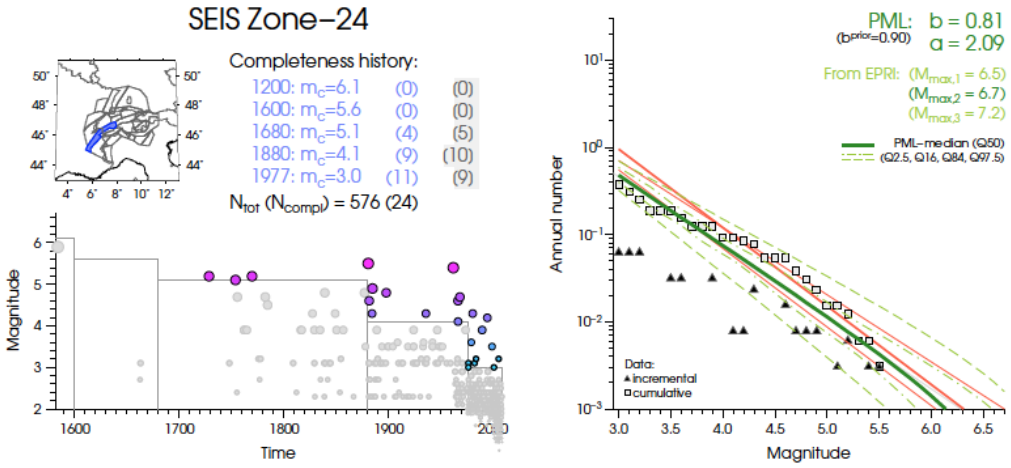
SEIS Zone–24
Completeness history:
1200: mc=6.1 (0) (0)
1600: mc=5.6 (0) (0)
1680: mc=5.1 (4) (5)
1880: mc=4.1 (9) (10)
1977: mc=3.0 (11) (9)
Ntot (Ncompl) = 576 (24)
Magnitude
Time
PML: b = 0.81
(bprior=0.90) a = 2.09
From EPRI: (Mmax,1 = 6.5)
(Mmax,2 = 6.7)
(Mmax,3 = 7.2)
PML–median (Q50)
(Q2.5, Q16, Q84, Q97.5)
Data:
incremental
cumulative
Annual number
Magnitude

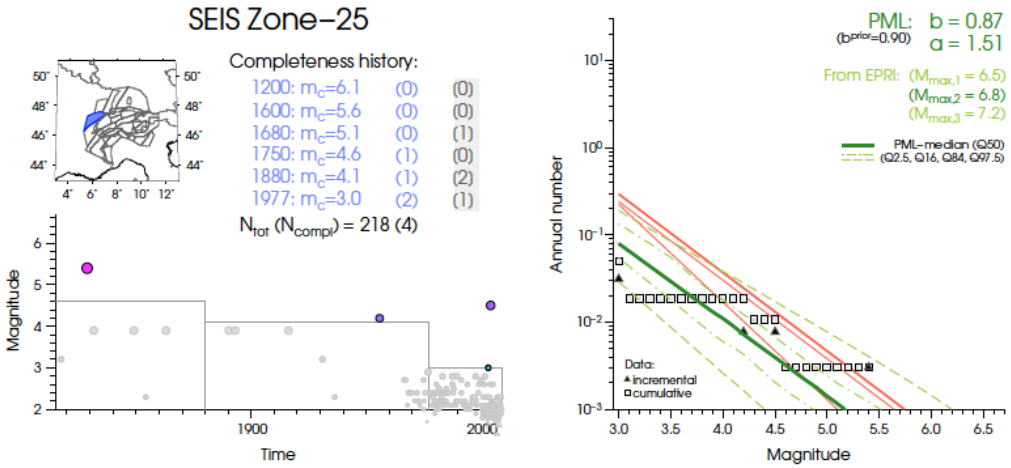
SEIS Zone–25
Completeness history:
1200: mc=6.1 (0) (0)
1600: mc=5.6 (0) (0)
1680: mc=5.1 (0) (1)
1750: mc=4.6 (1) (0)
1880: mc=4.1 (1) (2)
1977: mc=3.0 (2) (1)
Ntot (Ncompl) = 218 (4)
Magnitude
Time
PML: b = 0.87
(bprior=0.90) a = 1.51
From EPRI: (Mmax,1 = 6.5)
(Mmax,2 = 6.8)
(Mmax,3 = 7.2)
PML–median (Q50)
(Q2.5, Q16, Q84, Q97.5)
Data:
incremental
cumulative
Annual number
Magnitude

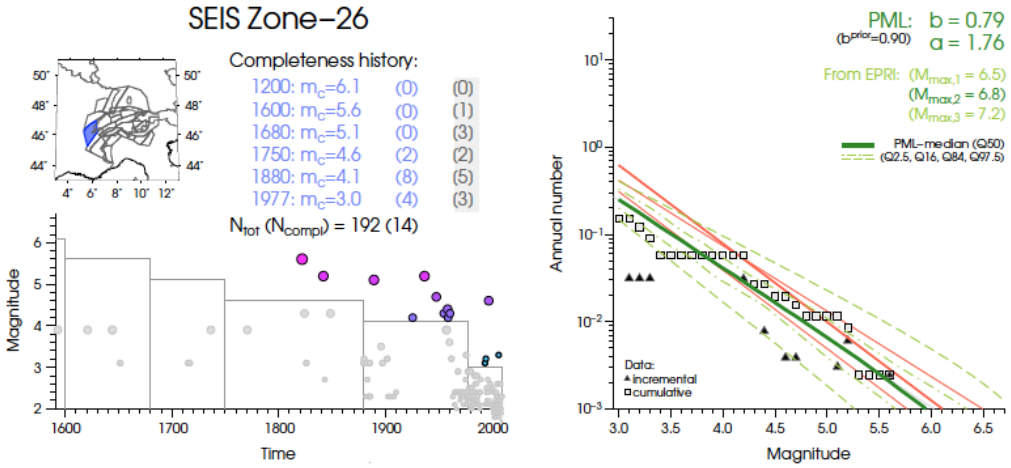
SEIS Zone–26
Completeness history:
1200: mc=6.1 (0) (0)
1600: mc=5.6 (0) (1)
1680: mc=5.1 (0) (3)
1750: mc=4.6 (2) (2)
1880: mc=4.1 (8) (5)
1977: mc=3.0 (4) (3)
Ntot (Ncompl) = 192 (14)
Magnitude
Time
PML: b = 0.79
(bprior=0.90) a = 1.76
From EPRI: (Mmax,1 = 6.5)
(Mmax,2 = 6.8)
(Mmax,3 = 7.2)
PML–median (Q50)
(Q2.5, Q16, Q84, Q97.5)
Data:
incremental
cumulative
Annual number
Magnitude